



University  
of Glasgow

<https://theses.gla.ac.uk/>

Theses Digitisation:

<https://www.gla.ac.uk/myglasgow/research/enlighten/theses/digitisation/>

This is a digitised version of the original print thesis.

Copyright and moral rights for this work are retained by the author

A copy can be downloaded for personal non-commercial research or study, without prior permission or charge

This work cannot be reproduced or quoted extensively from without first obtaining permission in writing from the author

The content must not be changed in any way or sold commercially in any format or medium without the formal permission of the author

When referring to this work, full bibliographic details including the author, title, awarding institution and date of the thesis must be given

Enlighten: Theses

<https://theses.gla.ac.uk/>  
[research-enlighten@glasgow.ac.uk](mailto:research-enlighten@glasgow.ac.uk)

" A THEORETICAL AND PHOTOELASTIC INVESTIGATION OF THE STRESS  
CONCENTRATION EFFECTS OF DISCONTINUITIES  
IN TENSION PLATES."

A THESIS PRESENTED FOR THE DEGREE OF  
DOCTOR OF PHILOSOPHY OF THE  
UNIVERSITY OF GLASGOW

by

D. S. ROSS, B.Sc.(Eng.), A.R.C.S.T., A.M.I.Mech.E., A.M.I.Prod.E., A.M.Inst.R.

3, KEIR DRIVE,  
BISHOPBRIGGS,  
GLASGOW.

NOVEMBER, 1960.



ProQuest Number: 10646155

All rights reserved

INFORMATION TO ALL USERS

The quality of this reproduction is dependent upon the quality of the copy submitted.

In the unlikely event that the author did not send a complete manuscript and there are missing pages, these will be noted. Also, if material had to be removed, a note will indicate the deletion.



ProQuest 10646155

Published by ProQuest LLC (2017). Copyright of the Dissertation is held by the Author.

All rights reserved.

This work is protected against unauthorized copying under Title 17, United States Code  
Microform Edition © ProQuest LLC.

ProQuest LLC.  
789 East Eisenhower Parkway  
P.O. Box 1346  
Ann Arbor, MI 48106 – 1346

## I N D E X

	<u>PAGE NO.</u>
ABSTRACT .....	1
LIST OF SYMBOLS .....	3
INTRODUCTION .....	4
CHAPTER I      REVIEW OF PUBLISHED LITERATURE .....	9
CHAPTER II     THEORETICAL ANALYSIS .....	65
CHAPTER III    EXPERIMENTAL WORK .....	91
CHAPTER IV     ANALYSIS AND DISCUSSION OF RESULTS .....	106
CHAPTER V      SUMMARY AND CONCLUSIONS .....	114
CHAPTER VI     BIBLIOGRAPHY AND AUTHOR INDEX .....	119
CHAPTER VII    APPENDICES .....	131
ACKNOWLEDGMENTS .....	174

ooo000ooo

# C O N T E N T S

	<u>PAGE NO.</u>
ABSTRACT.	1
LIST OF SYMBOLS.	3
INTRODUCTION.	4
<u>CHAPTER I - REVIEW OF PUBLISHED LITERATURE:</u>	
I.1    Theoretical Investigations.	9
I.2    Experimental Investigations.	41
I.3    Critical Summary.	62
<u>CHAPTER II - THEORETICAL ANALYSIS:</u>	
<u>Part 1</u> <u>The Method of Complex Potentials</u> <u>Applied to Tension Plates</u> <u>Containing Holes.</u>	
II.1    Basic Stress Equations in Complex Form.	65
II.2    Selection of Transformation Form.	71
<u>Part 2</u> <u>Stress Conditions due to the</u> <u>presence of a Cruciform Crack</u> <u>in a Tension Plate.</u>	
II.3    Transformation Form.	75
II.4    Derived Complex Potentials.	78
II.5    Distribution of Principal Stresses along Axis of Symmetry.	88
<u>Part 3</u> <u>Stress Concentration Factors.</u>	
II.6    Stress Concentration Factors for a Selection of Polygonal Discontinuities in the Interior of a Tension Plate.	89
<u>CHAPTER III - EXPERIMENTAL WORK:</u>	
III.1    Determination of Transformation Form by the Analogue Computer.	91
III.2    Determination of the Sum of the Principal Stresses by the Conducting Paper Analogy.	96
III.5    Determination of the Difference of the Principal Stresses by Photoelasticity.	100

<u>CHAPTER IV</u>	-	<u>ANALYSIS AND DISCUSSION OF RESULTS:</u>	<u>PAGE NO.</u>
IV.1		The Cruciform Crack.	106
IV.2		Comparison of Theoretical and Experimental Stress Concentration Factors for a variety of Discontinuities.	109
IV.3		Correlation of Stress Concentration Factors for design purposes.	111
<u>CHAPTER V</u>	-	<u>SUMMARY AND CONCLUSIONS:</u>	
V.1		The Cruciform Crack.	114
V.2		The Analogue Technique.	116
V.3		Stress Concentration Factors.	117
V.4		Design Chart for Stress Concentration Factors.	118
<u>CHAPTER VI</u>	-	<u>BIBLIOGRAPHY AND AUTHOR INDEX.</u>	119
<u>CHAPTER VII</u>	-	<u>APPENDICES:</u>	
VII.1		Theory of Complex Potentials in Two Dimensional Elasticity.	131
VII.2		Digital Computer Programme for Theoretical Stress Distribution for Cruciform Crack Case.	146
VII.3		Calculations for Theoretical Stress Concentration Factors.	149
VII.4		Investigation of Rothman's suggested Complex Potentials for Cruciform Crack, and Digital Computer Programme for same.	155
VII.5		Investigation of Reliability and Suitability of Conducting Paper Analogy for Cases of Tension and Torsion.	169
<u>ACKNOWLEDGMENTS.</u>			174

A B S T R A C T

This thesis presents a comprehensive illustrated review of published literature on the effect of stress raisers in the form of holes, notches and fillets in plane stress fields.

A theoretical analysis is given of the effect of a cruciform type 'crack' in an infinite plate under uniform tension at infinity, using the MUSKHELISHVILI method, the 'crack' being simulated by two machined slits at  $90^\circ$  to each other. The analysis is extended to include a further range of discontinuities, in the forms of 'square', 'triangular' and 'star' type openings, and in all, six theoretical stress concentration factors are derived, corresponding to the selected discontinuities investigated experimentally. The selection of suitable conformal transformations was greatly simplified by the use of a function generator built by the writer, together with a Minispace Analogue Computer, this application being believed to be original. The influence on basic shape and root radius of curvature, of the number of terms and their coefficients used in the series transformation forms employed, is shown pictorially by oscilloscope pattern photographs. The numerical evaluation of the stress concentration factors associated with the chosen transformation forms, was facilitated by the use of a Deuce Digital Computer, the programme for these calculations being given in the Appendix.

The results of an extensive photoelastic investigation into the stress concentration effects of a range of twenty-seven geometric forms of edge and internal discontinuities are reported, with examples of the stress distributions/

distributions along the axes of symmetry being shown in graphical form. Stress concentration factors are quoted in all cases, and selected fringe photographs are presented. The photoelastic work was supplemented by the use of a Conducting Paper Analogy, devised and built by the writer, for the rapid determination of the distribution of the sum of the principal stresses along the axes of symmetry. Details of this Analogue are given in the text, and the reliability check results are displayed in graphical form partly in the text and partly in the Appendix.

The experimental results are correlated graphically using INGLIS theory for non-elliptical holes, the experimental values being related to an elliptic hole whose major axis is at  $90^\circ$  to the axis of tension. As an extension to this, the theoretical stress concentration factors for certain forms of holes, given by SAVIN and STEVENSON, are correlated in a similar fashion. Using this as a basis, a design chart for holes in tension plates has been drawn up, expressing stress concentration factors as a function of the ratio of hole dimension to minimum radius of curvature, and this chart is presented as a suitable form for use in design practice.

The appendix includes a report of an investigation into complex potentials suggested by ROTHMAN, and the results (which were inconclusive) are stated.

A Bibliography, containing references to sixty-three publications consulted in the preparation of the thesis, is presented together with a related Author Index.

# L I S T O F S Y M B O L S

## THEORETICAL WORK

The theoretical presentation follows GODFREY'S translation of SAVIN'S work, the notation used being as follows:-

$x, y$ .....	Cartesian co-ordinates
$\rho, \theta$ .....	Curvilinear co-ordinates
$\left. \begin{aligned} Z &= x + iy \\ \bar{Z} &= x - iy \end{aligned} \right\} \dots\dots\dots$	Conjugate complex variables
$\left. \begin{aligned} \xi &= \xi + i\eta \\ \bar{\xi} &= \xi - i\eta \end{aligned} \right\} \dots\dots\dots$	" " "
$\sigma_x, \sigma_y, \tau_{xy}$ .....	Components of stress in cartesian co-ordinates.
$\sigma_\rho, \sigma_\theta, \tau_{\rho\theta}$ .....	Components of stress in curvilinear co-ordinates.
$\sigma_0, \sigma_\rho$ .....	Principal stresses at infinity.
$\Phi = \sigma_x + \sigma_y$ .....	Combinations of stress components.
$\Phi = \sigma_y - \sigma_x + 2i\tau_{xy}$ .....	" " " "
$\Phi' = \sigma_\rho + \sigma_\theta = \Phi$ .....	" " " "
$\begin{aligned} \Phi' &= \sigma_\theta - \sigma_\rho + 2i\tau_{\rho\theta} \dots\dots\dots \\ &= e^{2i\alpha} \Phi \dots\dots\dots \end{aligned}$	Where $\alpha$ is the angle between the normal to the curve $\rho = \text{constant}$ and the $x$ - axis.
$\phi(Z), \psi(Z)$ .....	Complex potentials.
$\mu$ .....	Modulus of Rigidity.
$\nu$ .....	Poisson's ratio.

## EXPERIMENTAL WORK

$\sigma_1, \sigma_2$ .....	Principal stresses in the plane of the plate.
$\sigma_0$ .....	Uniform tension stress (corresponds to $\sigma_0$ of theory).

## I N T R O D U C T I O N

The subject of stress concentration is of paramount importance in the field of engineering design.

Nominal stress is no longer regarded as sufficient for design purposes, since the form of the part considered may be such as to produce local maximum stresses, the magnitude of which may be the over-riding factor determining strength. It is particularly important where high strength to weight ratios are required, that magnitude of stress concentration should be assessable, in order to achieve maximum efficiency in the utilisation of material.

The determination of the degree of stress concentration presents considerable difficulty, since the avenues of approach require a good working knowledge either of advanced mathematics, or of the many available experimental methods.

Analytical methods vary, the form of the solution depending to a large extent on the initial basic assumptions, and also upon the limitations introduced by the mathematics involved. Hence, while it may be possible theoretically to state a form of solution for the assessment of stress concentration effect, it may be extremely difficult physically to arrive at a numerical result. Thus it is often necessary, in the analytical approach, to resort to an approximate form of solution.

Theoretical methods are broadly divisible into two categories, firstly those solutions which employ the classical Stress Function technique, and secondly the more recently developed and more elegant form/



form of solution in terms of Complex Potentials. Even within these two main groups there are subdivisions. For example, in the Stress Function Method, the stress function may be expressed in terms of an infinite series or alternatively in terms of complex variables. Within the Complex Potential group of solutions, either the 'tentative' method of STEVENSON<sup>(1)</sup> may be employed, in which case the complex potentials are assumed and subsequently tested to satisfy the boundary conditions, or alternatively the 'direct' method of MUSKHELISHVILI<sup>(2)</sup>, in which the complex potentials are deduced from the conditions imposed by the problem.

Generally, these analytical methods have been applied to simple forms of discontinuities, in particular the circular hole in the infinite plate, and only in comparatively recent years have solutions for other geometrical forms been forthcoming, such as in the work of COX<sup>(3)</sup> and SAVIN<sup>(4)</sup>. Comparatively little analytical work has appeared on edge discontinuities, due to the difficulty involved in the mathematical specification of the boundaries in a form suitable to be handled by the method of solution.

Experimental methods for determining stress concentration effects in two dimensional stress fields are numerous. Brittle models, accurate extensometers and wire resistance or foil strain gauges are well-known techniques for stress analysis work. The brittle lacquer method has been employed fairly widely in recent years for assessing the magnitude of stress concentration effects by examining the lacquer crack pattern around discontinuities of various types. The photoelastic method has been applied very extensively to stress distribution work, in both two- and three-dimensional stress analysis cases.

With/

With experimental methods, the accuracy of assessment of stress concentration effect is often limited by the technique employed, so that different methods applied to the same problem give variations in stress concentration factor. Of all the available methods, the photoelastic method stands out as being particularly suitable for the determination of stress concentration effect, and for stress distribution in general, provided that suitable models can be made for the purpose.

From the design point of view, these theoretical and experimental methods are not rapid methods of assessing values of stress concentration effect, and empirical formulae become desirable. Such formulae require some degree of care in application, particularly in non-standard cases of stress concentration, otherwise inaccurate assessments may occur, with obvious repercussions. Clearly, extreme accuracy is not possible, nor is it necessary, since even an approximate stress concentration factor is satisfactory for the designer's requirements.

It is evident that the state of knowledge of stress concentration effect, although extensively investigated theoretically and experimentally, is by no means far advanced, except in particular cases of discontinuities. Analytical methods are severely limited in their application by their complexity, experimental methods by the skill and patience required, and empirical rules by their scarcity. A review has shown that there is a need for some simplification of the method of assessment of stress concentration, so that the available results may be more readily applied to design.

It/

It is justifiable therefore to endeavour to integrate the available stress concentration information into a simple form which will be suitable for use by those unfamiliar with either the theoretical or the experimental methods of approach. Such authors as COX<sup>(3)</sup>, SAVIN<sup>(4)</sup>, PETERSON<sup>(5)</sup> and HEYWOOD<sup>(6)</sup> have been pioneers in this field, and in the case of the last mentioned writer, much has been done in the correlation of results from the collected published works of other authors.

In this thesis, a review of published literature dealing with stress concentrations in two-dimensional fields shows that there is a relative lack of analytical and experimental work on 'crack' type discontinuities, particularly of the cruciform type, together with other geometrical forms of edge and internal openings in tension plates.

In the case of crack type discontinuities, an analytical method of solution proposed by ROTHMAN<sup>(7)</sup> for the stress distribution around cruciform type cracks has been investigated by the author, but the results obtained have not been satisfactory. An alternative approach, using the Complex Potential Method of MUSKHELISHVILI<sup>(2)</sup>, has yielded a satisfactory solution.

The Photoelastic Method, in conjunction with the Conducting Paper Analogy, has been used successfully by the author to obtain stress concentration factors and stress distributions for a wide range of discontinuities, both edge and internal, in tension plates, including the case of the cruciform crack.

An attempt has been made also, to correlate in a simple manner,

the stress concentration factors for a wide variety of discontinuities in thin plates in uni-axial tension, from both theoretical and experimental results, and this correlation is presented in graphical form for ease of application in design practice.

CHAPTER I - REVIEW OF PUBLISHED LITERATURE

The review presents a critical survey of theoretical and experimental investigations of stress concentrations produced by internal and external discontinuities of regular geometric form in thin plates of infinite, semi-infinite and finite widths subjected to uni-axial and bi-axial tensions in the plane of the plate. Single discontinuities are considered only, but it is of interest to note that the effect of multiple discontinuities in close proximity is to reduce the stress concentration. Figure 1 shows this effect, in the case of edge notches of semi-circular form.

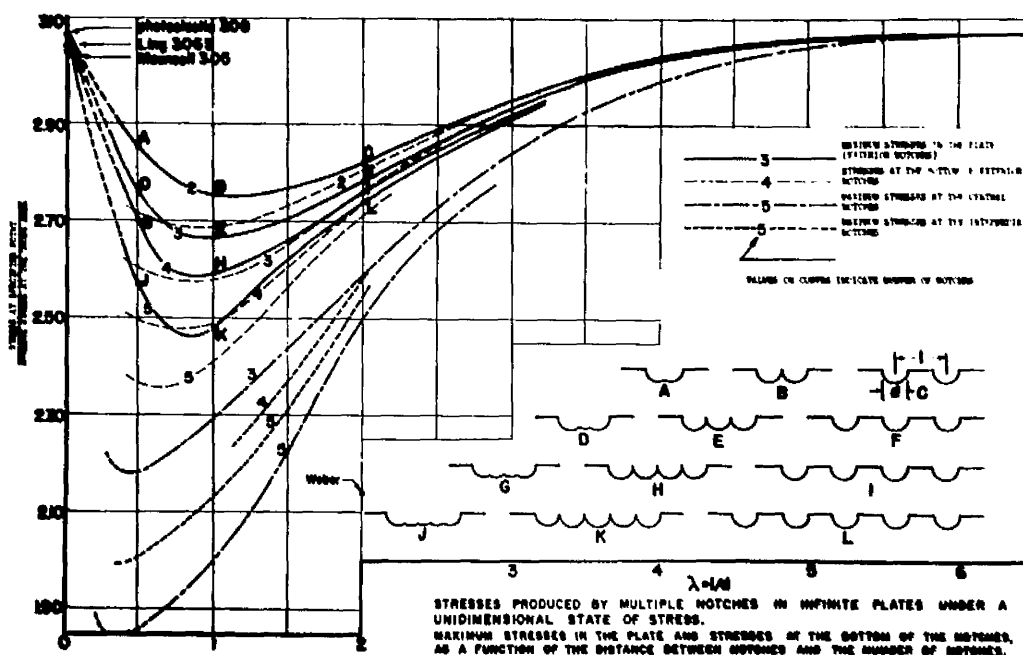


Fig.1.

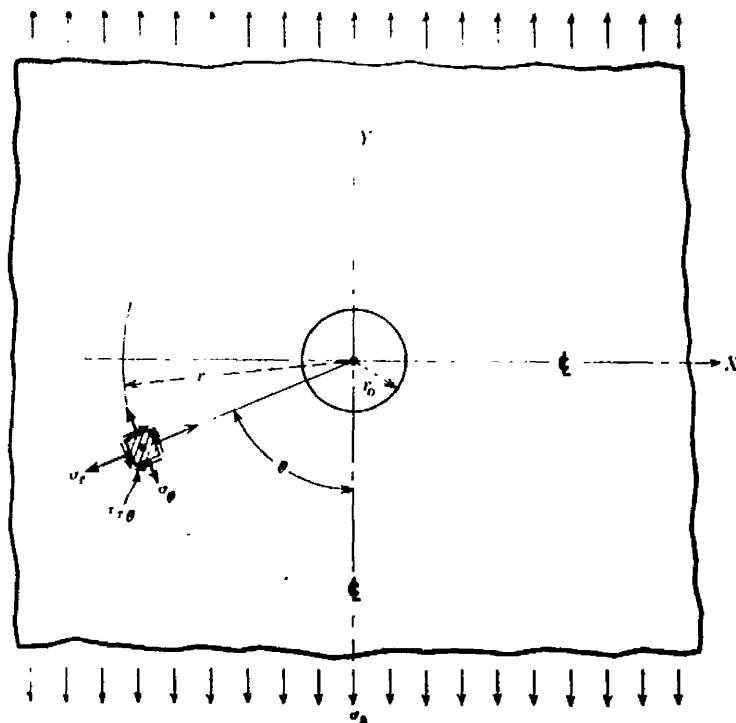
I.1 THEORETICAL INVESTIGATIONSINTERNAL DISCONTINUITIES:I.1 (a) Circular Hole

- (i) Infinite Plate
- (ii) Finite Plate
- (iii) Semi-infinite Plate.

I.1 (b) Elliptical Hole in Infinite PlateI.1 (c) Internal Crack in Infinite PlateI.1 (d) Miscellaneous Internal DiscontinuitiesEXTERNAL DISCONTINUITIES:I.1 (e) External CracksI.1 (f) External NotchesI.1 (g) Miscellaneous External Discontinuities

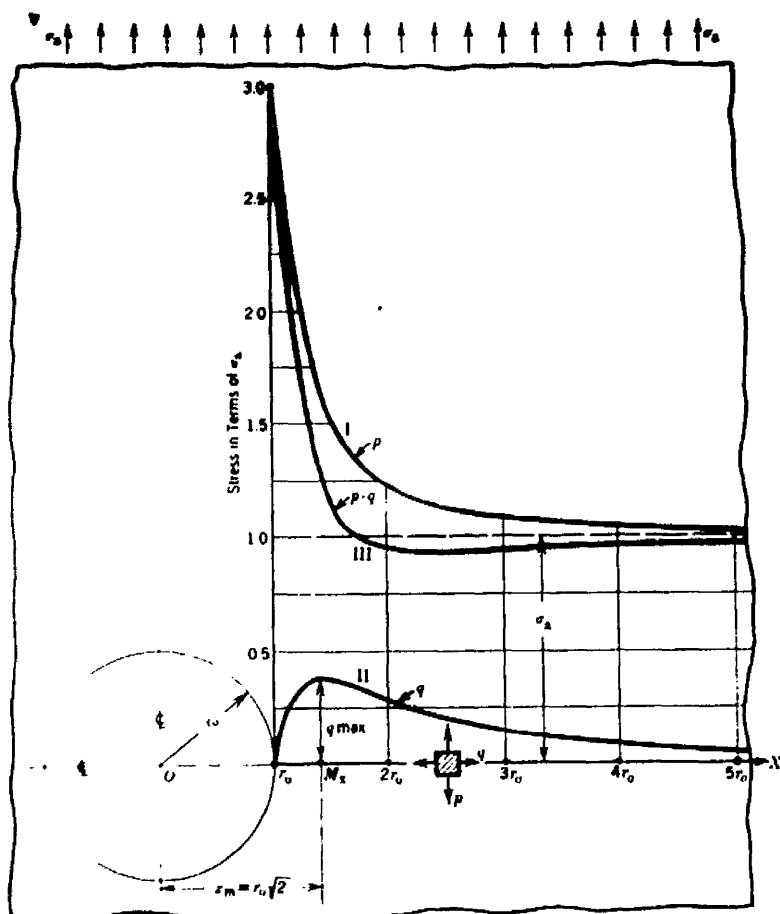
000 000 000 000 000 000 000 000 000 000 000 000 000 000 000

Fig.2.



Stresses in Polar Coordinates around a Circular Hole in a Bar in Tension.

Fig.3.





(I.1)

I.1(a) Circular Hole.(i) Infinite Plate

In 1898, KIRSCH<sup>(8)</sup> published the first rigorous solution for the stress distribution around a central circular hole in a thin infinite plate under uni-axial tension in the plane of the plate, the stresses being given by equations of the following form:-

$$\sigma_r = \frac{\sigma_0}{2} \left(1 - \frac{r_0^2}{r^2}\right) + \frac{\sigma_0}{2} \left(1 - \frac{4r_0^2}{r^2} + \frac{3r_0^4}{r^4}\right) \cos 2\theta \dots\dots\dots (1.1)$$

$$\sigma_\theta = \frac{\sigma_0}{2} \left(1 + \frac{r_0^2}{r^2}\right) - \frac{\sigma_0}{2} \left(1 + \frac{3r_0^4}{r^4}\right) \cos 2\theta \dots\dots\dots (1.2)$$

$$\tau_{r\theta} = -\frac{\sigma_0}{2} \left(1 + \frac{2r_0^2}{r^2} - \frac{3r_0^4}{r^4}\right) \sin 2\theta \dots\dots\dots (1.3)$$

where the notation is as shown in Fig.2.

Equation (1.2) gives the hoop stress round the boundary of the hole when

$$r = r_0.$$

$$\text{Thus } \sigma_\theta = \sigma_0 (1 - 2 \cos 2\theta)$$

which has a maximum value when  $\theta = 90^\circ$ . Hence the stress concentration factor is given by  $\sigma_\theta/\sigma_0 = 3.0$  for this case.

The distribution of principal stresses along the vertical and horizontal central lines of the plate are given in Figs. 3 and 4 respectively.

Strictly, this solution is true only for a plate which is very thin relative to the hole diameter. Where these dimensions are of the same order, the stress concentration factor is somewhat greater than 3 at the mid-plane of the plate and slightly less than 3 at the surface of the plate since in this case the conditions of generalised plane stress no longer hold.

The/

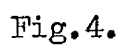


Fig. 4.

The effect of ratio of plate thickness to hole diameter was examined in 1949 by STERNBERG and SADOWSKY<sup>(9)</sup>, who found that for design purposes the stress concentration factor of 3 for a circular hole could be assumed valid for plates of arbitrary thickness ratio, as the increase in stress concentration factor at the mid plane of the plate was less than 3% and the decrease at the surface did not exceed 10%. For example, with a ratio of plate thickness to hole diameter of 0.75, the stress concentration factor at the mid plane was found to be 3.1 and at the surface 2.8.

The findings of these authors were based on an approximate three dimensional solution for the stress distribution in an infinite plate of arbitrary thickness, containing a circular hole. These conclusions support the assertion that factors of stress concentration based upon two dimensional analysis are applicable to plates of arbitrary thickness ratio.

#### I.1(a) Circular Hole

##### (ii) Finite Plate

The case of a transverse central circular hole in a plate of finite width was treated by HOWLAND<sup>(10)</sup> in 1929. The plate was assumed to be bounded by two parallel edges and under conditions of generalised plane stress.

The stress function method was adopted, using successive approximations with infinite series, the hoop stress around the hole boundary being given by

$$\sigma_{\theta} = \sigma_0 (p_0 - p_2 \cos 2\theta - p_4 \cos 4\theta \dots) \dots \dots \dots (1.4)$$

$$\text{and } \sigma_r = \tau_{r\theta} \dots \dots \dots (1.5)$$

the/

Fig. 5.

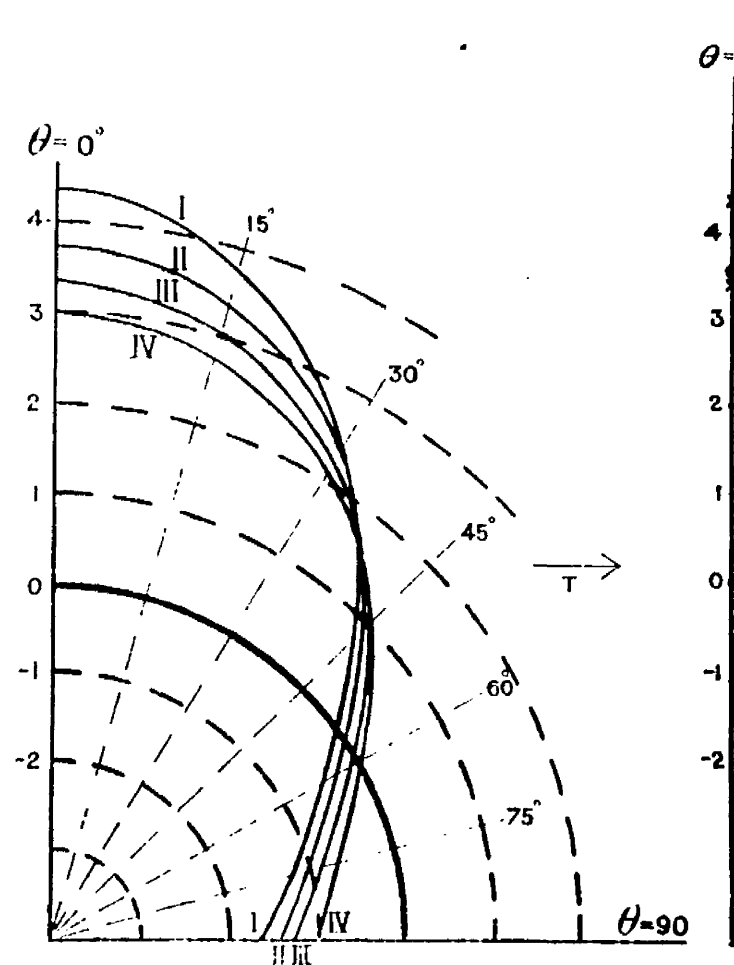
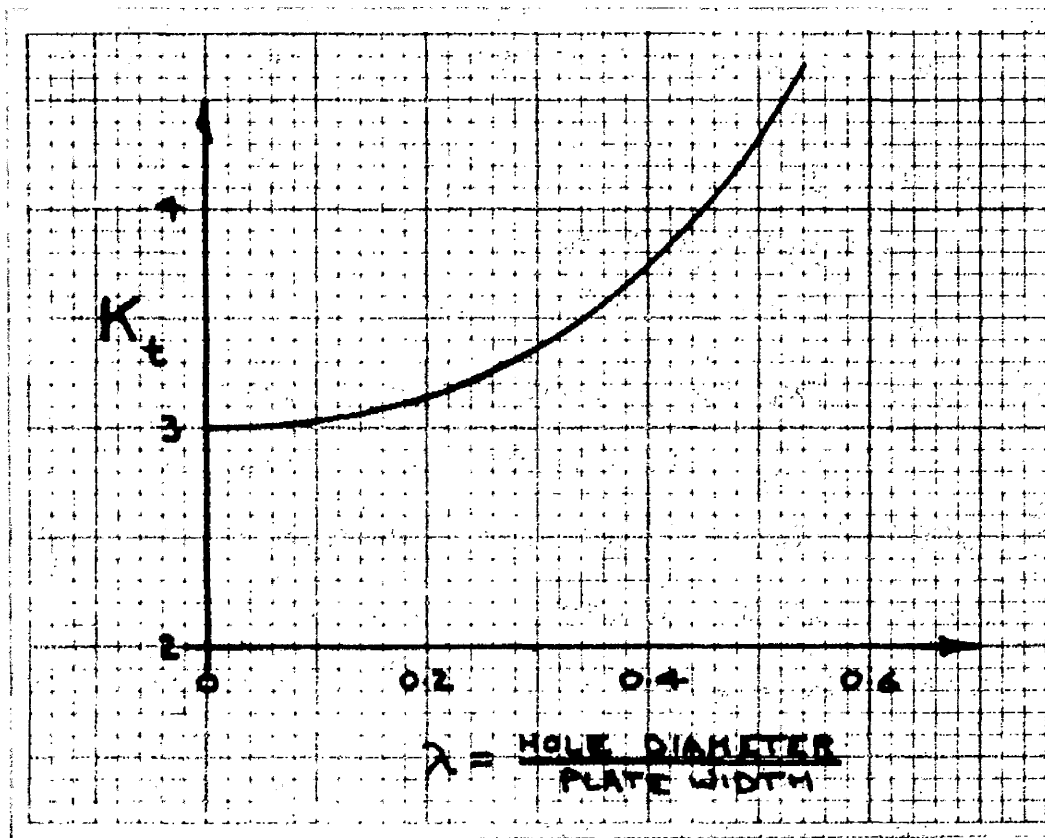


Fig. 6.



the notation being as given in Fig. 2, and  $p_0$ ,  $p_2$ , etc. vary with the ratio of hole diameter/plate width as follows:-

$$\begin{array}{ccccc} 0 & \longrightarrow & \lambda & \longrightarrow & 0.5 \\ 1.0 & \longrightarrow & p_0 & \longrightarrow & 1.06 \\ 2.0 & \longrightarrow & p_2 & \longrightarrow & 2.91 \end{array}$$

Hence as  $\lambda$  increases,  $\sigma_\theta$  increases as shown in Fig. 5.

For  $\lambda = 0$ , equation (1.4) reduces to KIRSCH'S solution for an infinite plate, namely  $\sigma_\theta = \sigma_0(1 - 2 \cos 2\theta)$ .

A graph of the variation of stress concentration factor based on the gross cross section of the plate is shown in Fig. 6, which indicates the field of application of stress concentration factors derived on the assumption of a plate being of infinite width.

In 1950, SJOSTROM<sup>(11)</sup> presented the solution for the case of a finite plate in tension, containing an eccentrically located hole, the results as summarised by PETERSON, being shown in Fig. 7.

### I.1(a) Circular Hole

#### (iii) Semi-Infinite Plate

A paper by MINDLIN<sup>(12)</sup> in 1948 gave the stress distribution produced by a circular hole located near one edge of a plate in tension, the other edge being at infinity, this set of conditions being regarded as a semi-infinite plate. Plane stress conditions were assumed and the solution was obtained by the Stress Function Method, a conformal transformation being employed to obtain the curvilinear co-ordinate system used in the analysis.

The stress variation along the straight edge of the plate near the /

Fig.7.

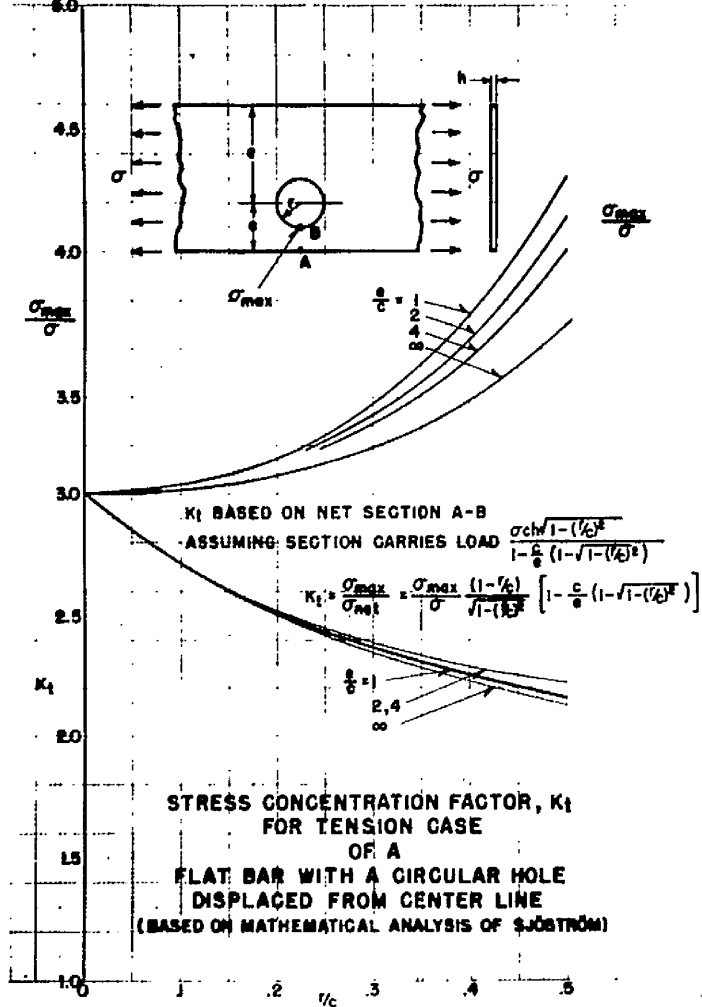
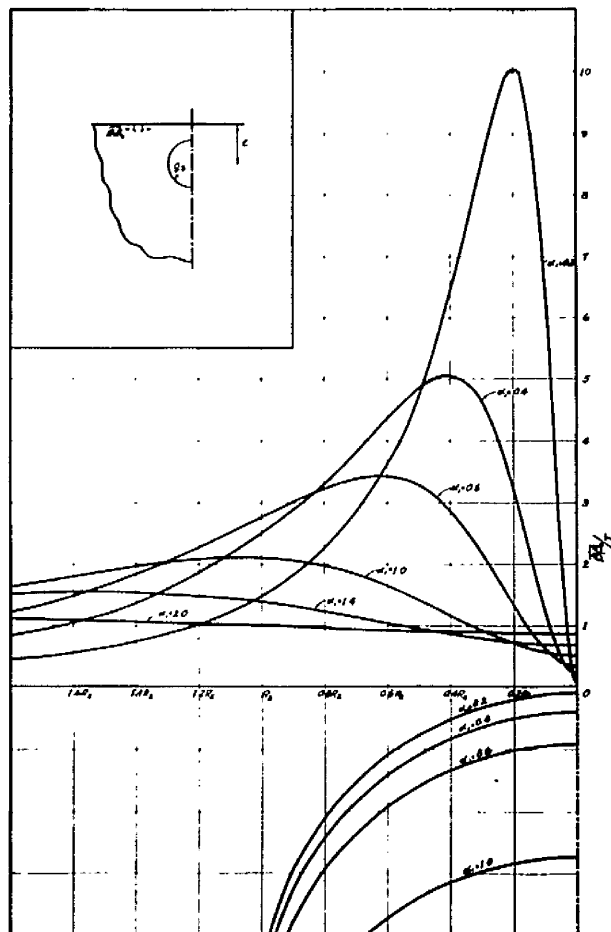


Fig.8.



Variation of stress along the straight edge (from mathematical solution).

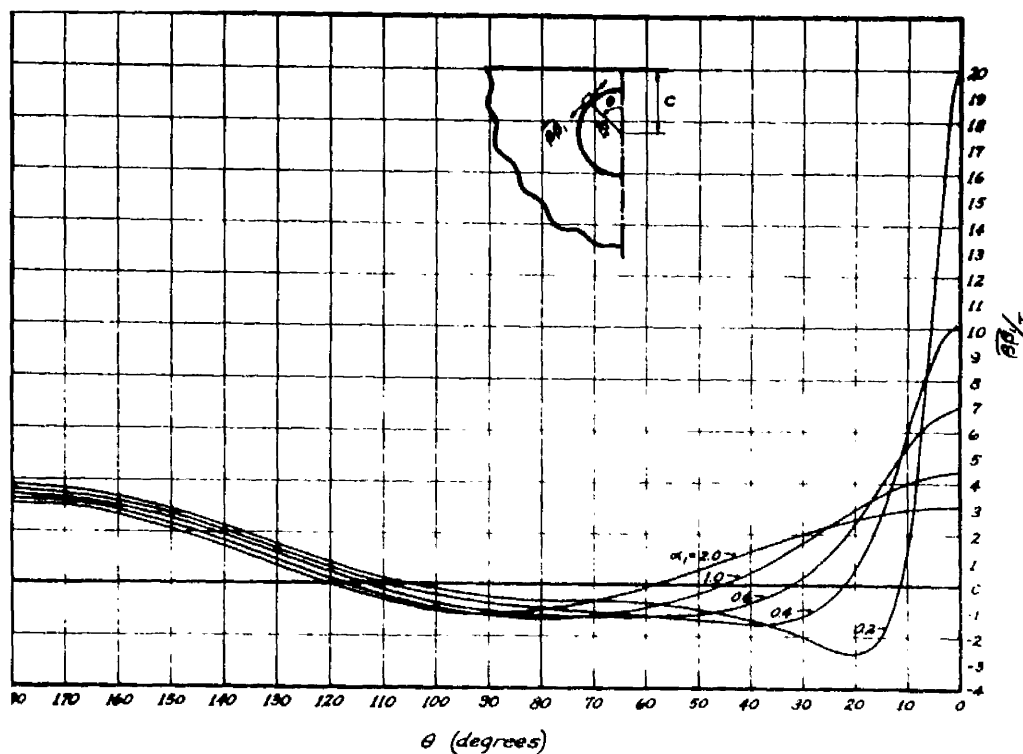


Fig. 9.

Variation of stress along the edge of the hole (from mathematical solution).

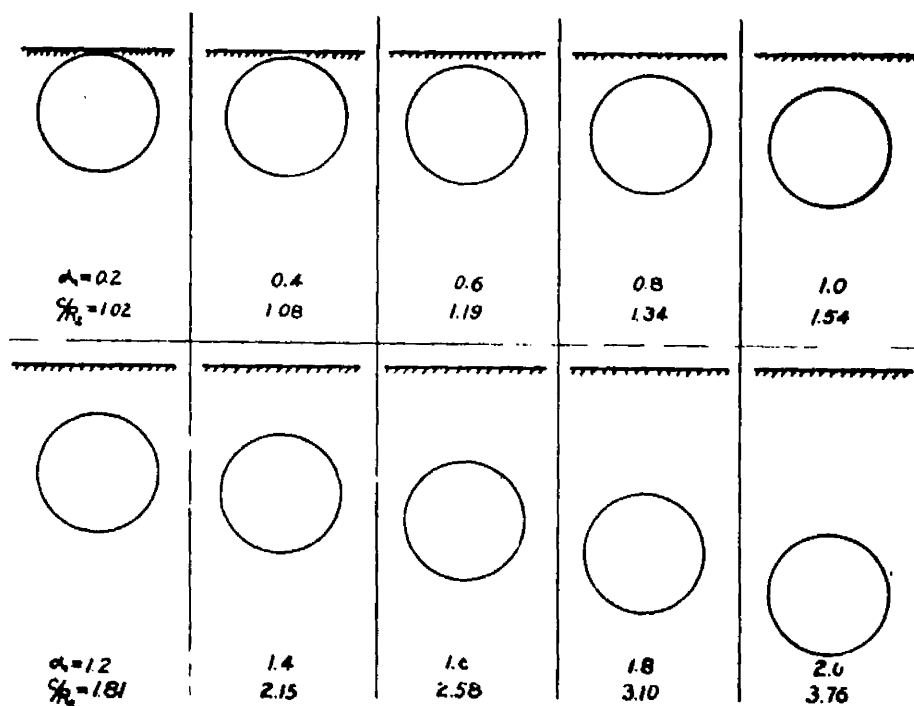


Fig. 10.

Proximity of hole to edge of plate for values of  $\alpha_1$  (and the corresponding values of  $c/R_2$ ) selected for computation.

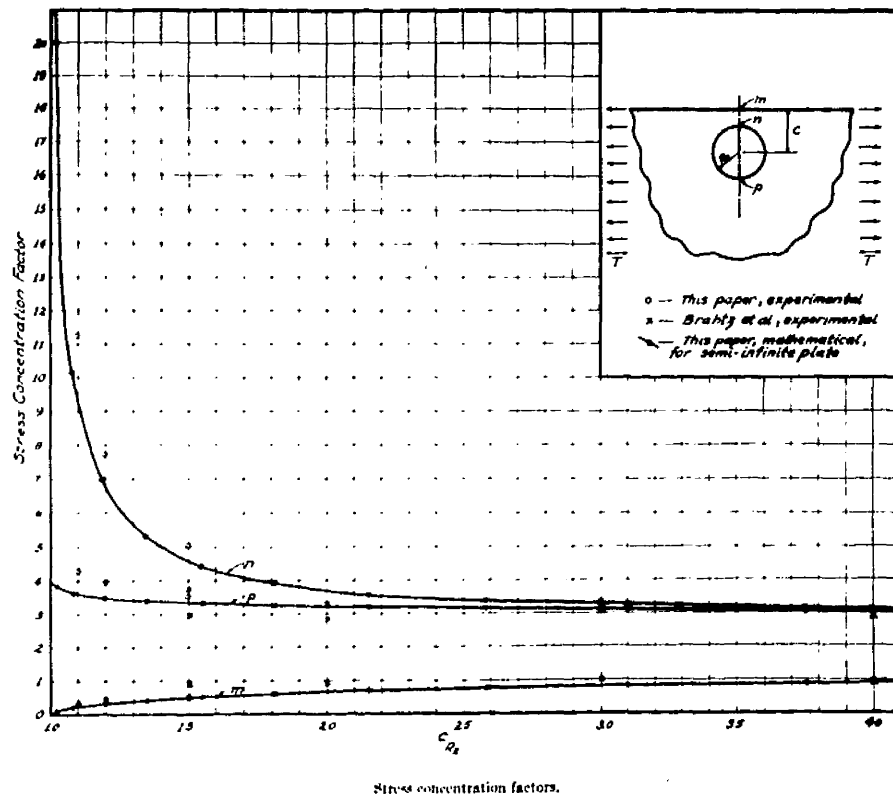


Fig.11.

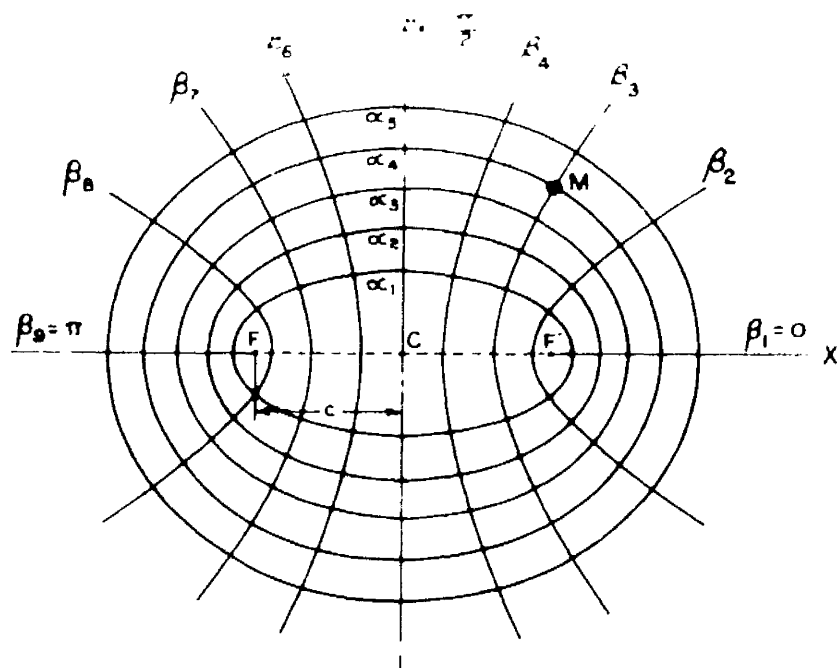


the hole, also the hoop stress variation round the hole are shown in Figs. 8 and 9 respectively, corresponding to various values of the parameter  $\alpha_1$ . The relation between this parameter and the proximity of the hole to the edge of the plate is shown in Fig. 10.

From Fig. 8 it is evident that as the thickness of the section between the hole and the free edge of the plate decreases, the stress at the section of symmetry on the face edge tends to zero. This effect has been substantiated by photoelastic tests.

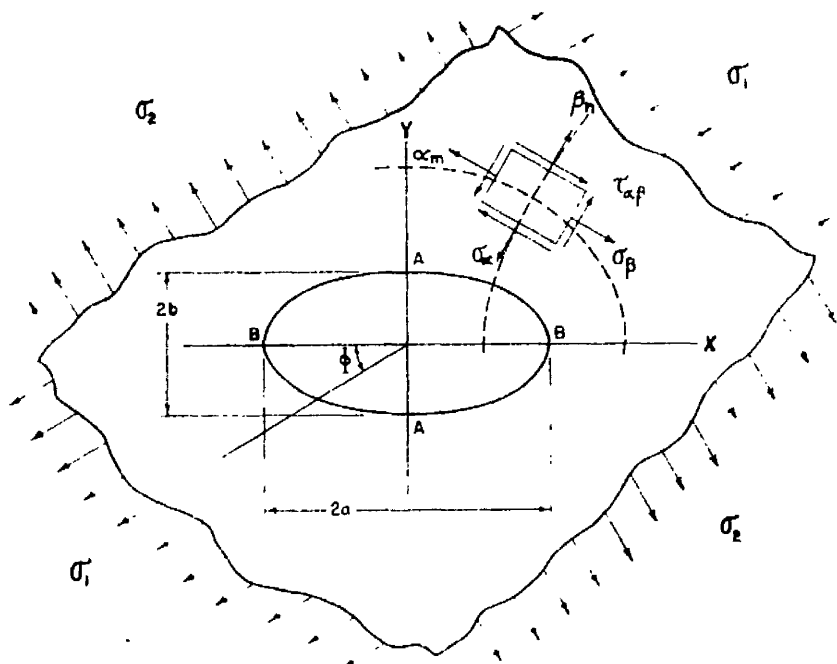
Referring to Fig. 11, the stress concentration factors based on the gross section at points p, m and n are shown for various values of  $C/R_2$ . The special case corresponding to the SJÖSTRÖM solution is in agreement. This graph clearly shows that for  $C/R_2 \geq 4$ , the plate containing the eccentric circular hole can be regarded as infinite for design purposes.

Fig. 12a.



Elliptical Coordinates. Point  $M$  is defined by  $(\alpha_4, \beta_3)$

Fig. 12b.



Stresses Around an Elliptical Hole in a Plate Subjected to Two Perpendicular Uniformly Distributed Loads

I.1(b) Elliptical Hole in Infinite Plate

The solution of the problem of a wide plate containing a centrally located elliptical hole was given by KOLOSOFF<sup>(15)</sup> in 1909, using for the first time in this work the theory of Complex Variables. His methods were later extended by INGLIS<sup>(14)</sup>, COKER and FILON<sup>(15)</sup>, and POSCHL<sup>(16)</sup>. The method examined the stresses acting on the surface of an element which was defined by curvilinear co-ordinates. Since the stress components were stated in terms of infinite series, very lengthy expressions were produced. The combined works of the above authors cover completely the stress analysis for tension plates containing an elliptical hole, under uni-axial or bi-axial tensions applied at an angle to the major axis of the ellipse. DURELLI and MURRAY<sup>(17)</sup> have supplied a useful summary of these works, a brief resume of which is now given.

$$\sigma_{\theta} = \frac{(\sigma_0 + \sigma_p) \sinh 2\alpha_0 + (\sigma_0 - \sigma_p) [\cos 2\phi - e^{2\alpha_0} \cos 2(\phi - \beta)]}{\cosh 2\alpha_0 - \cos 2\beta} \dots (1.6)$$

when  $\sigma_r = \tau_{r\theta} = 0$ , the notation being shown in Fig. 12, and

$\alpha_0$  = the elliptical parameter defining the hole boundary

$\phi$  = the angle between the major axis  $2a$  of the ellipse and the direction of  $\sigma_0$ .

When the directions of  $\sigma_0$  and  $\sigma_p$  coincide with the axes of  $2b$  and  $2a$  respectively,  $\phi = \frac{\pi}{2}$  and equation (1.6) reduces to

$$\sigma_{\theta} = \frac{(\sigma_0 + \sigma_p) \sinh 2\alpha_0 + (\sigma_0 - \sigma_p)(e^{2\alpha_0} \cos 2\beta - 1)}{\cosh 2\alpha_0 - \cos 2\beta} \dots (1.7)$$

and for the case of uni-axial tension when say  $\sigma_p = 0$ ,

equation/

equation (1.7) becomes

$$\sigma_{\theta} = \sigma_0 \left[ \frac{\sinh 2\alpha_0 + e^{2\alpha_0} \cos 2\beta - 1}{\cosh 2\alpha_0 - \cos 2\beta} \right] \dots\dots\dots (1.8)$$

This has a maximum value when  $\beta = 0$  or  $\pi$ , corresponding to points A at each end of the major axis of the elliptic hole, giving the maximum hoop stress as

$$\sigma_A = \sigma_0 \left[ \frac{\sinh 2\alpha_0 + e^{2\alpha_0} - 1}{\cosh 2\alpha_0 - 1} \right] \dots\dots\dots (1.9)$$

Using the relationships  $e^{2\alpha_0} = \sinh 2\alpha_0 + \cosh 2\alpha_0$

$$\text{and } \frac{\sinh 2\alpha_0}{\cosh 2\alpha_0 - 1} = \coth \alpha_0$$

the maximum hoop stress can be shown to be

$$\sigma_A = \sigma_0 \left( 1 + \frac{2a}{b} \right) \dots\dots\dots (1.10)$$

$$\text{or Stress Concentration Factor } \frac{\sigma_A}{\sigma_0} = 1 + \frac{2a}{b} \dots\dots\dots (1.11)$$

In a similar manner, the hoop stress at the ends B of the minor axis of the elliptic hole is determined using  $\beta = \frac{\pi}{2}$  in equation (1.8), giving  $\sigma_B = -\sigma_0$  at points B, or

$$\text{Stress Concentration Factor } \frac{\sigma_B}{\sigma_0} = -1.0 \dots\dots\dots (1.12)$$

For  $\sigma_0 = 0$ ,  $\sigma_p$  becomes the uni-axial tension.

Putting  $\beta = 0$  or  $\pi$  gives the hoop stress at the end of the major axis as  $\sigma_A = -\sigma$  and with  $\beta = \pm \frac{\pi}{2}$

the hoop stress at the ends of the minor axis becomes

$$\sigma_B = \sigma \left( 1 + \frac{2b}{a} \right) \dots\dots\dots (1.13)$$

These/

Fig.13.

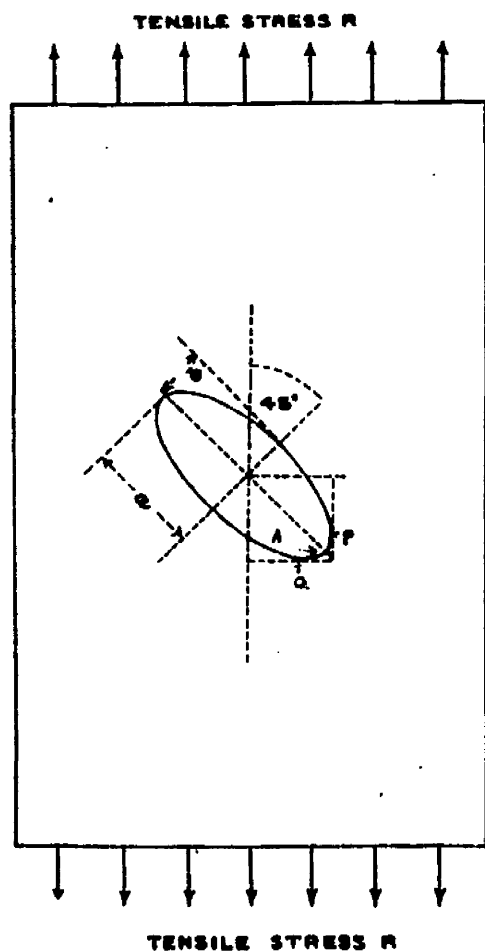
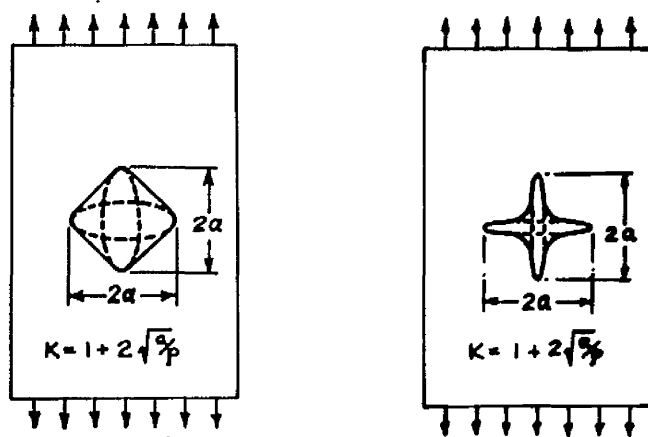


Fig.14.



These results apply for cases of uni-axial tension normal and parallel to the major axis respectively. For any combination of bi-axial tensions  $\sigma_o$  and  $\sigma_p$  parallel to the respective axis, the hoop stress at points A and B is given using the principle of superposition,

$$\text{by } \sigma_A = \sigma_o \left(1 + \frac{2a}{b}\right) - \sigma_p \dots\dots\dots(1.14)$$

$$\text{and } \sigma_B = \sigma_p \left(1 + \frac{2b}{a}\right) - \sigma_o \dots\dots\dots(1.15)$$

These two equations are usually attributed to INGLIS<sup>(14)</sup>. It is of interest to note the special case that for constant or uniform hoop round the boundary of the elliptical hole, then  $\frac{\sigma_o}{\sigma_p} = \frac{b}{a}$ , this relationship being obtained by equating (1.14) and (1.15).

Referring to equation (1.8) for uni-axial tension  $\sigma_o$  applied at angle  $\phi$  to the major axis of the ellipse, INGLIS showed that for  $\phi = \pi/4$  (that is with the axis of the ellipse inclined at  $45^\circ$  to the axis of tension), the point of maximum hoop stress lies between points A and F as shown in Fig. 13. If the ratio  $b/a$  is fairly small a good approximation to this maximum stress value is given by

$$\sigma = \sigma_o \frac{a}{2b} \left[ 1 + \frac{\sqrt{2a^2 + 2b^2}}{a - b} \right] \dots\dots\dots(1.16)$$

and the stresses at A, P and Q are given respectively by

$$\sigma_A = \sigma_o \cdot \frac{a}{b} \quad ; \quad \sigma_P = \sigma_o \left(1 + \frac{a}{b} + \frac{b}{a}\right) \quad ; \quad \sigma_Q = -\sigma_o$$

The relationship between the semi-axes  $a$  and  $b$  of the ellipse and the radius of curvature  $\rho$  at the ends of the major axes is given by  $b = \sqrt{a\rho}$

Hence/

Fig.15.

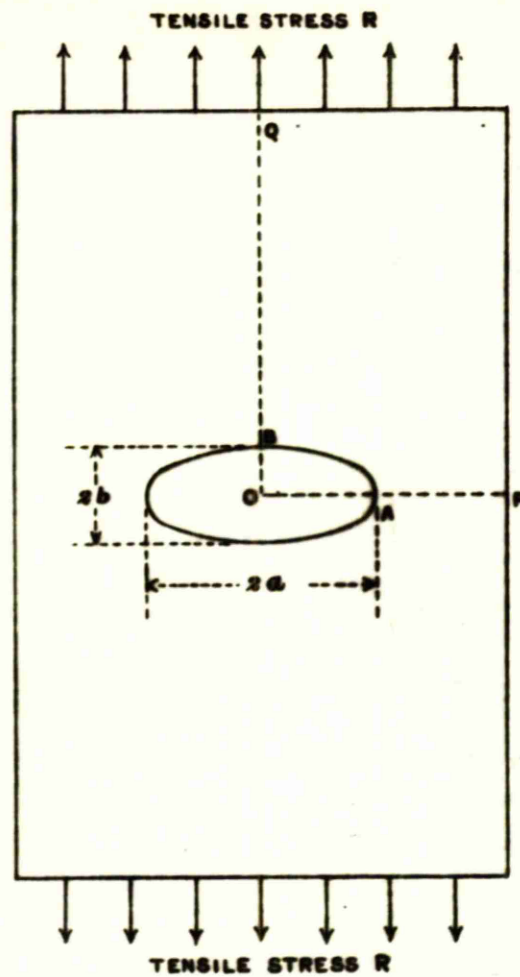
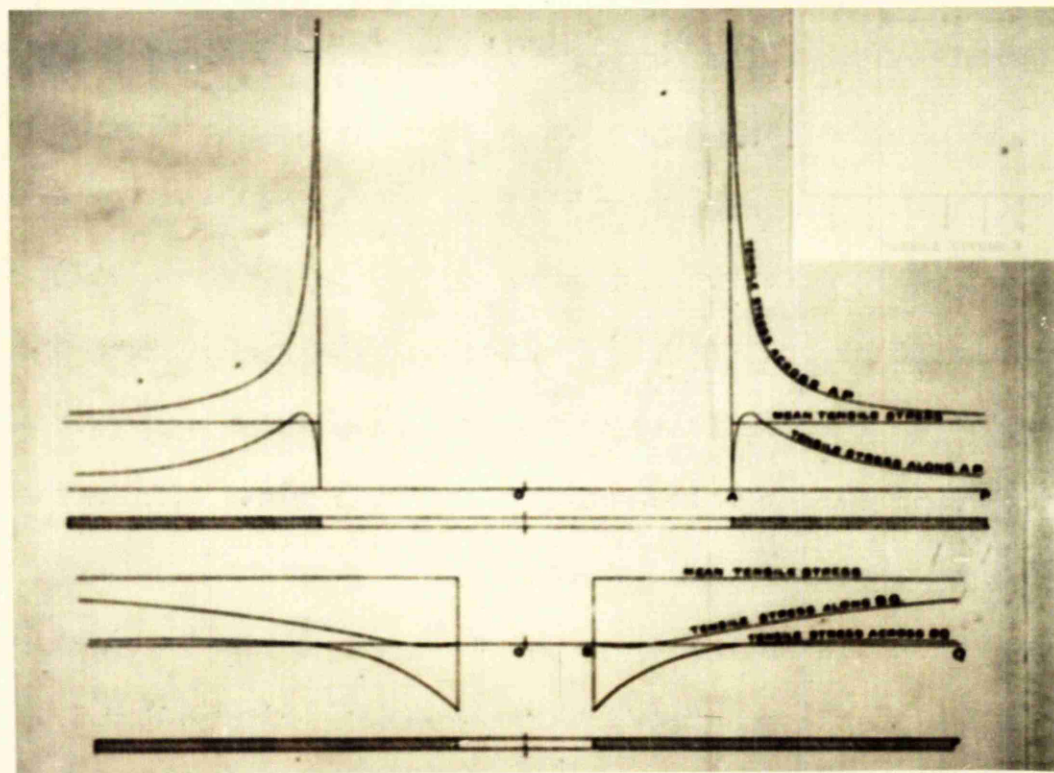


Fig.16.



Hence equations (1.10) and (1.16) may be reduced to

$$\sigma_A = \sigma_0 (1 + 2 \sqrt{a/\rho}) \dots\dots\dots(1.17)$$

$$\sigma = \frac{\sigma_0}{2} \sqrt{\frac{a}{\rho}} \left( 1 + \frac{\sqrt{2a + 2\rho}}{\sqrt{a} - \sqrt{\rho}} \right) \dots\dots\dots(1.18)$$

The first of these equations gives the maximum hoop stress on the boundary of an elliptical hole in a thin plate under uni-axial (or simple) tension, the major axis normal to the applied tension, and the second for the major axis at 45° to the applied tension. From these equations, INGLIS determined approximate solutions for the maximum stress concentration factor produced by internal discontinuities of square and star forms in wide plates in simple tension. The  $a$  and  $\rho$  values used were respectively the length of the major axis of the equivalent ellipse and the corner radius, as in Fig. 14. At that time, INGLIS' solution was the only treatment available for these forms of discontinuity. The complete stress distributions along the horizontal and vertical axes for a plate in simple tension containing an elliptical hole, are given in Figs. 15 and 16 respectively.

An interesting extension to INGLIS' work on elliptical forms was published by DONNELL<sup>(18)</sup> in 1941. This paper gives the stress distribution in an infinite plate, under uniform edge stress, containing an elliptical region filled with a material whose stiffness is  $K$  times that of the plate. Thus as  $K$  increases from zero through unity to infinity, the discontinuity takes the form of a hole, part of the homogenous plate, and finally a very stiff reinforcement.

For a plate of varying thickness, this theory gives a reasonable indication/



indication of the general effect produced by a change in section if  $K$  is taken as the ratio of thickness - times - modulus inside to thickness - times - modulus outside the region. The theoretical approach to this case was a generalisation of INGLIS' work, and for the particular case of a tensile load, the stresses at the boundary of the discontinuity are given as:-

$$\beta = 0, \quad \sigma_r = 3K(1 - K)(r^2 - r)N \dots\dots\dots(1.19)$$

$$\sigma_\theta = [(8 + 2K - K^2)r^2 + (4 + 13K + K^2)r + 9K]N \dots\dots\dots(1.20)$$

$$\beta = \frac{\pi}{2}, \quad \sigma_r = 3K[3(K + r^2) + (1 + 5K)r]N \dots\dots\dots(1.21)$$

$$\sigma_\theta = -(1 - K)[3K + (4 + 5K)r]N \dots\dots\dots(1.22)$$

$$\text{where } N = \frac{\sigma_0}{9K(r^2 + 1) + 2(2 - K - 8K^2)r}$$

$$r = \frac{a}{b}$$

$\beta$  = eccentric angle of the ellipse as defined in Fig. 12.

and  $\sigma_0$  = the applied tension, parallel to the axis  $2b$  of the ellipse.

This solution agrees with INGLIS' solution for an elliptical hole, when  $K \neq 0$  giving

$$\beta = 0, \quad \sigma_r = 0, \quad \sigma_\theta = (1 + 2r)\sigma_0$$

$$\beta = \frac{\pi}{2}, \quad \sigma_r = 0, \quad \sigma_\theta = -\sigma_0$$

When  $K = 1$ , the discontinuity in the plate disappears

$$\text{and } \beta = 0, \quad \sigma_r = 0, \quad \sigma_\theta = \sigma_0$$

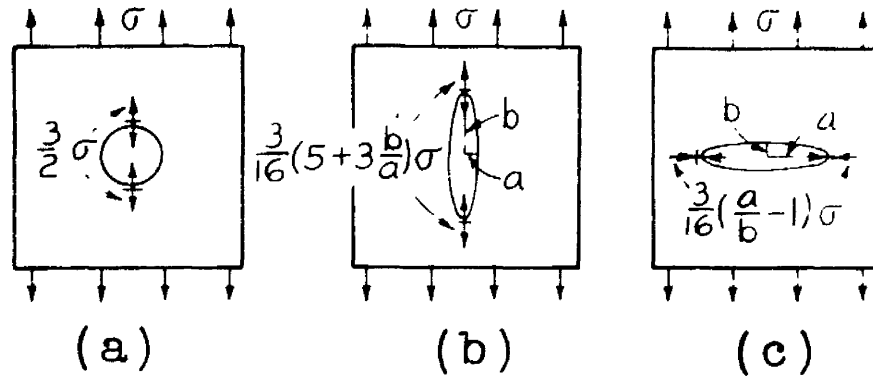
$$\beta = \frac{\pi}{2}, \quad \sigma_r = \sigma_0, \quad \sigma_\theta = 0$$

For  $K = \infty$ , representing a very stiff reinforcement,  $\sigma_r$  is always the critical value as  $\sigma_\theta = \frac{1}{3} \sigma_r$

$$\text{and } \beta = 0, \quad \sigma_r = \frac{3}{16}(1 - \frac{a}{b})\sigma_0 \dots\dots\dots(1.23)$$

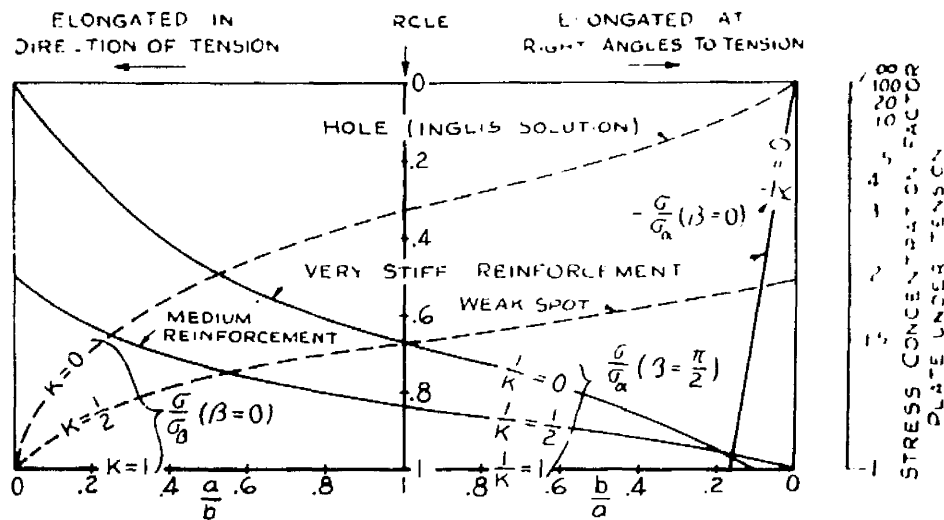
$$\beta = \frac{\pi}{2}, \quad \sigma_r = \frac{3}{16}(5 + \frac{3b}{a})\sigma_0 \dots\dots\dots(1.24)$$

Fig.17.



Stress concentra-  
tions due to very stiff  
reinforcements.

Fig.18.



Summary of critical stress concentrations  
due to elliptical discontinuities.



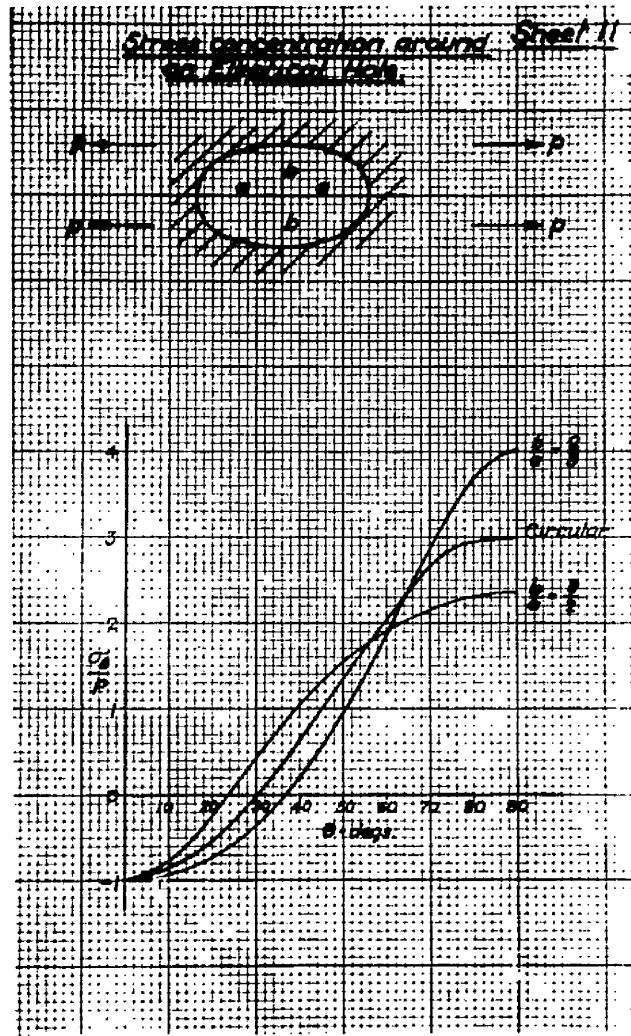


Fig.19.

The conditions corresponding to equations (1.23) and (1.24) respectively are shown in Figs. 17c and 17b and for the case of a circular hole in Fig. 17a.

A summary of critical stress concentrations is given graphically in Fig. 18, where only stresses which may be critical under certain conditions are shown.

The problem of an elliptical hole in an infinite plate in simple tension, at an angle and alternatively under bi-axial tension, has also been investigated by MUSKHELISHVILI<sup>(19)</sup> and STEVENSON<sup>(1)</sup> both of whom used the complex potential form of solution.

SAVIN<sup>(4)</sup>, in an extension of the work of MUSKHELISHVILI, referring to the case of simple tension, investigated the variation in stress concentration factor with the orientation of the ellipse, the results being shown in Fig. 19.

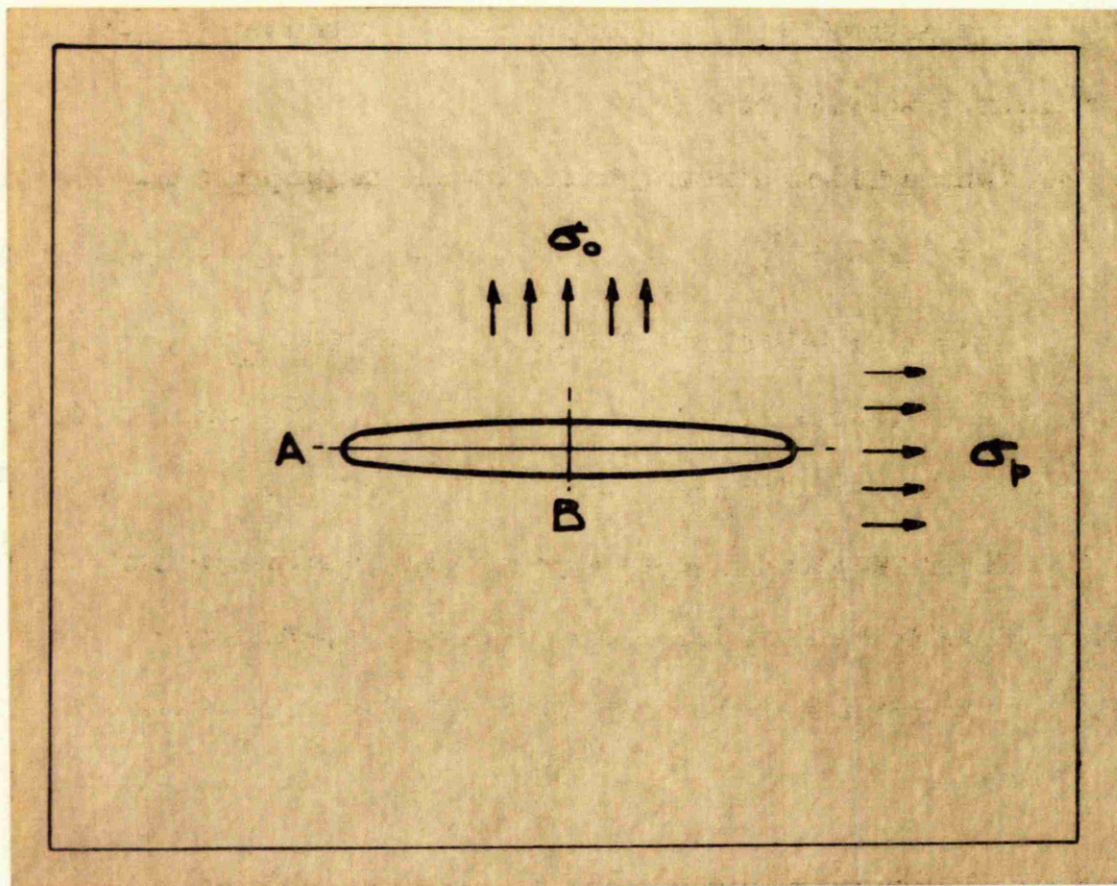


Fig. 20.

I.1(c) Internal Crack in Infinite Plate.

The internal crack in an infinite plate under simple tension was considered also by INGLIS (1913)<sup>(14)</sup>, using the Airy stress function method, the crack being considered as the limiting form of an elliptical hole, the minor axis of which tends to zero. Plane strain conditions were assumed and the hoop stresses produced at the ends of the major axis (Fig. 20) are

(i) for the applied stress normal to the major axis  $2a$

$$\sigma_A = \sigma_0 \left(1 + \frac{2a}{b}\right) \dots\dots\dots (1.25)$$

Thus with an  $\frac{a}{b}$  ratio of 1000,  $\sigma_A = 2001 \sigma_0$  and the ellipse would appear as a fine straight crack. Hence a very small pull across the crack would set up stresses at the ends, sufficient to tear the material. The increase in length due to the tear would increase the stress still further and rapid crack propagation would result.

(ii) for the applied stress parallel to the major axis

$$\sigma_A = -\sigma, \quad \sigma_B = \sigma \left(1 + \frac{2b}{a}\right) \dots\dots\dots (1.26)$$

Thus with an  $\frac{a}{b}$  ratio of 1000,  $\sigma_B = 1.002 \sigma$  and hence a crack running in the direction of the applied tension would not produce a great local stress effect.

GRIFFITH<sup>(20)</sup> in 1920, employing INGLIS' solution of the two-dimensional equations of elastic equilibrium in the space bounded by two concentric ellipses, determined the effect of the presence of a crack on the energy of an elastic body under the influence of a tensile stress.

From this analysis were presented criteria of rupture for cases of plane stress and plane strain in the form of critical values of applied stress./

It has been shown, however, by SNEDDON<sup>(21)</sup>, that in general these criteria do not apply, since the high concentrations of stress at the ends of a crack will induce local plastic flow, thus departing from the elastic conditions assumed by GRIFFITH.

A numerically different criterion was developed in 1934 by OROWAN<sup>(22)</sup> from assumptions similar to those employed by GRIFFITH.

WESTERGAARD<sup>(23)</sup> in 1934 produced a rather lengthy solution for the crack problem using stress functions in terms of infinite series.

In a later paper, WESTERGAARD<sup>(24)</sup> gave solutions for stress distribution as influenced by bearing pressures and cracks, under various conditions, and in this work the Airy stress function was represented by functions of a complex variable, assuming plane strain conditions to apply. In all cases, the shear stress along the axis of propagation was zero. Stress functions are given for an internal crack in an infinite plate under uni-axial tension, also for an internal crack subjected to liquid pressure, this latter case being equivalent to equal bi-axial tensions.

The GRIFFITH theory of rupture was extended in 1946 by SACK<sup>(25)</sup> to include three-dimensional problems, by considering the conditions for rupture in the case of a disc-shaped crack when one of the principal stresses acts normal to the plane of the crack, thus leading to another criterion for crack propagation.

In the same year SNEDDON<sup>(20)</sup>, using WESTERGAARD'S stress function, derived equations for the stress distribution in the interior of an infinite 'two-dimensional' elastic medium, produced by the opening of an internal crack subject to uniform hydrostatic pressure. This analysis/



Fig. 21.

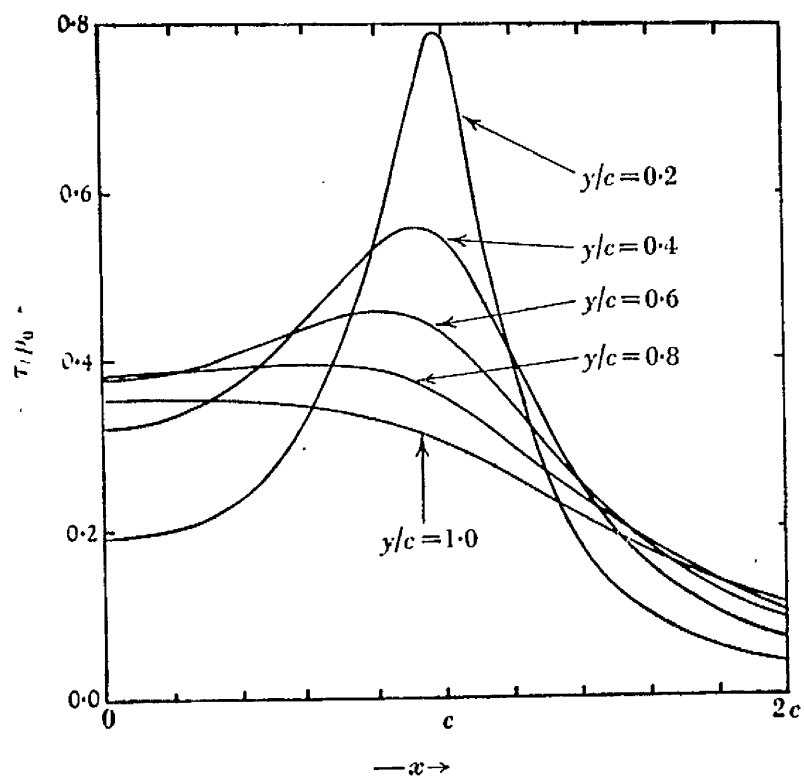
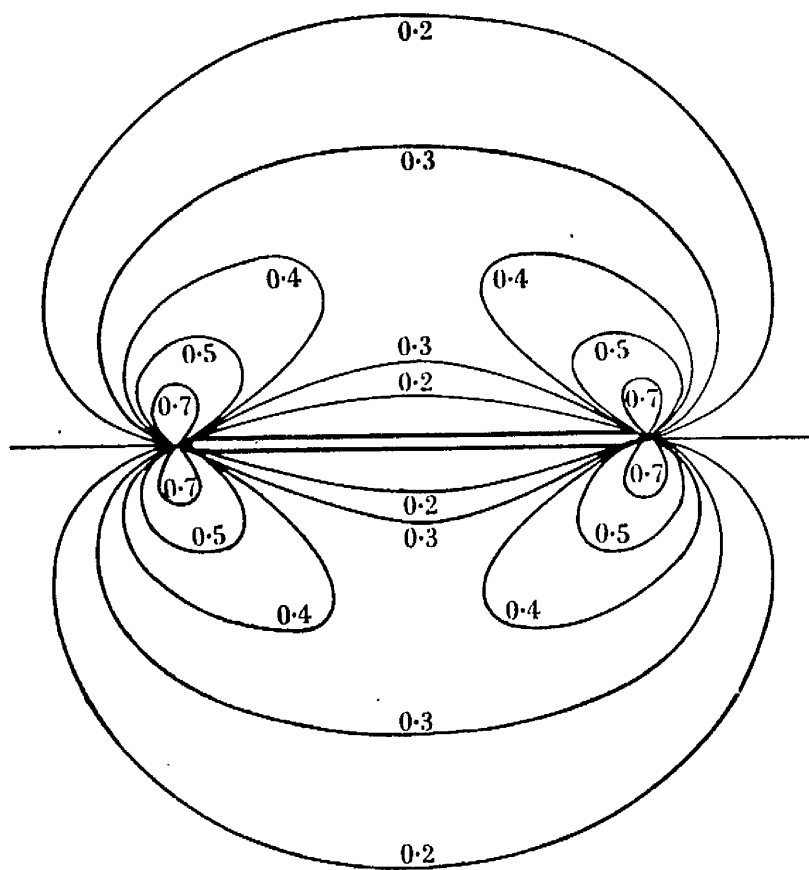


Fig. 22.





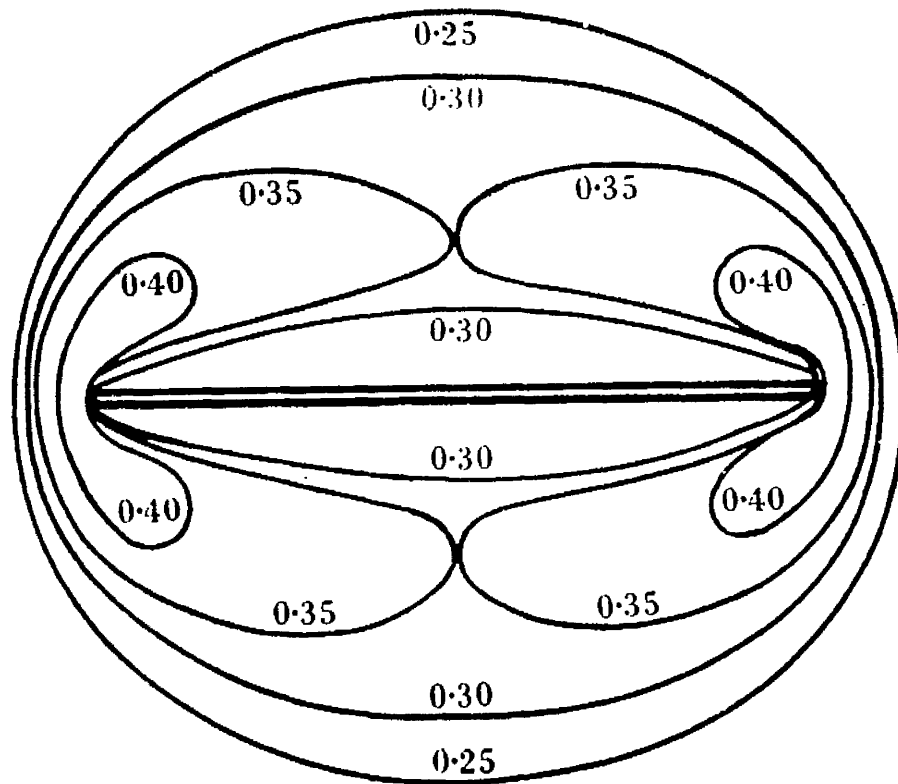


Fig. 23.

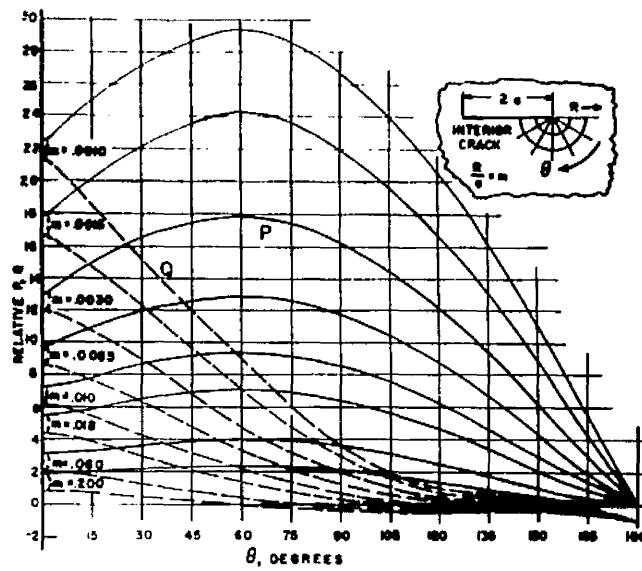
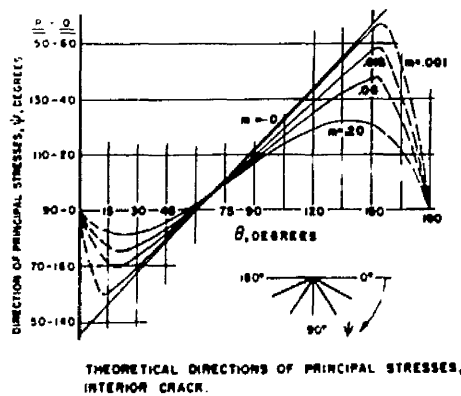


Fig. 24.



analysis is more simple than INGLIS' and employs Cartesian co-ordinates throughout. The principal shear stress distribution graph is illustrated in Fig. 21, and from this the isochromatics of Fig. 22 were constructed. The GRIFFITH criterion for rupture in the case of a stress free crack in a body under the influence of a uniform tensile stress is given as an extension to the first solution. The disc-shaped crack is also considered by SNEDDON, the crack surface being subjected to uniform hydrostatic pressure. It is shown that the crack, assumed to be initially a thin disc-shaped cavity, takes the form of a flat ellipsoid of revolution under the action of hydrostatic pressure. The isochromatic lines for this case are shown in Fig. 23.

For stresses due to straight, narrow cracks spreading at high velocities in a uniform tensile field under plane strain conditions, YOFFE<sup>(26)</sup> in 1951, employed stress wave equations, and assumed that the crack while not itself extending, moved across the material in a direction normal to the maximum tensile stress. The stresses thus computed are dependent on the wave velocity. Thus for zero velocity, these equations agree exactly with those of INGLIS.

In 1954, POST<sup>(27)</sup> adjusted the plane strain solutions of INGLIS, WESTERGAARD and YOFFE for the case of a crack in an infinite plate under simple tension, to represent the conditions of generalised plane stress encountered in thin walled members, and computed values for the stress system, as shown in Fig. 24.

The solution for the class of plane problems in elasticity corresponding to a distribution of radial cracks, equal and finite in length/

Fig. 25.

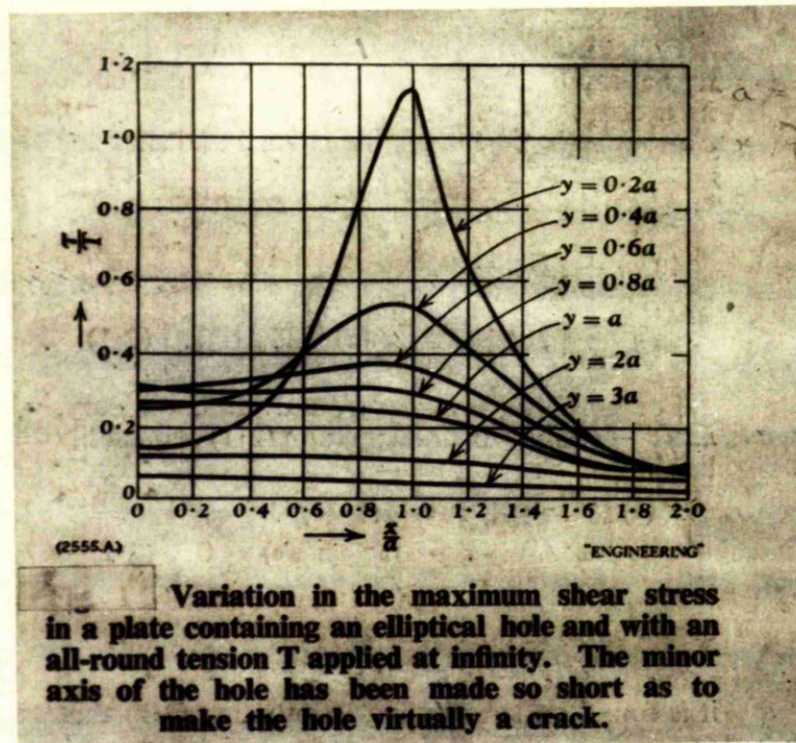
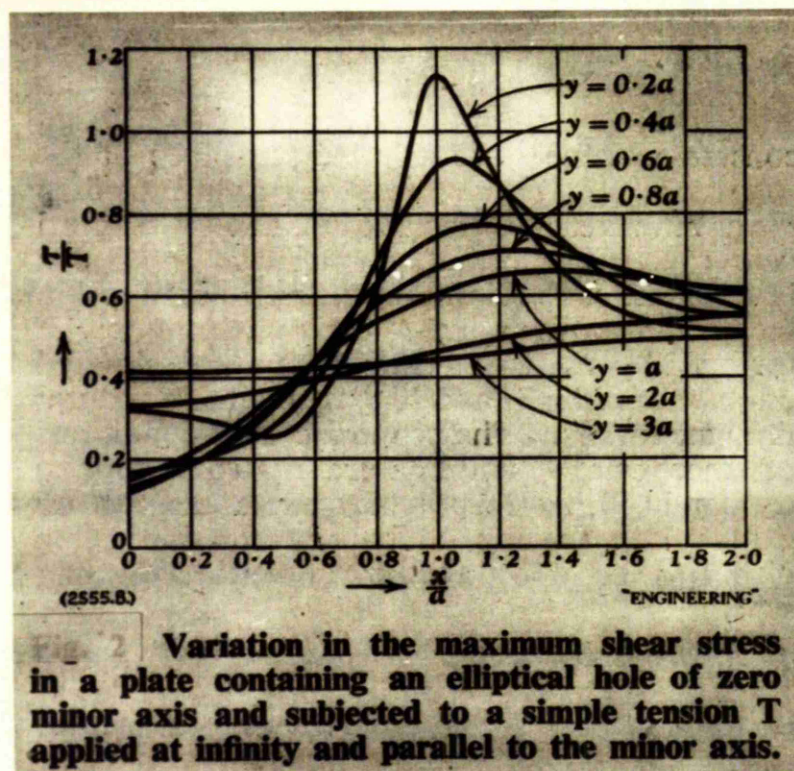


Fig. 26.

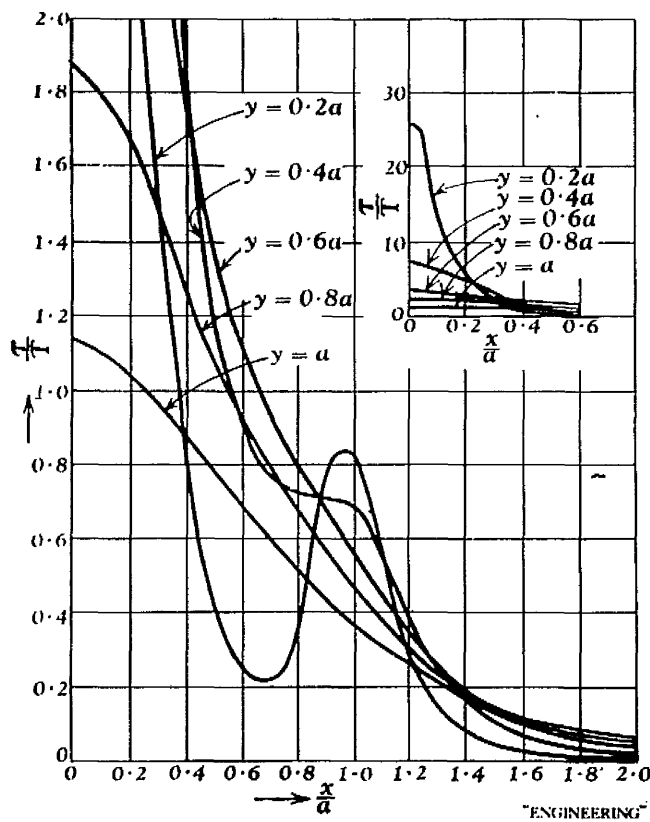


length, originating at the boundary of a circular hole in an infinite plate, has been given by BOWIE<sup>(28)</sup>. The complex variable method of MUSKHELISHVILI is employed and depends upon the representation of the Airy stress function in terms of two analytical functions of a complex variable. Criteria for rupture based on the GRIFFITH hypothesis are formulated, and numerical results obtained for the cases of a single crack and two cracks. It is shown that one solution is consistent with the well-known result that a single crack in an infinite plate is unaffected by tension in the direction of the crack. For cracks longer than the hole radius, it is shown that the effect of the stress field caused by the hole is negligible so far as the critical load for rupture is concerned. On the other hand, it is stated that for very small crack lengths, the critical load appears to be governed primarily by the local stress field of the hole.

In 1950, COX<sup>(2)</sup> investigated the effect of hair cracks on the stress concentration produced by an internal elliptical hole. The analysis was restricted to the elliptical form since stress concentrations due to certain forms of holes quite different from elliptical do not differ considerably from the stress concentration due to 'equivalent elliptical' holes. The general method of solution is similar to that of INGLIS, but the analysis is more direct and more elegant, by the use of complex variables. The conclusion is reached that the presence of small hair cracks on the boundary of a hole, reduces the stress concentration factor, and renders it less sensitive to changes in the ratio  $a/\rho$ , in comparison with the approximate formula  $K = 1 + 2 \sqrt{a/\rho}$ .

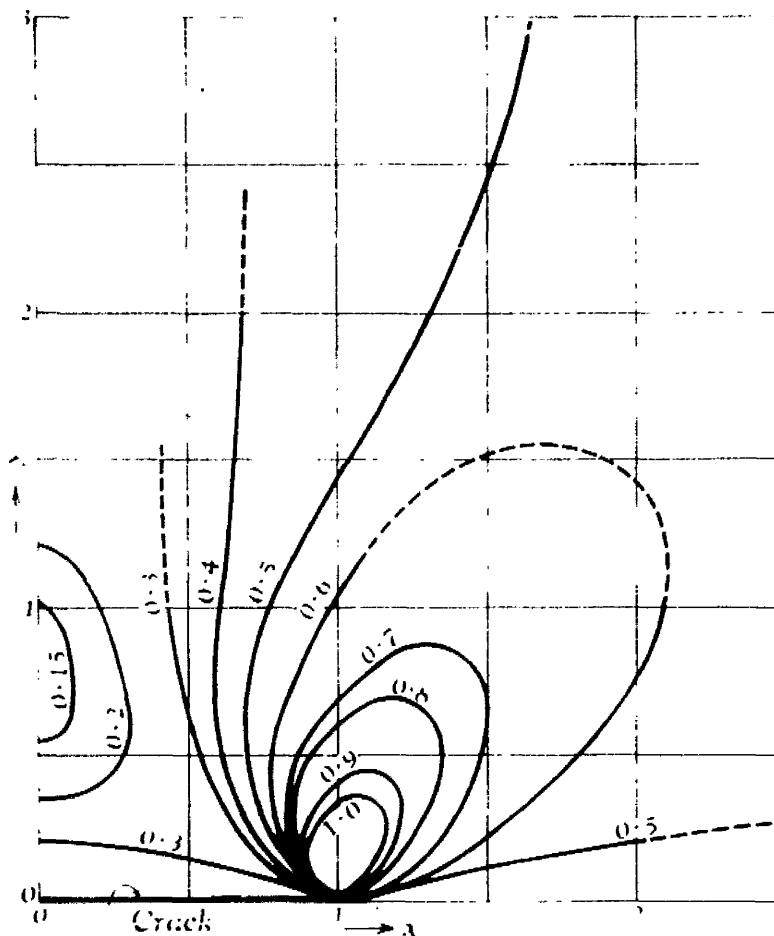
Using the complex potential method, ROTHMAN and ROSS<sup>(29)</sup> in 1955 reproduced/

Fig.27.



Variation in the maximum shear stress in a plate containing an elliptical hole of zero minor axis and with diametrically opposite forces applied at the ends of the minor axis. This state is comparable with a wedge being driven into the hole or crack.

Fig.28.



reproduced SNEDDON'S equations for an interior crack subject to uniform pressure on its boundary. The cases of all round tension, simple tension and diametrically opposite forces applied to the 'minor axis' of the crack, were analysed also. Graphs, similar to those of SNEDDON, were used to illustrate the variation in maximum shear stress, and from these the isochromatic lines were constructed for the simple tension case, as shown in Figs. 25, 26, 27 and 28.

It may be noted, referring to Figs. 22 and 28 that all the isochromatics pass through the end of the crack, showing that the principal shear stress is infinite.

Thus, even for small loads, plastic flow must occur at the ends of the crack to relieve this infinite stress. Therefore, there is no purely 'elastic' solution of the problem. If however, the applied tension is not too great, the region of plastic flow will be small and will not appreciably affect the distribution of stress at points in the material at a distance from the ends of the crack.



I.1(d) Miscellaneous Internal Discontinuities

It has been shown by INGLIS<sup>(14)</sup> in his paper on the elliptical hole in an infinite plate that

- (i) the stresses at the ends of a discontinuity depend almost entirely on its length and on the form of the ends.
- (ii) if the ends of a discontinuity are approximately elliptical in form, it is legitimate, in calculating the stresses at these points, to replace the discontinuity by an 'equivalent ellipse' having the same overall length and end formation.

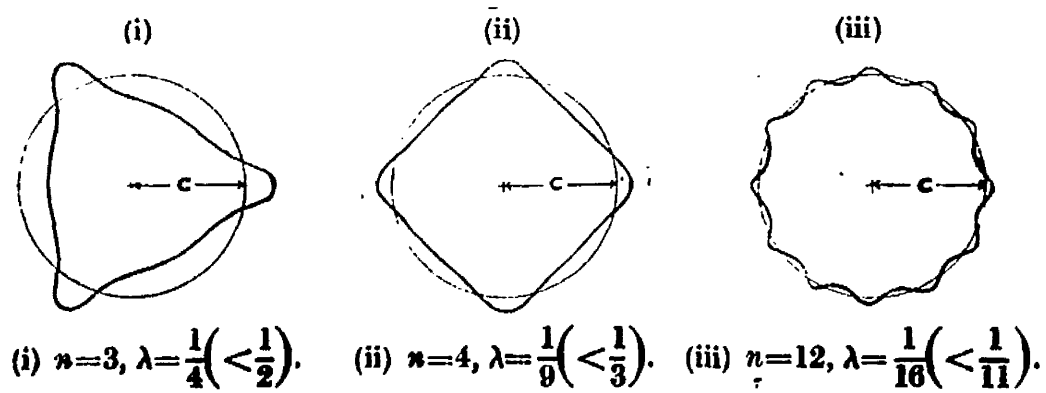
By application of these ideas, the determination of the stress concentration effects produced by internal discontinuities of various forms becomes possible (using equations 1.17 and 1.18) as has been indicated for openings of square and 'star' forms.

In addition to these approximate formulae, direct theoretical solutions for certain problems are also available.

The work of STEVENSON<sup>(50)</sup> in 1943 developed an approach to two-dimensional isotropic elastic theory (plane strain and generalised plane stress), using the complex variable technique. This resulted in elegant solutions having a considerable economy of effort in the investigation of problems formerly examined by means of the Airy stress function and the allied displacement function. The power of the complex potential method is demonstrated by finding appropriate complex potentials for a number of problems such as a curvilinear regular polygon of 'n' sides and 'n' rounded vertices, such that

n = 1	or $\infty$	corresponds to a circular hole.
n = 2	.....	" " elliptical "
n = 3	.....	" " triangular "
n = 4	.....	" " square.

etc.



**Examples of curvilinear polygonal boundary curve of hole.**

Fig. 29.

The forms of the boundary for  $n = 3, 4$  and  $12$  are shown in Fig. 29.

By the complex potentials for such boundaries, the stress distribution in an infinite plate containing the appropriate hole may be determined.

The stress concentration factors at the vertices of the hole are obviously important, and when the plate is under simple tension  $\sigma_0$ , this factor is given by

$$\frac{\sigma_\theta}{\sigma_0} = \frac{1}{1 - \lambda(n-1)} \left[ 1 + \lambda(n-1) - \frac{2 \cos 2\beta [1 + \lambda(n-3)]}{1 - \lambda^2(n-3)} \right] \dots\dots\dots (1.27)$$

and in this case  $n = 3$  (Ref. 31, STEVENSON)

where  $\lambda =$  a form factor,  $0 \leq \lambda(n-1) \leq 1$

$\beta =$  angle between the applied tension  $\sigma_0$  and the horizontal direction (x - axis) with reference to Fig. 29.

The stress concentration factor at the other vertices may be deduced by replacing  $\beta$  by  $\beta - \frac{2r\pi}{n}$  where  $r = 1, 2, \dots\dots\dots(n-1)$ . For  $\beta = \frac{\pi}{2}$ , that is with the plate under simple tension in the vertical direction (y axis), with reference to Fig. 29, equation (1.27) reduces to

$$\frac{\sigma_\theta}{\sigma_0} = \frac{1}{1 - \lambda(n-1)} \left[ 1 + \lambda(n-1) + \frac{2[1 + \lambda(n-3)]}{1 - \lambda^2(n-3)} \right] \dots\dots\dots (1.28)$$

As  $n \rightarrow \infty$  (and thus  $\lambda \rightarrow 0$ ), the stress concentration factor tends to the exact theoretical value of 3.0 for the circular hole, while for the three boundary shapes shown in Fig. 29, the appropriate factors are 7, 5.375 and 15.764.

For all round tension  $\sigma_0$ , the stress concentration factor for all vertices is given by

$$\frac{\sigma_\theta}{\sigma_0} = 2 \left[ \frac{1 + \frac{(n-1)\lambda}{(n-1)\lambda}}{1 - \frac{(n-1)\lambda}{(n-1)\lambda}} \right] \dots\dots\dots (1.29)$$

whilst at the mid point of the sides of the boundaries it has the reciprocal value. If  $n \rightarrow \infty$  (and thus  $\rightarrow 0$  as before), equation (1.29) gives the exact theoretical value of 2.0 for the circular hole. For the other boundaries of Fig. 29, the appropriate factors are 6, 4 and 10.8.

A paper by SEN<sup>(32)</sup> in 1948 on similar lines to that of STEVENSON<sup>(30)</sup> gives solutions for the case of a hole in an infinite plate under all-round uniform tension, the form of the hole being either (i) the inverse of an ellipse, (ii) the loop of a lemniscate (iii) an elliptic limaçon or (iv) an approximate square. In the latter case, which is of special interest, by assuming the transformation

$$Z = e^{\zeta} + ce^{-3\zeta} \quad \text{where } Z = x + iy \quad \text{and } \zeta = \xi + i\eta$$

and putting  $\xi = 0$ , an approximate square is obtained, and employing the usual notation for conformal representation, the stress concentration factor is given by

$$\frac{\sigma_{\theta}}{\sigma_0} = \frac{2(1 - 9c^2)}{1 - 6c \cos 2\eta + 9c^2} \dots\dots\dots (1.30)$$

where  $c$  is a form factor similar to  $\lambda$  in STEVENSON'S solution.

The method used by SEN consists of representing stress components explicitly in terms of certain harmonic functions in such a way that a proper choice of one of these functions leads at once to the solution of the problem. This method appears to be useful in many simple problems of plates with curvilinear boundaries.

The subject of thin, isotropic flat plates of infinite width under plane strain or generalised plane stress conditions, containing holes of/

Fig. 30.

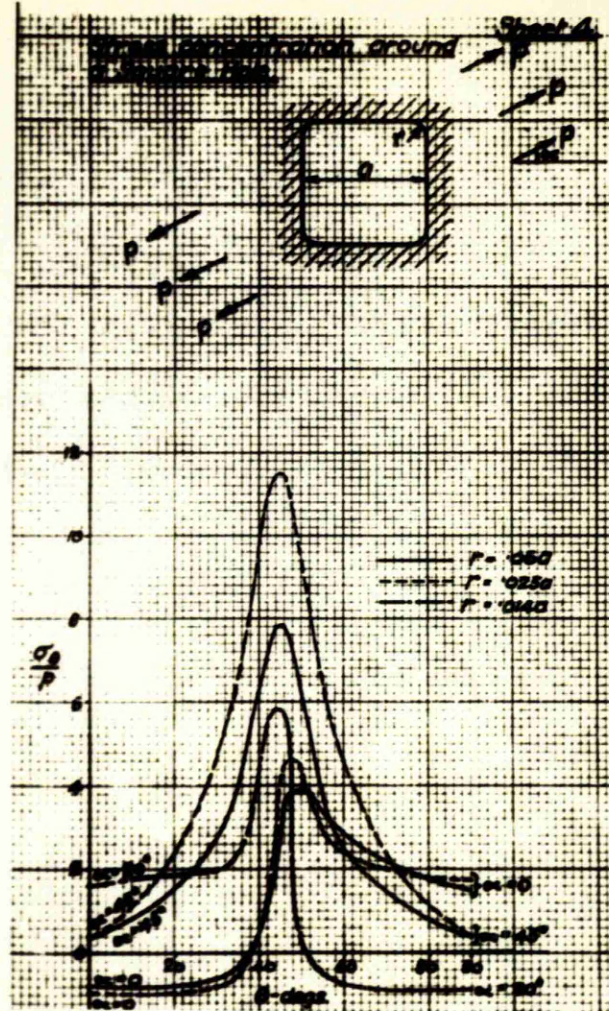
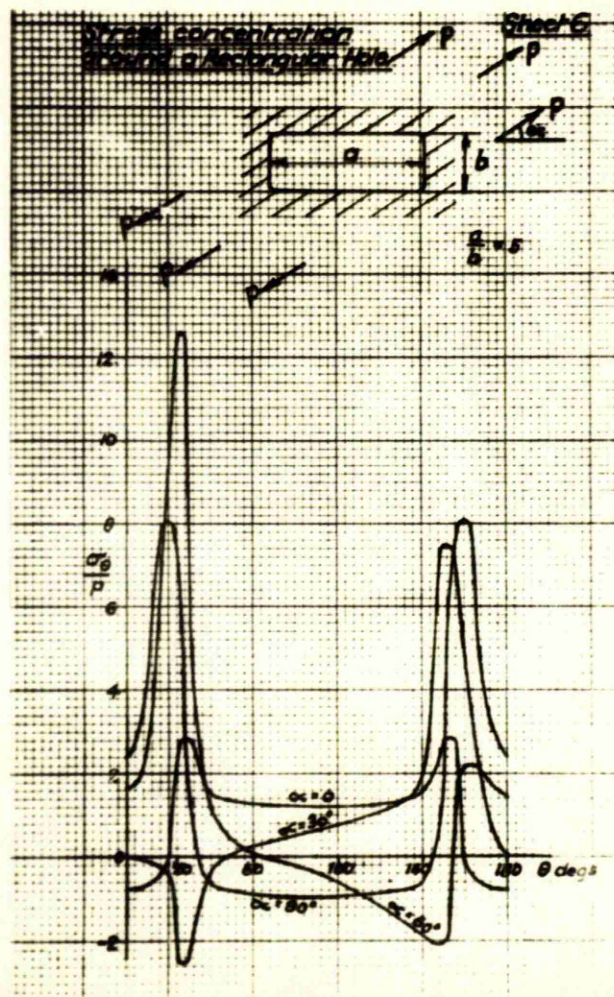


Fig. 31.



of various shapes was treated in 1951 by SAVIN<sup>(4)</sup>. This work stems from the original work on complex potentials by KOLOSOFF<sup>(15)</sup> and later by MUSKHELISHVILI(19). Selected charts of particular interest are given in Figs. 30, 31, 32 and 33. The conversion charts relating the parameter  $\theta$  with the physical angle  $\phi$  for these discontinuities are given in Figs. 34 and 35.



Fig. 32.

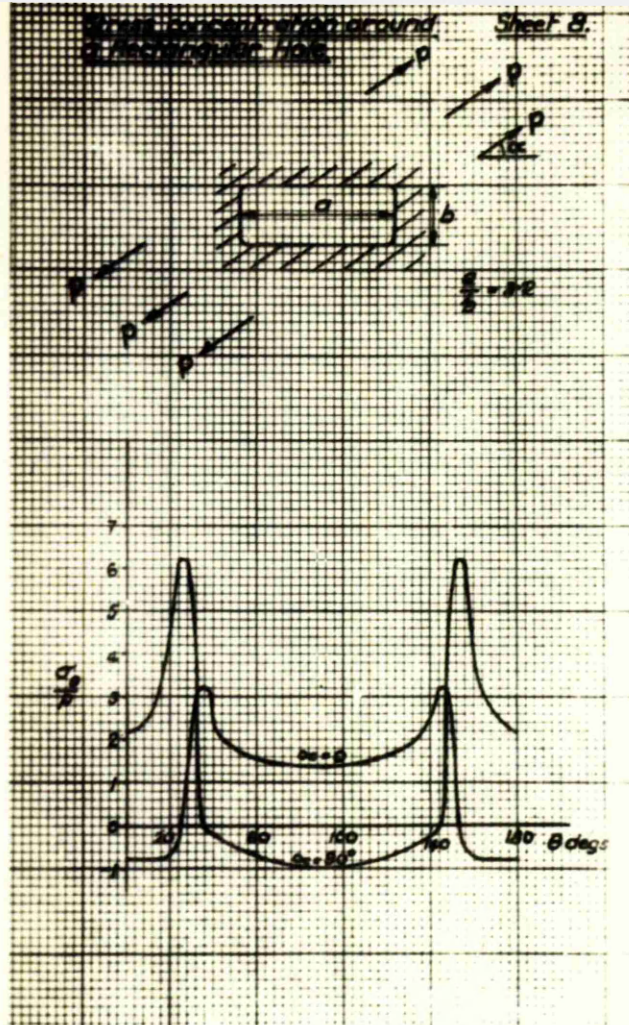
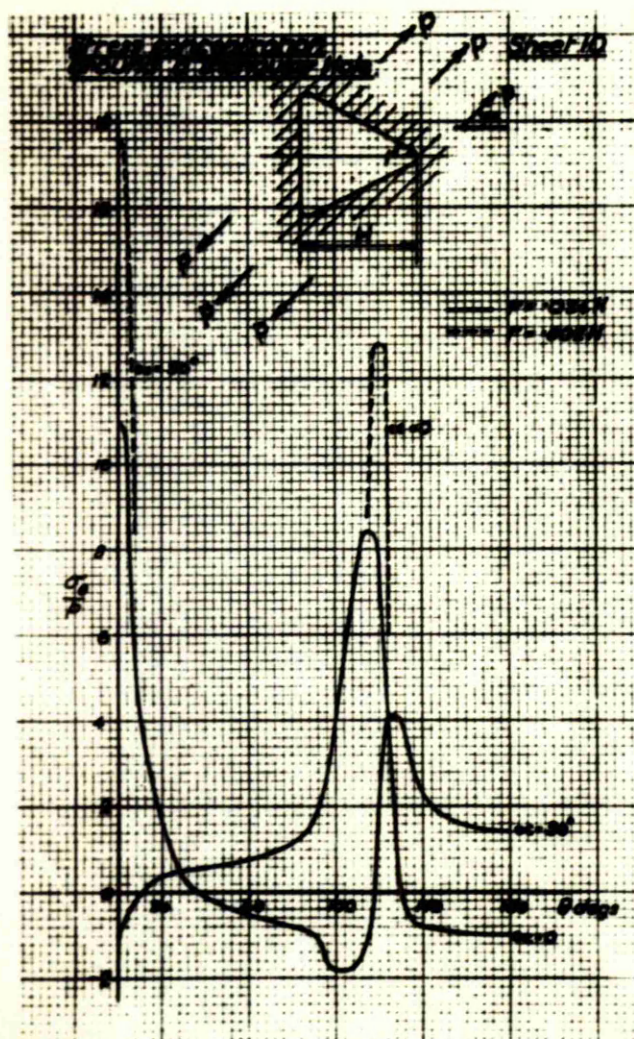


Fig. 33.





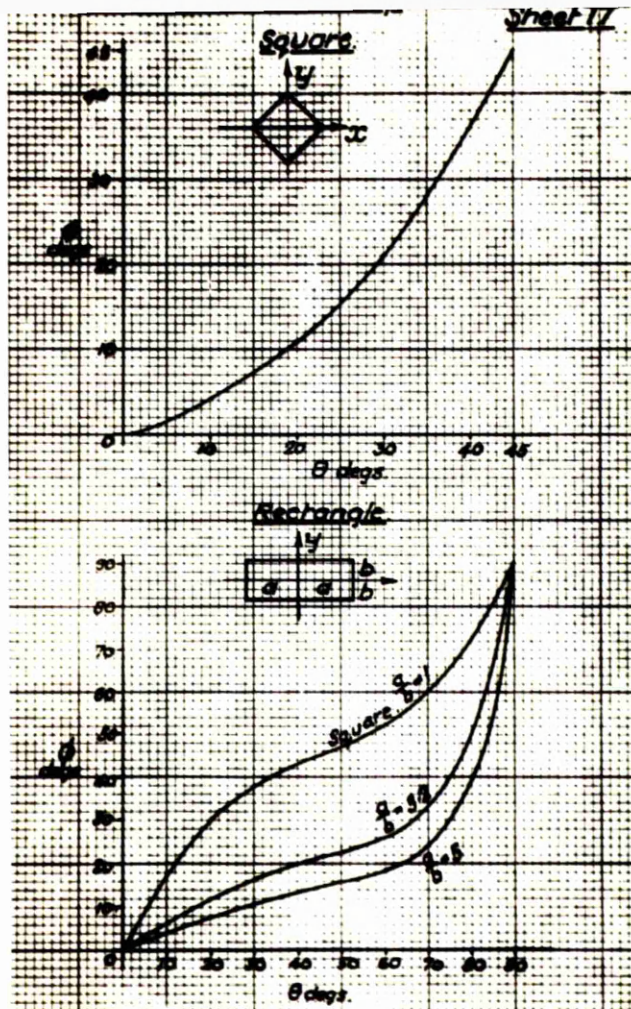


Fig. 34.

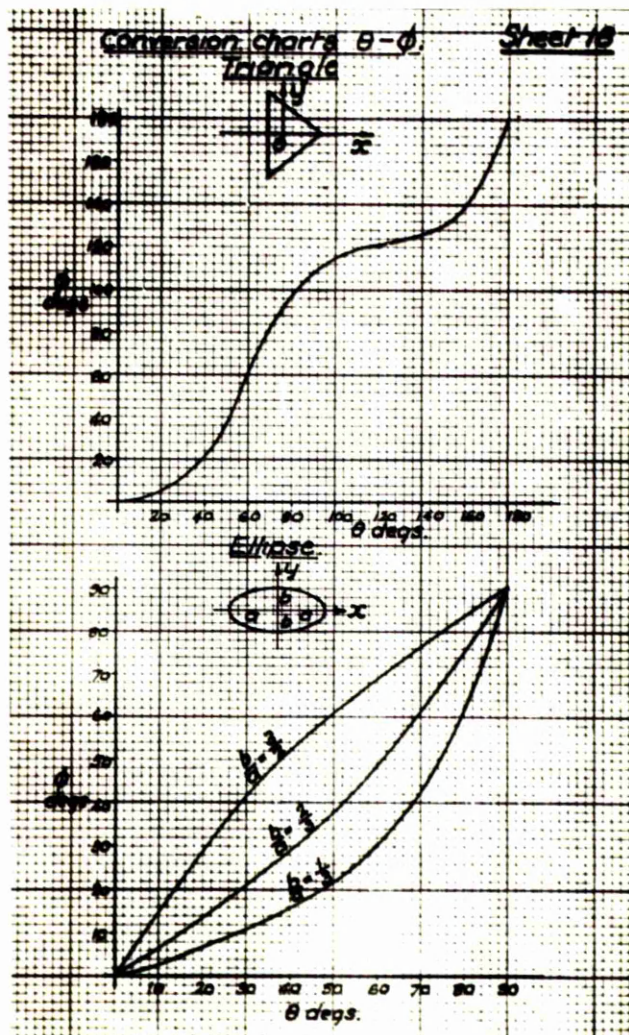


Fig. 35.



CHAPTER I.2. - EXPERIMENTAL INVESTIGATIONS

Fig. 36.

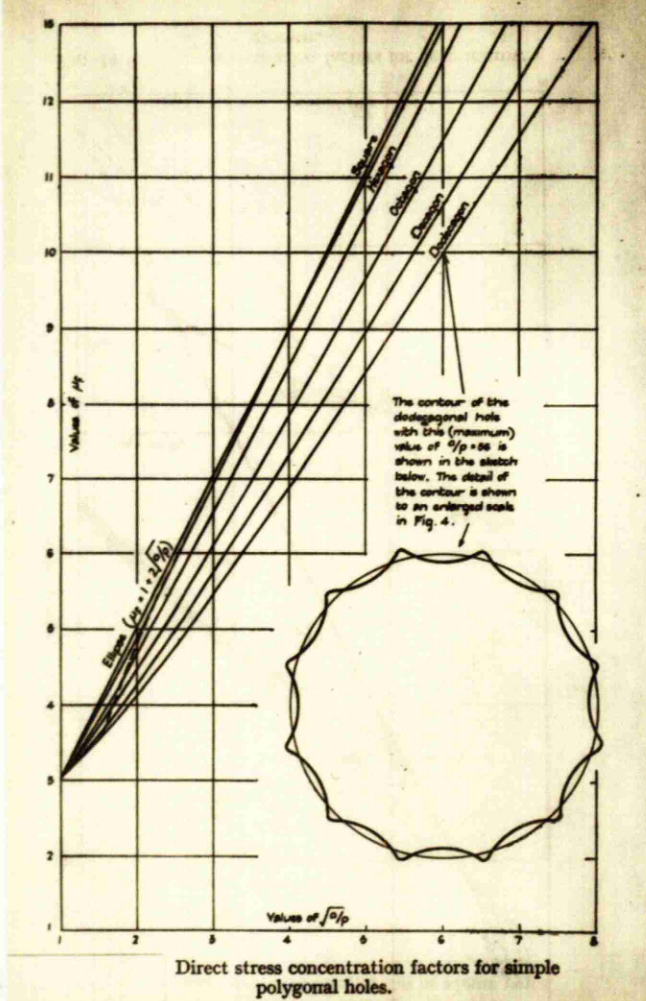
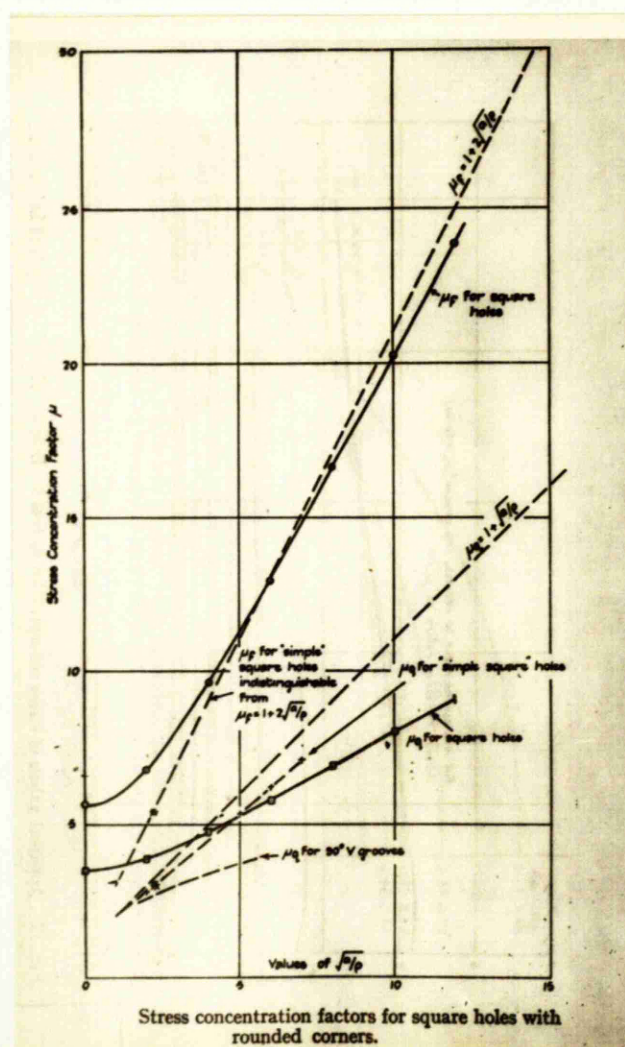


Fig. 37.



COX<sup>(3)</sup> in 1950, computed the stress distribution in the neighbourhood of holes of the general polynomial type in infinite plates under simple tension. The stress concentration factors obtained are compared with the approximate INGLIS solution, as shown in Figs. 36 and 37. Fig. 36 shows that the INGLIS form is a reasonable approximation.

Nevertheless the error in this form  $K_t = 1 + 2\sqrt{a}/\rho$  may be considerable in some cases, particularly for holes in which the radius of curvature varies rapidly round the contour near the point of maximum stress. This point is illustrated by Fig. 37, at low values of  $a/\rho$ ; but it is brought out most clearly in the case of a simple polygonal hole with an infinite number of sides. As expected this hole form is indistinguishable from a true circle and the stress concentration factor takes the value of 3.0, but in fact the radius of curvature of the contour oscillates indefinitely and rapidly between  $a/2$  and infinity, so that the value of  $1 + 2\sqrt{a}/\rho$  oscillates between 1.0 and  $1 + 2\sqrt{2}$ .

A recent paper by HELLER, BROCK and BART<sup>(35)</sup> published in 1958, re-examined the problem of a rectangular opening with rounded corners in a uniformly loaded plate, under bi-axial or uni-axial tension, and in this solution, the aspect ratio (length to width) and the radius of curvature at the corners were general. This solution overcame the obvious shortcomings of the work of INGLIS and SAVIN, and also of GREENSPAN<sup>(34)</sup>, whose solution by another method, for the square with rounded corners, failed to include a sufficient number of terms.

The solution by HELLER, BROCK and BART is an extension of the earlier work of BROCK<sup>(35)</sup> on a general solution for the entire family of squares with radiused corners.

Fig. 38.

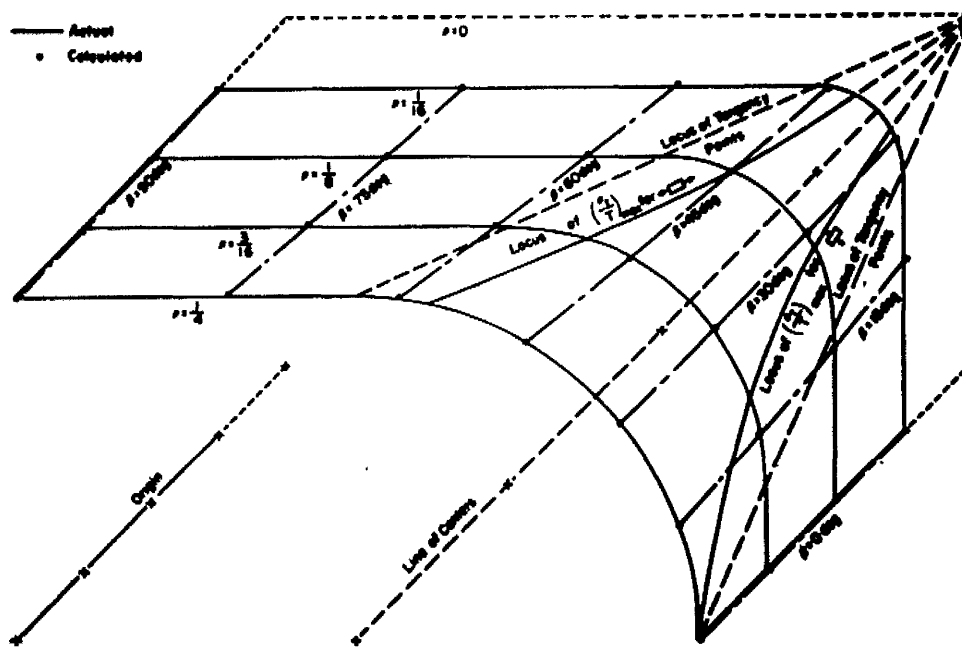
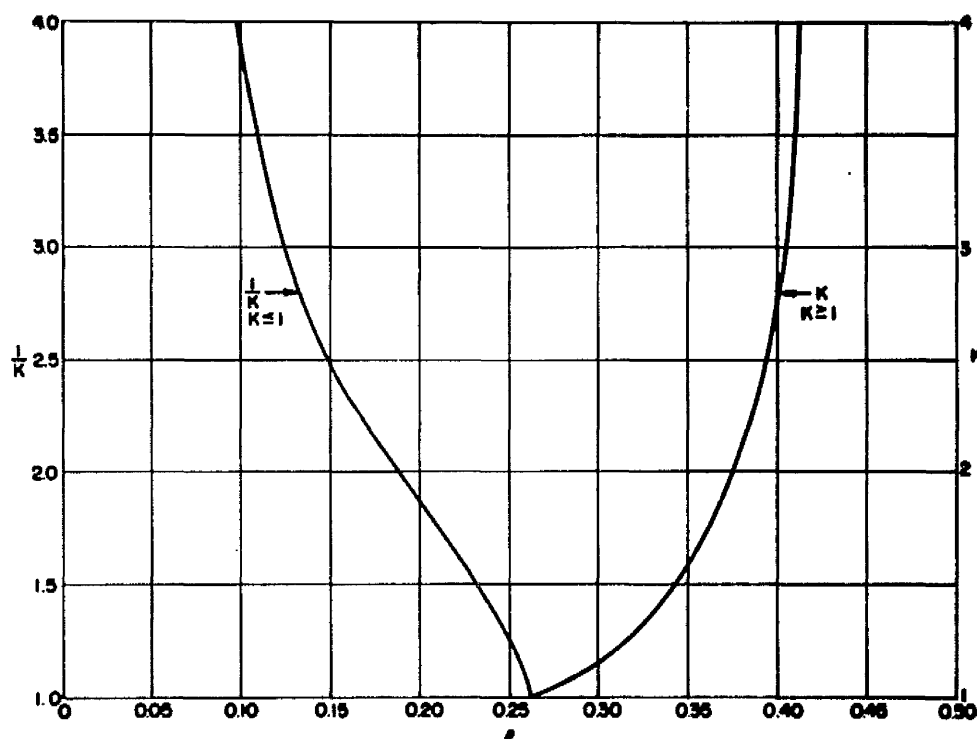


Fig. 39.





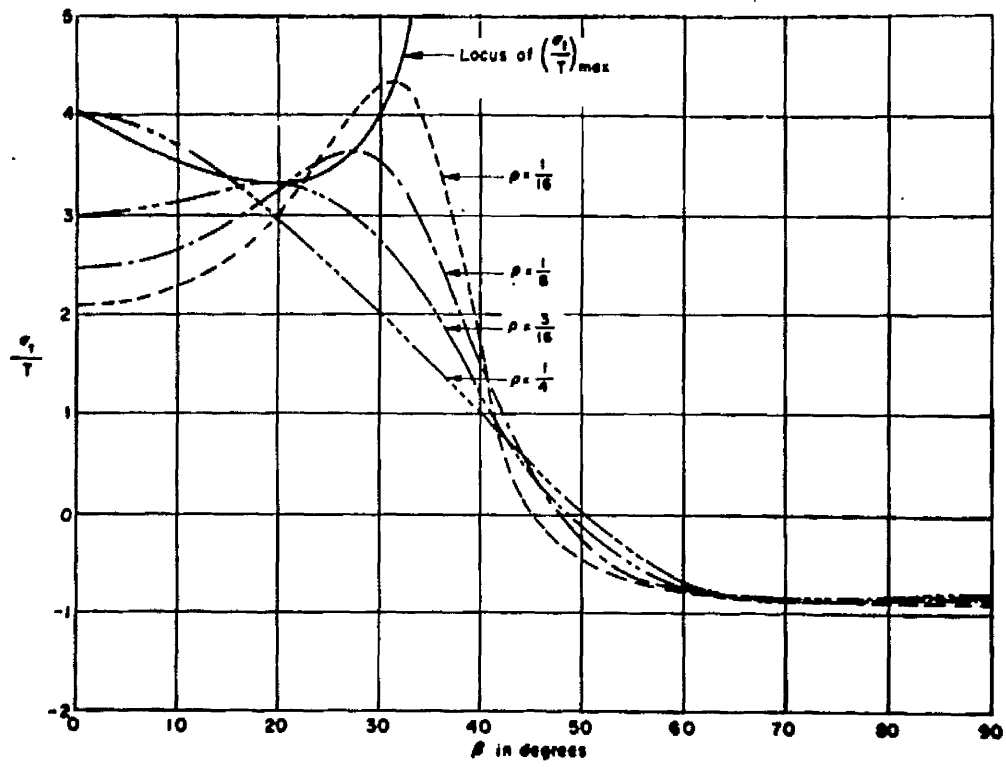


Fig. 40.

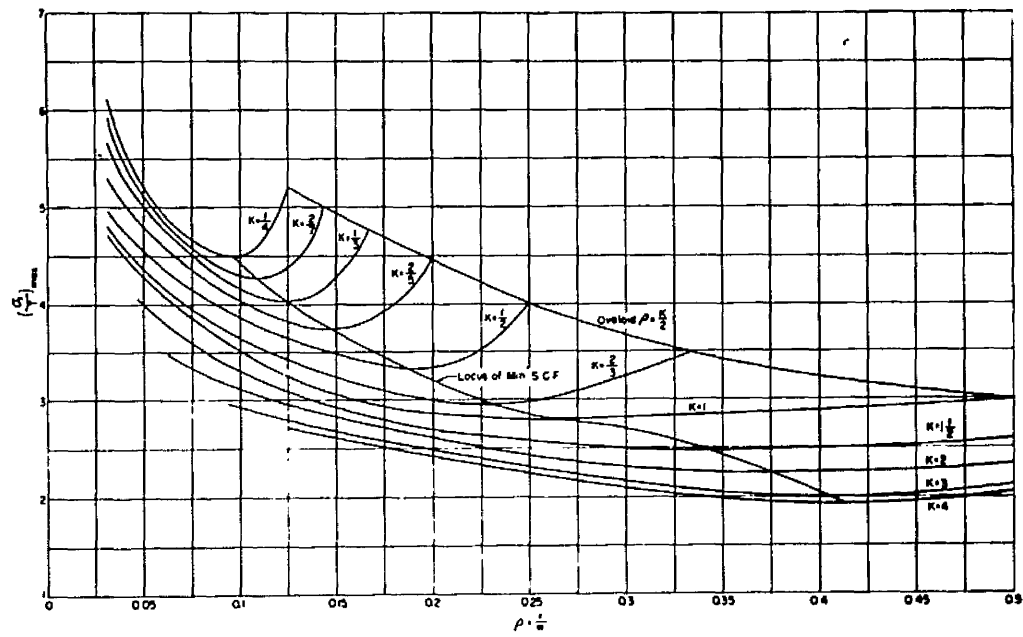


Fig. 41.

In the paper on rectangular openings, the solution is obtained by the complex variable method associated with MUSKHELISHVILI. The shape of rectangular opening is determined by the number of terms retained in the series for the mapping function, and for a reasonable degree of fit for practical openings, six coefficients were used. The solution of the nine simultaneous transcendental equations required the use of an electronic computer, and it was also necessary to use an approximation based on NEWTON'S method. Thus the work involved was considerable.

The solution was shown to agree with the solutions of GREENSPAN for an ovaloid, INGLIS for an ellipse, KIRSCH for a circle, and BROCK for a square with rounded corners.

Numerical results for uni-axial tension were calculated for the family of rectangles with aspect ratio 1 : 2, and the results are illustrated in Figs. 38, 39, 40 and 41.

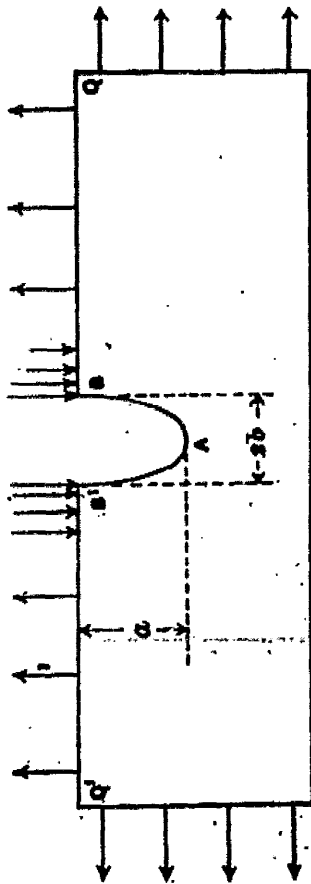


Fig. 42a.

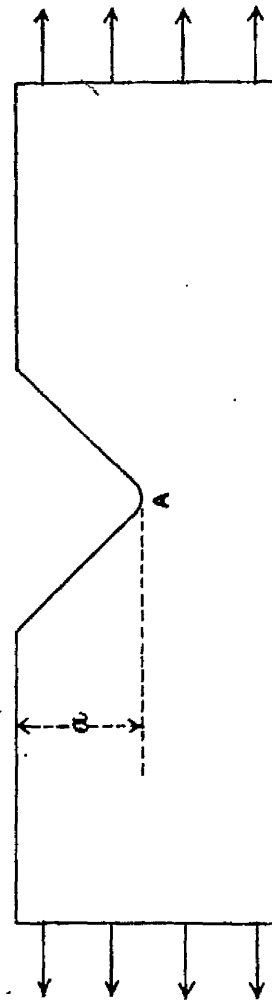


Fig. 42b.



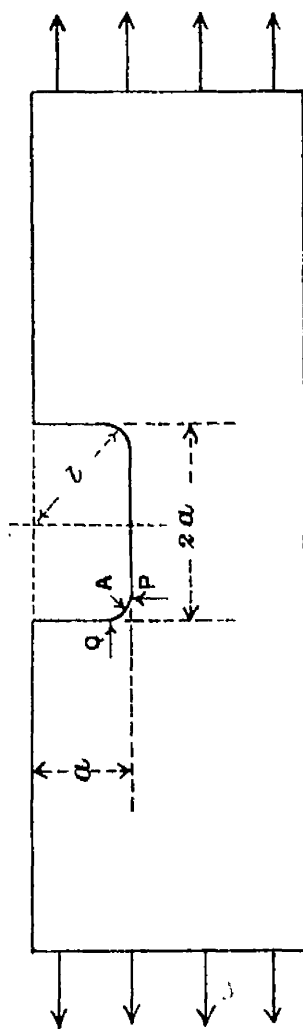
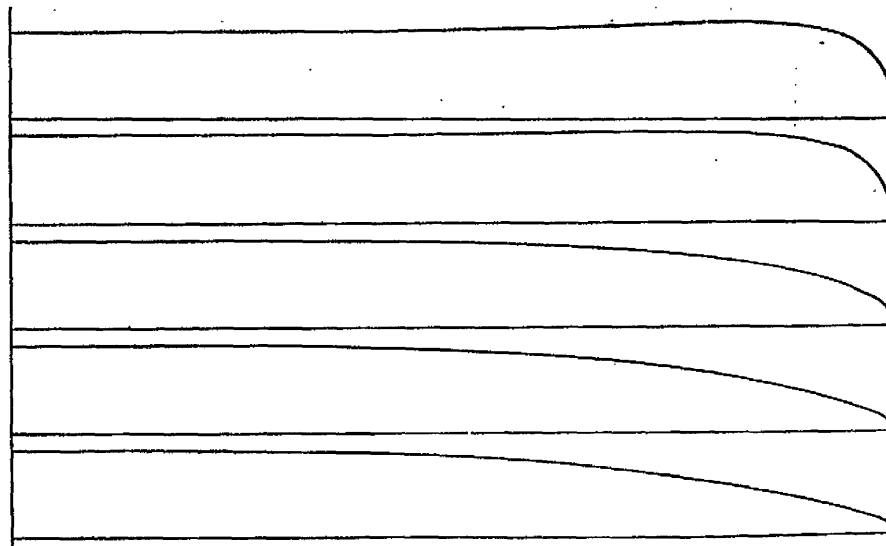


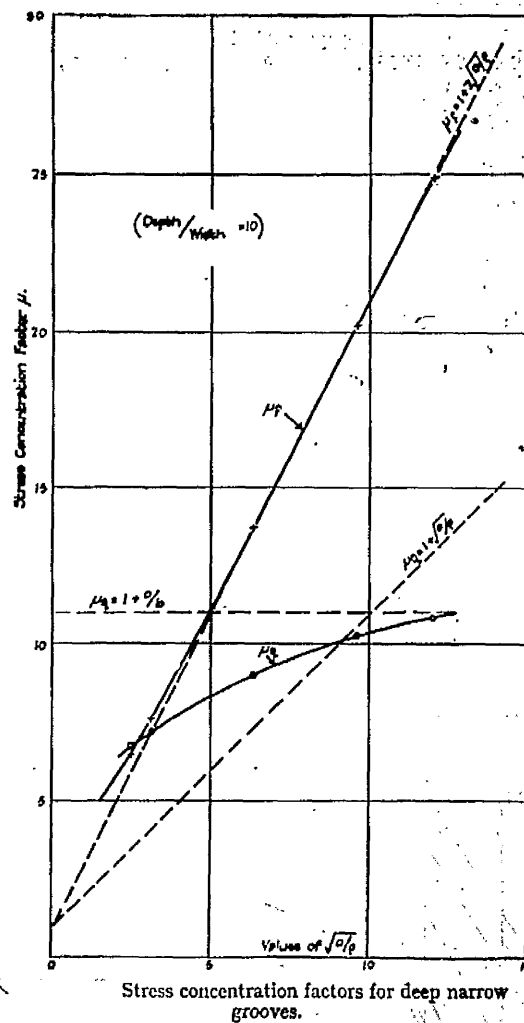
Fig.42c.

Fig.43.



Forms of deep narrow groove.

Fig.44.



External Discontinuities

Since the work of INGLIS also includes the treatment of a wide range of external discontinuities, it is convenient to preface this section on external discontinuities by reference to his work.

If one half of the tension plate shown in Fig. 15 is considered, the notched plate of Fig. 42a is the result. The reasoning advanced for this case is as follows. As the total force action on the edge Q'Q amounts to zero, the stresses on Q'Q have a negligible effect on the maximum stress produced at A. Accordingly the stress at A for the elliptic notch of depth 'a' is given by the expression for the stress at A on the equivalent internal discontinuity, that is an elliptic hole of semi-axis 'a' as shown in Fig. 15.

$$\text{Thus } \sigma_A = \sigma_0 (1 + 2\sqrt{a}/\rho) \dots\dots\dots(1.31)$$

Carrying this form of reasoning further, it is proposed by INGLIS that other external discontinuities, not elliptical in form, may be treated in a similar manner, and that by using an 'equivalent ellipse', stress concentration factors for such discontinuities as vee, triangular, rectangular notches, etc. may thus be determined (Figs. 42b, c).

A similar consideration was made by COX into the application of INGLIS' approximate form of  $K = 1 + 2\sqrt{a}/\rho$ , and as in his previous work on internal discontinuities, the analysis was considerably simplified by the adoption of complex variables. Values of stress concentration factor for the notch forms shown in Fig. 43 were calculated and compared with those obtained from the approximate formulae, and Fig. 44 shows that the latter gives very close approximations to the theoretical values.

The/

The approximate form for the determination of the stress concentration factor is especially valuable where a rapid estimate of the stress concentration factor is required and where there is no known theoretical solution.

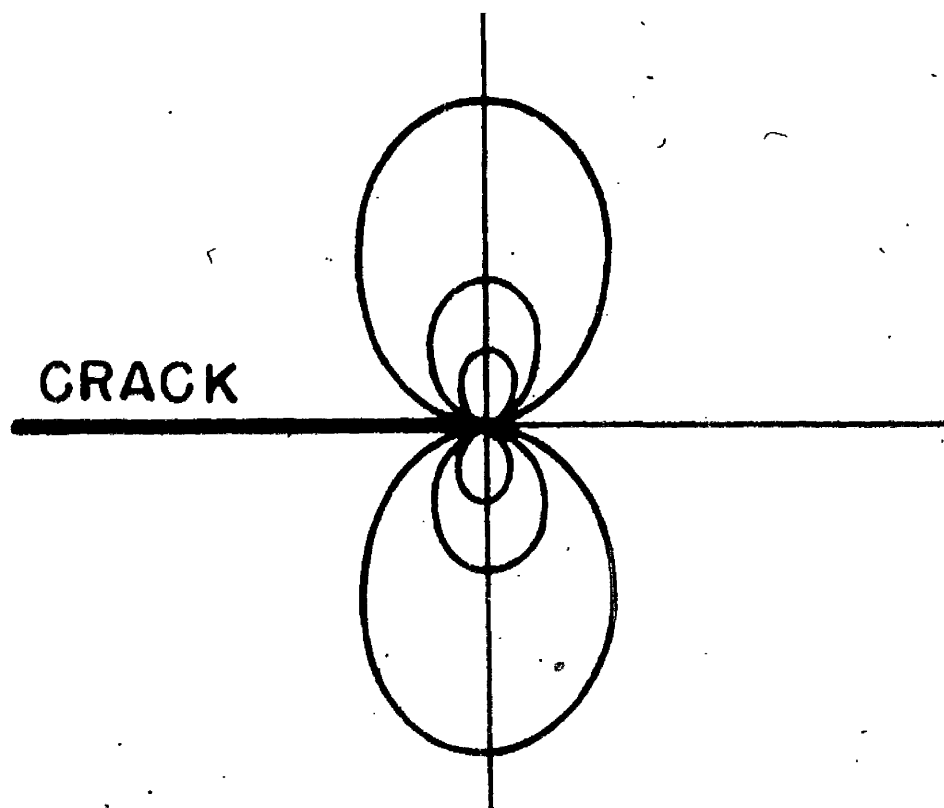


Fig.45.

I.1(e) External Cracks

Photoelastic work by POST<sup>(27)</sup> in 1954 confirms INGLIS' theory that the highly stressed zone at the head of a crack is unaffected by the shape of the structural part at some distance from it. It is reasonable therefore to refer the solution for an edge crack to that for the equivalent internal crack having a total length equal to twice the depth of penetration of the edge crack.

There is however an exact solution for the external crack problem, produced in 1957 by WILLIAMS<sup>(36)</sup> who examined the stress distribution in the region of a stationary edge crack in a thin, semi-infinite plate. The plane stress distributions near the vertex of an infinite sector of included angle  $\alpha$  for various boundary conditions were considered. Thus when the two radial edges of the plate are unloaded, and the wedge angle approaches  $2\pi$ , the conditions pertaining to the edge crack are reproduced. Using the Airy stress function method, expressions for the sum and difference of the principal stresses were obtained, and hence the isochromatic lines around the end of the crack, as shown in Fig. 45. It should be noted that the shear stress is zero along the line of propagation of the crack. Also there is a tendency for a state of two-dimensional or hydrostatic tension which consequently may permit the elastic analysis to apply more closely to the end of the crack than was previously supposed. From this it is evident that an isotropic point may exist at the end of the crack. Furthermore as the distance from the crack increases, the stress becomes non-hydrostatic and the suggestion is that there may be a yielded region ahead of the crack.

There/

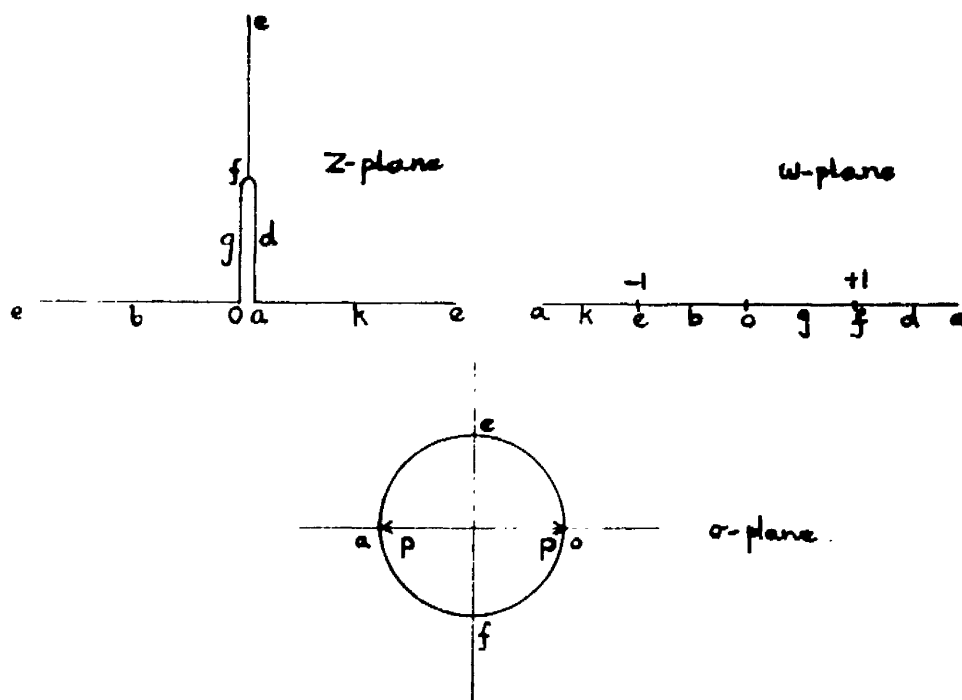


Fig.46.

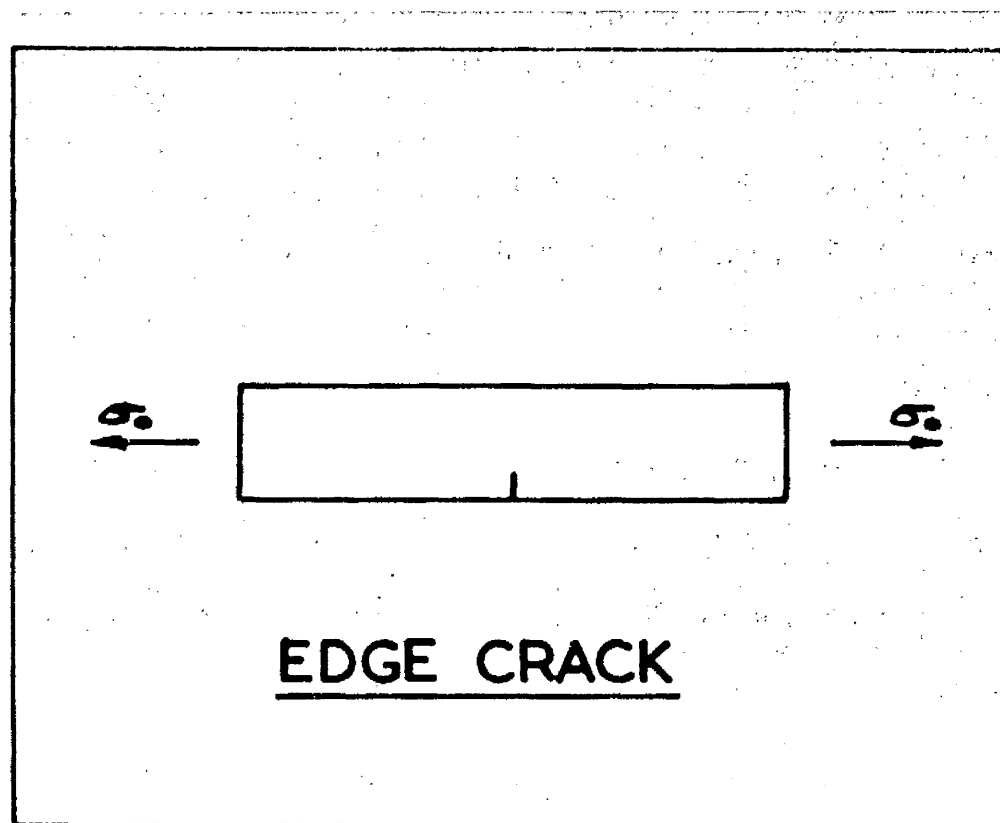


Fig.47.

There is also a distinct possibility of more highly yielded regions at  $\pm 70^\circ$  from the line of the crack, and the maximum tensile stress is found to occur at  $\pm 60^\circ$  from the line of the crack.

These findings are corroborated by the photoelastic analysis by POST, the results of which are reported in paragraph I.2(c)

The complex potential method was used by ROTHMAN<sup>(7)</sup> in 1957 to investigate the edge crack problem.

For the case of a crack in a plate of semi-infinite width, with reference to Fig. 46, the transformation

$$Z = \frac{2i\omega^{\frac{1}{2}}}{\omega + 1} \quad \text{or} \quad \omega = \frac{\left[1 + (1+Z^2)^{\frac{1}{2}}\right]^2}{Z^2} \dots\dots\dots(1.32)$$

is used to transform the 'cracked' boundary of the z-plane into the straight line of the w-plane, and the further transformation

$$\sigma = \frac{i + \omega}{i - \omega} \dots\dots\dots(1.33)$$

transforms the upper half of the w-plane on to the outside of the unit circle in the  $\sigma$ -plane. Stress equations are developed for the crack under various forms of boundary loading such as fluid pressure and wedge forces.

These solutions are also extended to the case of a crack in a plate of finite width, and it is stated that the stress solution for the edge crack case shown in Fig. 47 can be obtained using this method of analysis.



Stresses in the neighbourhood of the notch.

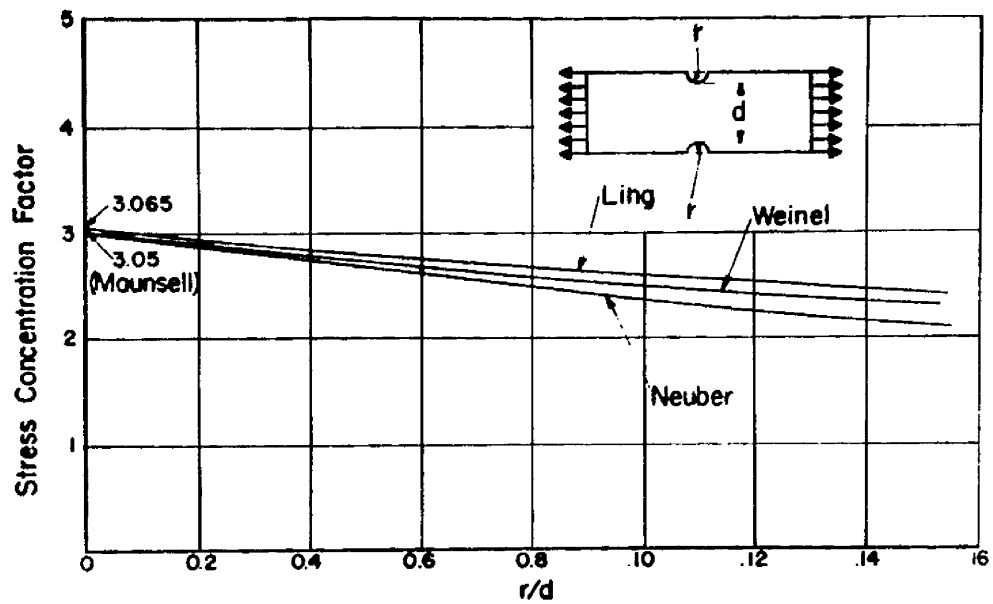


Fig. 49.

## FACTORS OF STRESS CONCENTRATION FOR SEMI-CIRCULAR NOTCHES

I.1(f) External Notches

The work of INGLIS giving an approximate solution for the stress concentration effects of notches of varying depth has been supplemented by direct theoretical approaches for the complete stress distribution around a notch. MAUNSELL<sup>(37)</sup> in 1936 applied the stress function method, and investigated the stress distribution around a semi-circular notch at the boundary of a thin plate of semi-infinite width, under generalised plane stress conditions. Due to the form of the boundary being composed of two intersecting parts, the mathematical treatment is rendered difficult, and thus the solution for the stress distribution shown in Fig. 48 may contain very slight errors.

In 1947, LING<sup>(38)</sup> investigated the case of a bar of finite width containing symmetrical semi-circular notches, using the Airy stress function technique. Later, in 1957, LING<sup>(39)</sup> repeated this solution but this time used the 'promotion of rank' process to diminish the labour involved in solving a problem of this type. The stress concentration factor based on the net section, for a semi-circular notch was computed by NEUBER<sup>(40)</sup>. In 1937, a comparison with LING'S solution<sup>(38)</sup> being shown in Fig. 49. Slight disagreement is evident (see Page 55 also) and ATSUMI<sup>(41)</sup> claims that LING'S results<sup>(38)</sup> are unreliable. Also shown in Fig. 49 is a solution by WEINEL<sup>(42)</sup> for this same problem, and in this case a new theoretical approach was presented, in which the tension plate was divided into three longitudinal strips, a central strip of uniform width and two boundary strips equal in width to the notch depth, the boundary conditions being re-established on the central strip. The stress concentration factors thus found compare favourably with those of NEUBER.

The complete field of shallow and deep notches was included in NEUBER'S original investigation, the semi-circular notch being a particular case. The general solution involved an interpolation between the two limiting cases of a shallow elliptic notch in an infinite plate and deep hyperbolic notches in a finite plate. NEUBER sought a function in the intermediate region which would interpolate between these two boundary cases, and which would give the proper limiting values at these two extremes. He found the function to be

$$K_t = 1 + \frac{(K_s - 1)(K_d - 1)}{\sqrt{(K_s - 1)^2 + (K_d - 1)^2}} \dots\dots\dots (1.34)$$

where  $K_s$  = the stress concentration factor for the limiting case of a shallow elliptic notch in an infinite plate.

$$= 1 + 2\sqrt{a}/\rho$$

and  $K_d$  = the stress concentration factor for the limiting case of deep hyperbolic notches in a finite plate.

$$= \frac{2\left(\frac{d}{2\rho} + 1\right) \sqrt{\frac{d}{2\rho}}}{\left(\frac{d}{2\rho} + 1\right) \tan^{-1} \sqrt{\frac{d}{2\rho}} + \sqrt{\frac{d}{2\rho}}}$$

where  $a$  = depth of elliptic notch.

$\rho$  = radius of curvature of notch.

$d$  = width of the net section.

This form gives the stress concentration factor based on the net section for a plate with notches of varying depth.

For semi-circular notches, the notch depth equals the notch radius and  $K_s = 3.0$ . In this case, equation (1.34) becomes

$$K_t = 1 + \frac{2(K_d - 1)}{\sqrt{4 + (K_d - 1)^2}} \dots\dots\dots (1.35)$$

From/

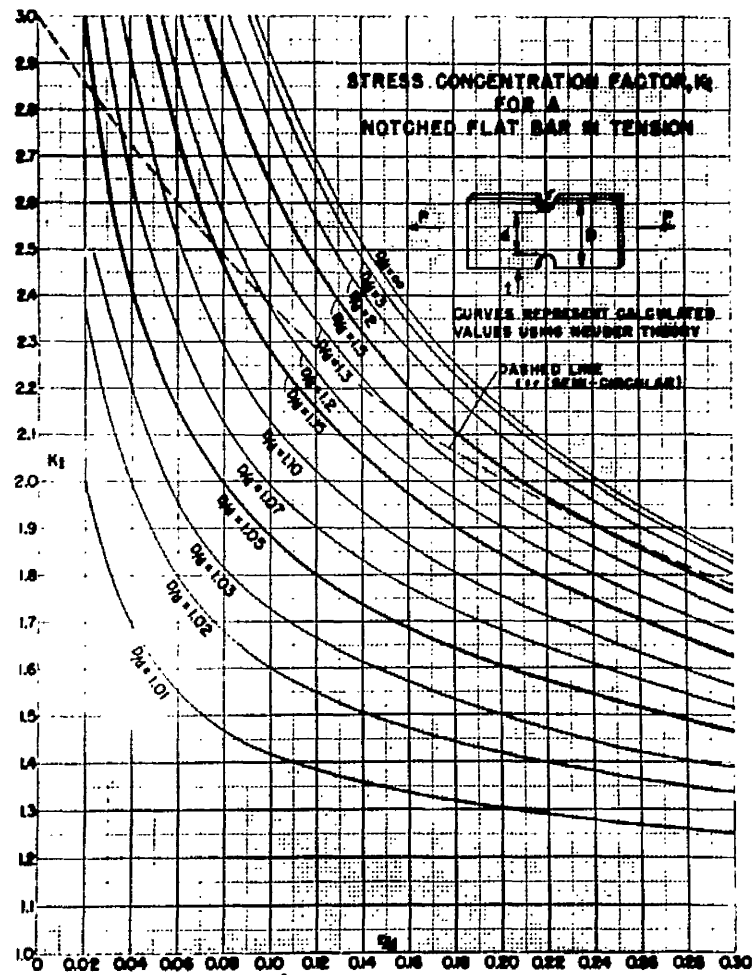
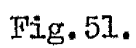


Fig. 50.

From this equation the curve of Fig. 49 was obtained.

The complete range of solutions for symmetrical notches, based on NEUBER'S theory is given in Fig. 50.



**Variation of stress concentration factor at B with  
depth of notch.**

I.1(g) Miscellaneous External Discontinuities

The problem of a semi-infinite plate bounded by a cubic curve was considered by STEVENSON<sup>(45)</sup> in 1945, the boundary taking the form of a single smooth notch of the form shown in Fig. 51, corresponding to  $\lambda = \frac{9}{10}$ . This curve has the polar equation

$$r = c \sec \theta - \lambda c \cos \theta$$

where the depth of the notch is given by  $\lambda c$ . Hence  $\lambda \leq 1$  restricts the form to a notched boundary for which the depth is less than or equal to  $c$ . For  $\lambda = 1$  the cubic has a cusp. For  $\lambda > 1$ , the point  $O'$  in Fig. 51 becomes a double point and the curve has a loop, hence this case is excluded for consideration.

For simple tension, under generalised plane stress conditions, using the method of complex potentials, STEVENSON expressed the stress concentration factor at the root of this notch form as

$$K_t = \frac{2 + \lambda}{(2 - \lambda)(1 - \lambda)} \dots\dots\dots (1.36)$$

Using various values of  $\lambda$ , the graph of Fig. 52 was obtained, showing the variation in stress concentration factor with depth of notch.

ROTHMAN and ROSS<sup>(29)</sup> in 1955 re-examined this form of notch and obtained expressions enabling the maximum shear stress at any point on the boundary to be computed.

### I.2 (a) Circular Hole

- (i) Centrally positioned
- (ii) Eccentrically positioned

### I.2 (b) Elliptical hole

### I.2 (c) Internal Cracks

### I.2 (d) Miscellaneous Internal Discontinuities.

**EXTERNAL DISCONTINUITIES:**

### I.2 (e) External cracks

### I.2 (f) External Notches

## I.2 (g) External Fillets

### I.2 (h) Miscellaneous External Discontinuities.



I.2(a) Circular Holes

In experimental work, infinitely wide plates are simulated by means of finite plates, in which the ratio of plate width to hole width is greater than 4.0, as this has been shown by various experimenters to give stress distributions which approximate closely to the infinite plate stress distribution.

(i) Central circular hole

The results of several photoelastic investigations of the stress concentration effects produced by a central circular hole in a thin plate in simple tension, are summarised as shown in Fig. 53.

HOWLAND'S<sup>(10)</sup> mathematical results for values of the ratio plate width/hole diameter greater than 0.5 are plotted, as a basis of comparison, together with an empirical solution by HEYWOOD<sup>(6)</sup>, of the form  $K_t = 2 + \left(\frac{b}{D}\right)^5 \dots\dots\dots(1.37)$

This problem was apparently first tackled experimentally in 1912 by COKER<sup>(44)</sup> who, using a celluloid model, determined the stresses in the plate around the discontinuity with the aid of a tungsten filament lamp polariscope.

Due to difficulties in experimental techniques, however, accurate determination of the stresses at the edge of the hole was not possible, the main trouble lying in the use of a compensator method, which tends to give the average fringe value at points of localised stress concentration, rather than the maximum value. In comparison with HOWLAND'S figures, COKER'S results are low. More recently, HENNING<sup>(45)</sup> published results from specimens of optical quality glass, and these results/

Fig. 53.

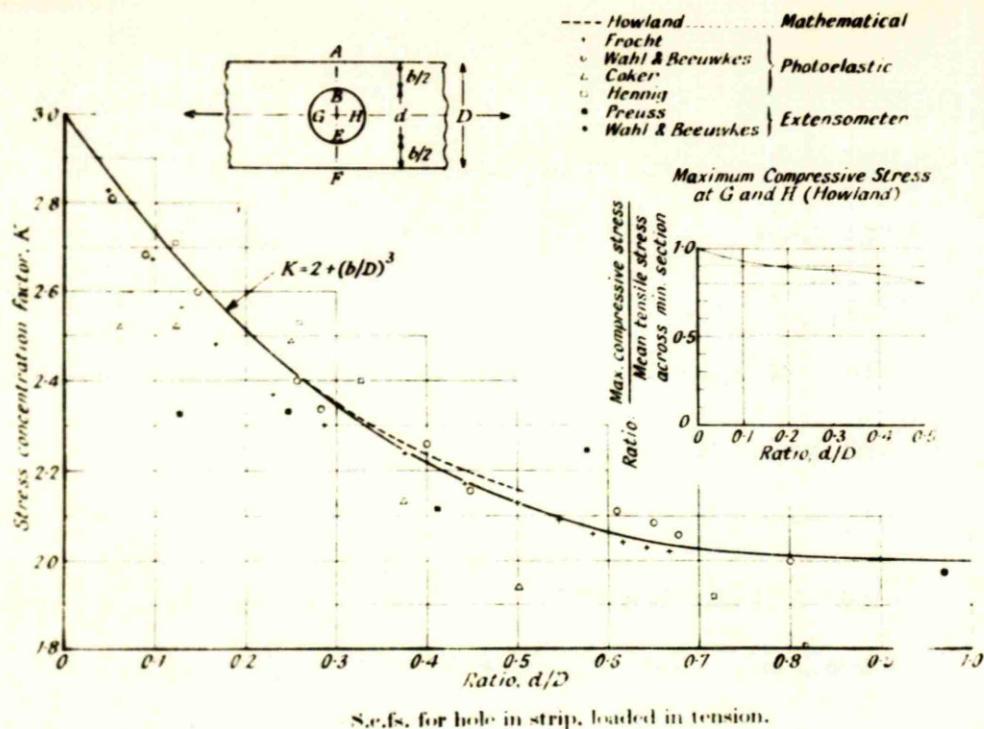
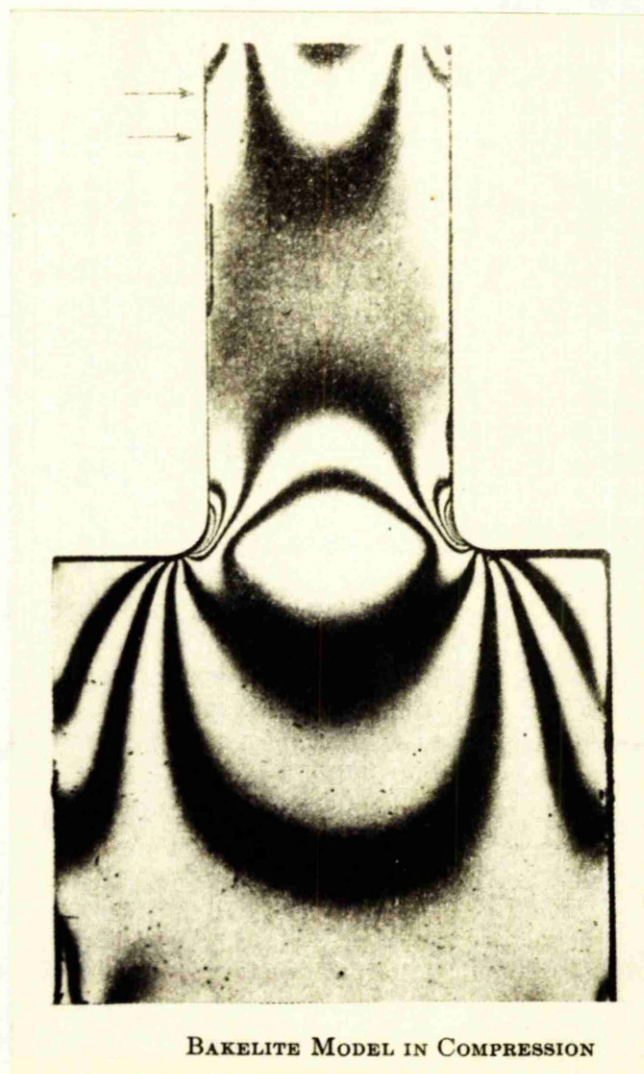


Fig. 54.



results are also slightly different from the mathematical results. In 1934 WAHL and BEEUWKES<sup>(46)</sup>, using a monochromatic light source polariscope, together with bakelite specimens, succeeded in producing the first results of high accuracy. It was at that time currently believed that the photoelastic method obscured the true boundary of the specimen and hence could not be used for accurate determination of the boundary stresses.

In overcoming this difficulty, WAHL and BEEUWKES engraved reference lines on the model and measured the distances between the lines and from them to the true boundaries of the model. Measurement of the distance between these reference lines on the stress pattern picture enabled a magnification factor to be used, and hence the positions of the true boundaries relative to the stress pattern were determined, followed by the boundary stresses. An empirical formula quoted by the authors gives results in approximate agreement with their experimental figures, thus:-

$$K_t = 3 - 3.15\frac{d}{D} + 3.76\left(\frac{d}{D}\right)^2 - 1.71\left(\frac{d}{D}\right)^3 \dots\dots\dots(1.38)$$

the notation being as shown in Fig. 53.

In a discussion of this paper, FROCHT<sup>(47)</sup> refuted the necessity of using engraved lines as a datum for determining the true boundaries and claimed that these boundaries could be clearly shown on the stress pattern picture. As evidence of this, a stress pattern photograph (Fig. 54) was given, on which were visible two lines, one a fine scratch at 0.0025" from the edge, and the other of 0.006" width at 0.004" from the edge. WAHL and BEEUWKES disputed this claim, but in 1935 FROCHT<sup>(48)</sup> produced results/

Fig. 55.

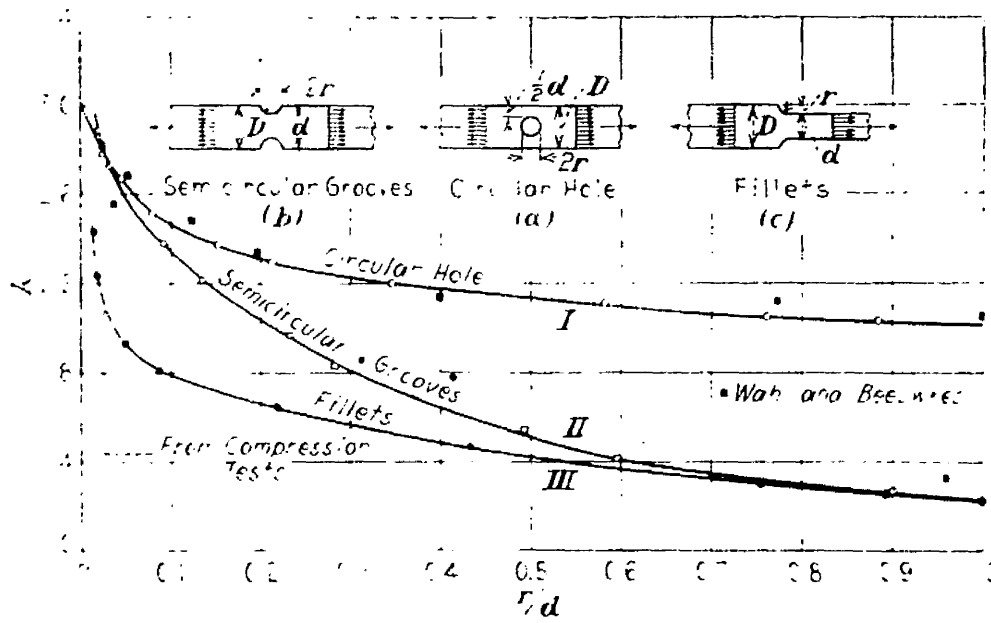
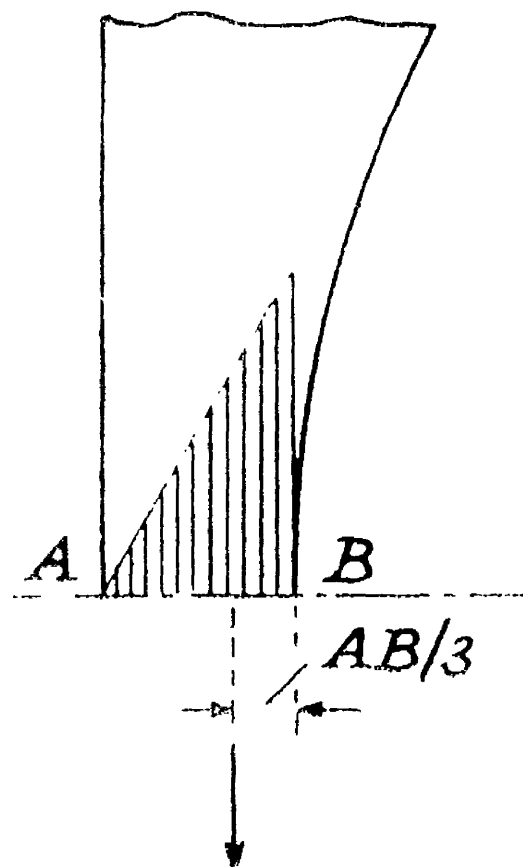


Fig. 56.



results as shown in Fig. 55, comparable with those of HOWLAND and of WAHL and BEEUWKES, from a photoelastic investigation of a tension specimen with a central circular hole, the boundaries and boundary stress values being obtained directly from the stress pattern without the use of engraved lines. Thus the work of FROCHT gave results of high accuracy with a much easier technique than that of WAHL and BEEUWKES. This method for determining the boundary stresses directly from the fringe pattern is now generally used in photoelastic investigations. With the great improvements in photoelastic materials has come further confirmation of the degree of accuracy obtainable from FROCHT'S method of boundary determination. In 1953, FROCHT, in association with GUERNSEY and LANDSBERG<sup>(49)</sup>, published the results of a photoelastic investigation of a tension member containing a central circular hole, the results varying from HOWLAND'S classical solution by only 1.8%.

In examining the extreme case of hole diameter tending to plate width, WAHL and BEEUWKES, in their original investigation obtained the single point in Fig. 53 for a value of  $d/D = 0.97$ , from a test on a steel model, using an extensometer. The model was 4.1/8" wide and contained a 4" diameter central hole. The 0.3" gauge length of the extensometer was large compared with the hole diameter, and the experimental results tend to be a few per cent low.

The stress distribution for a thin section is known to be linear, and this evidently applies to the two thin sections at the hole in this case. As the load is transmitted assymmetrically to the sections, they tend to collapse inwards with the result that as the thickness/

Fig. 57.

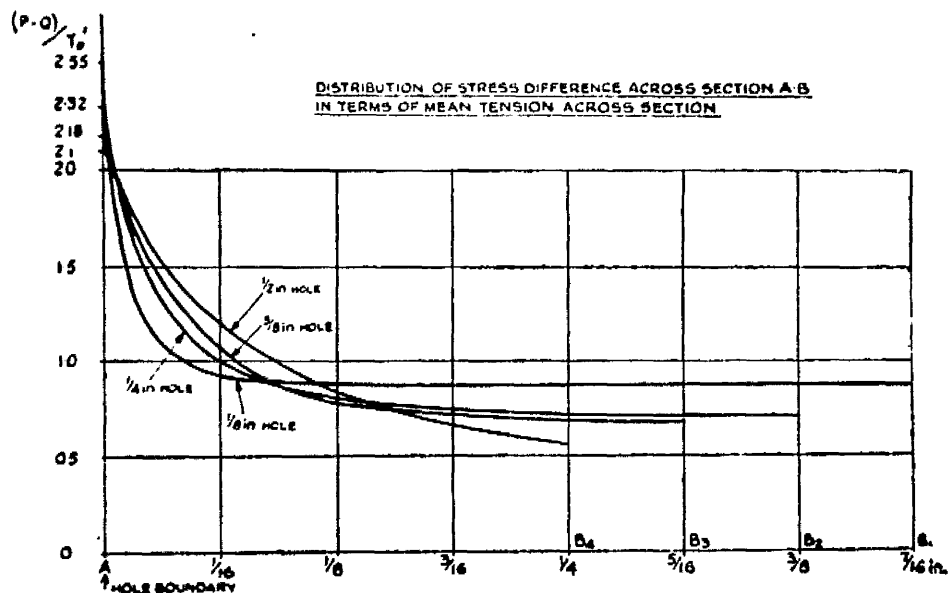
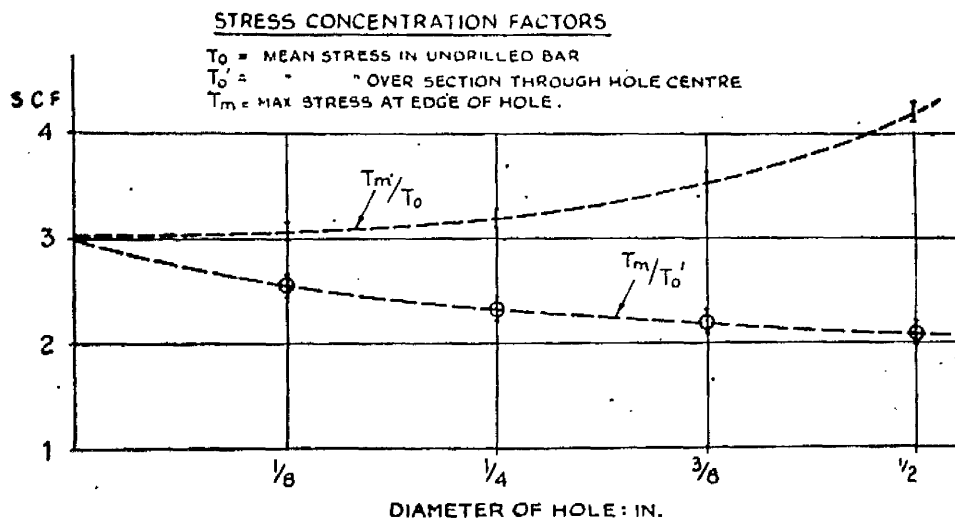


Fig. 58.



thickness tends to zero, no stress whatsoever is produced at the outer edges. As the stress at the outer edge tends to zero, the stress at the hole boundary tends to twice the average stress in the thin section as shown in Fig. 56. Hence as  $d/D$  tends to 1.0, the stress concentration factor based on the net section tends to 2.0, as shown in Fig. 53. This shows an error in HENNIG'S results, which indicate that the stress concentration factor based on the net section tends to 1.0 as  $d/D$  tends to 1.0.

In 1955 JESSOP and SNELL<sup>(50)</sup> conducted a systematic investigation of the effect upon the stress distribution at the cross-section through the hole centre, of variation of the ratio of hole diameter to width of bar. The variations in the stress difference and in the separate stresses were determined from a 1" wide strip of Araldite resin, the central hole being progressively increased in diameter for each test. Their comparison of the distribution of stress difference under loads which produced the same mean tension across the section through the hole centre is shown in Fig. 57. The values obtained for the stress concentration factor based on the net section at the edge of the hole, as shown in Fig. 58, compare favourably with those obtained previously by WAHL and BEEUWKES, and also FROCHT.

#### (ii) Eccentric Circular Hole

Using the model shown in Fig. 59, MINDLIN<sup>(9)</sup> in 1948 investigated the stress distribution along the straight edge of the plate and around the boundary of the hole. The stress variation along the straight edge was found to vary as shown in Fig. 60 with a minimum value at the minimum cross-section. Thus the stress at the minimum section/

Fig. 59.

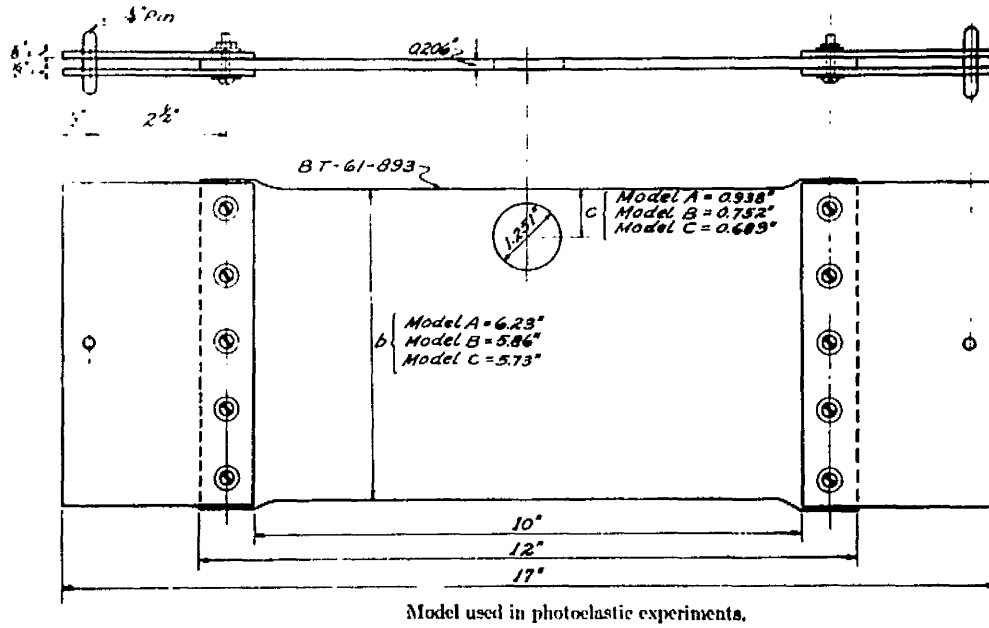
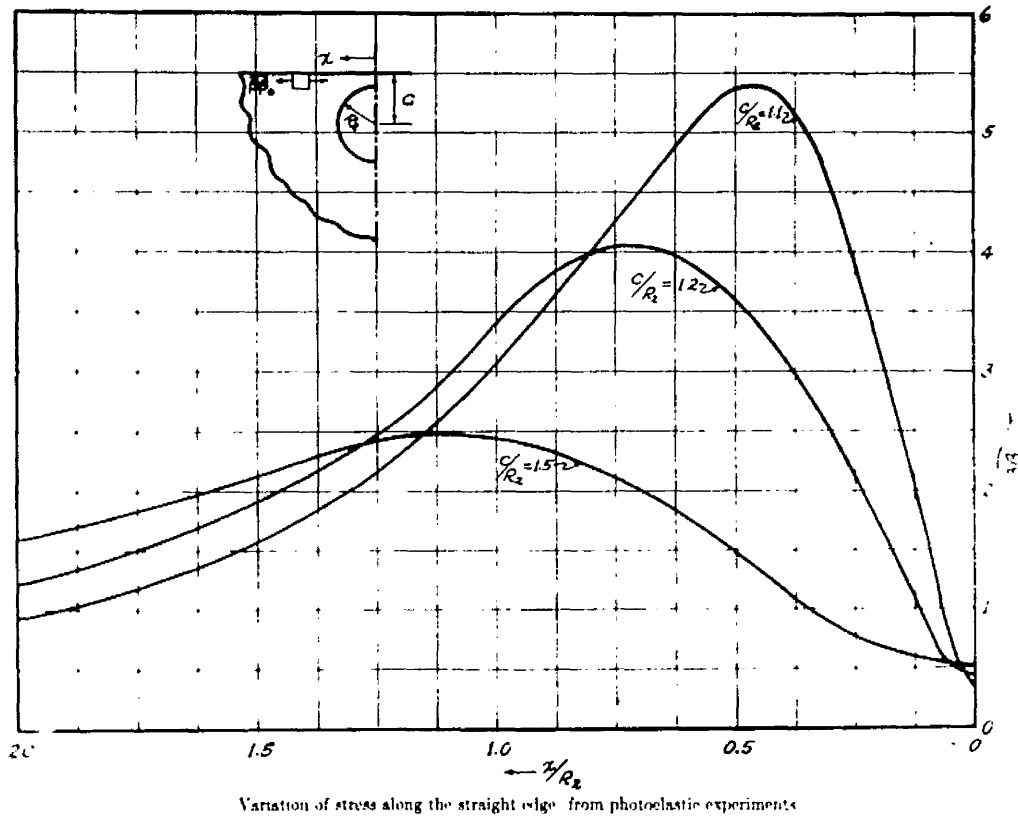
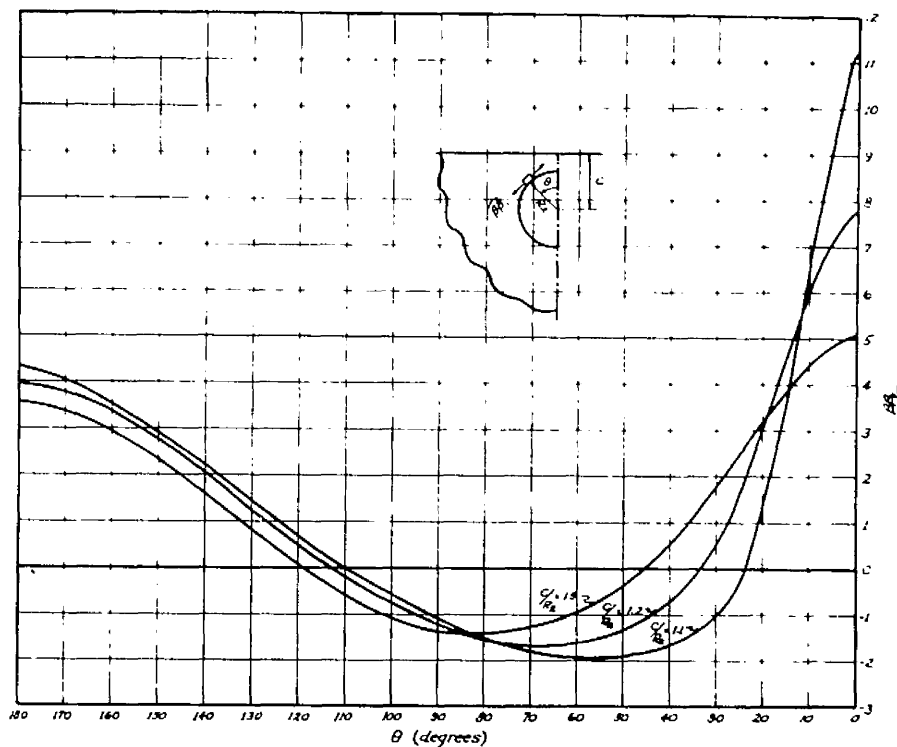


Fig. 60.





section tends to zero, as the ratio  $c/r_2$  tends to unity, which is in agreement with WAHL and BEEUWKES. The variation in the hoop stress round the hole boundary is shown in Fig. 61. Quantitative agreement was observed between these results and MINDLIN'S theoretical results for a semi-infinite plate. Comparison of the experimental and theoretical stress concentration factors at the minimum section of the hole boundary and plate edge are given in Fig. 11, for comparison with the theoretical results.



Variation of stress along the edge of the hole (from photoelastic experiments).

Fig. 61.

# STRESS AT BOUNDARY OF ELLIPTICAL HOLE

CASE  $\frac{a}{b} = \frac{3}{2}$

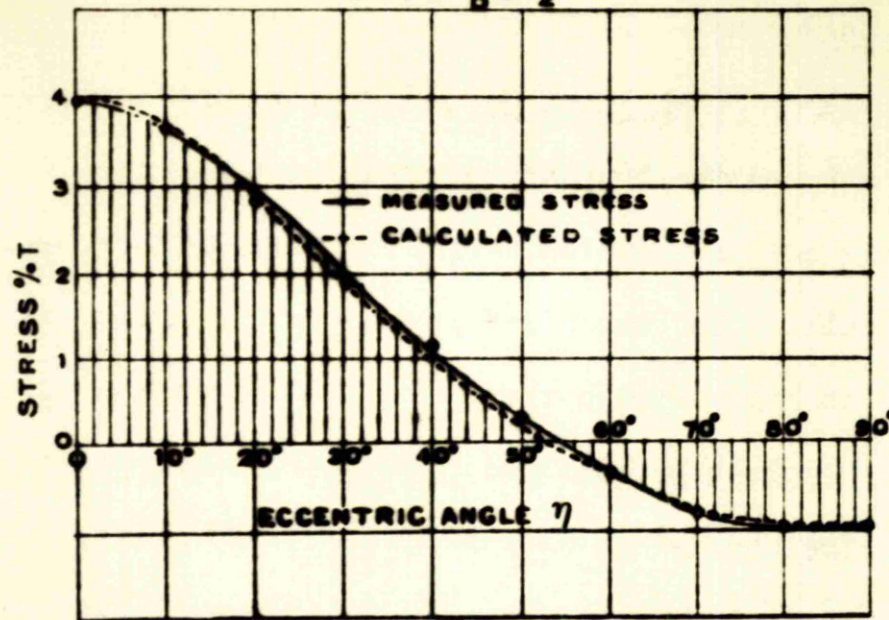


Fig.62.

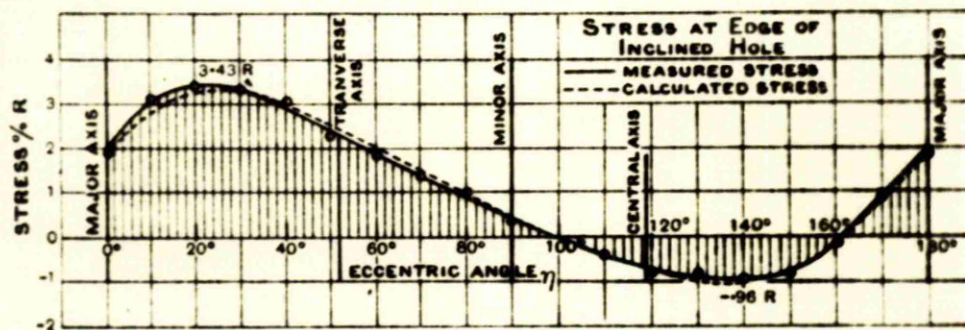


Fig.63.

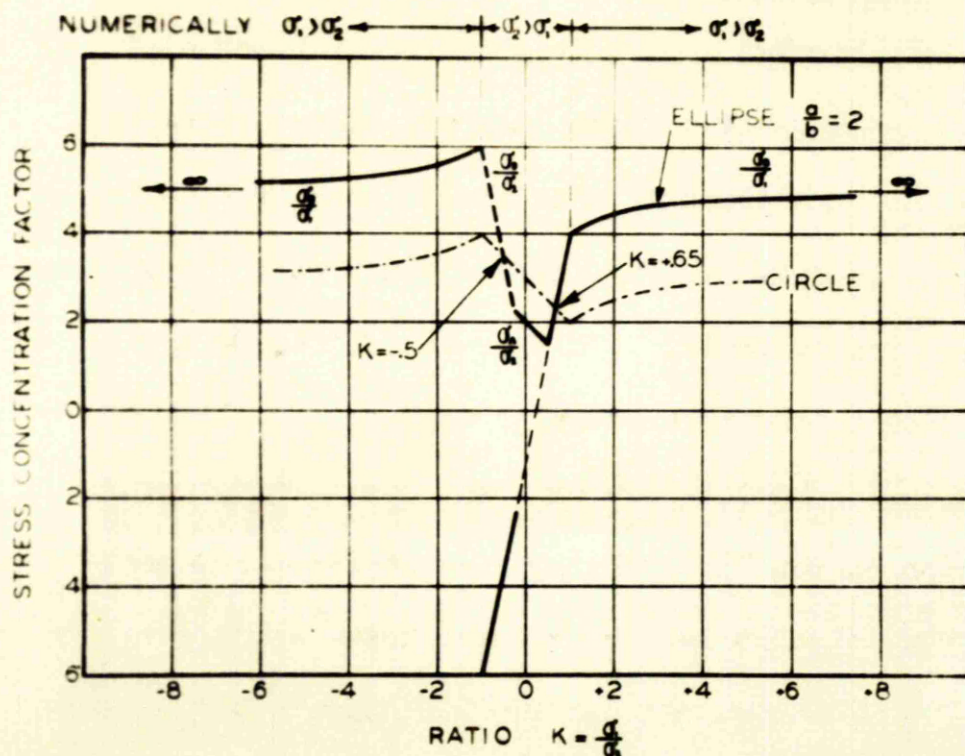


Fig.64.

Stress Concentration Factor as a Function of  $k$

I.2(b) Elliptical Hole

In 1920, COKER and KIMBALL<sup>(51)</sup> investigated the stress concentration round the boundary of an elliptical hole of axes ratio  $3/2$  in a field of pure tension, with the major axis perpendicular to the line of pull. The experimental results for the boundary stresses are compared in Fig. 62 with the INGLIS solution for a plate of infinite width, given by equation (1.8). The same authors investigated the case of an ellipse with the major axis at an angle of  $49^\circ$  to the axis of tension, and the results for this case are compared in Fig. 63 with the INGLIS solution, as found from equation (1.6) with  $\sigma_p = 0$ . Experimental and theoretical results are in good agreement in both cases, and thus indicate that, provided the width of a test specimen is large relative to the width of the discontinuity, the stress distribution closely approximates to that of an infinite plate.

DURELLI and MURRAY<sup>(17)</sup> in 1945 gave results for an elliptical hole of axis ratio  $2/1$  in a wide plate under bi-axial tensions  $\sigma_o$  and  $\sigma_p$ . The parameter  $K = \sigma_o/\sigma_p$  was varied from a negative to a positive value. A graph of the stress concentration factor as a function of  $K$  is given in Fig. 64, together with the corresponding graph for a circular hole. This graph verifies the validity of the statement made in the theoretical treatment of elliptic holes that for uniform stress round the hole boundary, that is for minimum stress concentration factor,  $K = \frac{\sigma_o}{\sigma_p} = \frac{b}{a}$  ( $= 0.5$  for this case). This criterion also applies to the circular hole, which is a special form of an ellipse, in which case  $K = b/a = 1.0$  gives a stress concentration factor of 2.0 as the minimum value.

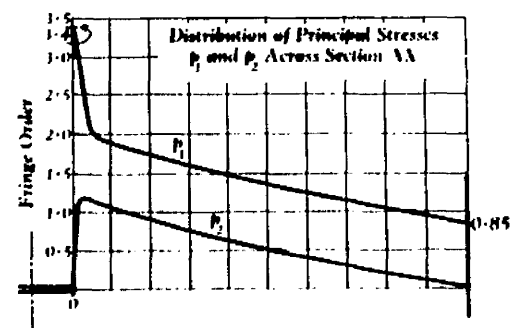
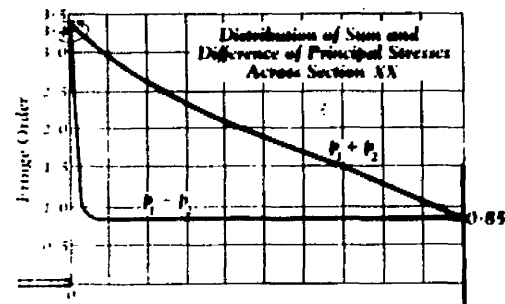
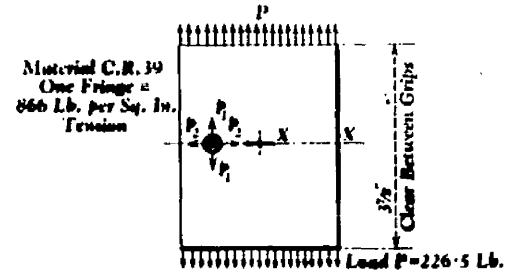


Fig. 65.

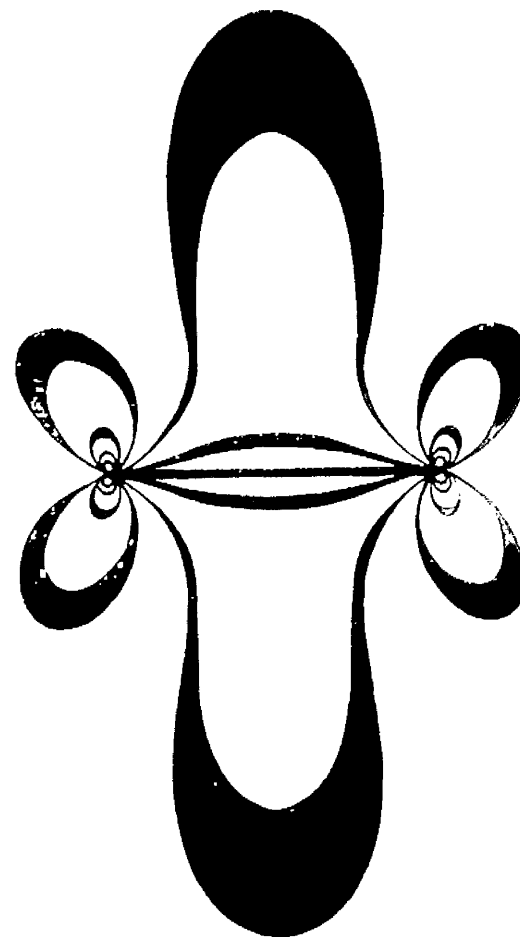


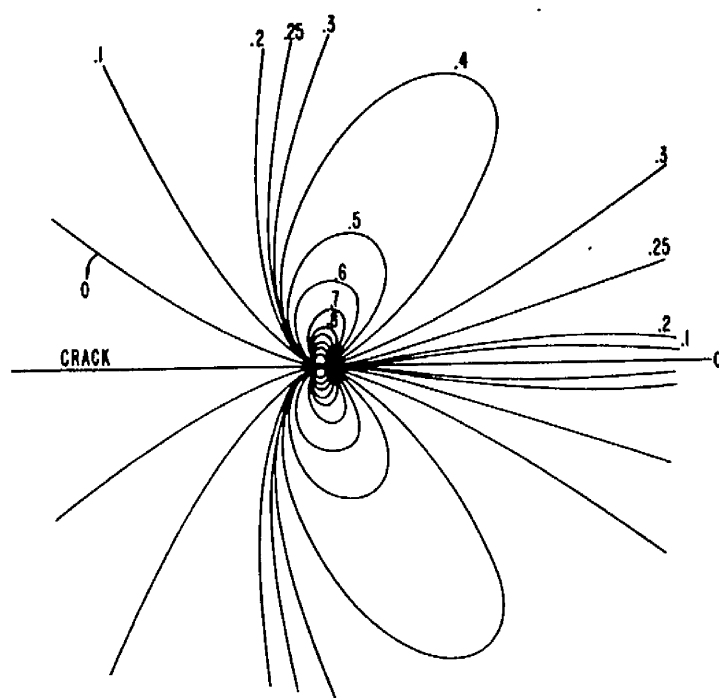
Fig. 66.

I.2(c) Internal Cracks

The major difficulty experienced in the experimental investigations of straight internal cracks lies in producing the crack in a specimen test plate. One method commonly employed is to drill two small holes at the ends of the 'crack' and machine a slot between these two holes. In photoelastic work, drilled holes are best avoided, due to the danger of machining stresses, hence a narrow machined slit gives an approximation to a crack in the plate. The latter technique was used by ROTHMAN and ROSS<sup>(29)</sup> in an investigation of the stress distribution along the axis of symmetry lying in the direction of the crack in a 4" wide tension plate. The machined slit was 0.015" wide and 0.5" long and the stress distribution obtained is shown in Fig. 65. The isochromatic fringe pattern (Fig. 66) shows excellent agreement with the theoretical fringe pattern shown in Fig. 28.

It is also interesting to compare the theoretical pattern with the experimental isochromatic fringe pattern obtained by POST<sup>(27)</sup> for an edge crack as shown in Fig. 67. For the region at the end of the crack, the fringe distributions are seen to be identical, and it is only on the parallel sides of the crack that the secondary effects of location in the plate make themselves apparent.

Unpublished experimental work by DIXON<sup>(52)</sup> in 1956 examined the stress distribution due to a central 'crack' in a flat tension plate. The form of the 'crack' was simulated by connecting two drilled holes of .055" diameter with a slit of .042" width. The effects of plate width/plate length and crack length/plate width were examined, and indicated firstly that the method of loading affected the stress concentration factor/



factor and secondly that an increase in the crack length/plate width value produced an increase in the stress concentration factor, if this were based on the mean stress at the minimum cross-section, or alternatively a decrease if based on the mean stress at the gross cross-section. Since the plate width/crack length ratios used were 5.76, 5.64, 2.44, 1.87 and 1.5 it is evident that infinite plate conditions are not satisfied, and that some deviation from infinite plate theory must be expected, as suggested by DIXON to the writer. This work also examined the effect of 'strain barriers' on the stress distribution around these simulated cracks, and indicated that the barriers had very little effect on the stress concentration factor, unless it were placed 'very near' to the end of the crack.



Fig.68.

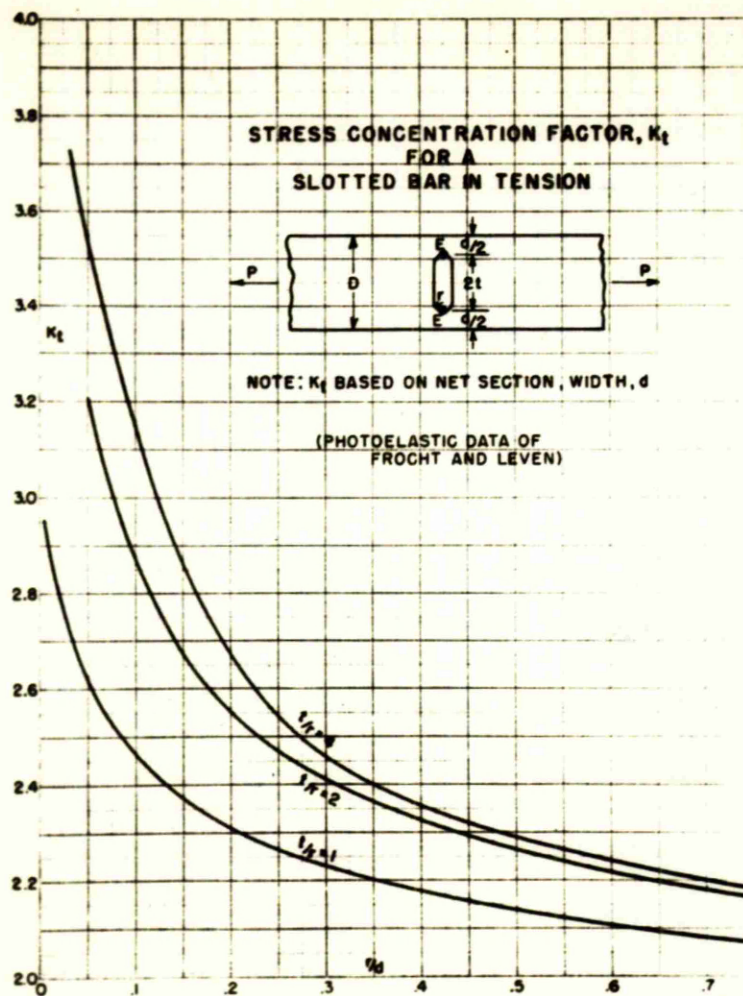
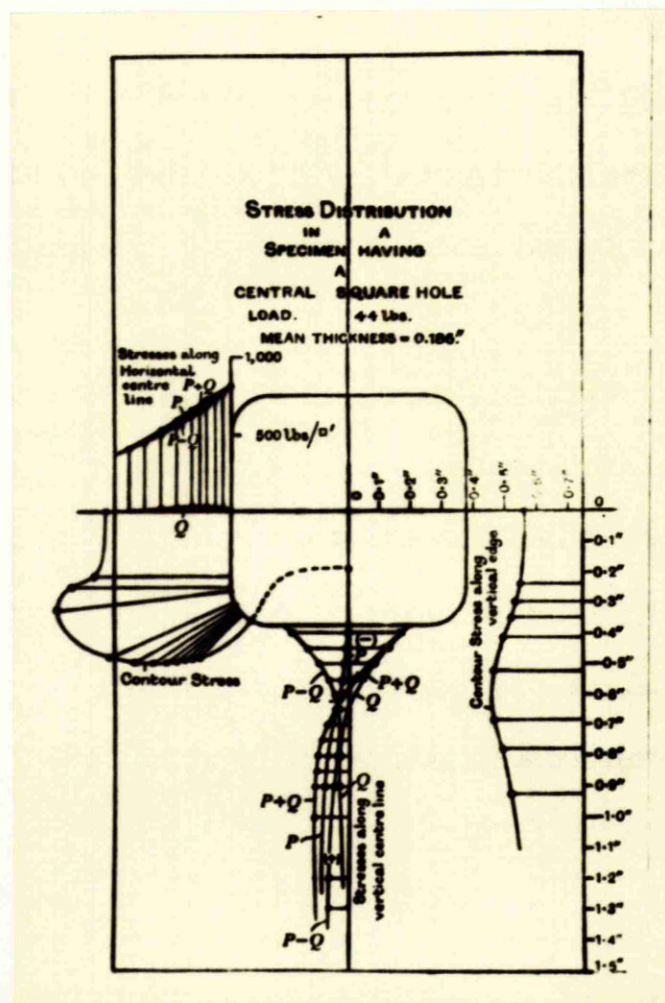


Fig.69.





I.2(d) Miscellaneous Internal Discontinuities

The results of a photoelastic test by FROCHT and LEVEN<sup>(53)</sup> on a slotted bar in tension, were published in 1951. The stress concentration factor based on the net section is shown in Fig. 68, for the cases considered. For the ratio  $t/r = 1$ , the results are in good agreement with HOWLAND'S classical solution for a circular hole in a finite tension member.

COKER and FILON<sup>(15)</sup> investigated the stress distribution caused by a variety of internal forms of opening. One most interesting example was a thin plate under uniform uni-axial compression with a central square hole of width equal to half the plate width and with corner radii equal to one twelfth the plate width. Their stress distribution results are shown in Fig. 69. Points worthy of note are as follows:-

- (i) the maximum hoop stress occurs at a point on the corner radii just immediately away from the straight vertical sides.
- (ii) across the central horizontal section, the longitudinal stress is almost linearly variable, rising to its maximum values at the hole boundary.
- (iii) along the outer vertical edges of the plate, the edge stress is a minimum at the horizontal axis of symmetry and rises to a maximum value at some distance away from the discontinuity.

These findings have been seen to be applicable to the case of a circular hole in a plate of limited width.

A photoelastic investigation on internal discontinuities in wide plates was carried out by the writer<sup>(54)</sup> in 1958, and the experimental solutions for stress concentration factors for a range of geometric/

# FORMS OF DISCONTINUITIES TESTED

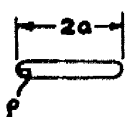
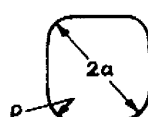
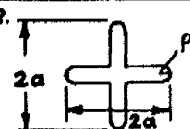
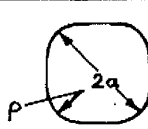
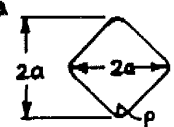
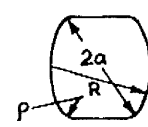

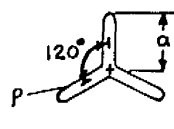
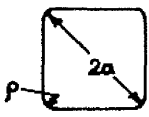
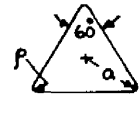
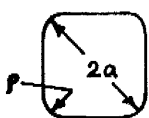
1.  $2a = 0.506''$ $\rho = 0.015''$	7.  $2a = 0.584''$ $\rho = 0.125''$
2.  $2a = 0.500''$ $\rho = 0.015''$	8.  $2a = 0.552''$ $\rho = 0.1875''$
3.  $2a = 0.503$ $\rho = 0.015$	9.  $2a = 0.604$ $\rho = 0.047$ $R = 0.500$
4.  $2a = 0.495''$ $\rho = 0.015''$	10.  $2a = 0.510''$ $\rho = 0.015''$
5.  $2a = 0.695''$ $\rho = 0.015''$	11.  $2a = 0.556''$ $\rho = 0.015''$
6.  $2a = 0.692''$ $\rho = 0.0625''$	

Fig. 70.

geometric forms, as indicated in Fig. 70, are compared with those for INGLIS' equivalent elliptic forms. The detailed experimental results are given in Chapter III of this thesis. It should be noted that this corresponds with the work of COX who investigated the accuracy of using the equivalent elliptic form by comparing theoretical solutions for stress concentration factors for polygonal holes and for deep edge notches with the INGLIS approximate solutions.

The writer suggests that the INGLIS' theory tends to overestimate the stress concentration factor for cases where the equivalent elliptic form is enclosed by the actual discontinuity, whereas if the discontinuity is enclosed by the equivalent elliptic form, the INGLIS value is in agreement with the experimental value.

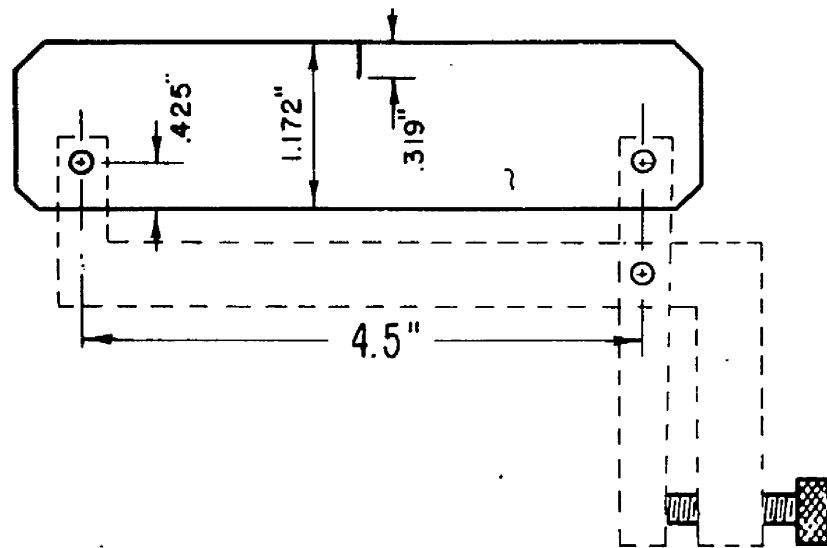


Fig. 71.

I.2(e) External Cracks

The stress distribution around an edge crack was found experimentally by POST<sup>(27)</sup> in 1954, by independent determination of the sums (isopachic pattern) and differences (isochromatic pattern) of the principal stresses. The isopachic pattern indicates minute changes in the model thickness through a simple two beam interference effect, which produces a fringe pattern whose fringe order is proportional to change of thickness.

In certain respects this method is preferable to other photoelastic techniques which may involve graphical work and/or arithmetical computation, and may often be derived from vaguely defined isoclinic lines. However, since distinct interference fringe patterns require a unique velocity of light through the model, the model material must not be permanently or artificially birefringent. Thus the isopachic-isochromatic fringe method requires two models of identical shape to be subjected to identical loading. Another argument against the method is that a change of thickness in a model is a measure of a principal stress sum only where a two dimensional stress system is realised. Where the radius of curvature of the discontinuity is small compared to the thickness of the model, lateral stresses develop in the interior of the model near the discontinuity, and may influence the experimental results. The work of STERNBERG and SADOWSKY<sup>(9)</sup> for a circular hole would, however, indicate that this effect is of negligible magnitude.

The specimen dimensions and method of loading used by POST are shown in Fig. 71, the model thickness and eccentricity of loading being varied. Real cracks were produced by the wedging action of a steel razor blade/

Fig. 72a.

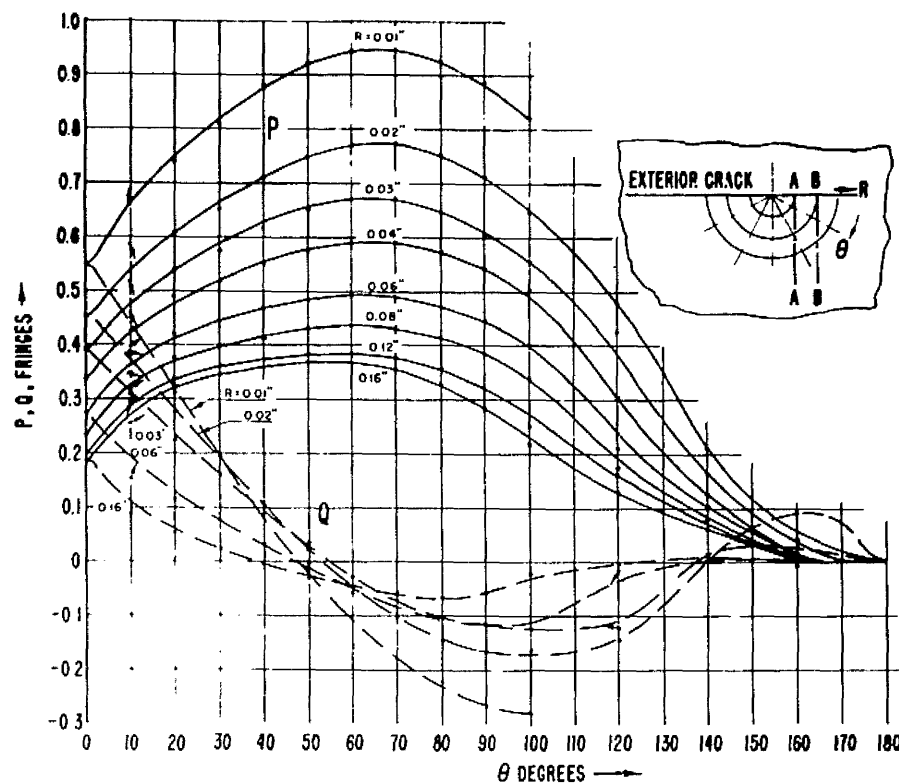
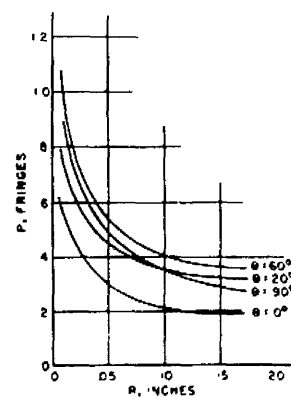
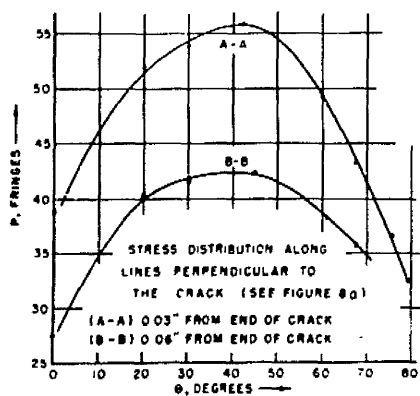


Fig. 72b.



blade inserted in a small machined groove, so that the crack was initiated from the root of the groove and propagated ahead of the blade. The estimated radius of curvature at the root of the crack was  $10^{-4}$  to  $10^{-5}$  ins. The stress distribution round the crack is shown graphically in Fig. 72. Changes of model thickness from  $1/32''$  to  $1/8''$  produced no visible change in the fringe pattern, indicating as expected that the tri-axial stress system which must exist immediately adjacent to the crack does not seriously affect the isochromatic pattern over a very short distance from the crack. The eccentricity of the loading or degree of non-uniformity of the tensile field appeared to have no effect on the orientation and shape of the inner loops of the isochromatic pattern, though the outer loops were slightly affected. One interesting feature is that, contrary to common concepts, the maximum normal stress at a given distance from the root of the crack does not occur directly ahead of the crack but rather at a large angle away from this direction. Also, the stress distribution at the root of the edge crack was found to be very similar to that for an equivalent internal crack (see Page 48). Therefore, POST'S work indicates that the stress gradients around the root of the crack are so severe that the shape and location of the crack, the stress gradients round the root of the crack, and the non-uniformity of the tensile loading, have little effect on the stress distribution at the head of the crack.

The stress distribution along the axis of symmetry through an edge 'crack' was investigated experimentally by ROTHMAN and ROSS<sup>(29)</sup> in 1955. The 'crack' was simulated by a machined slit of  $0.020''$  width and  $0.300''$  depth in a sheet of Columbia Resin  $1/8''$  thick. The stress distribution, as shown in Fig. 73 shows general agreement with POST'S solution for  $\theta = 90^\circ$ .

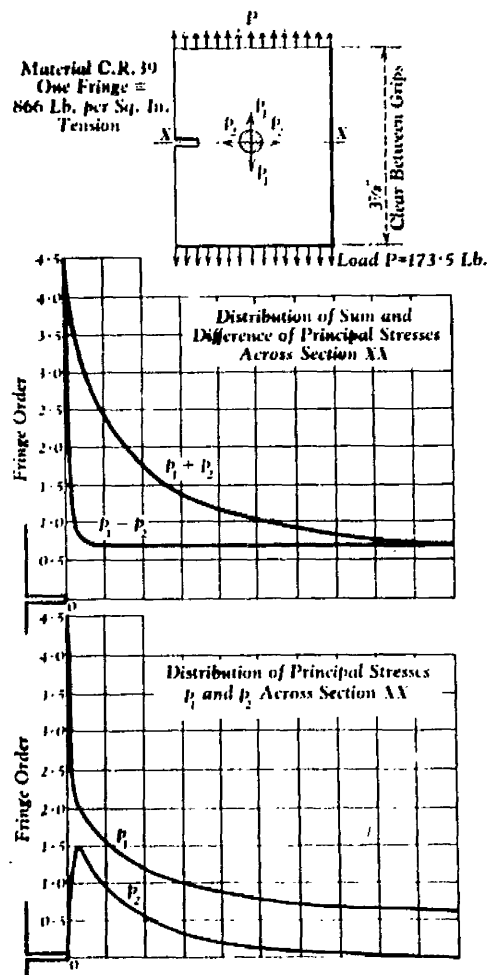


Fig. 73.

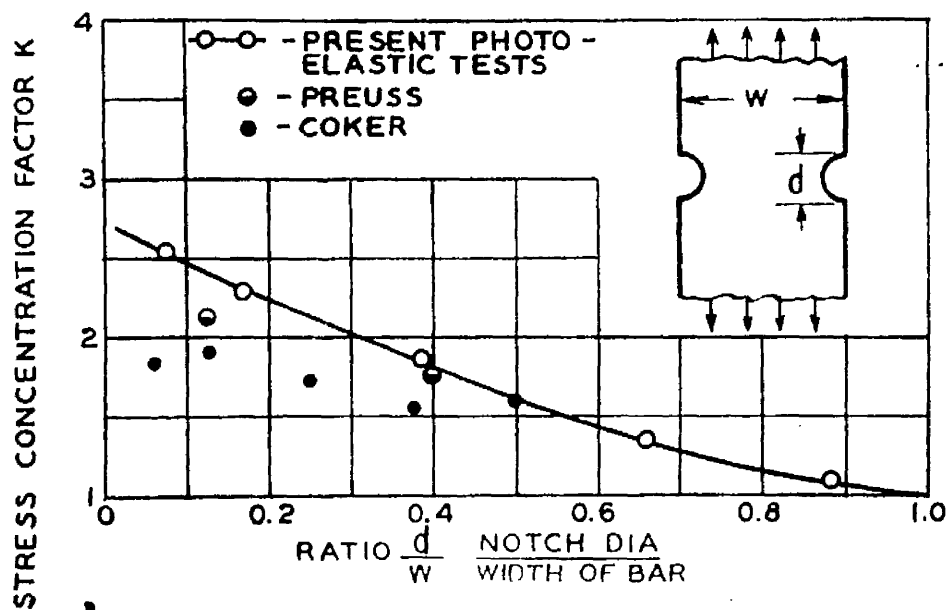


Fig. 74.

STRESS CONCENTRATION FACTOR Vs.  $d/w$  FOR FLAT BAR



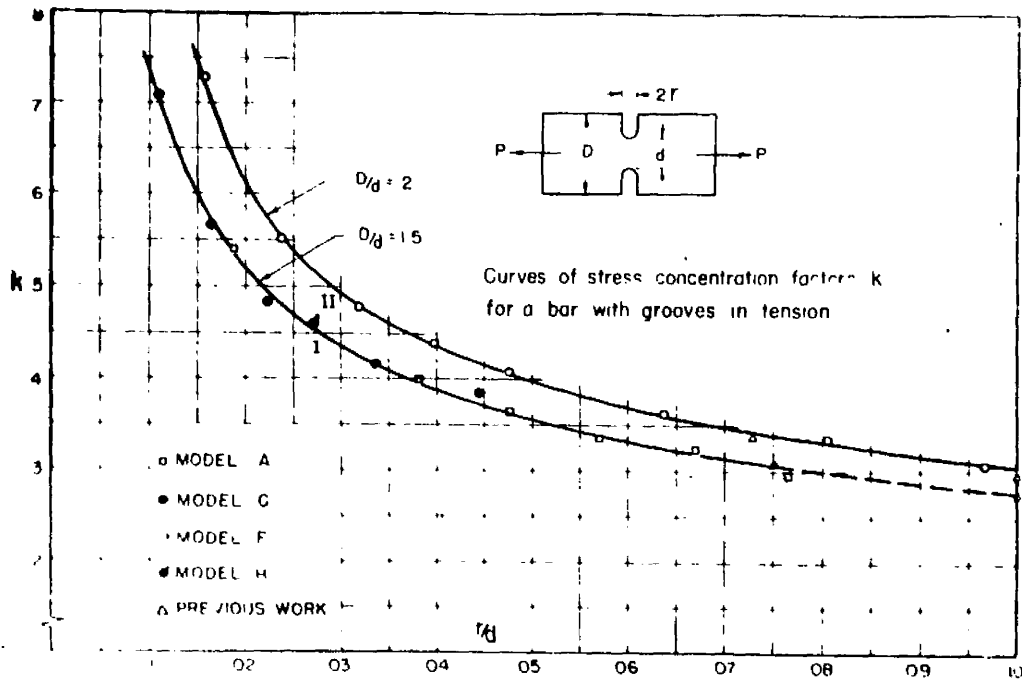


Fig.75.

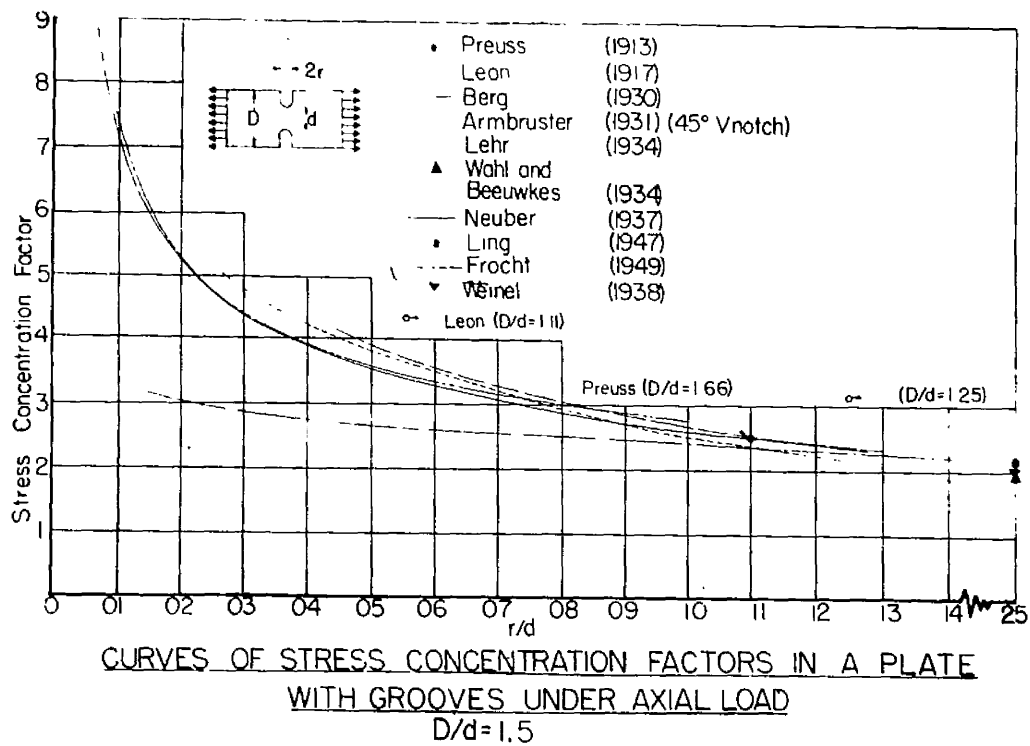


Fig.76.

Fig. 77.

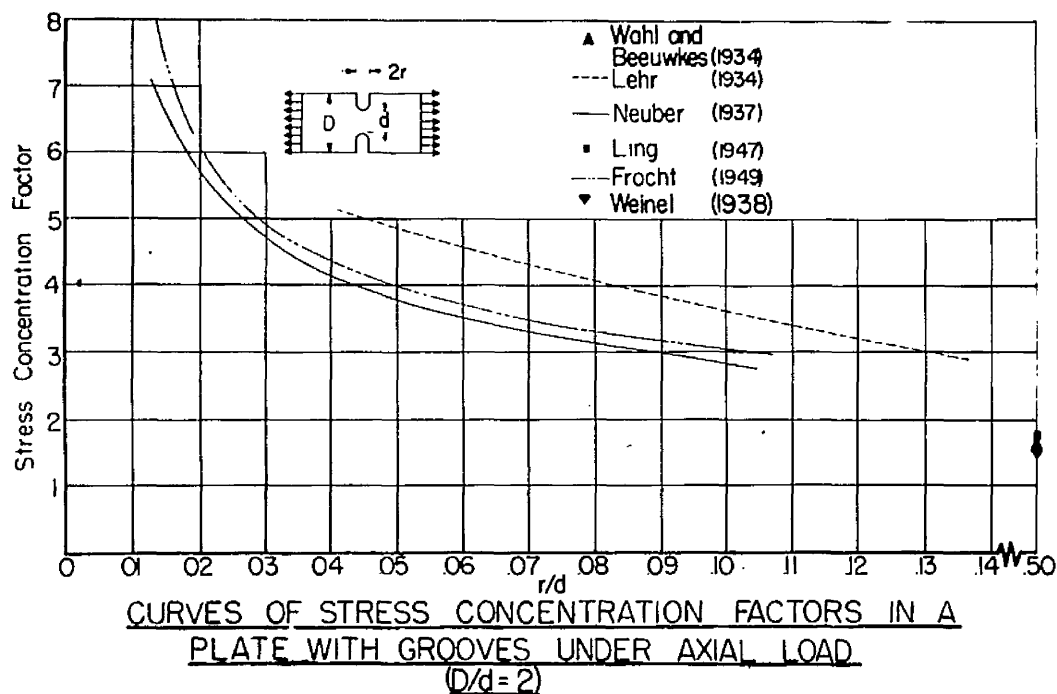
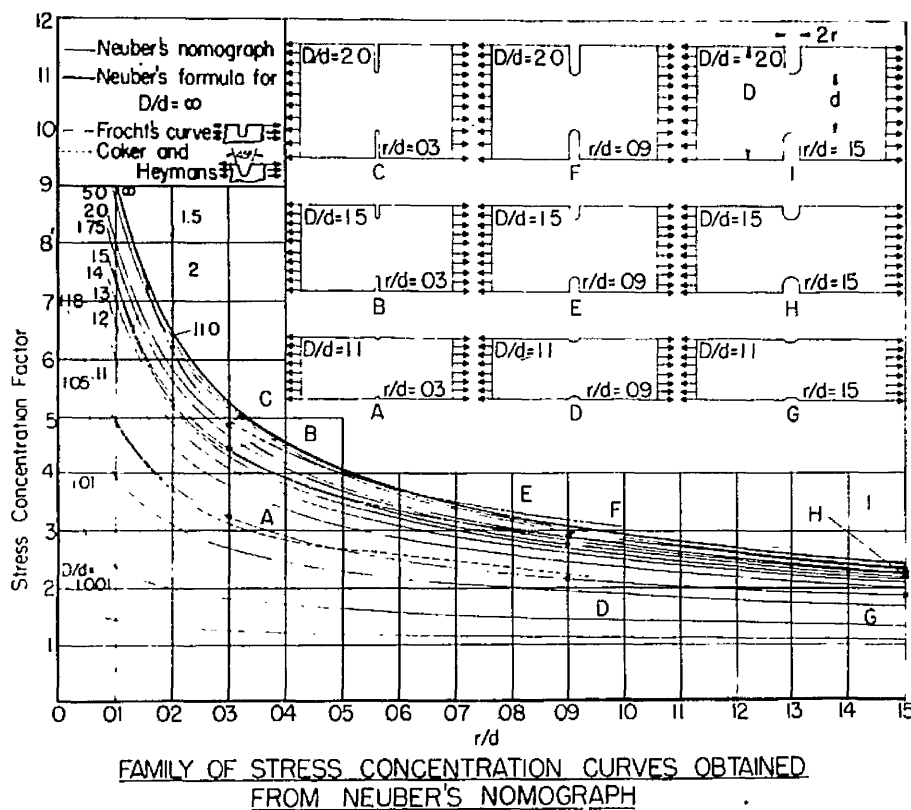


Fig. 78.



I.2(f) External Notches

COKER<sup>(44)</sup> published in 1912 the results of the first photoelastic investigation of the stress concentration effects produced by semi-circular notches in a thin finite plate under simple tension.

A comparison of these results with those obtained by WAHL and BEEUWKES<sup>(46)</sup> in 1934 is given in Fig. 74, indicating that, as in the case of the circular hole, COKER'S results are low, probably due to the use of the compensation method for determining the boundary fringe orders, and perhaps also partly due to the use of the relatively insensitive (and then the only suitable) celluloid material for specimens.

In 1936 FROCHT<sup>(48)</sup>, using the improved experimental light-field technique mentioned earlier, produced results for semi-circular notches, which are compared with those of WAHL and BEEUWKES in Fig. 55. FROCHT also extended the field of investigation of deep and shallow grooves commenced by COKER and HEYMANS<sup>(55)</sup> in 1912. In 1951 FROCHT and LANDSBERG<sup>(56)</sup> published the results shown in Fig. 75 for notches. This graph clearly shows that the stress concentration factor for notches of varying depth increases with increase of notch depth and with decrease in notch root radius.

In a discussion on this paper, DURELLI and JACOBSON<sup>(57)</sup> compiled all the available information from theoretical and experimental sources in the graphical forms shown in Figs. 76, 77 and 78. The theoretical results of NEUBER show closest agreement with FROCHT'S experimental results<sup>(56)</sup>, indicating the reliability for design purposes of NEUBER'S curve for deep and shallow notches.

The/

Fig. 79.

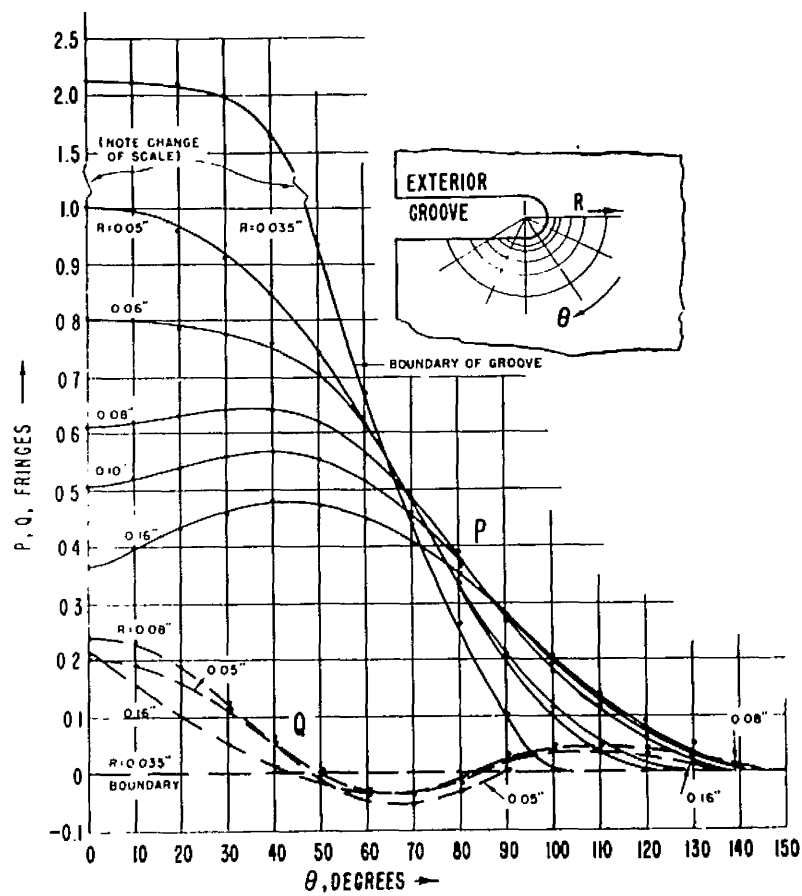
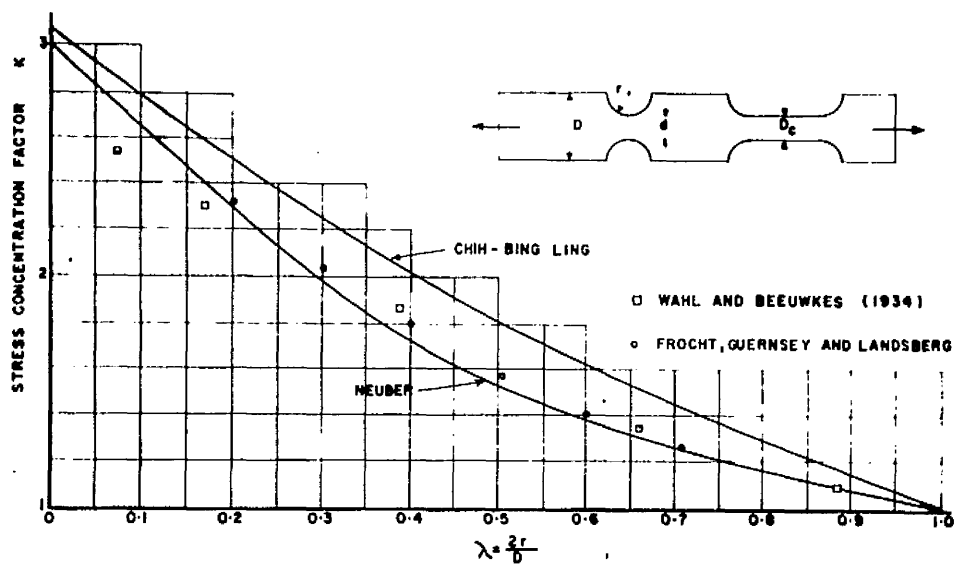


Fig. 80.



The paper by POST<sup>(27)</sup> in 1954, gave also the results of an investigation of the case of a single edge notch of root radius of curvature 0.035" and depth 0.319". This was for comparison of his edge crack case, and the general model dimensions and method of loading were identical to that case (see Fig. 71).

The resulting stress distribution is shown in Fig. 79, showing that as is logically assumed, the largest stress occurs at the intersection of the free boundary with the axis of symmetry. It is notable that for the larger radii there is a tendency for the maximum stress to occur off the axis of symmetry. Hence the maximum principal stress at a given distance from the stress raiser is shown to be largest at a considerable angle away from the axis of symmetry. This resembled the distribution of stress around a crack.

In 1953, FROCHT, GUERNSEY and LANDSBERG<sup>(49)</sup> published a paper comparing the theoretical solutions of NEUBER and LING<sup>(36)</sup> for a semi-circular notch with the latest photoelastic results. In the discussion on this paper, DURELLI<sup>(58)</sup> also included in the comparison the results of WAHL and BEEUWKES (see Fig. 80), which show remarkable agreement with the results obtained from modern tests using the latest techniques and the newest and more sensitive photoelastic materials. The variation between the curves from the theoretical treatments of NEUBER and LING is seen to be too large to be ascribed solely to secondary errors, though NEUBER'S curve again shows the best agreement with the results from photoelastic tests.

HEYWOOD, in his book, analysed the results of the aforementioned photoelastic/

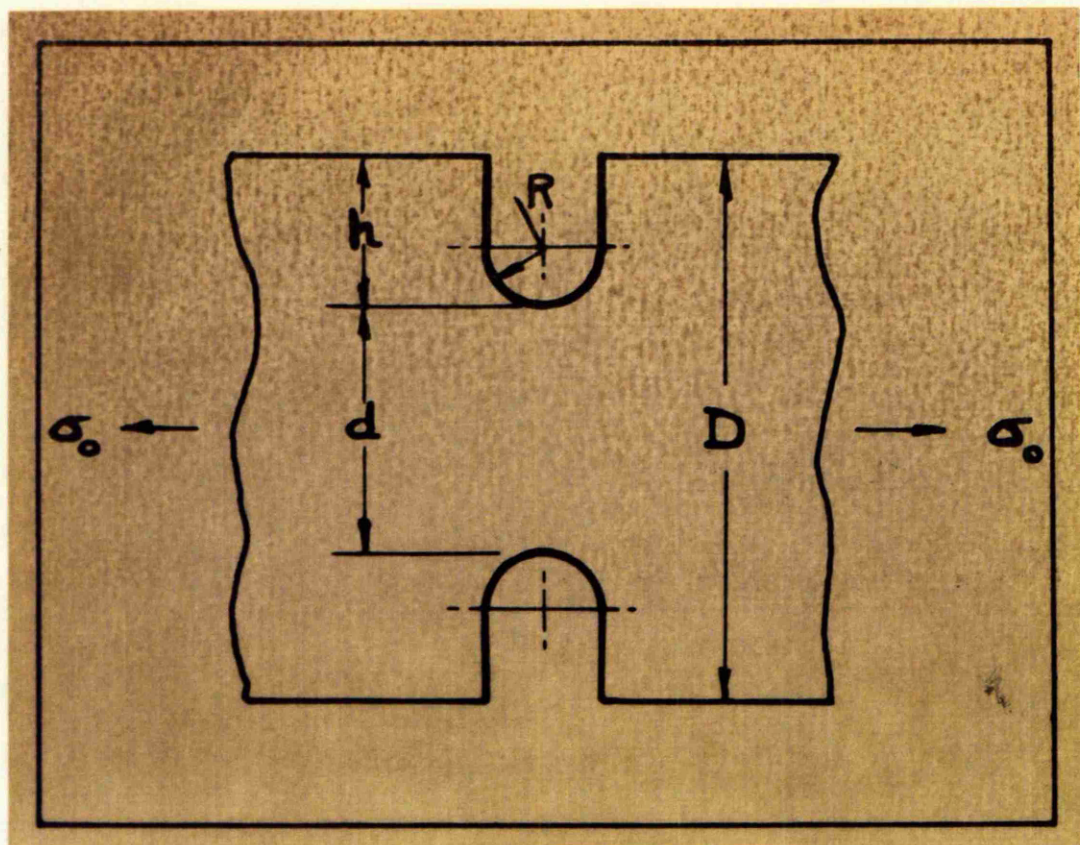


Fig. 81.

photoelastic investigations, and deduced the following empirical formula, which is applicable to shallow, semi-circular and deep notches:-

$$K_t = 1 + \left[ \frac{\Delta - 1}{2(1.55 - 1.3)} \frac{d}{R} \right]^n \dots\dots\dots (1.39)$$

where  $k_t = \frac{\text{maximum stress at base of notch}}{\text{average stress across minimum section.}}$

$$= D/d$$

$$n = \frac{(\Delta - 1) + 0.5 \sqrt{h/r}}{(\Delta - 1) + \sqrt{h/r}}$$

the notation being as shown in Fig. 81.

Fig. 82.

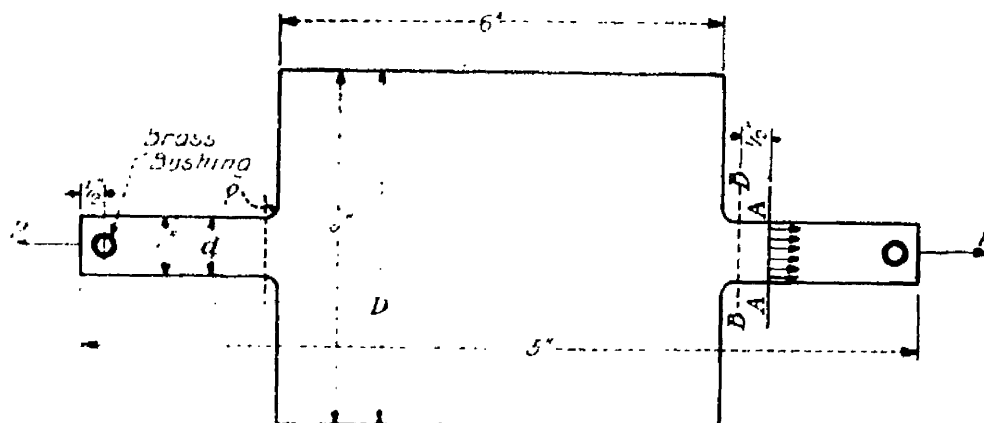
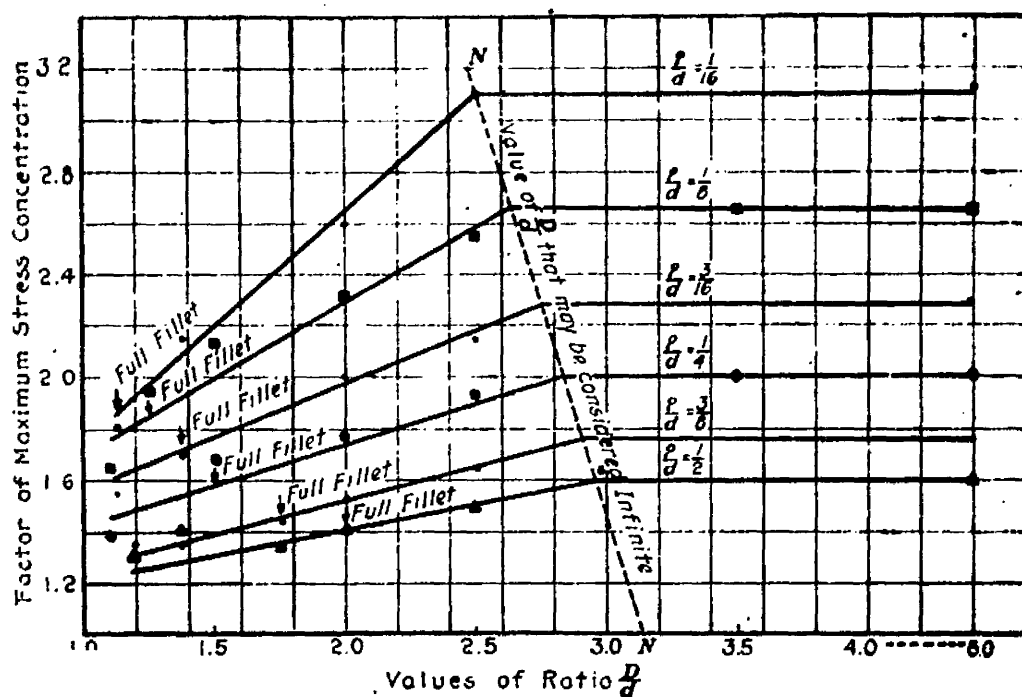


Fig. 83.



CURVES FOR STRESS CONCENTRATION VS. REDUCTION OF CROSS-SECTION



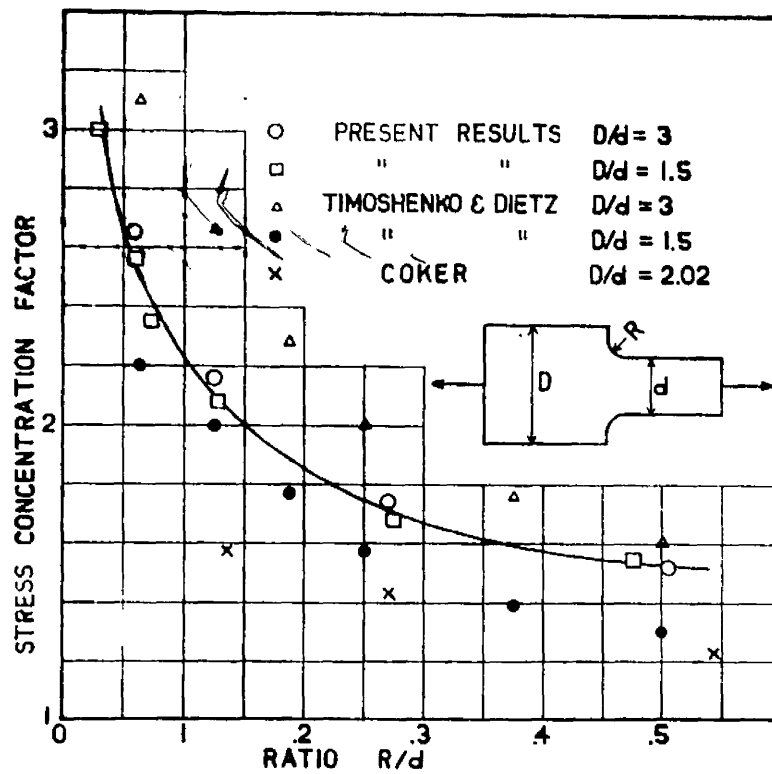


Fig. 84.

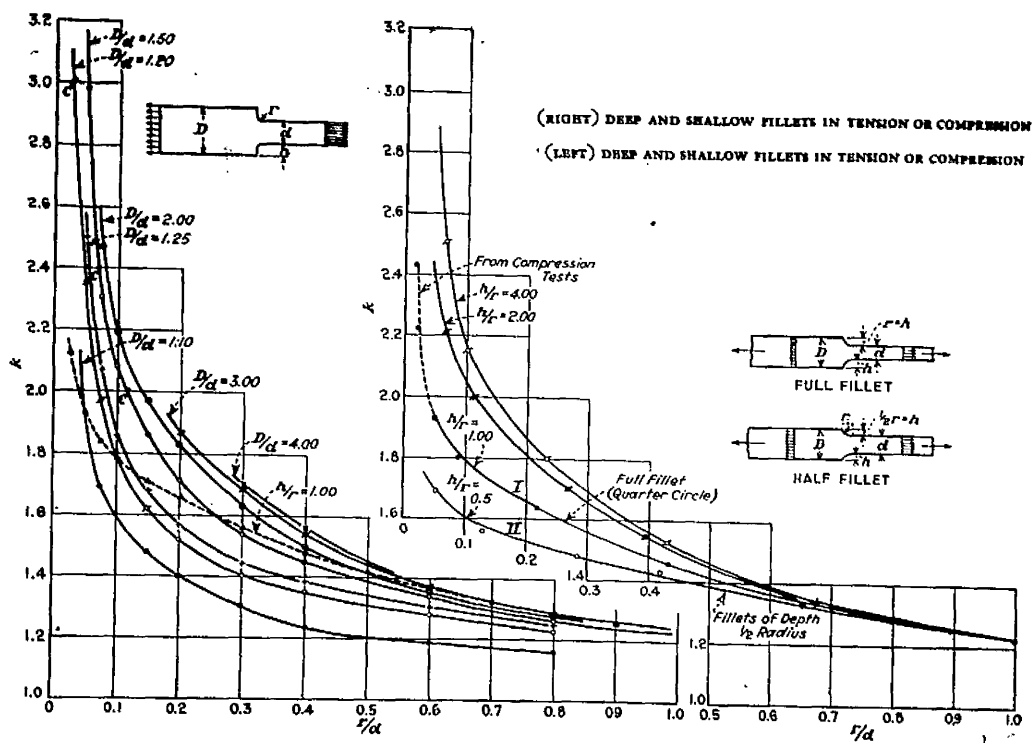


Fig. 85.

Fig. 86.

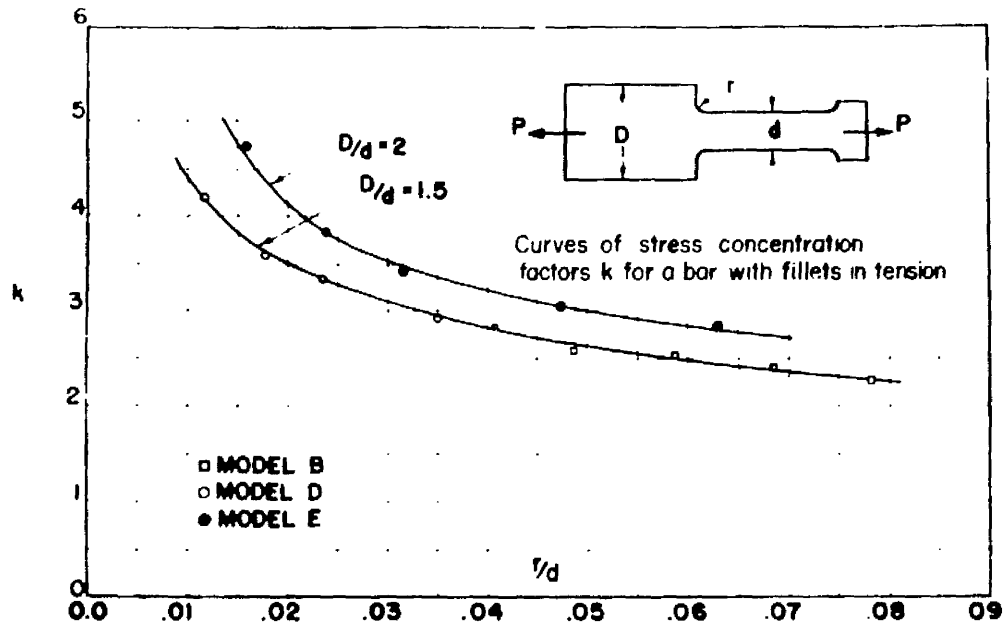


Fig. 87a.

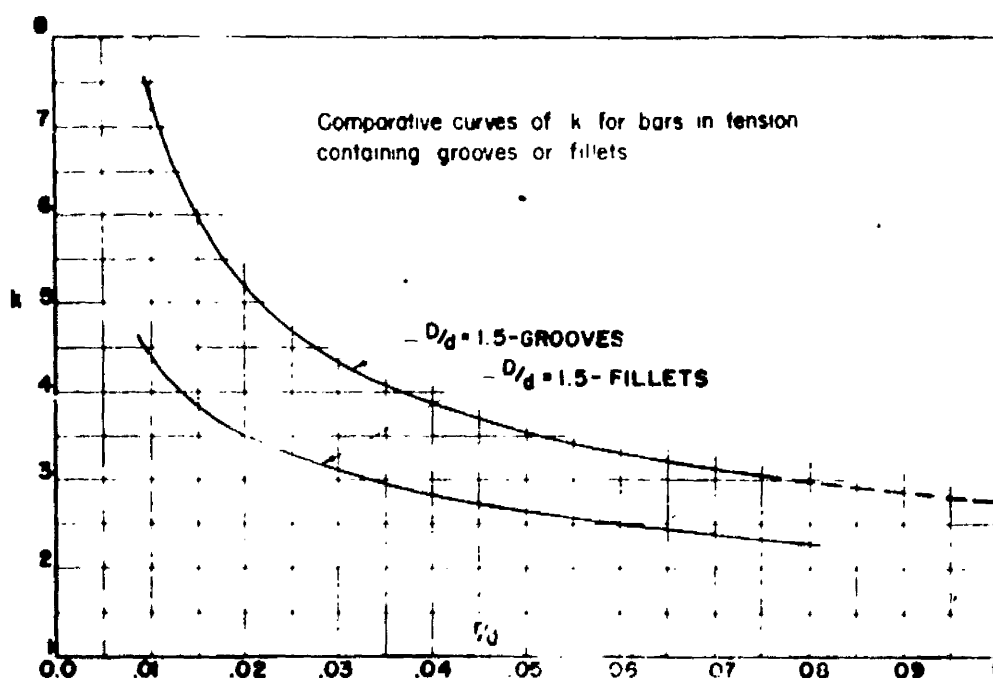
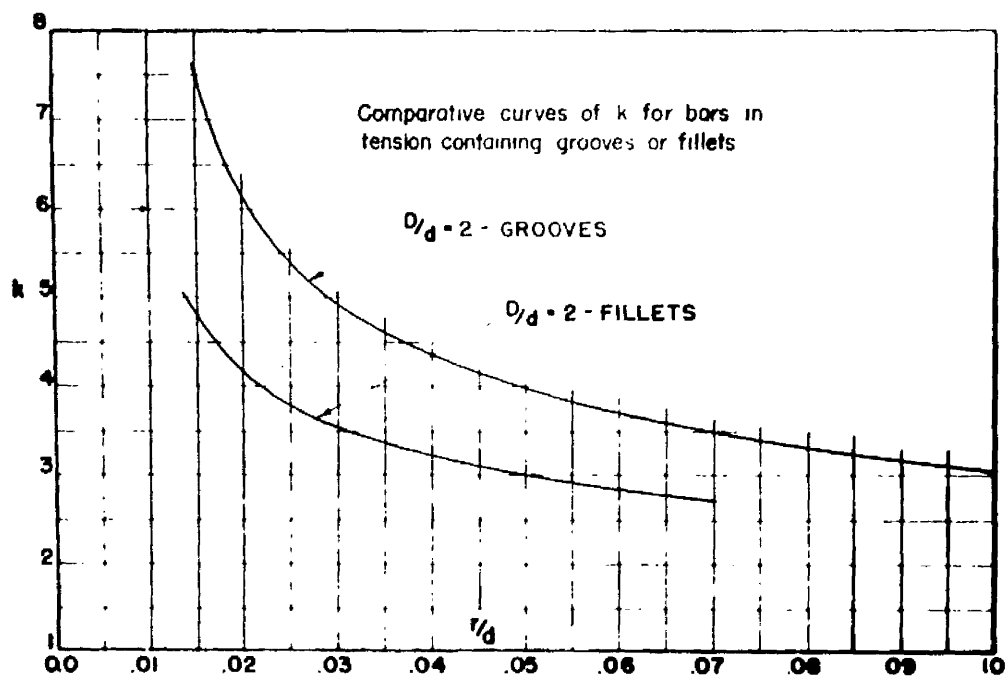


Fig. 87b.



I.2(g) External Fillets

Stress concentration factors for tension members of the form shown in Fig. 82 were determined photoelastically by TIMOSHENKO and DIETZ<sup>(59)</sup> in 1925. Using celluloid models, and the compensation method for stress determination, the results of Fig. 83 were obtained, the stress concentration factor being based on the stress at the minimum section. The graph shows that for a fixed  $\rho/D$  ratio, the stress concentration factor increases with the  $D/d$  ratio until a certain limit is reached, whereupon variation in the width  $D$  no longer materially affects the maximum stress concentration factor at the fillet.

This work extended the original investigation of COKER<sup>(60)</sup> in 1921, who used the same experimental methods. WEIBEL<sup>(61)</sup> in 1934 sought results of higher accuracy by using Bakelite and Phenolite models, with the monochromatic fringe-photograph method. A comparison of his results with those of COKER, TIMOSHENKO and DIETZ is given in Fig. 84. WEIBEL'S results show negligible variation in stress concentration factor with the ratio  $D/d$  for the range considered, which is in contrast with the findings of TIMOSHENKO and DIETZ. In the ensuing discussion on WEIBEL'S paper, however, criticism by FROCHT, WAHL and BEEUWKES produced admission from WEIBEL that, due to the short length of the wide portion of his test specimens, the results might be low for the ratio  $D/d = 3$ .

FROCHT<sup>(48)</sup> published in 1936 the results shown in Fig. 85 and later in 1951<sup>(56)</sup> the results shown in Fig. 86, for a smaller range of  $r/d$  ratios. These results show agreement with those of TIMOSHENKO and DIETZ in that the stress concentration factor increases with decrease in the ratio  $r/d$  and with increase in the ratio of  $D/d$ . However, the range of  $D/d$ ,/

Fig. 88.

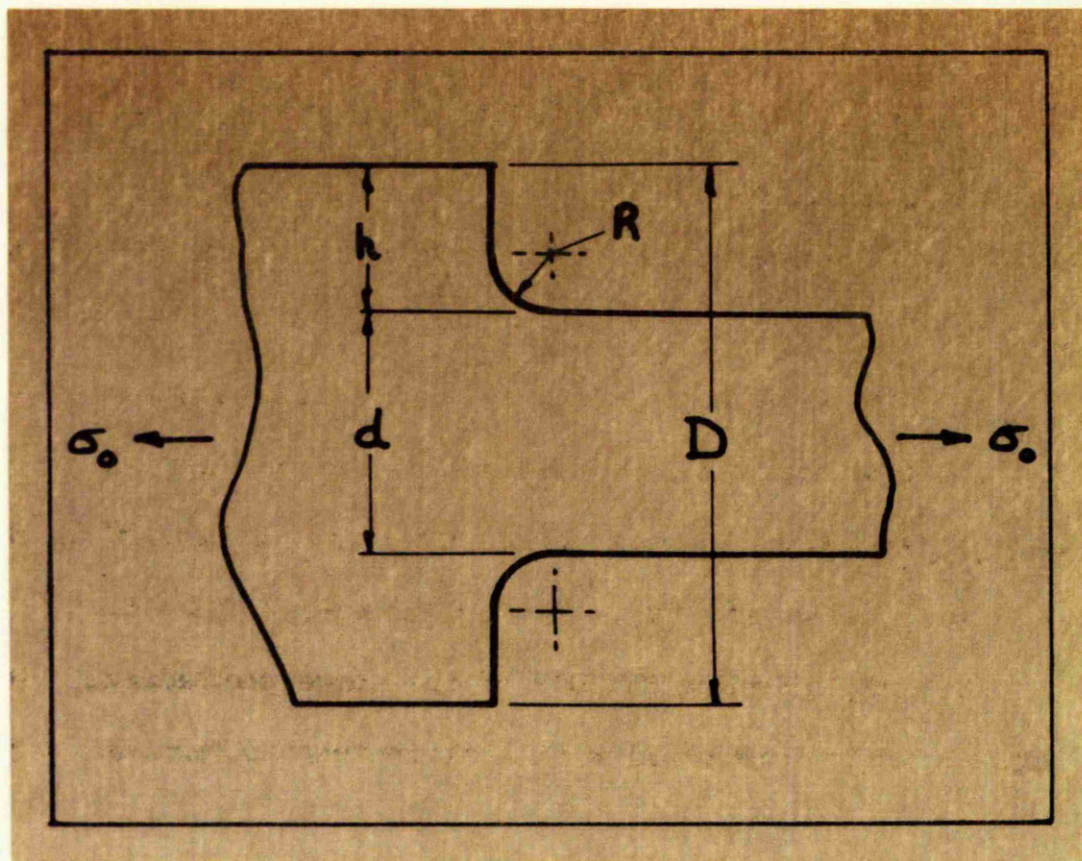
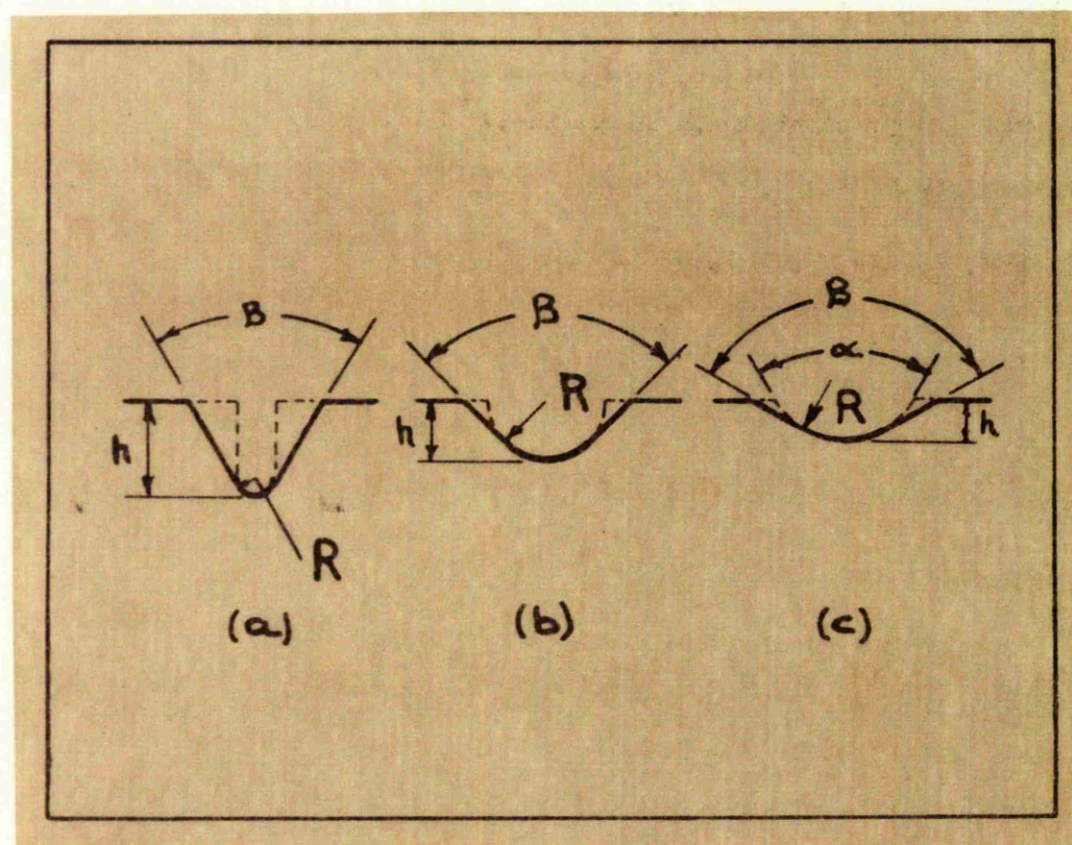


Fig. 89.



$D/d$  used (1.1 - 4.0) was too small to verify the conclusions of TIMOSHENKO and DIETZ with regard to the non-variance of the stress concentration factor with the width  $D$  above a certain value, as indicated by Fig. 85.

It should be noted that, as is logically expected, the stress raising effect of grooves is considerably greater than that of fillets of the same parameters. This is clearly shown in Fig. 87 which is a comparison of the results for  $\frac{D}{d} = 2.0$  from Figs. 75 and 86.

A correlation by HEYWOOD of the above photoelastic results for deep, semi-circular and shallow fillets in tension bars yielded the following empirical formula:-

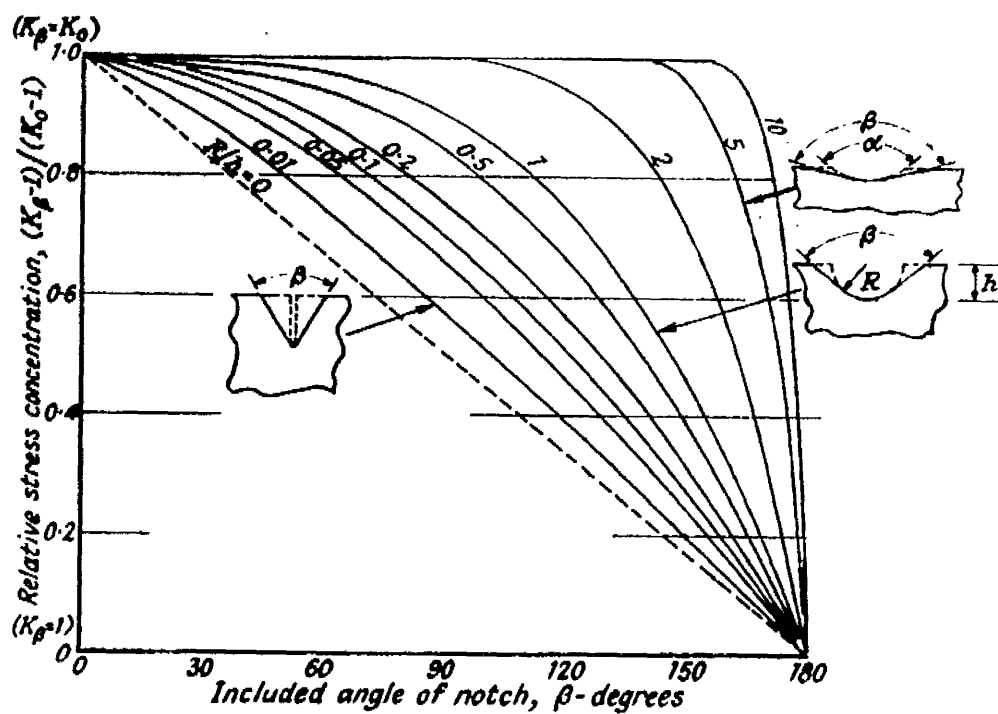
$$K_t = 1 + \left[ \frac{\Delta - 1}{2(2.8\Delta - 2)} \cdot \frac{d}{R} \right]^{0.65} \dots\dots\dots(1.40)$$

where  $k_t = \frac{\text{maximum stress in fillet of shoulder}}{\text{mean stress in minimum section}}$

and  $\Delta = D/d$

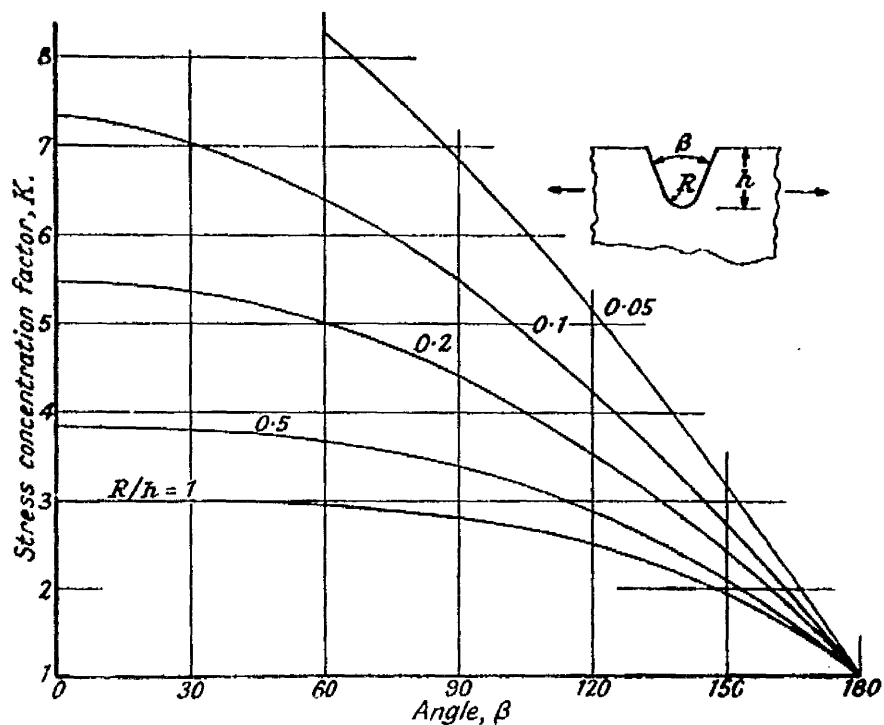
the notation being as shown in Fig. 88.

Fig. 90.



-Relative stress concentration in V grooves compared with that in U grooves.

Fig. 91.



-Effect of included angle on the s.c.f. for a small V groove in a plate loaded in tension.

I.2(h) Miscellaneous External Discontinuities(i) Vee grooves

Vee grooves of the form shown in Fig. 89 should obviously be expected to have lower stress concentration factors than the corresponding parallel-sided notches, as in the former case there is a greater tendency to streamline the lines of principal stress. An analysis by HEYWOOD of the conditions obtaining in the vee groove, led to an empirical estimate of the correction necessary to allow for the effect of the groove angle  $\beta$  on the stress concentration factor.

If  $k_0$  = Stress concentration factor for a notched plate of the form shown in Fig. 81.

and  $k_\beta$  = Stress concentration factor for the corresponding grooved plate conforming to the series shown in Fig. 89, and the notation for  $d$ ,  $D$  etc. is as shown in Fig. 81, then for the cases (a) and (b) of Fig. 89

$$k_\beta = 1 + (k_0 - 1) \left[ 1 - \left( \frac{\beta}{180} \right)^1 + 2.4 \sqrt{R/h} \right] \dots\dots\dots (1.41)$$

and for case (c) where the ratio  $R/h$  is greater than unity,

$$k_\beta = 1 + (k_0 - 1) \left[ 1 - \left( \frac{\beta - \alpha}{180 - \alpha} \right)^1 + 2.4 \sqrt{R/h} \right]$$

These results are applicable to any type of plate loading for which the stress concentration factor  $k_0$  is available. A pictorial representation of the stress concentration factors for all shapes of vee groove is given in Fig. 90.

For the particular case of a relatively small groove with

$k_0 = 1 + 2 \sqrt{h/r}$  (INGLIS approximate form), the stress concentration/

Fig.92.

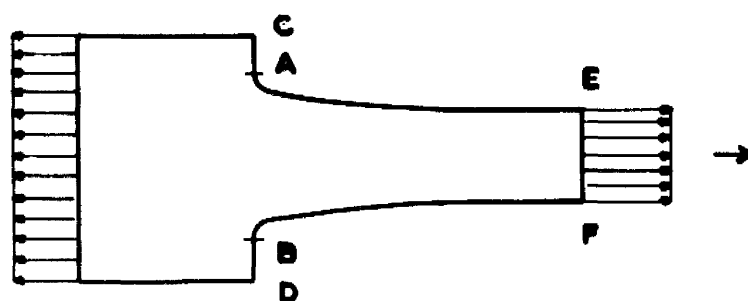
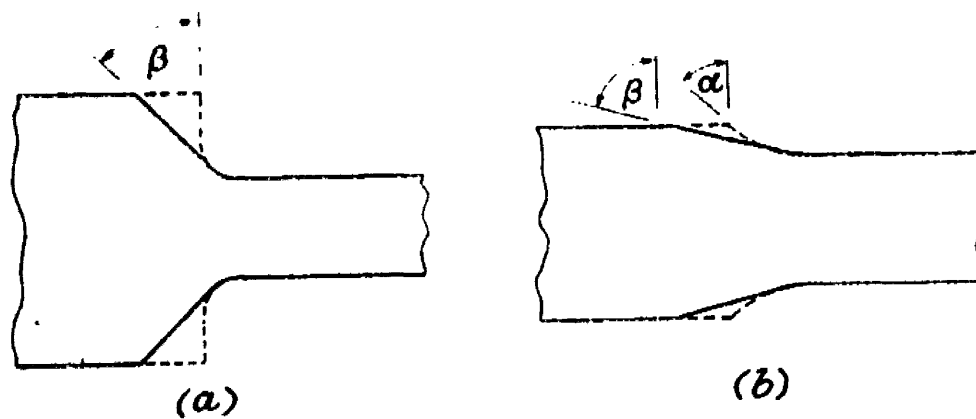
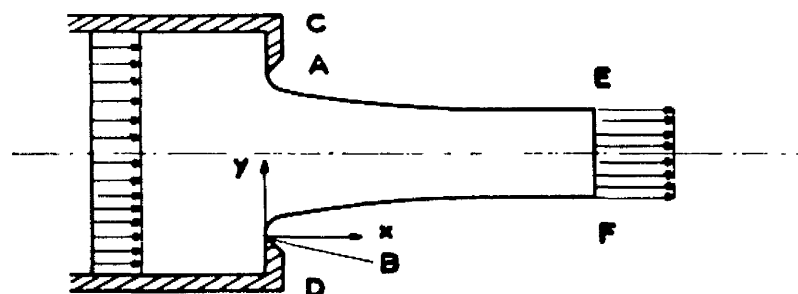


PLATE IN TENSION.

Fig.93.



TWO-DIMENSIONAL FLOW THROUGH A SLOT  
(OR THREE-DIMENSIONAL FLOW THROUGH A  
CIRCULAR ORIFICE).



concentration factor  $k_\beta$  is given directly in terms of  $R/h$  and angle  $\beta$ , and varies as shown in Fig. 91.

Figs. 90 and 91 indicate that the stress concentration factor  $k_\beta$  is especially sensitive to the approach of the inclined sides of the groove to the highly stressed region at the root radius on the section of symmetry.

(ii) Inclined shoulder fillets

For inclined shoulders of the form shown in Fig. 92, the stress concentration factor is again reduced due to the more gradual change in profile. HEYWOOD determined an empirical relationship with the stress concentration factor for standard fillets, as follows:-

$$\text{Case a} \quad k_\beta = 1 + (k_0 - 1) \left[ 1 - \left( \frac{\beta}{90} \right)^{1 + 2.4 \sqrt{R/h}} \right] \dots\dots\dots (1.42)$$

$$\text{Case b} \quad k_\beta = 1 + (k_0 - 1) \left[ 1 - \left( \frac{\beta - \alpha}{90 - \alpha} \right)^{1 + 2.4 \sqrt{R/h}} \right] \dots\dots\dots (1.43)$$

where  $k_0$  is the stress concentration factor for the standard shoulder, and  $k_\beta$  is the stress concentration factor for the inclined shoulder.

(iii) Streamline shoulder fillet.

Circular fillet radii at shoulders always produce stress concentration effects, but the ideal condition would be an optimum fillet profile giving constant stress along its boundary. LANSARD<sup>(62)</sup> in 1955 tested progressive curvature fillets which gave a close approximation to the optimum condition. The profile was obtained from an analogy with two dimensional flow through a slot of constant width (Fig. 93), the equivalent plate in tension being as shown. The profile co-ordinates are/

are given by

$$x = a \frac{V_1}{2\pi} \left[ L \frac{1 + \cos \theta}{1 - \cos \theta} - \frac{1}{2} \left( \frac{1}{V_1} - V_1 \right) L \frac{1 + V_1^2 + 2V_1 \cos \theta}{1 + V_1^2 - 2V_1 \cos \theta} \right] \dots\dots(1.44)$$

$$y = a \frac{V_1}{2\pi} \left( \frac{1}{V_1} - V_1 \right) \left[ 2 \tan^{-1} V_1 - \tan^{-1} V_1 \frac{2V_1 \sin \theta}{1 - V_1^2} \right] \dots\dots\dots(1.45)$$

where  $L$  = Napierian Logarithm.

$a$  = plate width.

$V_1$  = ratio of initial velocity to velocity in section EF.

$\theta$  = angle of profile tangent at point  $(x, y)$ .

Thus, use of this form of blending curve decreases the danger of failure by fatigue. Elliptical fillets reduce the stress concentration factor and CHAFFMAN<sup>(63)</sup> gave an illustration of achieving an increase of 30% in the 'bursting' speed of a high speed compressor wheel on changing from a circular to an elliptical fillet profile.

CHAPTER I. 3.      CRITICAL SUMMARY

### I.3 Critical Summary

The review of published literature on two dimensional cases of stress concentration has shown that a considerable amount of work, both theoretical and experimental, has been carried out regarding the stress concentration effects of discontinuities of various geometric forms.

There is however, a very marked lack of analytical work on discontinuities in the form of edge or internal cracks, and in particular, cracks of the cruciform type. Regarding the last mentioned the work of ROTHMAN, who used the tentative method of solution by complex potentials is the only one known to the writer.

The different theoretical methods have their own advantages and limitations, but it is apparent that the method of complex potentials is mathematically the most elegant.

With reference to the experimental results reviewed, these in general are seen to be in agreement with their respective analytical solutions. However, while much has been accomplished in the verification of these analytical solutions for certain forms of discontinuities, such as circular and elliptic holes, etc., there is an evident lack of experimental corroboration of the results for other geometric forms of discontinuities. Few experimental results have been published for rectangular forms and none at all have appeared for triangular, and barrel-shaped discontinuities, or for 'star' and 'cruciform' type cracks.

Dealing with the question of the application of the theoretical and experimental results to design, the only significant attempts at an integrated/

integrated approach have been made by COX, PETERSON and HEYWOOD, and these are not all-embracing in their scope.

The theoretical and experimental work of this thesis was planned with the foregoing deficiencies in view, and consequently it was arranged to cover the following:-

- (1) Theoretical analysis of the stresses around a cruciform type crack in a tension plate.
- (2) Theoretical evaluation of the stress concentration factors for selected forms of discontinuities such as square and triangular openings, and for star-type cracks, in plates in uniform tension.
- (3) Experimental investigation of the cruciform crack type discontinuity.
- (4) Experimental determination of the stress concentration factors for a variety of discontinuities, including those examined theoretically.
- (5) Preparation of a semi-empirical 'Design Chart' giving correlation of the theoretically and experimentally determined stress concentration factors, in a form which may rapidly give these factors without recourse to lengthy calculations.

## CHAPTER II - THEORETICAL ANALYSIS

### PART 1.      THE METHOD OF COMPLEX POTENTIALS.

(Note: The subject matter presented in the text is a Summary form of the more detailed treatment given in Appendix Chapter VII.1.)

NOTATION

The theoretical presentation follows GODFREY'S translation of SAVIN'S work, the notation used being as follows:-

$x, y$ .....	Cartesian co-ordinates
$\rho, \theta$ .....	Curvilinear co-ordinates
$\frac{Z}{\bar{Z}} = \frac{x + iy}{x - iy}$ } .....	Conjugate complex variables
$\frac{\xi}{\bar{\xi}} = \frac{\xi + i\eta}{\xi - i\eta}$ } .....	" " "
$\sigma_x, \sigma_y, \tau_{xy}$ .....	Components of stress in cartesian co-ordinates.
$\sigma_\rho, \sigma_\theta, \tau_{\rho\theta}$ .....	Components of stress in curvilinear co-ordinates.
$\sigma_o, \sigma$ .....	Principal stresses at infinity.
$\Theta = \sigma_x + \sigma_y$ .....	Combinations of stress components.
$\Phi = \sigma_y - \sigma_x + 2i\tau_{xy}$ .....	" " "
$\Theta' = \sigma_\rho + \sigma_\theta = \Theta$ .....	" " "
$\Phi' = \sigma_\theta - \sigma_\rho + 2i\tau_{\rho\theta}$ .....	" " "
$= e^{2i\alpha} \Phi$ .....	Where $\alpha$ is the angle between the normal to the curve $\rho = \text{constant}$ and the $x$ - axis.
$\phi(Z), \psi(Z)$ .....	Complex potentials.
$\mu$ .....	Modulus of Rigidity.
$\nu$ .....	Poisson's ratio.

BASIC EQUATIONS IN COMPLEX POTENTIAL FORM.(i) Conformal Transformation:

The SCHWARTZ-CHRISTOFFEL transformation is<sup>(4)</sup> used to map the region exterior to a hole in a plate on to the region inside the unit circle and is of the form

$$Z = \omega(\zeta) = R \frac{1}{\zeta} + m_1 \zeta + m_2 \zeta^2 + \dots + m_n \zeta^n \dots\dots\dots (2.1)$$

where  $m_1, m_2$  etc. are numerically less than unity, and diminish as the power of  $\zeta$  increases.

(ii) Stress - Complex Potential Equations:

Conditions of equilibrium are satisfied if

$$\frac{\partial \Phi}{\partial \bar{Z}} - \frac{\partial \bar{\Phi}}{\partial Z} = 0 \dots\dots\dots (2.2)$$

and the conditions of compatibility are satisfied if

$$\frac{\partial^2 \Phi}{\partial Z \partial \bar{Z}} = 0 \dots\dots\dots (2.3)$$

Thus  $\Phi$  which is real, may be expressed in the form

$$\Phi = 2 \left[ \phi'(Z) + \bar{\phi}'(\bar{Z}) \right] \dots\dots\dots (2.4)$$

where the dashes denote differentiation with respect

to the bracketed variable, and the bars denote the

conjugate complex quantity. Also, substitution for  $\Phi$

in (2.2) and integrating gives

$$\bar{\Phi} = 2 \left[ \bar{Z} \phi''(Z) + \psi'(Z) \right] \dots\dots\dots (2.5)$$

Thus the stress components at any point in the plane may

be determined from two complex potentials  $\phi(Z)$  and

$\psi(Z)$  in terms of which all other quantities may be obtained.



(iii) Boundary Condition and Resultant Force on the Boundary.

The boundary condition may be shown to be

$$f_1 + if_2 + \text{constant} = \phi(Z) + Z\bar{\phi}'(\bar{Z}) + \psi(Z) \dots\dots\dots(2.6)$$

If (X, Y) are the components of the resultant force on the hole boundary L, and  $Ry.f(Z)$  is the change in  $f(Z)$  where Z makes one circuit of L, then the boundary condition is satisfied when

$$X + iY = -\frac{1}{4}iRy \left[ \phi(Z) + Z\bar{\phi}'(\bar{Z}) + \bar{\psi}(\bar{Z}) \right] \dots\dots\dots(2.6a)$$

(iv) The Displacement:

If  $D = u + iv$  is the complex displacement in the x, y plane, then the stress combinations  $\phi$  and  $\Theta$  may be written as  $\phi = -4\mu \frac{\partial \bar{D}}{\partial Z} \dots\dots\dots(2.7)$

$$\Theta = \frac{2\mu}{1-2\nu} \left( \frac{\partial D}{\partial Z} + \frac{\partial \bar{D}}{\partial \bar{Z}} \right) \dots\dots\dots(2.8)$$

and from these it can be shown that an integral for D is given by

$$2\mu D = K\phi(Z) - Z\bar{\phi}'(\bar{Z}) - \bar{\psi}(\bar{Z}) \dots\dots\dots(2.9)$$

where  $K = (3-4\nu)$  for plane strain

$$= (3-\nu)/(1+\nu) \text{ for generalised plane stress.}$$

(v) Form of the complex potentials:

The complex potentials take the form

$$\phi(Z) = -\frac{(x+iy)}{2\pi(1+K)} \log Z + (B+iC)Z + \phi_1(Z) \dots\dots\dots(2.10)$$

$$\psi(Z) = -\frac{K(x-iy)}{2\pi(1+K)} \log Z + (B_1+iC_1)Z + \psi_1(Z) \dots\dots\dots(2.11)$$

where B,  $B_1$  and  $C_1$  are constants to be determined from the stresses/

stresses at infinity, and  $C$  corresponds to a rigid body displacement, taken herein to be zero. For principal stresses  $\sigma_o$  and  $\sigma_p$  at infinity with  $\sigma_o$  at an angle  $\alpha$  to the  $x$ -axis, then

$$\begin{aligned} B &= \frac{1}{4} (\sigma_o + \sigma_p) \\ B_1 &= \frac{1}{2} (\sigma_p - \sigma_o) \cos 2\alpha \\ C_1 &= \frac{1}{2} (\sigma_o - \sigma_p) \sin 2\alpha \dots\dots\dots(2.12) \end{aligned}$$

and for uni-axial tension  $\sigma_o$ ,  $\sigma_p$  is taken as zero in these equations.

(vi) Application of Conformal Transformation:

When the point  $\zeta$  is on the unit circle  $\gamma$ , it is denoted by  $\sigma$ , and the complex potentials are expressed in terms of  $\sigma$  using the conformal transformation

$$\phi(Z) = \phi[\omega(\sigma)] = \phi(\sigma)$$

so that the boundary condition (2.6) becomes

$$\phi(\sigma) + \omega(\sigma) \frac{\bar{\phi}'(\bar{\sigma})}{\bar{\omega}'(\bar{\sigma})} + \bar{\psi}(\bar{\sigma}) = f_1 + if_2 + \text{constant on } \gamma \dots\dots(2.13)$$

Also, using curvilinear co-ordinates, stress combinations can be written for  $\Phi'$  and  $\bar{\Phi}'$  thus:-

$$\Phi' = 2 \left[ \chi(\zeta) + \bar{\chi}(\bar{\zeta}) \right] \dots\dots\dots(2.14)$$

$$\bar{\Phi}' = \frac{2\zeta^2}{\rho^2 \bar{\omega}'(\bar{\zeta})} \left[ \bar{\omega}(\bar{\zeta}) \cdot \chi'(\zeta) + \psi'(\zeta) \right] \dots\dots\dots(2.15)$$

$$\text{Where } \chi(\zeta) = \frac{\phi'(\zeta)}{\omega'(\zeta)}$$

Using the transformation  $Z = \omega(\zeta)$ , the complex potentials become

$$\phi(\zeta) = \frac{X + iY}{2(1 + K)} \log \zeta + \frac{CB}{\zeta} + \phi_o(\zeta) \dots\dots\dots(2.16)$$

$$\psi(\zeta) = -\frac{K(X - iY)}{2\pi(1 + K)} \log \zeta + \frac{\zeta}{\zeta} (B_1 + iC_1) + \psi_0(\zeta) \dots \dots (2.17)$$

$$\text{where } \phi_0(\zeta) = \sum_1^{\infty} a_n \zeta^n, \quad \psi_0(\zeta) = \sum_0^{\infty} b_n \zeta^n \dots \dots \dots (2.18)$$

being two functions of  $\zeta$  which are analytic inside

the unit circle  $|\zeta| = 1$ , and are to be determined.

The MUSKHELISHVILI method is used for this determination

in the manner now described. The complex potentials

are substituted into the boundary equation (2.13), which

is then integrated round the unit circle boundary  $\gamma$ ,

applying HARNACK'S theorem, the various terms being evaluated

using CAUCHY'S Integral formula. Hence  $\phi_0(\zeta)$  and

$\psi_0(\zeta)$  are determined, when the form of the transformation

is given and, therefore, the complex potentials  $\phi(\zeta)$  and

$\psi(\zeta)$  can be found.

The stress combinations in Cartesian components of stress

at any point in the  $Z$  - region are given by

$$\Theta = \sigma_x + \sigma_y = 2 \left[ \frac{\phi'(\zeta)}{\omega'(\zeta)} + \frac{\bar{\phi}'(\bar{\zeta})}{\bar{\omega}'(\bar{\zeta})} \right] \dots \dots \dots (2.19)$$

$$\Phi = \sigma_y - \sigma_x + 2i\tau_{xy}$$

$$= 2 \left[ \bar{z} \left\{ \frac{\omega'(\zeta)\phi''(\zeta) - \omega''(\zeta)\phi'(\zeta)}{[\omega'(\zeta)]^3} \right\} + \frac{\psi'(\zeta)}{\omega'(\zeta)} \right] \dots \dots \dots (2.20)$$

Alternatively the equations for  $\Theta'$  and  $\Phi'$  giving the stress

combinations in curvilinear stress components may be employed.

### SELECTION OF THE TRANSFORMATION FORMS

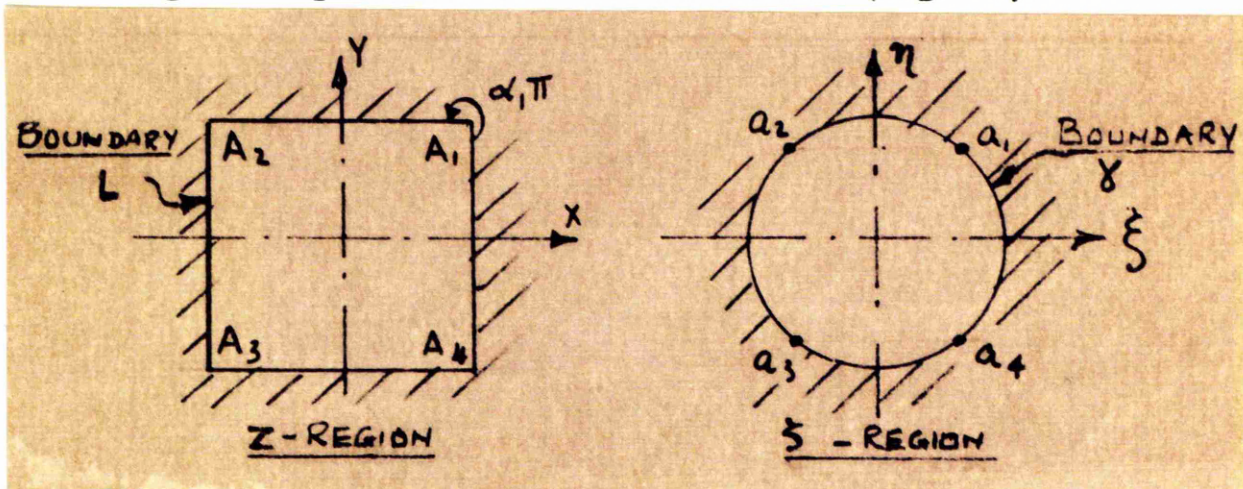
As stated in equation (2.1) the general form of the transformation used is given by the power series

$$Z = \omega(\zeta) = R\left(\frac{1}{\zeta} + m_1 \zeta + m_2 \zeta^2 + m_3 \zeta^3 + \dots + m_n \zeta^n\right)$$

where  $R$  is a scale factor.

By selection of the appropriate terms in this series, boundaries of various geometric forms can be represented, the number of terms used determining the degree of approximation to any desired shape of opening. The co-efficients may also be varied to give variations in the shape of opening, including the degree of sharpness of re-entrant corners.

As an example of the technique involved, following the method of SAVIN, the SCHWARTZ-CHRISTOFFEL transformation is used to transform the  $Z$ -region exterior to a square hole boundary on to the  $\zeta$ -region exterior to the unit circle, the sides of the hole being taken parallel to the  $X$  and  $Y$  axes. (Fig. 94).



$$Z = \omega(\zeta) = R \int_1^{\zeta} \left(1 - \frac{a_1}{\zeta}\right)^{\alpha_1 - 1} \cdot \left(1 - \frac{a_2}{\zeta}\right)^{\alpha_2 - 1} \cdot \left(1 - \frac{a_3}{\zeta}\right)^{\alpha_3 - 1} \cdot \left(1 - \frac{a_4}{\zeta}\right)^{\alpha_4 - 1} \cdot d\zeta \dots (2.21)$$

In/

In this case  $\alpha_1 = \alpha_2 = \alpha_3 = \alpha_4 = 3/2$  and for symmetry about both axes

$$a_1 = e^{i\pi/4} : a_2 = -e^{-i\pi/4} = -\bar{a}_1$$

$$a_3 = -e^{i\pi/4} : a_4 = e^{-i\pi/4} = \bar{a}_1$$

Substituting for  $a_1$ ,  $a_2$ ,  $a_3$  and  $a_4$  in the right hand side of equation (2.20) and grouping terms gives

$$(1 - \frac{a_1}{\zeta})^{\alpha_1-1} \cdot (1 - \frac{a_3}{\zeta})^{\alpha_3-1} = (1 - \frac{a_1^2}{\zeta^2})^{\frac{1}{2}} \dots\dots\dots (2.22)$$

and

$$(1 - \frac{a_2}{\zeta})^{\alpha_2-1} \cdot (1 - \frac{a_4}{\zeta})^{\alpha_4-1} = (1 - \frac{\bar{a}_1^2}{\zeta^2})^{\frac{1}{2}} \dots\dots\dots (2.23)$$

and multiplying these equations together gives

$$(1 - \frac{a_1^2}{\zeta^2})^{\frac{1}{2}} \cdot (1 - \frac{\bar{a}_1^2}{\zeta^2})^{\frac{1}{2}} = (1 + \frac{1}{\zeta^4})^{\frac{1}{2}} \dots\dots\dots (2.24)$$

Binomial expansion leads to

$$(1 + \frac{1}{\zeta^4})^{\frac{1}{2}} = (1 + \frac{1}{2\zeta^4} - \frac{1}{8\zeta^8} + \frac{1}{16\zeta^{12}} - \dots\dots\dots) \dots\dots\dots (2.25)$$

therefore the transformation becomes

$$Z = \omega(\zeta) = R \int_1^{\zeta} (1 + \frac{1}{2\zeta^4} - \frac{1}{8\zeta^8} + \frac{1}{16\zeta^{12}} - \dots\dots\dots) d\zeta \dots\dots\dots (2.26)$$

$$= R (\zeta - \frac{1}{6\zeta^3} + \frac{1}{56\zeta^7} - \frac{1}{176\zeta^{11}} + \dots\dots\dots) \dots\dots\dots (2.27)$$

and this expression transforms the Z - region exterior to the square hole boundary on to the  $\zeta$ -region exterior to the unit circle.

Replacing  $\zeta$  by  $\frac{1}{\zeta}$  gives

$$Z = \omega(\zeta) = R (\frac{1}{\zeta} - \frac{1}{6}\zeta^3 + \frac{1}{56}\zeta^7 - \frac{1}{176}\zeta^{11} + \dots\dots\dots) \dots\dots\dots (2.28)$$

which transforms the Z - region exterior to the square hole boundary on to the  $\zeta$ -region inside the unit circle.

The mathematical working is reduced if the latter form (2.28) of transformation is employed.

In GODFREY'S translation of SAVIN'S work, the general transformation form for polygonal holes is given as:-

$$Z = \omega(\zeta) = C \left[ \frac{1}{\zeta} + \frac{2}{n(n-1)} \zeta^{n-1} + \frac{n-2}{n^2(2n-1)} \zeta^{2n-1} + \frac{(n-2)(2n-2)}{3n^3(3n-1)} \zeta^{3n-1} + \frac{(n-2)(2n-2)(3n-2)}{12n^4(4n-1)} \zeta^{4n-1} \text{ etc.} \right] \dots (2.32)$$

for  $n = 3$  for triangular hole

$n = 4$  for square hole, etc.

From this expression are obtained the following transformation forms:-

(a) Square hole (with diagonals along axes)

$$Z = \omega(\zeta) = C \left( \frac{1}{\zeta} + \frac{1}{6} \zeta^5 + \frac{1}{56} \zeta^7 + \frac{1}{176} \zeta^{11} \text{ ----} \right) \dots (2.29)$$

where all the terms are now positive, this corresponding to a  $45^\circ$  rotation of the hole.

(b) Equilateral Triangular Hole (with one median along the axis)

$$Z = \omega(\zeta) = C \left( \frac{1}{\zeta} + \frac{1}{3} \zeta^2 + \frac{1}{45} \zeta^5 + \frac{1}{162} \zeta^8 + \frac{7}{2675} \zeta^{11} \text{ ----} \right) \dots (2.30)$$

(c) Elliptic Hole  $Z = \omega(\zeta) = C \left( \frac{1}{\zeta} + m \zeta \right) \dots (2.31)$

which represents the  $Z$ -region exterior to an elliptic hole on the inside of a unit circle. In order that the transformation is conformal at points inside  $|\zeta| = 1$  it is necessary that  $\omega'(\zeta)$  is non-zero so that  $|m| \leq 1$ .

It may be shown that the  $L$  boundaries represented by these transformations in the  $Z$ -plane are not geometrically identical to the desired/

desired form, e.g. the square is 'sway-backed' and has rounded corners. The closeness of the approximation depends upon the number of terms used in the series, but by using fewer terms and varying the co-efficients, a sufficiently accurate fit may be obtained. This is a necessary procedure, otherwise the numerical working would be so voluminous as to make the obtaining of a stress solution in any particular case extremely laborious.

The determination of the degree of fit is a lengthy task, if attempted by the usual method of calculation of co-ordinates for graphical plotting. For this reason, the writer devised the analogue computer application described in Chapter III, and this gives a rapid method of selecting the number of terms (up to five in the equipment used) and the values of the coefficients required for any desired degree of fit. Transformation forms for shapes other than quoted by GODFREY, as given by this process, are stated in Chapter III.

CHAPTER II (CONTD.)

PART 2. STRESS CONDITIONS DUE TO THE PRESENCE  
OF A CRUCIFORM CRACK IN A TENSION PLATE.

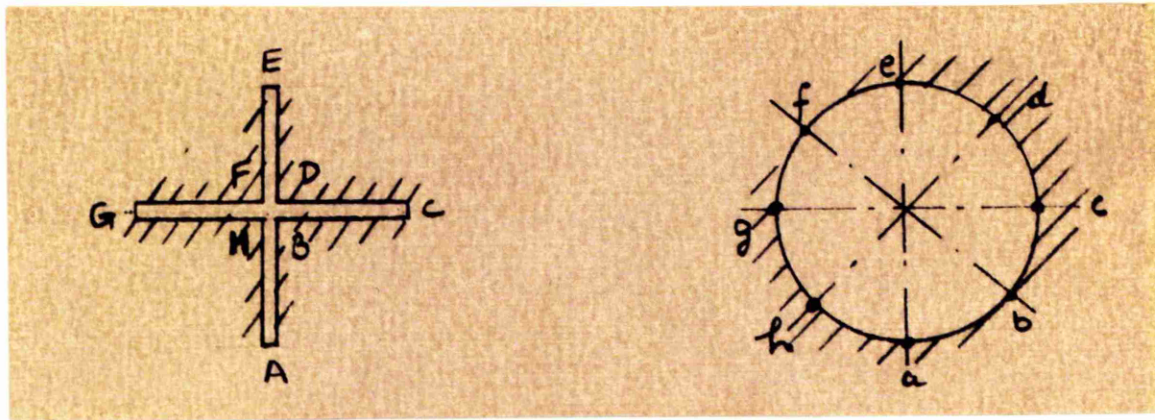


TRANSFORMATION FORM FOR CRUCIFORM CRACK

The region exterior to the cruciform 'crack' shown in Fig. 95 is mapped on to the region exterior to the unit circle by the transformation  $Z = \frac{1}{\sqrt{2}} (\zeta^2 + \frac{1}{\zeta^2})^{\frac{1}{2}}$  .....(2.33)

which on binomial expansion gives

$$Z = \frac{1}{\sqrt{2}} \left[ \frac{1}{\zeta} + \frac{1}{2} \zeta^3 - \frac{1}{8} \zeta^7 + \frac{1}{16} \zeta^{11} - \dots \right] \text{ .....(2.34)}$$



Z - region

ζ - region

Fig. 95

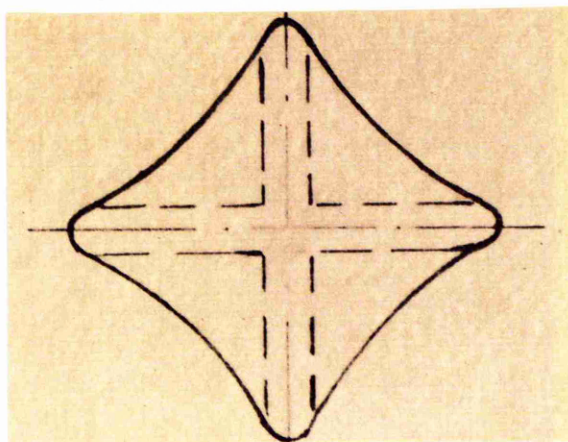
The use of this exact transformation in the MUSKHELISHVILI method presents certain difficulties in the determination of residues, and it was decided to use a modified form of this transformation which gave an approximation to the cruciform crack outline corresponding to the shape of opening used for the experimental specimen, in particular with respect to root radii at points A, C, E and G.

The form used, taking the first two terms of the series of (2.34) with an arbitrary coefficient m for the second term was

$$Z = \omega(\zeta) = R \left( \frac{1}{\zeta} + m \zeta^n \right) \text{ .....(2.35)}$$

which is a general form for 'square' holes, with  $R$  as a scale factor and  $\zeta = \rho e^{i\theta}$ . Using  $n = 5$  and  $0 \leq m \leq \frac{1}{n}$  gives a range of 'square' holes. If  $m$  is positive, the diagonals of the 'square' are parallel to the  $X$  and  $Y$  axes, and if  $m$  is negative, the sides of the 'square' are parallel to these axes.

By judicious selection of the coefficient  $m$  using the analogue computer method given in Chapter III, it was found possible to obtain a shape of opening giving end radii of the same order as used in the experimental specimen, the sides of the 'square' being curved inwards towards the centre. (Fig. 96)



This approximation is justifiable since the four re-entrant corners  $B$ ,  $D$ ,  $F$  and  $H$  of Fig. 96 must be stress free, and the approximation used is tantamount to removing some of this stress free material. From the analogue computer technique mentioned later, the required value of  $m$  was found to be  $m = \frac{1}{5.15} = 0.194$ .

II.4 Derived complex potentials:

The general transformation form is

$$Z = \omega(\zeta) = R\left(\frac{1}{\zeta} + m\zeta^n\right)$$

and the notation is  $\omega'(\zeta)$  etc. where the dash represents differentiation with respect to the bracketed variable. On the boundary of the unit circle  $|\zeta| = 1$ , then as before, when the point  $\zeta$  is on the boundary of the unit circle, it will be denoted by  $\sigma$ .

$$\text{Thus } \omega(\sigma) = R\left(\frac{1}{\sigma} + m\sigma^3\right) \dots\dots\dots (2.36)$$

$$\bar{\omega}(\bar{\sigma}) = R\left(\frac{1}{\bar{\sigma}} + m\bar{\sigma}^3\right) = R\left(\sigma + \frac{m}{\sigma^3}\right) \dots\dots\dots (2.37)$$

$$\omega'(\sigma) = R\left(-\frac{1}{\sigma^2} + 3m\sigma^2\right) \dots\dots\dots (2.38)$$

$$\bar{\omega}'(\bar{\sigma}) = R\left(-\frac{1}{\bar{\sigma}^2} + 3m\bar{\sigma}^2\right) = -R\left(\sigma^2 - \frac{3m}{\sigma^2}\right) \dots\dots\dots (2.39)$$

Derivation of Stress Combination  $\sigma' = \sigma_\theta + \sigma_\rho$ 

In the following the derivation of the stress combination

$$\sigma' = \sigma_\theta + \sigma_\rho \text{ is given.}$$

$$\frac{\omega(\sigma)}{\bar{\omega}'(\bar{\sigma})} = -\frac{\left(\frac{1}{\sigma} + m\sigma^3\right)}{\left(\sigma^2 - \frac{3m}{\sigma^2}\right)} \dots\dots\dots (2.40)$$

which after some reduction gives

$$\frac{\omega(\sigma)}{\bar{\omega}'(\bar{\sigma})} = -m\sigma \left[ 1 + \frac{5m^2+1}{m\sigma^4} (1 + 3m\sigma^{-4} + 9m^2\sigma^{-8} + \dots) \right] \dots\dots\dots (2.41)$$

The derived boundary condition (See Appendix Chapter VII.1)

for  $\phi_o(\zeta)$  and  $\psi_o(\zeta)$  takes the form

$$f_1^o + if_2^o = -\frac{\sigma_o}{2} \left[ \omega(\sigma) - e^{2i\alpha} \bar{\omega}(\bar{\sigma}) \right]$$

$$f_1^o - if_2^o = -\frac{\sigma_o}{2} \left[ \bar{\omega}(\bar{\sigma}) - e^{-2i\alpha} \omega(\sigma) \right]$$

and/

and substituting (2.36) and (2.37) in these equations gives

$$f_1^0 + if_2^0 = -\frac{\sigma_0 R}{2} \left[ \frac{1}{\sigma} - e^{2ia} \frac{m}{\sigma^3} + m\sigma^3 - e^{2ia} \sigma \right] \dots \dots \dots (2.42)$$

and

$$f_1^0 - if_2^0 = -\frac{\sigma_0 R}{2} \left[ \frac{m}{\sigma^3} - \frac{e^{-2ia}}{\sigma} + \sigma - e^{-2ia} m\sigma^3 \right] \dots \dots \dots (2.43)$$

From equation (2.42)

$$\frac{1}{2\pi i} \int_{\gamma} \frac{f_1^0 + if_2^0}{\sigma - \zeta} d\sigma = -\frac{\sigma_0 R}{4\pi i} \int_{\gamma} \left[ \frac{1}{\sigma} - e^{2ia} \frac{m}{\sigma^3} + m\sigma^3 - e^{2ia} \sigma \right] \frac{1}{\sigma} \sum_0^{\infty} \left(\frac{\zeta}{\sigma}\right)^r$$

which by the theorem of residues gives

$$-\frac{\sigma_0 R}{4\pi i} \cdot 2\pi i (m\zeta^3 - e^{2ia} \zeta) = \underline{\underline{\frac{m\sigma_0 R}{2} \left( \zeta^2 - \frac{e^{2ia}}{m} \right) \zeta}}$$

Similarly

$$\frac{1}{2\pi i} \int_{\gamma} \frac{f_1^0 - if_2^0}{\sigma - \zeta} d\sigma = -\frac{\sigma_0 R}{4\pi i} \int_{\gamma} \left[ \frac{m}{\sigma^3} - \frac{e^{-2ia}}{\sigma} + \sigma - e^{-2ia} m\sigma^3 \right] \frac{1}{\sigma} \sum_0^{\infty} \left(\frac{\zeta}{\sigma}\right)^r$$

which by the theorem of residues gives

$$\underline{\underline{-\frac{\sigma_0 R}{4\pi i} \cdot 2\pi i (\zeta - e^{-2ia} m\zeta^3) = \frac{m\sigma_0 R}{2} \left( \frac{1}{m} - e^{-2ia} \zeta^2 \right) \zeta}}$$

From the equation for the boundary condition for  $\phi_0(\zeta)$  and  $\psi_0(\zeta)$

(See Appendix VII.1) and using  $\phi_0(\sigma) = \sum_0^{\infty} a_n \sigma^n$ ,

$$\begin{aligned} \text{therefore } \frac{1}{2\pi i} \int_{\gamma} \frac{\omega(\sigma)}{\bar{\omega}(\bar{\sigma})} \bar{\phi}_0'(\bar{\sigma}) \frac{d\sigma}{\sigma - \zeta} &= -\frac{1}{2\pi i} \int_{\gamma} m\sigma \left[ 1 + \frac{3m^2 + 1}{m\sigma^4} (1 + 5m\sigma^{-4} + 9m\sigma^{-8}) \right] \times \\ &\times \left[ \bar{a}_1 + \frac{2\bar{a}_2}{\sigma} + \frac{3\bar{a}_3}{\sigma^2} + \dots \right] \frac{1}{\sigma} \sum_0^{\infty} \left(\frac{\zeta}{\sigma}\right)^r \end{aligned}$$

which/

which, by the theorem of residues, gives

$$= (\bar{m}\bar{\alpha}_1 \zeta + 2m\bar{\alpha}_2) = - \frac{m\bar{\alpha}_1 \zeta - 2m\bar{\alpha}_2}{\zeta}$$

Hence from

$$\phi_0(\zeta) + \frac{1}{2\pi i} \int_{\gamma} \frac{\omega(\sigma)}{\omega'(\sigma)} \bar{\phi}_0'(\sigma) \frac{d\sigma}{\sigma - \zeta} + \bar{\beta}_0 = \frac{1}{2\pi i} \int_{\gamma} \frac{f_1^0 + if_2^0}{\sigma - \zeta} \cdot d\sigma$$

so that

$$\alpha_1 \zeta + \alpha_2 \zeta^2 + \alpha_3 \zeta^3 + \dots - m\bar{\alpha}_1 \zeta - 2m\bar{\alpha}_2 + \beta_0 = -\frac{m\sigma_0 R}{2} \zeta^3 + \frac{\sigma_0 R}{2} e^{2i\alpha} \zeta \dots (2.44)$$

Equating coefficients

$$\bar{\beta}_0 = 0, \alpha_2 = 0, \bar{\alpha}_2 = 0, \alpha_3 = -\frac{m\sigma_0 R}{2}, \alpha_1 - m\bar{\alpha}_1 = \frac{\sigma_0 R e^{2i\alpha}}{2}$$

Putting  $\alpha_1 = x + iy, \bar{\alpha}_1 = x - iy$

gives  $x + iy - mx + miy = \frac{\sigma_0 R}{2} (\cos 2\alpha + i \sin 2\alpha)$

$$(1 - m)x = \frac{\sigma_0 R}{2} \cos 2\alpha \quad \text{or} \quad x = \frac{\sigma_0 R}{2} \frac{\cos 2\alpha}{(1 - m)}$$

$$(1 + m)y = \frac{\sigma_0 R}{2} \sin 2\alpha \quad \text{or} \quad y = \frac{\sigma_0 R}{2} \frac{\sin 2\alpha}{(1 + m)}$$

and  $\alpha_1 = \sigma_0 R \left[ \frac{\cos 2\alpha}{2(1-m)} + i \frac{\sin 2\alpha}{2(1+m)} \right]$

Thus

$$\phi_0(\zeta) = \alpha_1 \zeta + \alpha_3 \zeta^3 + \dots = \sigma_0 R \left\{ \left[ \frac{\cos 2\alpha}{2(1-m)} + i \frac{\sin 2\alpha}{2(1+m)} \right] \zeta - \frac{m}{2} \zeta^3 \right\} \dots (2.45)$$

But as shown in Appendix Chapter VII.1

$$\phi(\zeta) = \frac{1}{4} \sigma_0 \omega(\zeta) + \phi_0(\zeta) \quad \text{which on substituting for } \omega(\zeta) \text{ and}$$

$\phi_0(\zeta)$  gives

$$\begin{aligned}\phi(\zeta) &= \frac{1}{4} \sigma_o R \left( \frac{1}{\zeta} + m \zeta^3 \right) + \sigma_o R \left\{ \left[ \frac{\cos 2\alpha}{2(1-m)} + i \frac{\sin 2\alpha}{2(1+m)} \right] \zeta - \frac{m}{2} \zeta^3 \right\} \\ &= \sigma_o R \left[ \frac{1}{4\zeta} + \left( \frac{\cos 2\alpha}{2(1-m)} + i \frac{\sin 2\alpha}{2(1+m)} \right) \zeta - \frac{m}{4} \zeta^3 \right] \dots\dots\dots(2.46)\end{aligned}$$

For tension along the XX axis,  $\alpha = 0^\circ$

$$\text{so that } \phi(\zeta) = \sigma_o R \left[ \frac{1}{4\zeta} + \frac{1}{2(1-m)} \zeta - \frac{m}{4} \zeta^3 \right] \dots\dots\dots(2.47)$$

$$\text{and } \phi'(\zeta) = \sigma_o R \left[ -\frac{1}{4\zeta^2} + \frac{1}{2(1-m)} - \frac{3m}{4} \zeta^2 \right]$$

Thus

$$\chi(\zeta) = \frac{\phi'(\zeta)}{\omega'(\zeta)} = \frac{\sigma_o \left[ -\frac{1}{4\zeta^2} + \frac{1}{2(1-m)} - \frac{3m}{4} \zeta^2 \right]}{-\frac{1}{\zeta^2} + 3m\zeta^2}$$

which reduces to

$$\chi(\zeta) = \frac{\sigma_o \left[ -3m(1-m)\zeta^4 + 2\zeta^2 - (1-m) \right]}{4m(1-m)(3\zeta^4 - \frac{1}{m})}$$

$$\text{and } \bar{\chi}(\bar{\zeta}) = \frac{\sigma_o \left[ -3m(1-m)\bar{\zeta}^4 + 2\bar{\zeta}^2 - (1-m) \right]}{4m(1-m)(3\bar{\zeta}^4 - \frac{1}{m})}$$

Then

$$\sigma_\theta = \sigma_\theta + \sigma_\rho = 2[\chi(\zeta) + \bar{\chi}(\bar{\zeta})] \dots\dots\dots(2.48)$$

$$\text{For } \zeta = \rho e^{i\theta}, \quad \bar{\zeta} = \rho e^{-i\theta} \quad \text{and } \theta = 90^\circ$$

then

$$\sigma_\theta + \sigma_\rho = \sigma_o \left[ \frac{-2\rho^2 - (1-m)(3m\rho^4 + 1)}{(1-m)(3m\rho^4 - 1)} \right] \dots\dots\dots(2.49)$$

Similarly for  $\theta = 0^\circ$

$$\sigma_\theta + \sigma_\rho = \sigma_o \left[ \frac{2\rho^2 - (1-m)(3m\rho^4 + 1)}{(1-m)(3m\rho^4 - 1)} \right] \dots\dots\dots(2.50)$$

and/

and from these the distribution of  $\sigma_\theta + \sigma_\rho$  along the X and Y axes may be determined.

For the hoop stress on the hole boundary,  $\rho = 1$   
and  $\sigma_\rho = 0$ , with  $\zeta = e^{i\theta}$ ,  $\bar{\zeta} = e^{-i\theta}$

Hence equation (2.48) gives the stress concentration factor on the hole boundary as

$$\left[ \frac{\sigma_\theta}{\sigma_\infty} \right]_{\rho=1} = \frac{1}{2m(1-m)} \left[ \frac{-3(1-m)e^{i4\theta} + 2e^{i2\theta} - (1-m)}{5e^{i4\theta} - \frac{1}{m}} + \frac{-3m(1-m)e^{-i4\theta} + 2e^{-i2\theta} - (1-m)}{5e^{-i4\theta} - \frac{1}{m}} \right] \quad (2.51)$$

The maximum hoop stress occurs on the axis YY perpendicular to the axis XX which is the axis of tension, that is,  $\theta = 90^\circ$  giving the stress concentration factor as

$$\left[ \frac{\sigma_\theta}{\sigma_\infty} \right]_{YY} = \left[ \frac{3m(1-m) - 2 - (1-m)}{m(1-m)(5 - \frac{1}{m})} \right] \dots\dots\dots (2.52)$$

Derivation of Stress Combination  $\phi' = \sigma_\theta - \sigma_\rho + 2i\tau_{\rho\theta}$

In the following the derivation of the stress combination

$\phi' = \sigma_\theta - \sigma_\rho + 2i\tau_{\rho\theta}$  is given.

$$\frac{\bar{\omega}(\bar{\sigma})}{\omega'(\sigma)} = \frac{(\sigma + \frac{m}{\sigma^3})}{(-\frac{1}{\sigma^2} + 3m\sigma^2)} = \frac{m}{\sigma} \frac{(\frac{\sigma^4}{m} + 1)}{(3m\sigma^4 - 1)} \dots\dots\dots (2.53)$$

Therefore

$$\frac{1}{2\pi i} \int_\gamma \frac{\bar{\omega}(\bar{\sigma})}{\omega'(\sigma)} \frac{\phi_\theta'(\sigma) d\sigma}{\sigma - \zeta} = \frac{1}{2\pi i} \int_\gamma \frac{m(\frac{\sigma^4}{m} + 1) [\alpha_1 + 3\alpha_3\sigma^2 + \dots]}{\sigma(3m\sigma^4 - 1)(\sigma - \zeta)} d\sigma \dots\dots (2.54)$$

Poles/

Poles occur when (a)  $\sigma = 0$ , (b)  $\sigma = \zeta$ .

(a) When  $\sigma = 0$ , and using only the first two relevant terms in the series, to limit the mathematical working,

$$\frac{1}{2\pi i} \int_{\gamma} \frac{m(\frac{\sigma^4}{m} + 1)(\alpha_1 + 3\alpha_3 \sigma^2)}{(3m\sigma^4 - 1)(\sigma - \zeta)} d\sigma$$

$$\text{Residue} = \frac{m\alpha_1}{(-1)(-\zeta)} = \frac{m\alpha_1}{\zeta} \dots\dots\dots (2.55)$$

(b) When  $\sigma = \zeta$ ,

$$\frac{1}{2\pi i} \int_{\gamma} \frac{m(\frac{\sigma^4}{m} + 1)(\alpha_1 + 3\alpha_3 \sigma^2)}{\sigma(3m\sigma^4 - 1)(\sigma - \zeta)} d\sigma$$

$$\text{Residue} = \frac{m(\frac{\zeta^4}{m} + 1)(\alpha_1 + 3\alpha_3 \zeta^2)}{(3m\zeta^4 - 1)} \dots\dots\dots (2.56)$$

The residue on integration is therefore

$$\frac{m\alpha_1}{\zeta} + \frac{(\zeta^4 + m)(\alpha_1 + 3\alpha_3 \zeta^2)}{\zeta(3m\zeta^4 - 1)} \dots\dots\dots (2.57)$$

and applying the equation

$$\psi_0(\zeta) + \frac{1}{2\pi i} \int_{\gamma} \frac{\bar{\omega}(\bar{\sigma})}{\omega'(\sigma)} \frac{\phi_0'(\sigma)}{\sigma - \zeta} d\sigma = \frac{1}{2\pi i} \int_{\gamma} \frac{f_1^0 - if_2^0}{\sigma - \zeta} d\sigma$$

gives

$$\psi_0(\zeta) = -\frac{\sigma_0 R}{2} (\zeta - me^{-2i\alpha} \zeta^3) - \frac{m\alpha_1}{\zeta} - \left[ \frac{(\zeta^4 + m)(\alpha_1 + 3\alpha_3 \zeta^2)}{\zeta(3m\zeta^4 - 1)} \right] \dots\dots\dots (2.58)$$

$$= -\frac{\sigma_0 R}{2} (\zeta - me^{-2i\alpha} \zeta^3)$$

$$- \frac{\sigma_0 R}{2} \frac{m(\cos 2\alpha}{1+m} + \frac{i \sin 2\alpha}{1+m}) - \frac{\sigma_0 R}{2} \left[ \frac{(\zeta^4 + m)(\frac{\cos 2\alpha}{1-m} + \frac{i \sin 2\alpha}{1+m}) - 5m\zeta^2 \times (\zeta^4 + m)}{\zeta(3m\zeta^4 - 1)} \right]$$

which/



which after some reduction results in

$$\psi_0(z) = -\frac{\sigma_0 R}{2} \left[ -me^{-2i\alpha} z^3 + \frac{(3m^2+1) \left[ z^3 \left( \frac{\cos 2\alpha}{1-m} + i \frac{\sin 2\alpha}{1+m} \right) - z \right]}{(3mz^4 - 1)} \right] \dots (2.59)$$

Hence from

$$\psi(z) = -\frac{\sigma_0 R}{2} e^{-2i\alpha} \omega(z) + \psi_0(z)$$

$$\begin{aligned} \psi(z) = & -\frac{\sigma_0 R}{2} e^{-2i\alpha} \cdot \frac{1}{z} - \frac{\sigma_0 R}{2} me^{-2i\alpha} z^3 + \frac{\sigma_0 R}{2} me^{-2i\alpha} z^5 \\ & - \frac{\sigma_0 R}{2} \left[ \frac{(3m^2+1) \left[ z^3 \left( \frac{\cos 2\alpha}{1-m} + i \frac{\sin 2\alpha}{1+m} \right) - z \right]}{(3mz^4 - 1)} \right] \\ \psi(z) = & -\sigma_0 R \left[ \frac{e^{-2i\alpha}}{2z} + \frac{(3m^2+1) \left[ z^3 \left( \frac{\cos 2\alpha}{1-m} + i \frac{\sin 2\alpha}{1+m} \right) - z \right]}{2(3mz^4 - 1)} \right] \dots \dots \dots (2.60) \end{aligned}$$

Thus equations (2.46) and (2.60) give the complex potentials for tension at angle  $\alpha$  to the XX axis.

For tension along the YY axis,  $\alpha = 0^\circ$ , these potentials become

$$\phi(z) = \sigma_0 R \left[ \frac{1}{4z} + \frac{1}{2(1-m)} z - \frac{mz^3}{4} \right] \dots \dots \dots (2.61)$$

$$\psi(z) = -\sigma_0 R \left[ \frac{1}{2z} + \frac{(3m^2+1)z^5 - (1-m)(3m^2+1)z}{2(1-m)(3mz^4-1)} \right] \dots \dots \dots (2.62)$$

The stress combination

$$\bar{\phi}' = \sigma_\theta - \sigma_\rho + 2i\tau_{\rho\theta} = \frac{2z^2}{\rho^2 \bar{\omega}'(z)} \left[ \bar{\omega}(z) \chi'(z) + \psi'(z) \right] \dots \dots (2.63)$$

can now be formed.

The following are required in the formation of  $\bar{\phi}'$ .

$$\omega(z) = R \left( \frac{1}{z} + mz^3 \right) = \frac{R}{z} (mz^4 + 1) \dots \dots \dots (2.64)$$

$$\omega^{\circ}(\xi) = R\left(-\frac{1}{\xi^2} + 3m\xi^2\right) = \frac{R}{\xi^2}(3m\xi^4 - 1) \dots\dots\dots(2.65)$$

$$\omega''(\xi) = R\left(\frac{2}{\xi^3} + 6m\xi\right) = \frac{2R}{\xi^3}(3m\xi^4 + 1) \dots\dots\dots(2.66)$$

$$\bar{\omega}(\bar{\xi}) = \frac{R}{\bar{\xi}}(m\bar{\xi}^4 + 1) \dots\dots\dots(2.67)$$

$$\bar{\omega}'(\bar{\xi}) = \frac{R}{\bar{\xi}^2}(3m\bar{\xi}^4 - 1) \dots\dots\dots(2.68)$$

Equation (2.62) may be written:-

$$\psi(\xi) = -\sigma_o R \left[ \frac{1}{2\xi} + \frac{(3m^2 + 1)}{2(1-m)} \left\{ \frac{\xi^3 - \xi(1-m)}{(3m\xi^4 - 1)} \right\} \right] \dots\dots\dots(2.69)$$

$$\psi'(\xi) = -\sigma_o R \left[ -\frac{1}{2\xi^2} + \frac{(3m^2 + 1)}{2(1-m)} \left\{ \frac{\xi^2(3m\xi^4 - 1) - (1-m)(3m\xi^4 - 1)}{(3m\xi^4 - 1)^2} \right\} \right] \dots\dots\dots(2.70)$$

$$\text{Also } \chi(\xi) = \frac{\phi'(\xi)}{\omega'(\xi)}$$

$$\text{and } \chi'(\xi) = \frac{\omega'(\xi)\phi''(\xi) - \phi'(\xi)\omega''(\xi)}{[\omega'(\xi)]^2} \dots\dots\dots(2.71)$$

$$\text{or } \chi'(\xi) = \frac{\phi''(\xi)}{\omega'(\xi)} - \frac{\phi'(\xi)\omega''(\xi)}{[\omega'(\xi)]^2} \dots\dots\dots(2.72)$$

From equations (2.61) and (2.64) to (2.68) etc. the component parts of equation (2.72) are as follows:-

$$\phi'(\xi) = \sigma_o R \left[ -\frac{1}{4\xi^2} + \frac{1}{2(1-m)} - \frac{3m\xi^2}{4} \right] \dots\dots\dots(2.73)$$

$$\phi''(\xi) = \sigma_o R \left[ \frac{1}{2\xi^3} - \frac{3m\xi}{2} \right] = -\frac{\sigma_o R}{2\xi^3}(3m\xi^4 - 1) \dots\dots\dots(2.74)$$

$$\text{and } \frac{\phi''(\xi)}{\omega'(\xi)} = -\frac{\sigma_o}{2\xi} \dots\dots\dots(2.75)$$

$$\text{Also } [\omega'(\xi)]^2 = \frac{R^2}{\xi^4}(3m\xi^4 - 1)^2 \dots\dots\dots(2.76)$$

Hence after some reduction

$$\frac{\phi'(\xi)\omega''(\xi)}{[\omega'(\xi)]^2} = \frac{\sigma_0(3m\xi^4 + 1)(-1 + m + 2\xi^2 - 3m\xi^4 + 3m^2\xi^4)}{2\xi(3m\xi^4 - 1)^2(1-m)} \dots\dots\dots(2.77)$$

Then from (2.75) and (2.77)

$$\chi'(\xi) = -\frac{\sigma_0}{2\xi} \left[ 1 + \frac{(3m\xi^4 + 1)(3m^2\xi^4 - 3m\xi^4 + 2\xi^2 + m - 1)}{(1-m)(3m\xi^4 - 1)^2} \right] \dots\dots\dots(2.78)$$

Equations (2.67), (2.68) and (2.78) give

$$\frac{2\xi^2}{\rho^2\bar{\omega}'(\xi)} \bar{\omega}(\xi)\chi'(\xi) = -\frac{\sigma_0\xi^2(3m\xi^4+1)}{\rho^2(3m\xi^4-1)} \left[ 1 + \frac{(3m\xi^4+1)(3m^2\xi^4-3m\xi^4+2\xi^2+m-1)}{(1-m)(3m\xi^4-1)^2} \right] \dots\dots\dots(2.79)$$

and from (2.68) and (2.70)

$$\frac{2\xi^2}{\rho^2\bar{\omega}'(\xi)} \cdot \psi'(\xi) = -\frac{\sigma_0\xi^2\xi^2}{\rho^2(3m\xi^4-1)} \left[ -\frac{1}{\xi^2} + \frac{(3m^2+1)}{(1-m)(3m\xi^4-1)^2} \times \right. \\ \left. \times \left\{ 3\xi^2(3m\xi^4-1) + (1-m)(9m\xi^4+1) - 12m\xi^6 \right\} \right] \dots\dots\dots(2.80)$$

Equations (2.79) and (2.80) define the right hand side of equation (2.63).

It is easily shown that the boundary values at infinity are satisfied, by substituting for  $\rho = 0$  and  $\theta = 90^\circ$  and  $0^\circ$  respectively.

For  $\theta = 90^\circ$ , equation (2.79) is zero and equation (2.80) gives  $+\sigma_0$ . Hence from equation (2.63),  $\sigma_\theta = \sigma_0$  since  $\sigma_\rho$  and  $\tau_{\rho\theta}$  are both zero at infinity, parallel to the axis of tension. Therefore this gives uniform tension along the edge of the plate to infinity, parallel to the axis of tension. For  $\theta = 0^\circ$ , equation (2.79) is again zero and equation (2.80) gives  $-\sigma_0$ . Hence equation (2.63)

gives  $\sigma_\rho = \sigma_0$  since  $\sigma_\theta$  and  $\tau_{\rho\theta}$  are zero and this corresponds to uniform tension at infinity along the ends of the plate.

An expression for the hoop stress on the hole boundary corresponding to that obtained from equation (2.51) is given when  $\zeta = \rho e^{i\theta}$ ,  $\bar{\zeta} = \rho e^{-i\theta}$  and  $\rho = 1.0$ , the maximum hoop stress occurring when  $\theta = 90^\circ$  from the direction of tension.

Thus the right hand side of equation (2.79) becomes

$$= \frac{\sigma_0(m+1)}{(3m-1)} \left[ 1 + \frac{(3m+1)(3m^2-2m-3)}{(1-m)(3m-1)^2} \right] \dots\dots\dots (2.81)$$

and the right hand side of equation (2.80) becomes

$$= \frac{\sigma_0}{(3m-1)} \left[ 1 + \frac{(3m^2+1)}{(1-m)(3m-1)^2} \left\{ -3(3-m) + (1-m)(9m+1) + 12m \right\} \right] \dots\dots (2.82)$$

and as before the sum of these equations (2.81) and (2.82) gives the maximum hoop stress on the boundary of the hole, hence the stress concentration factor can be found.

In order to facilitate calculation of the stress distribution along the axes of symmetry, the general expressions for (2.79) and (2.80) were written as follows:-

$$\text{Right hand side of (2.79)} = - \frac{\sigma_0(m\rho^4+1)}{(3m\rho^4-1)} \left[ 1 + \frac{(3m\rho^4+1)(3m^2\rho^4-5m\rho^4-2\rho^2+m-1)}{(1-m)(3m\rho^4-1)^2} \right] \dots\dots (2.83)$$

Right hand side of (2.80) =

$$\frac{-\sigma_0\rho^2}{(3m\rho^4-1)} \left[ \frac{1}{\rho^2} + \frac{(3m^2+1)\{-3\rho^2(3m\rho^4-1) + (1-m)(9m\rho^4+1) + 12m\rho^6\}}{(1-m)(3m\rho^4-1)^2} \right] \dots\dots\dots (2.84)$$

Using equations (2.48) and (2.65), the sum and difference of  $\sigma_\theta$  and  $\sigma_\rho$  can be determined, and also the separate stresses, together with the shear stress distribution  $\tau_{\rho\theta}$  at any point in the plate.

Fig. 97.

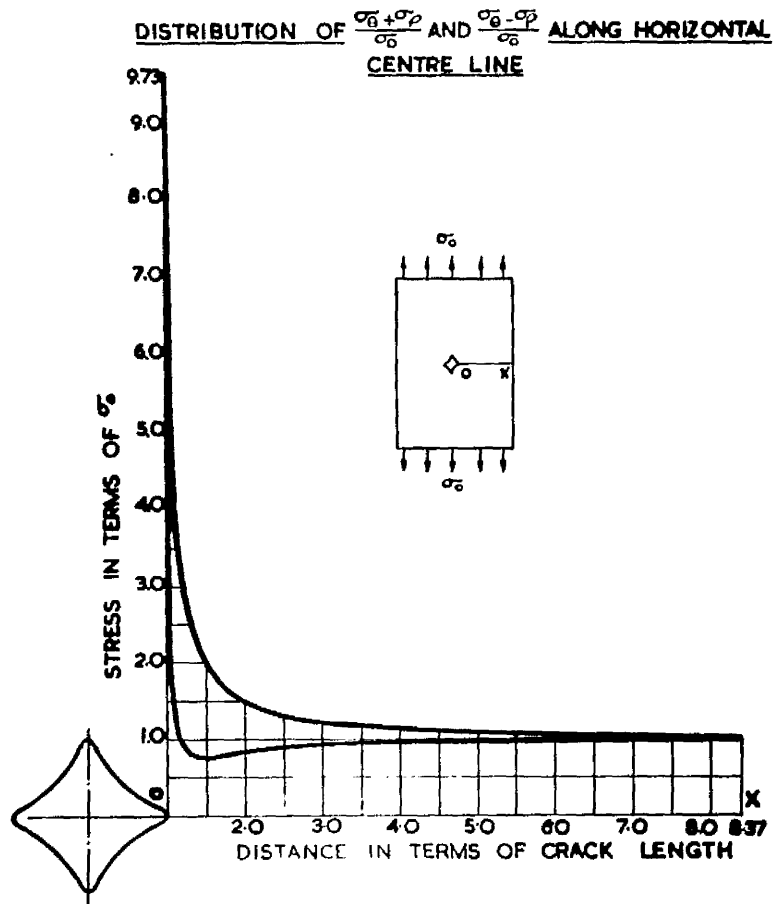
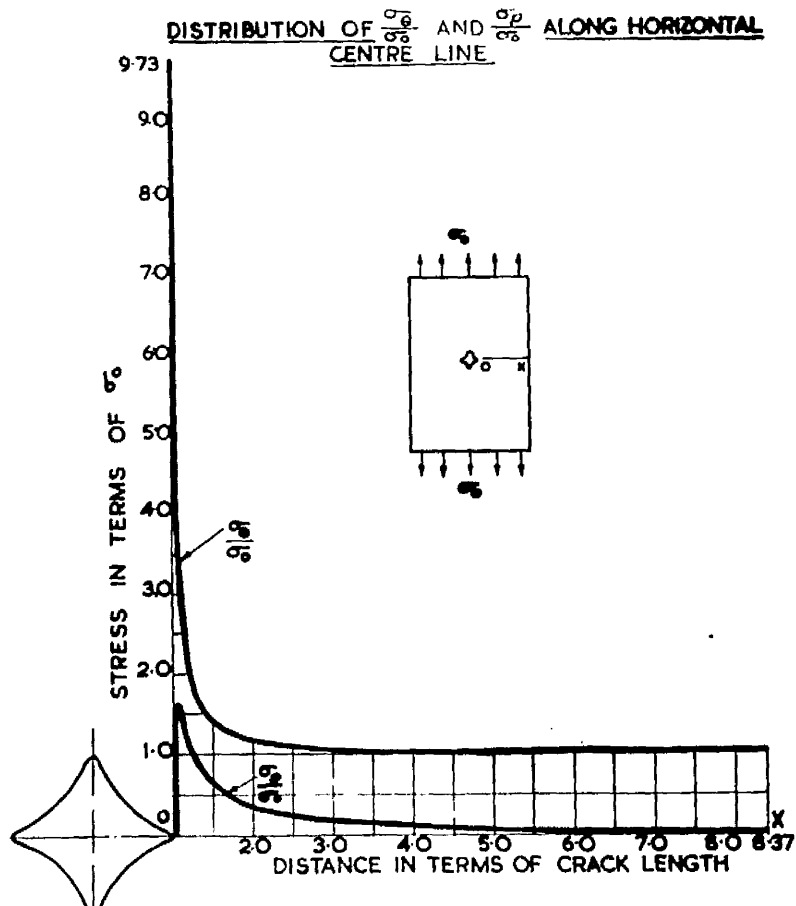


Fig. 98.



DISTRIBUTION OF PRINCIPAL STRESSES ALONG THE AXIS OF  
SYMMETRY PERPENDICULAR TO THE AXIS OF UNIFORM TENSION

The distributions of  $\frac{(\sigma_\theta + \sigma_\rho)}{\sigma_0}$  and  $\frac{(\sigma_\theta - \sigma_\rho)}{\sigma_0}$  are shown in Fig. 97.

The numerical evaluation of equations (2.46), (2.79) and (2.80) for varying values of  $\rho$  was facilitated using the Deuce Digital Computer at Glasgow University Computing Laboratory. The Alphacode Mark II system was employed. The programme and details are given in Appendix Chapter VII.2.

From the computer results, the distributions of  $\sigma_\theta/\sigma_0$  and  $\sigma_\rho/\sigma_0$  were obtained, using a hand calculating machine; these distributions are shown in Fig. 98.

These graphs show that the effect of a 'cruciform' hole in an infinite plate under uniform uniaxial tension at infinity, is a local one, and that the disturbance of stress diminishes rapidly a short distance away from the hole.

CHAPTER II (contd).

PART 3. STRESS CONCENTRATION FACTORS

TRANSFORMATION FORMS FOR A SELECTION  
OF POLYGONAL DISCONTINUITIES IN THE  
INTERIOR OF A TENSION PLATE.







	<u>TRANSFORMATION FORM</u>
1. 	$Z = \omega(\xi) = R \left( \frac{1}{\xi} + \frac{1}{5.15} \xi^3 \right)$
2. 	$Z = \omega(\xi) = R \left( \frac{1}{\xi} + \frac{1}{5.5} \xi^3 \right)$
3. 	$Z = \omega(\xi) = R \left( \frac{1}{\xi} - \frac{1}{4.63} \xi^3 \right)$
4. 	$Z = \omega(\xi) = R \left( \frac{1}{\xi} - \frac{1}{4.5} \xi^3 \right)$
5. 	$Z = \omega(\xi) = R \left( \frac{1}{\xi} - \frac{1}{3.15} \xi^2 \right)$
6. 	$Z = \omega(\xi) = R \left( \frac{1}{\xi} + \frac{1}{3.08} \xi^2 \right)$

Fig.99.

THEORETICAL STRESS CONCENTRATION FACTORS  
FOR A SELECTION OF POLYGONAL DISCONTINUITIES  
IN THE INTERIOR OF A TENSION PLATE







	<u>S.C.F.</u>
1. 	9.73
2. 	8.8
3. 	5.67
4. 	6.0
5. 	7.58
6. 	7.93

Fig.100.



STRESS CONCENTRATION FACTORS FOR A SELECTION OF  
POLYGONAL DISCONTINUITIES IN THE INTERIOR OF A TENSION PLATE.

Stress concentration factors for holes of different shapes were determined from general solutions for  $\bar{\phi}'/\sigma_0$  for each polygonal form under consideration. A typical derivation and calculation is given in Appendix Chapter VII.3. The maximum stress concentration factor was ascertained by interpolation, using incremental changes in the angle  $\theta$  which located the points on the hole boundary relative to the axis of tension, thus giving incremental variation in the stress concentration factor round the hole boundary. The transformation forms are given in Fig. 99.

A summary of the calculated values of the stress concentration factors found by this method is given in Fig. 100.

CHAPTER III.      EXPERIMENTAL WORK

The experimental work presented embraces

- (a) an adjunct to the theoretical work, using the analogue computer for the determination of suitable conformal transformations to give discontinuity forms similar to those used for the experimental specimens,
- (b) the determination of the principal stresses and stress concentration factors for the forms of discontinuities considered. In this work, the sums and the differences of the principal stresses at points in the tension plate were determined, and then combined to give their separate values.

Relaxation solutions, using SOUTHWELL'S method, for the determination of the sum of the principal stresses in the tension plate, were fully investigated by the writer, but were later replaced by a more rapid technique utilising the Conducting Paper Analogy.

Brief details of these methods are given at the beginning of each of the relevant subsections which follow.

DETERMINATION OF THE TRANSFORMATION FORM  
BY THE ANALOGUE COMPUTER.

As stated in paragraph II.3, this application of the Minispace Analogue Computer was devised by the writer to facilitate the determination of suitable conformal transformations, using an analogue computer.

THEORY: The general form of the power series is given in equation (2.32) and for say a 'square' hole is of the form given by (2.27),

$$\text{i.e. } Z = \omega(\zeta) = C \left[ \frac{1}{\zeta} + m_3 \zeta^3 + m_7 \zeta^7 + m_{11} \zeta^{11} + \dots \right]$$

$$\text{where } m_3 = -\frac{1}{6}, m_7 = +\frac{1}{56}, m_{11} = -\frac{1}{176}.$$

The complex number  $\zeta = \rho e^{i\theta}$  gives a circle on the Argand diagram for constant  $\rho$  and varying  $\theta$ . Also  $\zeta = \rho(\cos \theta + i \sin \theta)$  and for  $\rho = 1$  (unit circle),  $\zeta = (\cos \theta + i \sin \theta)$ .

Hence from (2.28)

$$Z = C \left( \cos \theta + m_3 \cos 3\theta + m_7 \cos 7\theta + m_{11} \cos 11\theta + \dots \right) \\ + iC \left( \sin \theta + m_3 \sin 3\theta + m_7 \sin 7\theta + m_{11} \sin 11\theta + \dots \right) \dots\dots\dots (3.1)$$

and this complex number gives a conformal transformation of the unit circle in the form of a 'square', on the Argand diagram.

The analogue computer can be used to continuously plot this transformation and display the result on an oscilloscope screen. For this application, using  $\theta = \omega t$  in equation (3.1) results in

$$Z = C \left( \cos \omega t + m_3 \cos 3\omega t + m_7 \cos 7\omega t + m_{11} \cos 11\omega t + \dots \right) \\ + iC \left( -\sin \omega t + m_3 \sin 3\omega t + m_7 \sin 7\omega t + m_{11} \sin 11\omega t \dots \right) \dots\dots\dots (3.2)$$

Fig.101.

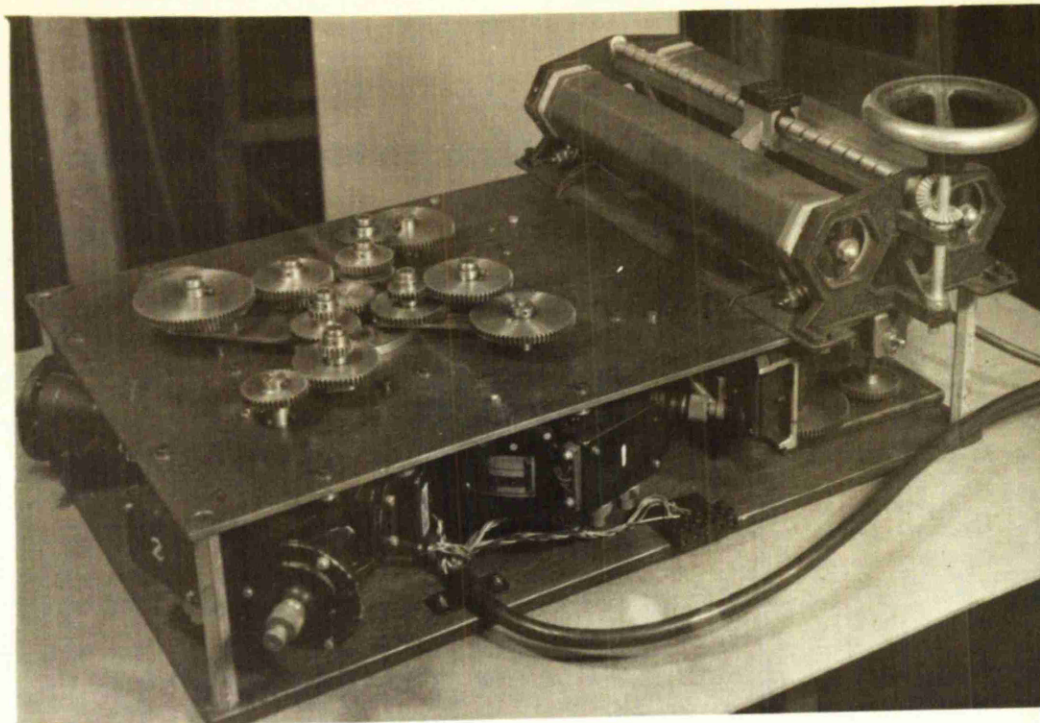
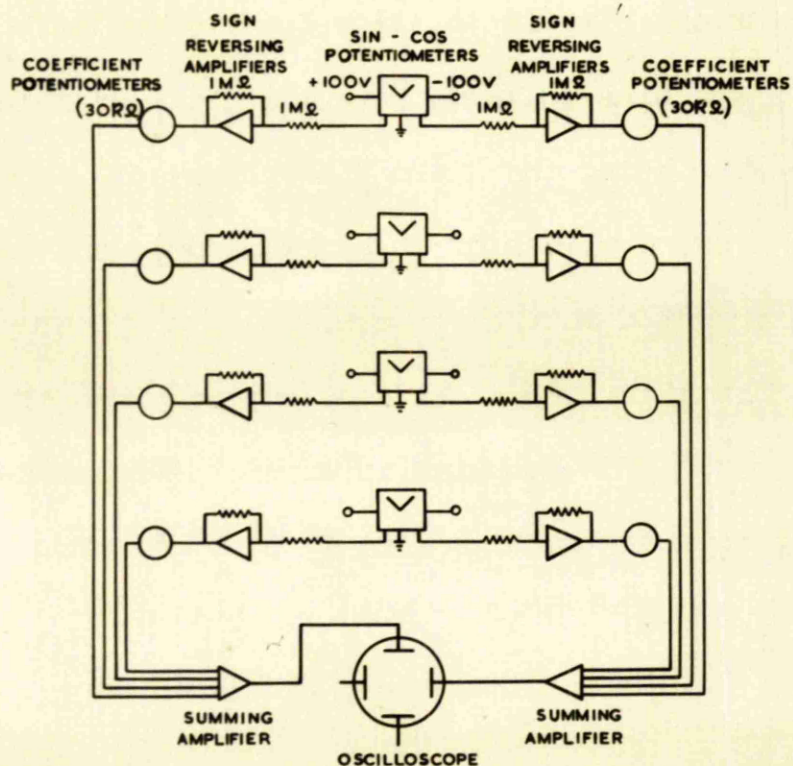


Fig.102.



COMPUTER ARRANGEMENT:

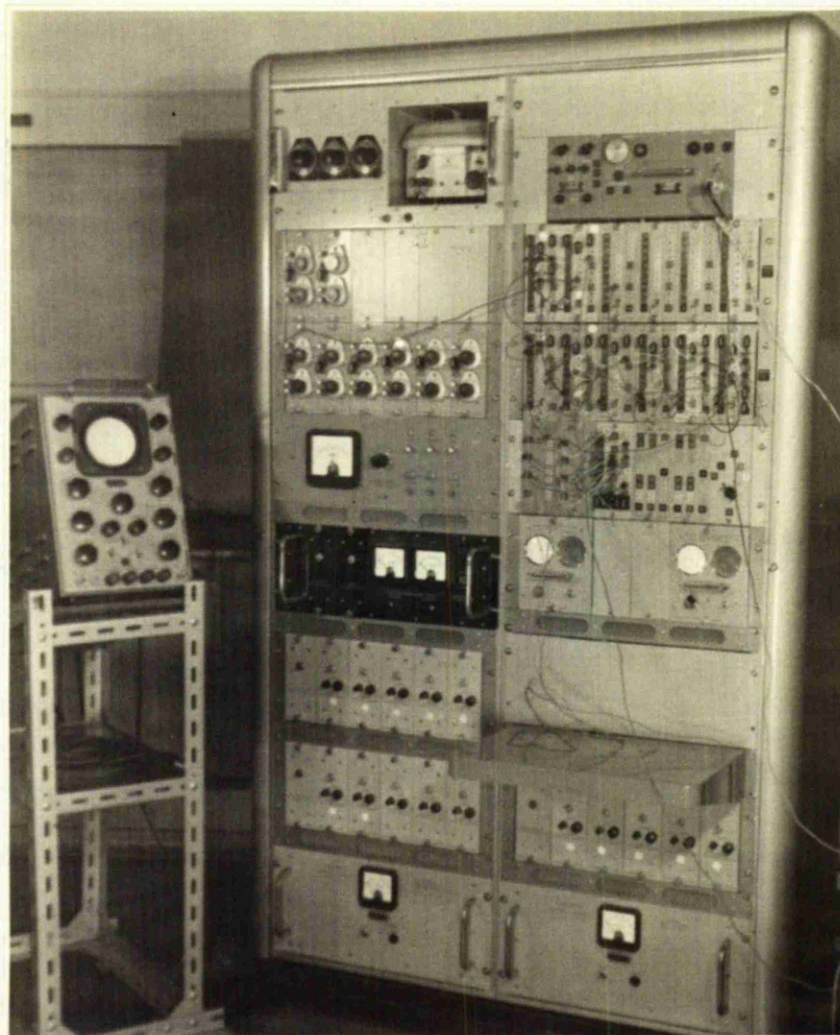
The function generator shown in Fig. 101 was built, using four sine-cosine potentiometers of the rectangular card type, motor driven at related speeds via change wheels, so that different speed ratios were available.

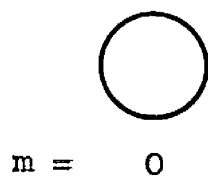
For the transformation of equation (3.2), the potentiometer speeds were  $\omega$ ,  $3\omega$ , and  $7\omega$  and  $11\omega$  radians/sec. The wiring diagram is shown in Fig. 102. The potentiometers were fed from a common  $\pm 100$  volt supply, and the phasing adjusted to produce voltages of  $100 \cos \omega t$ ,  $-100 \sin \omega t$ ,  $100 \cos 5\omega t$  etc. Each voltage was then passed through a sign-reversing amplifier to reduce loading errors in the sine-cosine potentiometers, and thence to an adjustable 10 turn helical potentiometer.

Each potentiometer could be set to give the required coefficients  $m_3$ ,  $m_7$ ,  $m_{11}$ , etc. to an accuracy of 0.1% of its full scale travel, using a bridge circuit to allow for loading effects. The resulting cosine and sine voltages were added in separate summing amplifiers, the sums being the X and Y component of  $Z = \omega(\dot{S})$ . These were fed to the X and Y plates of an oscilloscope, and as the potentiometers generated their respective waveform components, the resultant transformation form was traced out continuously on the oscilloscope screen. The computer is shown in Fig. 103 and the resulting transformations in Figs. 104 a, b, c, d, etc.



Fig.103.





$$\frac{1}{5} + m\zeta^3$$

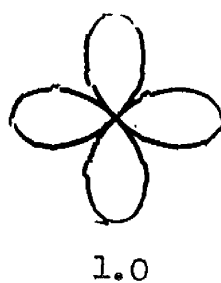
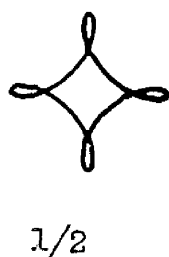
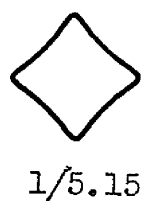
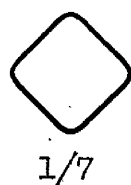


Fig.104a.

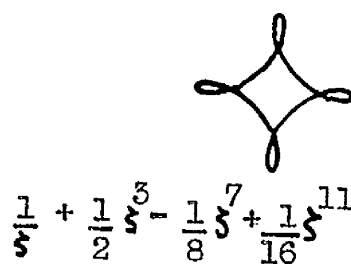
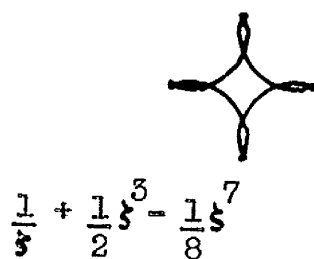
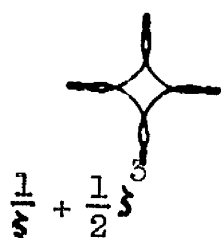


Fig.104b.



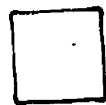


Fig.104c.

$$\frac{1}{z} + \frac{1}{6}z^3$$

$$\frac{1}{z} - \frac{1}{6}z^3 + \frac{1}{56}z^7$$

$$\frac{1}{z} - \frac{1}{6}z^3 + \frac{1}{56}z^7 - \frac{1}{176}z^{11}$$



$$0.146\cos\theta - j 0.102\sin\theta$$



$$-0.03z^3$$



$$-0.1z^3$$



$$-0.16z^3$$



$$-0.16z^3 - 0.038z^5$$

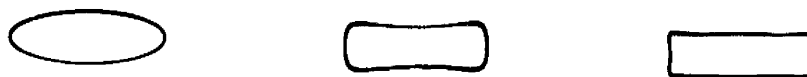


$$-0.16z^3 - 0.038z^5 - 0.01z^7$$



$$0.146\cos\theta - j 0.102\sin\theta - 0.16z^3 - 0.038z^5 - 0.02z^7$$

Fig.104d.



$$\frac{1}{f} + 0.5f$$

$$\frac{1}{f} + 0.5f - 0.125f^3$$

$$\frac{1}{f} + 0.5f - 0.125f^3 - 0.038f^5$$

Fig. 104e.

$$\frac{1}{f} + 0.643f$$

$$\frac{1}{f} + 0.643f - 0.098f^3$$

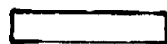
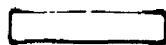
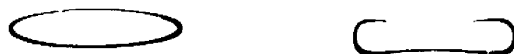


Fig. 104f.

$$\frac{1}{f} + 0.643f - 0.098f^3 - 0.038f^5$$

$$\frac{1}{f} + 0.643f - 0.098f^3 - 0.038f^5 - 0.011f^7$$



$$\frac{1}{\zeta}$$



$$\frac{1}{\zeta} + \frac{1}{10}\zeta^2$$



$$\frac{1}{\zeta} + \frac{1}{6}\zeta^2$$



$$\frac{1}{\zeta} + \frac{1}{4}\zeta^2$$



$$\frac{1}{\zeta} + \frac{1}{5}\zeta^2$$



$$\frac{1}{\zeta} + \frac{1}{3}\zeta^2$$



$$\frac{1}{\zeta} + \frac{1}{2}\zeta^2$$



$$\frac{1}{\zeta} + \frac{2}{3}\zeta^2$$



$$\frac{1}{\zeta} + \zeta^2$$



$$\frac{1}{\zeta} + \frac{1}{3}\zeta^2$$



$$\frac{1}{\zeta} + \frac{1}{3}\zeta^2 + \frac{1}{45}\zeta^5$$



$$\frac{1}{\zeta} + \frac{1}{3}\zeta^2 + \frac{2}{45}\zeta^5$$

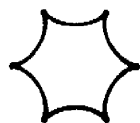


$$\frac{1}{\zeta} + \frac{1}{3}\zeta^2 + \frac{2}{45}\zeta^5 + \frac{1}{162}\zeta^8$$



$$\frac{1}{\zeta} + \frac{1}{3}\zeta^2 + \frac{1}{45}\zeta^5 + \frac{1}{162}\zeta^8$$

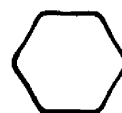
Fig.104g.



$$\frac{11}{5} + \frac{1}{5} \zeta^5$$

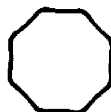


$$\frac{1}{5} + \frac{1}{8} \zeta^5$$



$$\frac{1}{5} + \frac{1}{16} \zeta^5$$

Fig.104h.



$$\frac{1}{5} + \frac{1}{25} \zeta^7$$

Fig.104i.

CHOICE OF TRANSFORMATION FORM.

From the results illustrated, it is evident that the basic shape produced by the transformation is mainly determined by the first two terms in the series, while the higher terms, having smaller coefficients, have a minor effect on the basic shape, but obviously affect the corner radii.

The method was therefore applied in two stages, firstly to determine the changes in shape due to the use of the first two terms in the series, with variation of the coefficient of the second term, and secondly to examine the changes in shape due to the addition of successive terms in the series. It is shown by the results (see Fig. 104) that it is possible to reduce the corner radii at the expense of loss of straightness of the sides of the transformed openings.

It was possible using the first method of application, to determine suitable two-term transformations to give a reasonable degree of correspondence to the forms of discontinuities considered in the theoretical analysis given in Chapter II.

It was noted that the number of sides of a transformation outline was one greater than the highest power in the  $\zeta$  - series.

In the case of the rectangular form, the terms  $\frac{1}{\zeta} + m\zeta$  are combined to give an ellipse of axes  $(1 + m)$  and  $(1 - m)$  then terms in  $\zeta^3$  and  $\zeta^5$  are added to give 'rectangular' outlines.

$$\begin{aligned} \text{That is } Z = \omega(\zeta) &= \frac{1}{\zeta} + m\zeta + m_3\zeta^3 + m_5\zeta^5 + \dots \\ &= \left[ (1 + m)\cos \omega t + m_3\cos 3\omega t + \dots \right] \\ &\quad + i \left[ -(1 - m)\sin \omega t + m_3\sin 3\omega t + \dots \right] \dots\dots\dots (3.5) \end{aligned}$$

This application of a Minispace analogue computer is to the writer's knowledge original, and is a rapid technique for the determination of

DETERMINATION OF THE SUM OF THE PRINCIPAL STRESSES USING  
THE CONDUCTING PAPER ANALOGY AS AN ADJUNCT TO THE PHOTOELASTIC ANALYSIS

THEORY: The distribution of steady state potential  $V$  in a thin conducting sheet of constant thickness and uniform resistivity is governed by the LAPLACE differential equation

$$\frac{\partial^2 V}{\partial x^2} + \frac{\partial^2 V}{\partial y^2} = 0 \quad \dots\dots\dots(3.4)$$

where  $x$  and  $y$  are co-ordinates in the plane of the sheet. Also, the distribution of the sum of the principal stresses  $(\sigma_1 + \sigma_2)$  in a tension field are governed by a similar equation

$$\frac{\partial^2(\sigma_1 + \sigma_2)}{\partial x^2} + \frac{\partial^2(\sigma_1 + \sigma_2)}{\partial y^2} = 0 \quad \dots\dots\dots(3.5)$$

and this forms the basis of the analogy.

NOTE: Additionally to the above, equations of the POISSON type

$$\frac{\partial^2 \rho}{\partial x^2} + \frac{\partial^2 \rho}{\partial y^2} = \text{constant} \quad \dots\dots\dots(3.6)$$

can be transformed into the LAPLACE form, and hence the analogy can be extended to include such cases. In particular, for cases of torsion, the distribution of the modified stress function  $\psi$  in plane sections under pure torsion, is governed by the equation

$$\frac{\partial^2 \psi}{\partial x^2} + \frac{\partial^2 \psi}{\partial y^2} = 0 \quad \dots\dots\dots(3.7)$$

where  $\psi = \phi + \frac{G\theta}{2} (x^2 + y^2)$

$\phi$  = shear stress function

$G$  = modulus of rigidity

$x, y$  = co-ordinates of points in the plane of the section.

Fig.105.

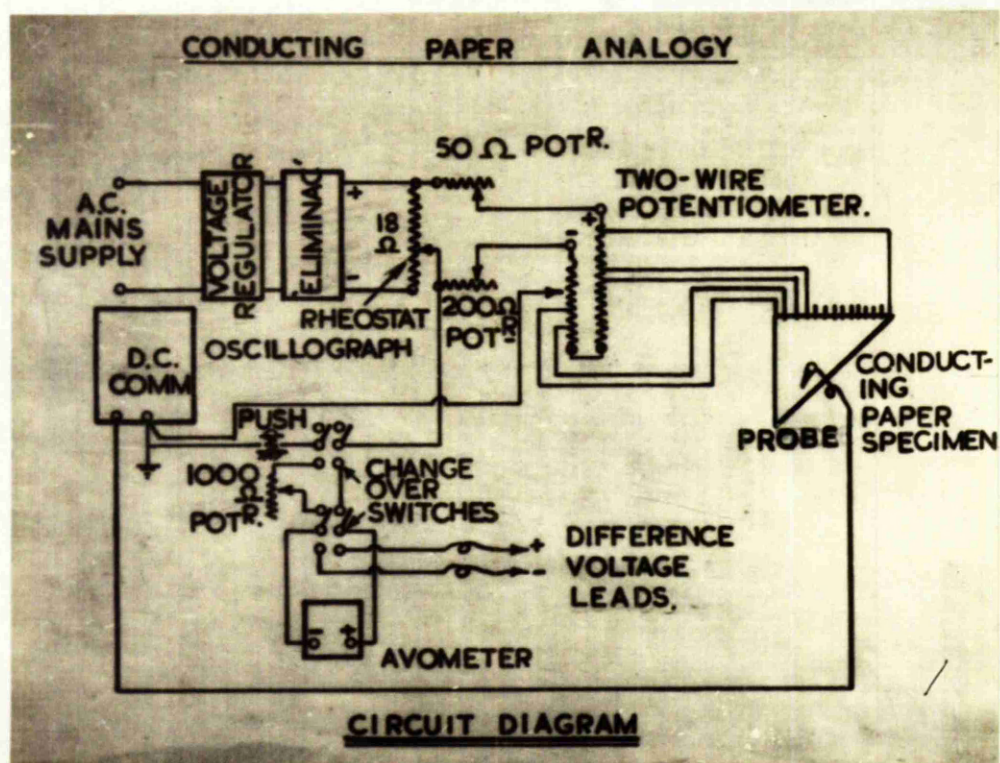
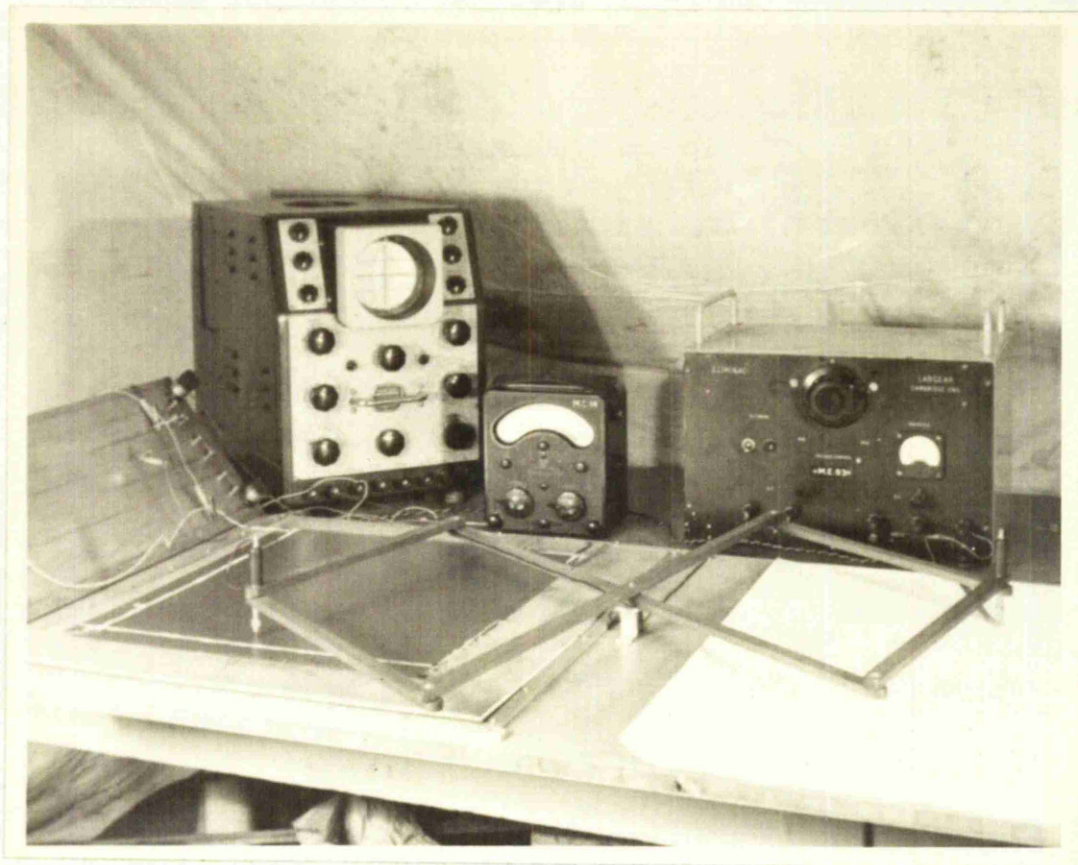


Fig.106

In this application, the use of the symbols  $\phi$ ,  $\psi$  and  $\theta$  are confined strictly to the case of torsion, which was used as an accuracy check on the conducting paper method, and they bear no relation to the symbols used in the theoretical treatment for complex potentials.

#### APPARATUS AND TECHNIQUE:

The equipment is shown in Fig. 105 and the circuit diagram in Fig. 106.

The arrangement provided means of supplying boundary voltages from a potentiometer, to the conducting paper specimen, the boundary voltages (in volts/fringe) corresponding to the known boundary stresses determined from the stress specimen. Boundary voltage wires were soldered to office staples which pierced the conducting paper at the selected points, which were then spotted with silver solution. The conducting paper specimens were cut from 21" wide rolls of Teledeltos recording paper of resistance approximately 2500 ohms per square. The outline was an enlarged version of the photoelastic model, with the exception that dimensions taken across the paper were modified by multiplying these measurements by  $\rho_y/\rho_x$  where  $\rho_y$  and  $\rho_x$  are the resistivities along and across the roll respectively. This allowed for non-uniform resistivity of the material available.

Voltages at points on the paper were measured by a probe, using an oscilloscope as a null reading indicator, the balancing voltages then being read by an Avometer. The pantograph arrangement (Fig. 105) facilitated the plotting and recording of voltage contours and voltage values at hole boundaries.



912 DISTRIBUTION OF  $\frac{\sigma_1 + \sigma_2}{\sigma_0}$  ALONG HORIZONTAL CENTRE  
LINE FOR ELLIPTIC HOLE IN TENSION PLATE  $\frac{b}{a} = 2.45$

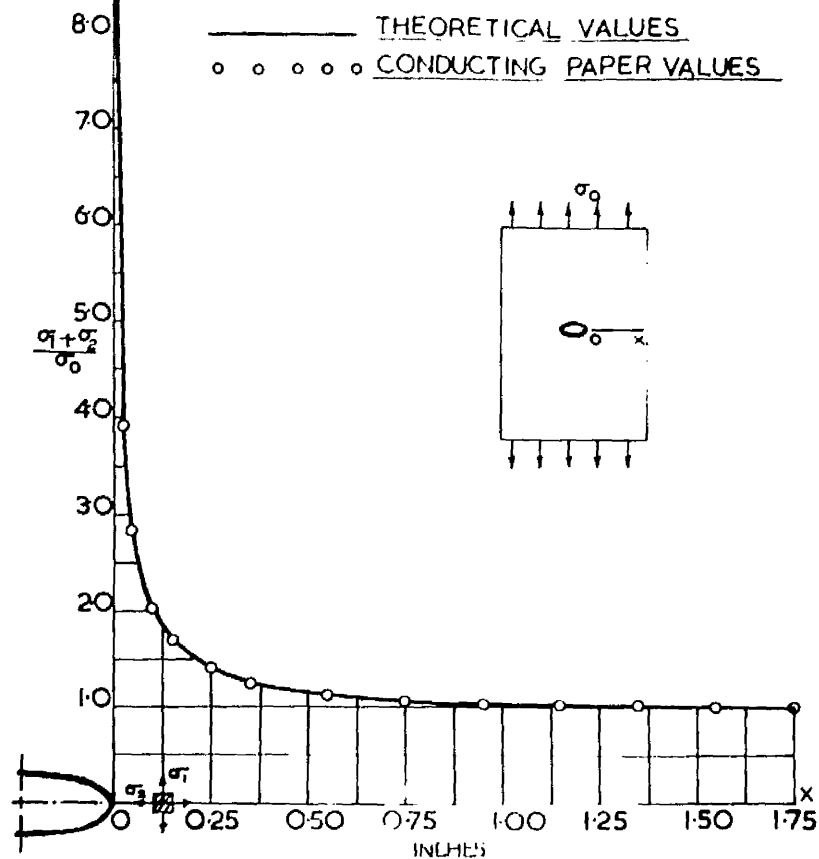


Fig.107.

DISTRIBUTION OF  $\frac{\sigma_1 + \sigma_2}{\sigma_0}$  ALONG HORIZONTAL CENTRE LINE  
FOR ELLIPTIC HOLE IN TENSION PLATE  $\frac{b}{a} = \frac{2}{3}$

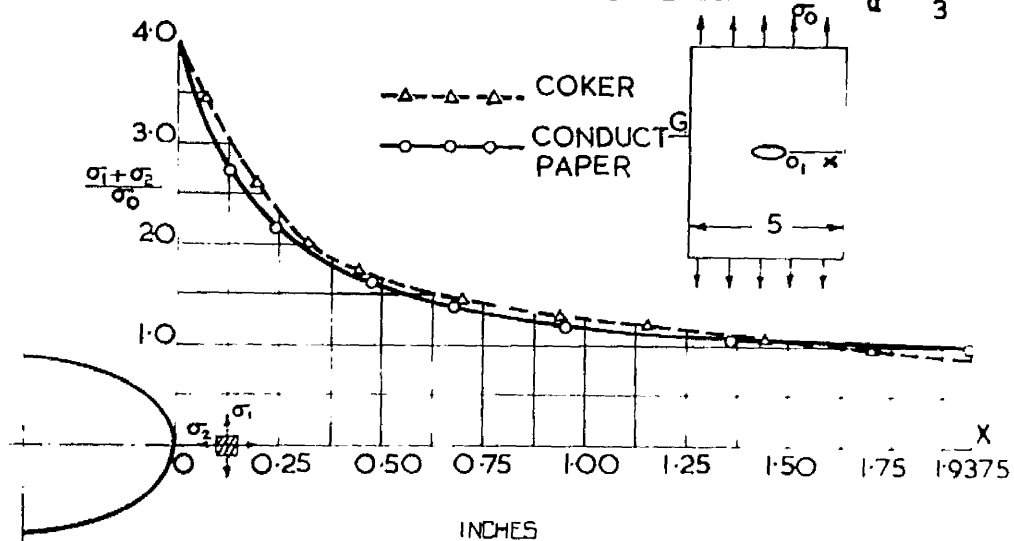


Fig.108a.

ESTABLISHMENT OF RELIABILITY:

The reliability of the method was established in three ways, the first two of which are described here, the third being a torsion case which is given in Appendix Chapter VII.5.

- (i) A comparison was made between the exact theoretical and conducting paper distributions for the sum of the principal stresses  $(\sigma_1 + \sigma_2)$  along an axis of symmetry through the major axis of an elliptical discontinuity in a tension plate, corresponding to theoretical boundary values. The direction of tension was taken perpendicular to the major axis of the ellipse. The results are shown in Fig. 107 and it is evident that excellent agreement was obtained. It should be noted that this ellipse is the 'equivalent' ellipse for the horizontal arm of the cruciform 'crack', and that the distribution of  $\frac{\sigma_1 + \sigma_2}{\sigma_0}$  was calculated using the appropriate exact theoretical solution for this form of opening as quoted by COKER and FILON in their 'Treatise on Photoelasticity'.
- (ii) A comparison was made between COKER'S experimental  $(\sigma_1 + \sigma_2)$  distribution and the conducting paper distribution, for an elliptical hole as in (i), using COKER'S experimental boundary values. The results obtained for axes through the major and minor axes of the ellipse are given in Fig. 108a and 108b. It is seen that the conducting paper method provides a relatively more consistent variation than that given by COKER, while remaining in close agreement with same.

The maximum deviation in both of the foregoing tests was only 2.1/2%.

Fig.108b.

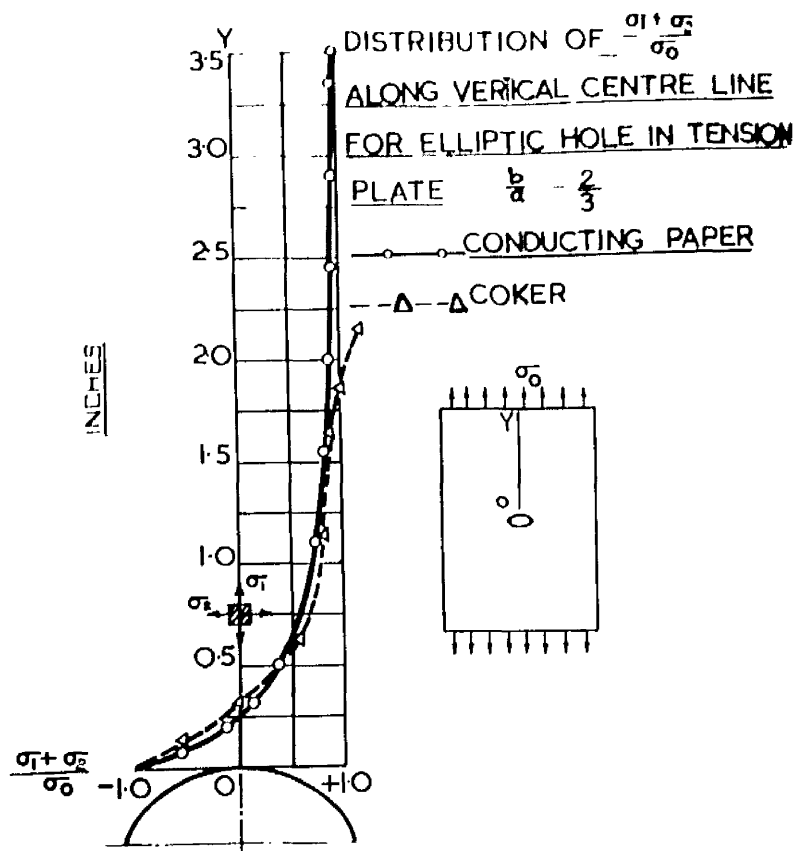
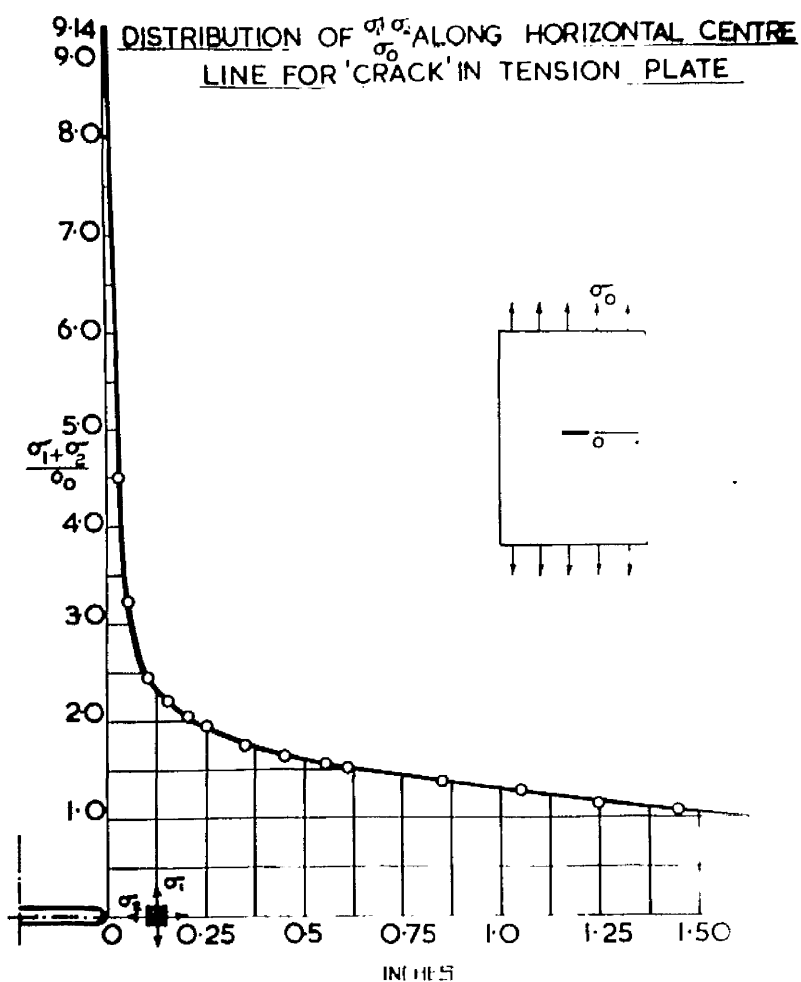


Fig.109.



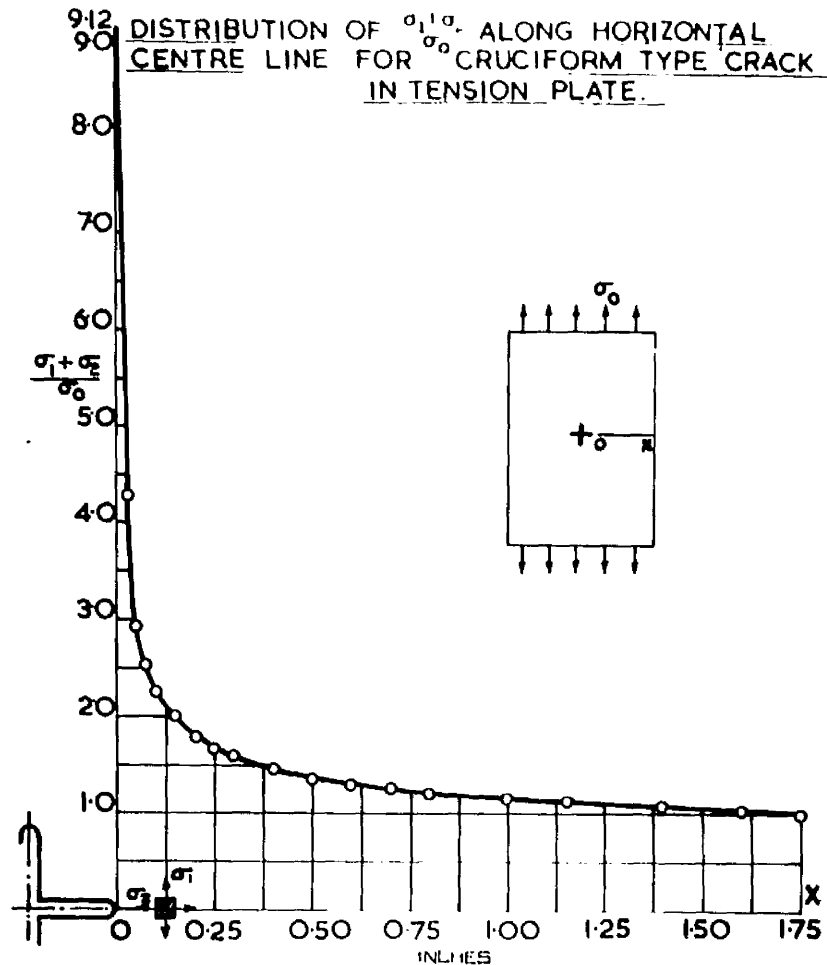


Fig.110.

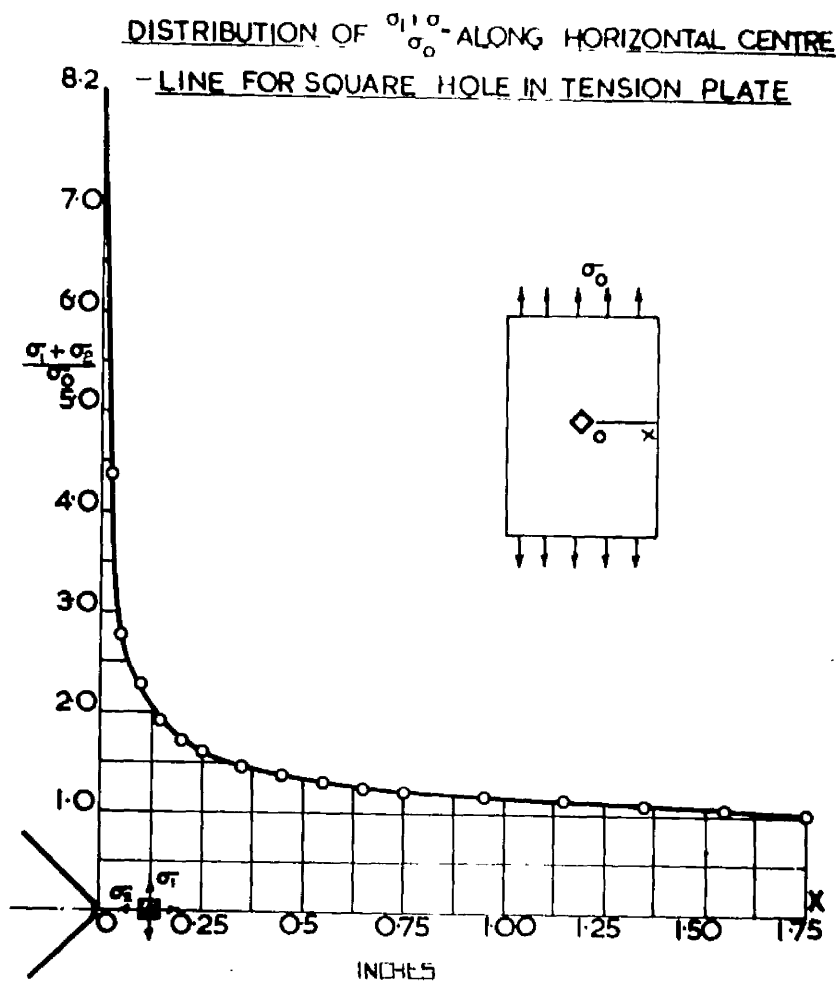


Fig.111.

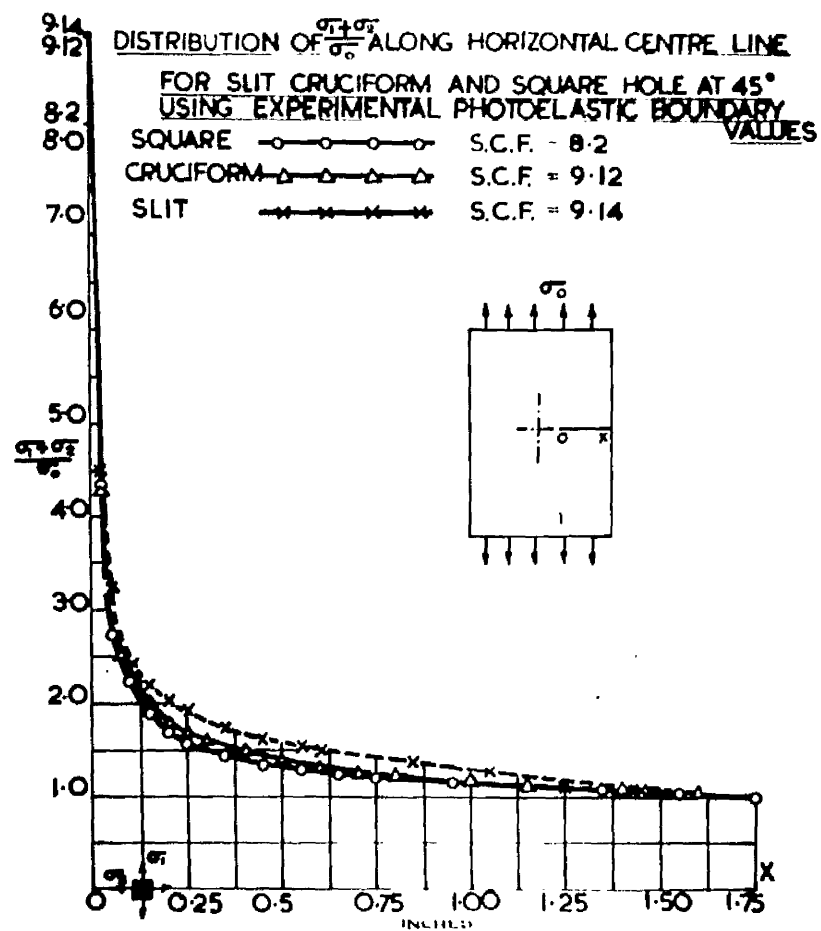


Fig.112.

APPLICATION:

The sums of the principal stresses ( $\sigma_1 + \sigma_2$ ) along the horizontal centre lines of plates in uniaxial tension containing different shapes of discontinuities, were determined by the conducting paper analogy. The types of discontinuities considered were a 'crack' in the form of a narrow slit, a cruciform type 'crack' and a square discontinuity with diagonals parallel and alternatively perpendicular to the axis of the applied tension.

The boundary values applied to the conducting paper specimen were related to the stress values obtained from the photoelastic tests described in paragraph III.3.

The  $(\sigma_1 + \sigma_2)/\sigma_0$  distributions obtained are shown in Figs. 109, 110, and 111, and also together with the photoelastic results of the next section (III.5). These distributions are superimposed for comparison in Fig. 112.

(NOTE: The third test for reliability of the conducting paper technique was made on specimens of rectangular cross-section, together with a shaft section containing a British Standard keyway, all subjected to torsion. The results are given in Appendix 7.3)

In all of the foregoing, it has been conclusively established that the conducting paper analogy is a reliable and accurate method for the determination of the sum of the principal stresses in tension fields.

DETERMINATION OF THE DIFFERENCE OF THE PRINCIPAL  
STRESSES BY PHOTOELASTICITY

BASIS:

The photoelastic method is so well-known that only a brief outline of its basic concepts is introduced here. The method is used primarily for the determination of the difference of the principal stresses ( $\sigma_1 - \sigma_2$ ) in plane stress fields. The model material has the characteristic property of birefringence when subjected to stress. The stressed, transparent plastic model is viewed in a beam of plane or circularly polarised light, the relative retardation of the appropriate light wave components being directly related to the principal stress difference ( $\sigma_1 - \sigma_2$ ) at the particular point viewed. This relative retardation is measured by optical interference fringes, which can be stress-scaled by means of a calibration specimen.

In the determination of stress concentration factors and stress distributions, there is usually no need to calculate the actual stress values, since the stress values may be expressed in terms of photoelastic fringe values, relative to the boundary fringe value  $\sigma_0$ . This method has been adopted in the photoelastic work described herein.

Specimen Material

The material used for the tests was Columbia Resin (C.R. 59). This resin, being cast-polymerised between glass plates is highly transparent, hard, strong and has optical clarity equal to that of plate glass. The stress-optical sensitivity of Columbia Resin is high, and compares well with Bakelite B.T. 81 - 695.

The stress-retardation curve is linear up to approximately 3000 lb/in<sup>2</sup>. Optical creep is not pronounced at stresses well below this figure, but at the higher end of the linearity range, can prove troublesome.

Time-edge stress effects and machining stress edge effects may also be evident, but can be avoided by careful machining followed by immediate testing of the specimen.

From a typical calibration specimen of 0.105 in<sup>2</sup> cross-sectional area, loaded in tension to 267 lb. the third order fringe appeared, and from this the

$$\text{Model Fringe Value} = \frac{P}{An} = \frac{267}{0.105 \times 5} = 866 \text{ lb/in}^2/\text{fringe tension.}$$

#### SPECIMEN SIZE:

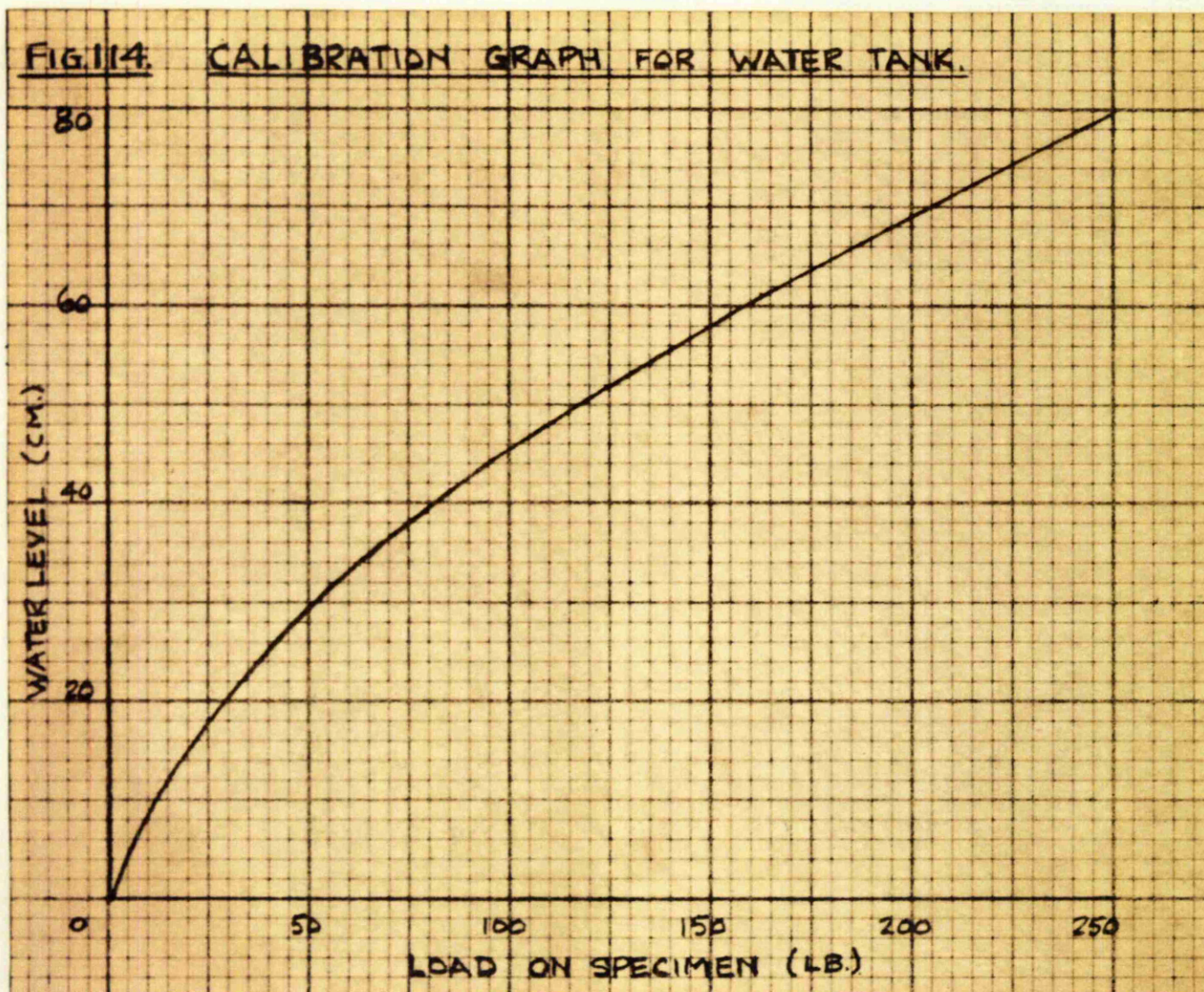
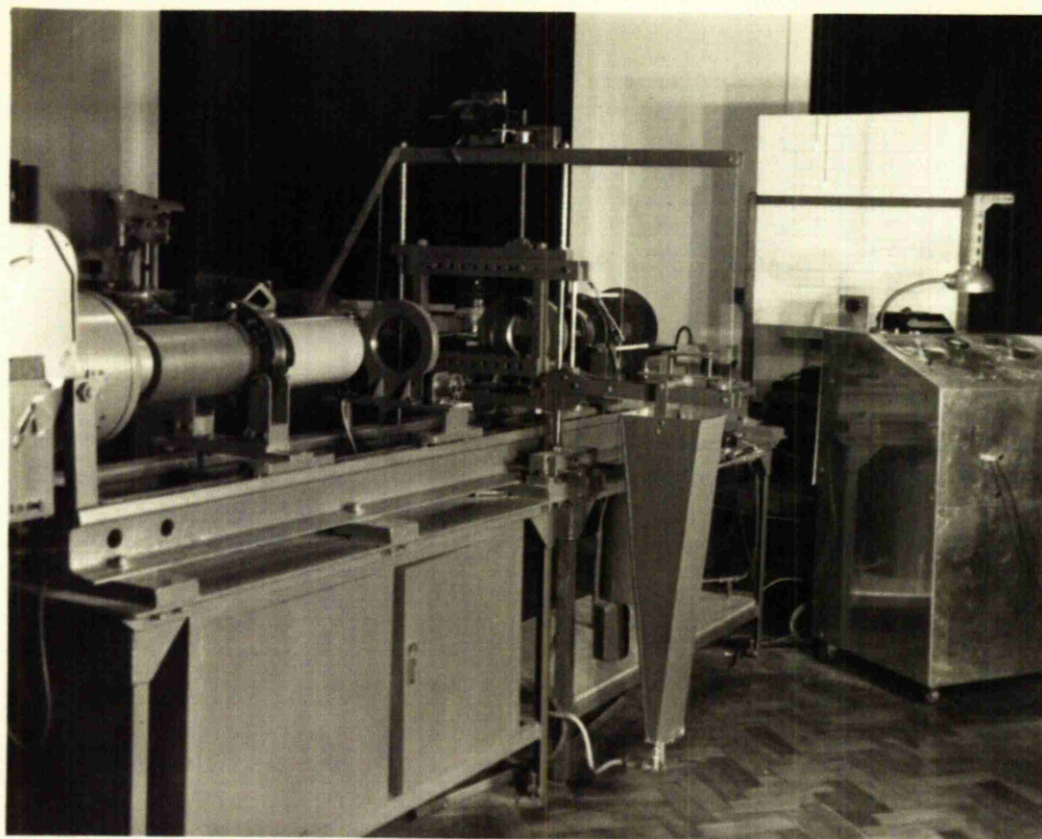
Each specimen was 6.1/4" long x 4" wide x 1/16" thick, and the maximum width of discontinuity was 1/2". This gave a discontinuity width/plate width ratio of 1/8, and as has been shown by the writer in previously published work, (29, 54) a minimum ratio of 1/6 gives, for practical purposes, infinite plate conditions.

#### SPECIMEN PREPARATION:

The specimens were cut from the main sheet by a pantograph engraving machine, using enlarged templates for the profiles of the discontinuities. The cutter diameter was .050", and fine cuts at high speeds and light feeds were employed, with a copious supply of cutting compound. This produced specimens with clean cut edges, free from machining stress fringes. The actual dimensions of the various discontinuities cut in the plates were measured using an Engineers' microscope.



Fig. 113.



APPARATUS AND EXPERIMENTAL TECHNIQUE:

The photoelastic polariscope used, which was designed and built by the writer, is shown in Fig. 113 and consisted of 5 inch aperture collimating and collecting lenses of 12 inch focal length, together with remotely controlled, rotatable 5" diameter polaroids and mica quarter-wave-plates. The light sources were a 10 volt, 240 watt compact source tungsten-filament prefocus lamp, and a 250 volt, 500 watt compact source mercury vapour pre-focus lamp, together with a rear parabolic reflector. Wratten 77 and 58 filters were employed to isolate the mercury green line when required.

Photography of the overall fringe patterns was carried out using a 5" x 4" technical plate camera, and for regions of high stress, where the fringes were closely spaced, a microscope and microscope camera were employed. In every test, light and dark field photographs were taken, as a standard routine. For measuring the relative positions of these closely spaced fringes, a travelling microscope was used to directly view and measure the fringe pattern spacing. Loading of the specimens was carried out via friction grips, by a lever system employing a water loading tank, giving variable loading rates. The calibration graph for the water tank is shown in Fig. 114.

For the determination of uniform tension fringe orders, and for fractional fringe orders in the specimen, the fringe patterns were projected on to a 3 ft. square white projection screen carrying a photo-multiplier which was coupled to a moving coil galvanometer. The Sénarmont method of compensation was employed to establish the fringe values required.



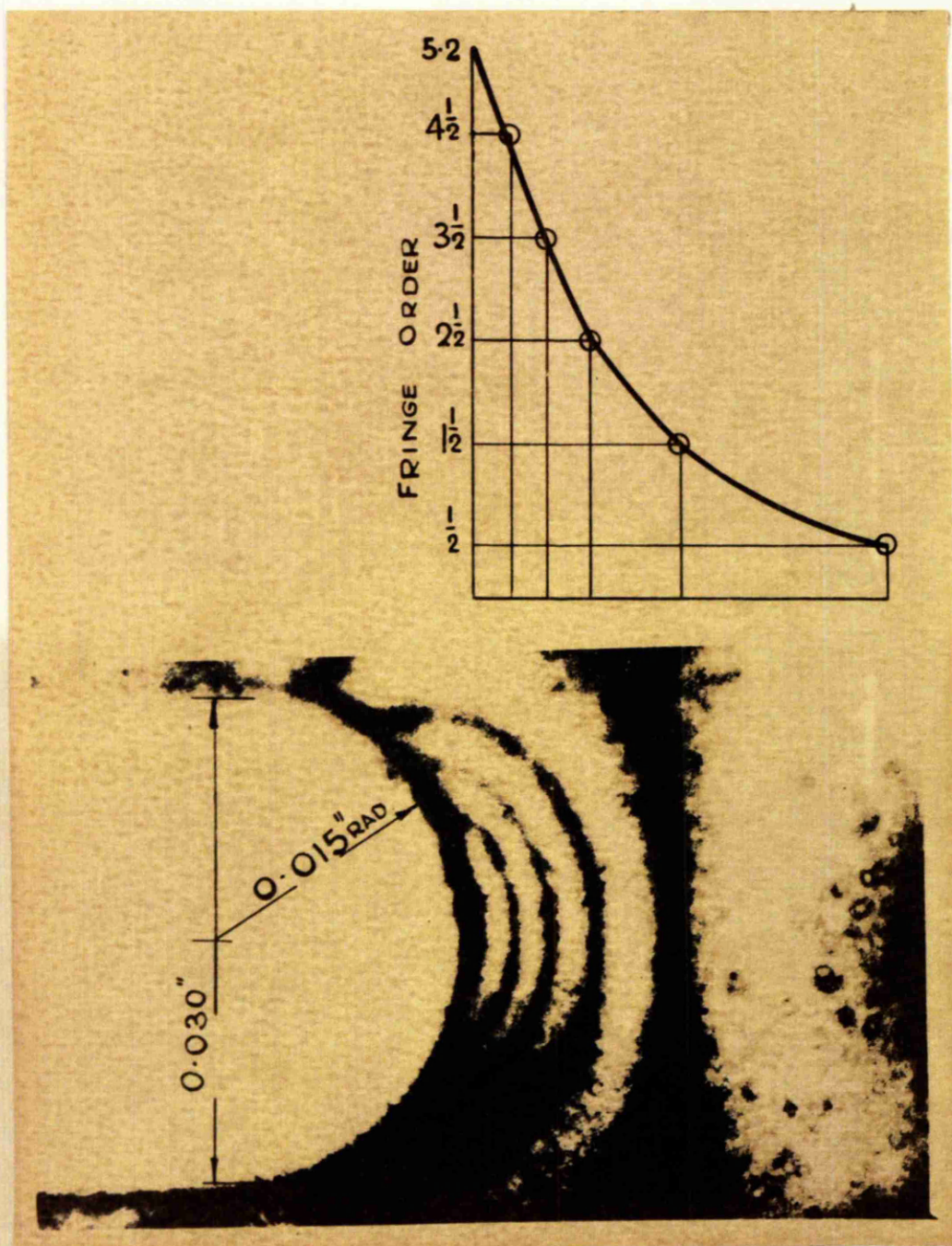


Fig.115.

Boundary fringe values in regions of high stress were found by plotting the fringe order distribution along selected axes, and extrapolating to meet the boundary (Fig. 115).



Fig.116a.

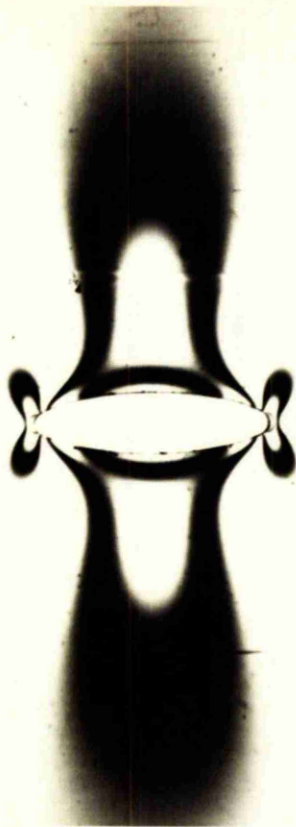


Fig.116b.

EXPERIMENTAL RESULTS

A total of twenty-seven different types of discontinuities were investigated experimentally. In addition to light and dark field photographs of the area around the discontinuity, similar photographs were also taken through the microscope, of the area in the region of the highest stress. To demonstrate the clarity of the fringe patterns produced for these highly stressed regions, Fig. 115 shows the light field photograph of the region at the end of the horizontal arm of a cruciform type 'crack' opening in a tension plate, the magnification being about 80X, as photographed by the microscope camera and subsequently enlarged by a 35 mm. enlarger. A selection of typical light field photographs are shown in Figs. 116a, b, c, d, etc. the boundaries of the specimens being clearly visible.

The distributions of the differences of the principal stresses along selected axes were determined for a representative range of eleven of these specimens. In the case of three of these the complete stress analysis procedure was carried out, the  $(\sigma_1 - \sigma_2)$  graphs obtained from the photoelastic fringe patterns being combined with the corresponding  $(\sigma_1 + \sigma_2)$  graphs obtained by the conducting paper method, all values being expressed in terms of the uniform tension fringe value  $\sigma_0$ . The distributions of the separate principal stresses, expressed in terms of the uniform tension fringe value are shown in Figs. 117 to 125.

For the remaining sixteen specimens, values of maximum stress concentration were determined, from the ratio of the maximum fringe order at the discontinuity to the uniform tension fringe order, and these stress

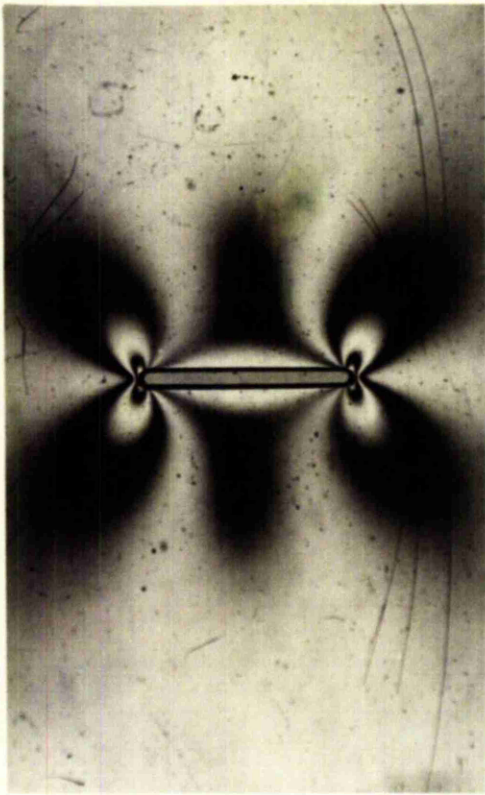


Fig. 116c.

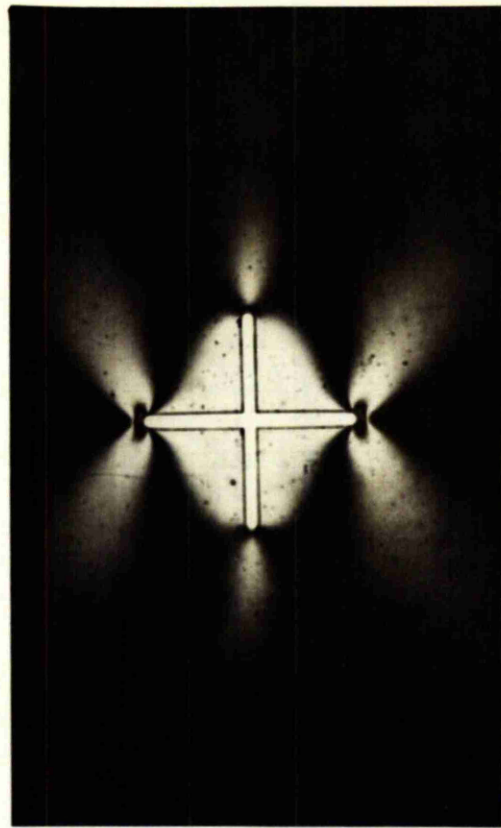


Fig. 116d.

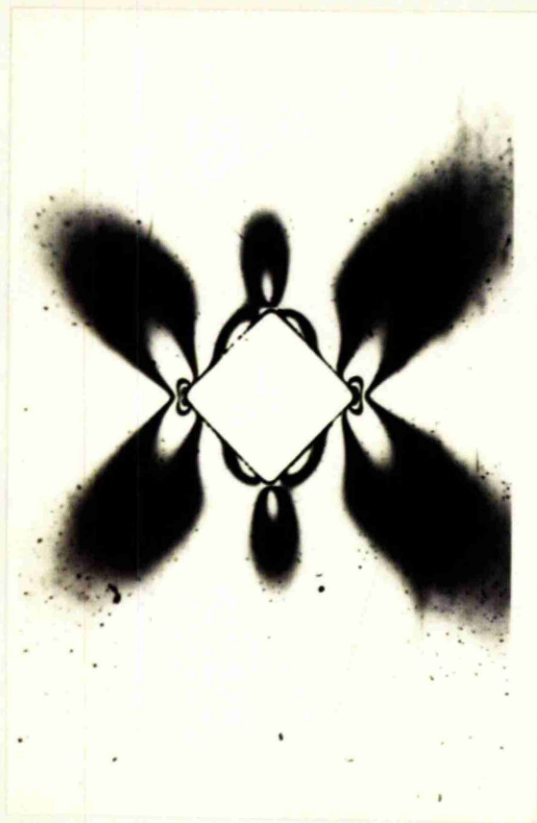


Fig. 116e.

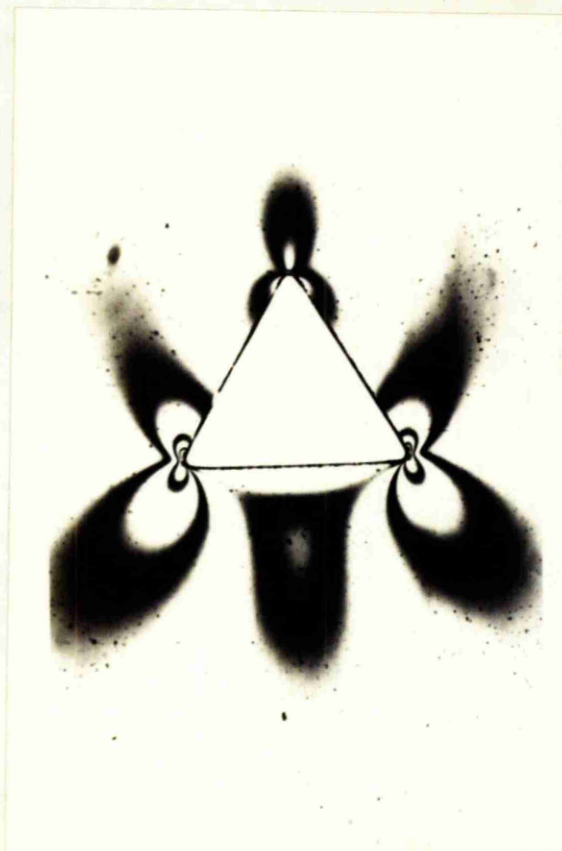


Fig. 116f.



stress concentration factors are shown together with the stress concentration factors for the rest of the specimens, in the comprehensive table of Fig. 126.

For the range of square and 'barrel' shaped discontinuities investigated experimentally, the fringe orders round the openings were determined, and these values, expressed in terms of the uniform tension fringe order  $\sigma_0$ , give the variation in stress concentration factor round the boundary of the discontinuities. These results are shown in Fig. 127.

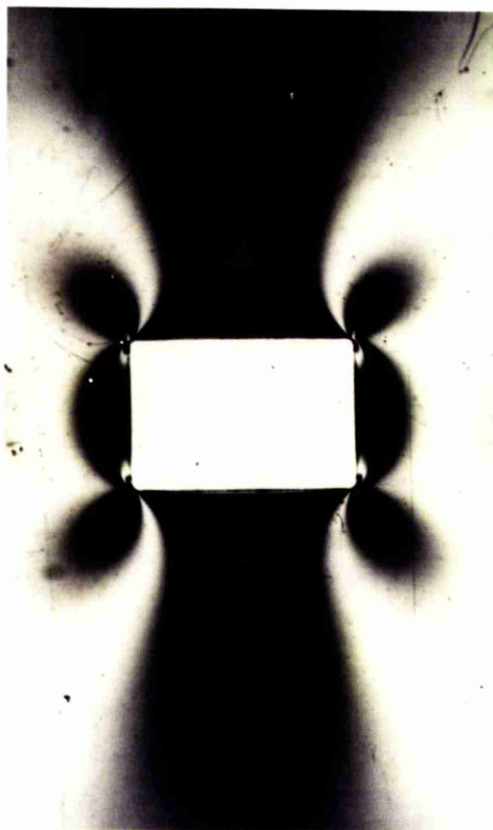


Fig.116g.

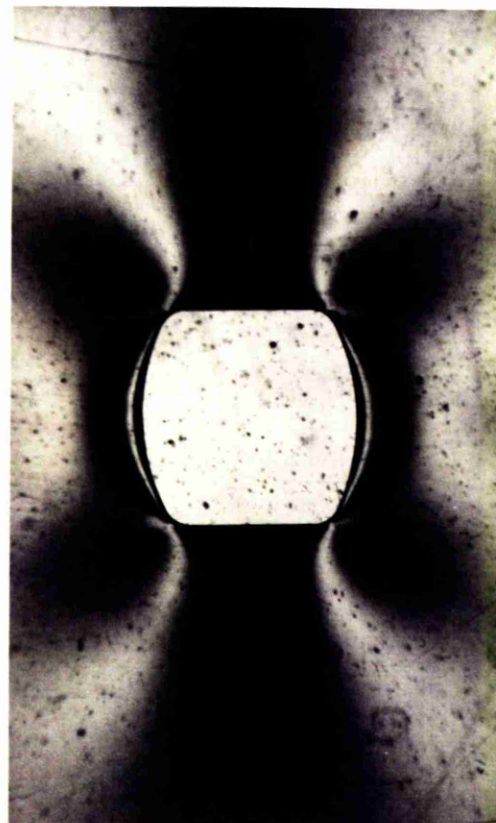


Fig.116h.



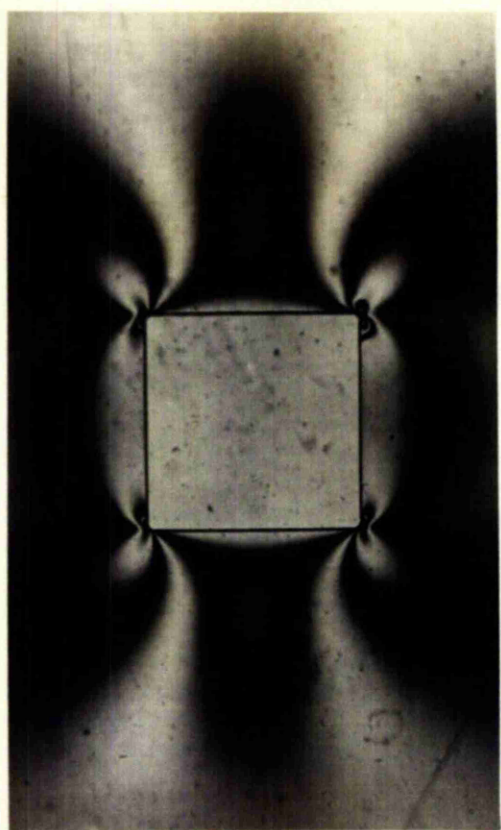


Fig. 116 i.

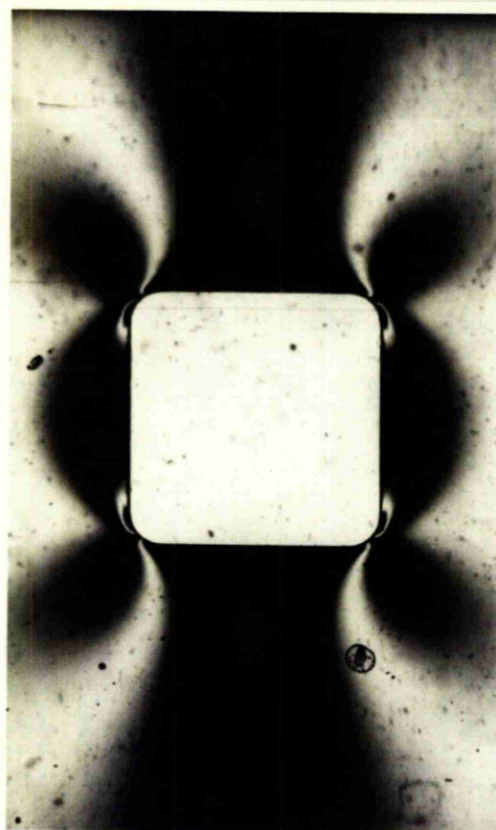


Fig. 116 j.

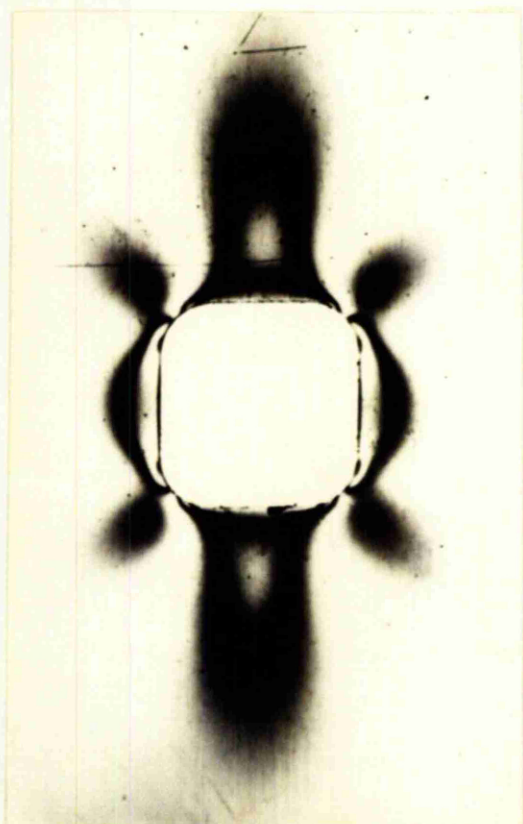


Fig. 116 k.

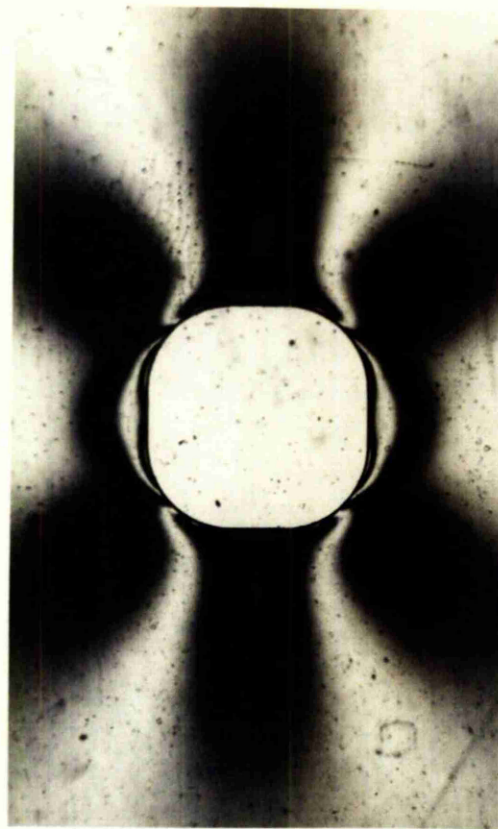


Fig. 116 l.

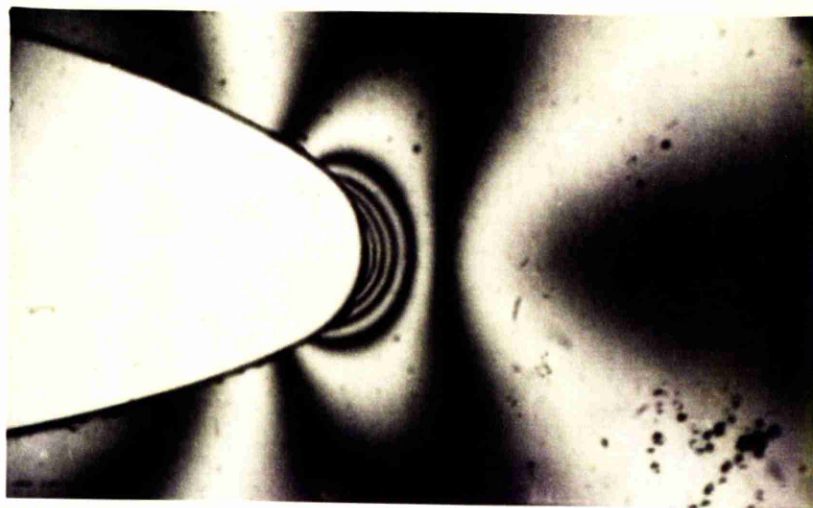
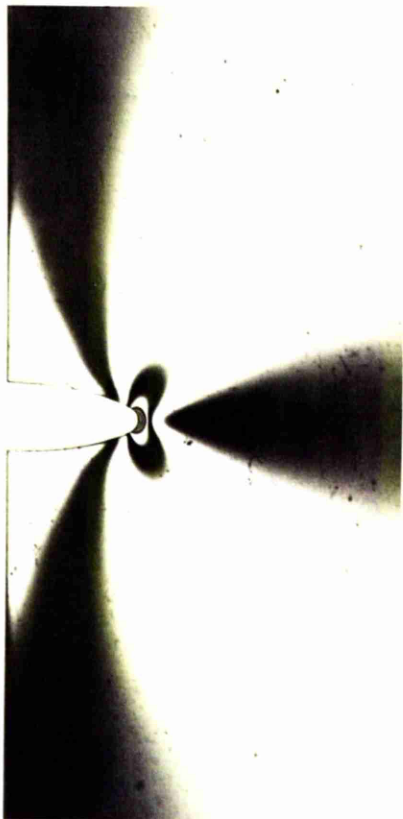


Fig.116 m.

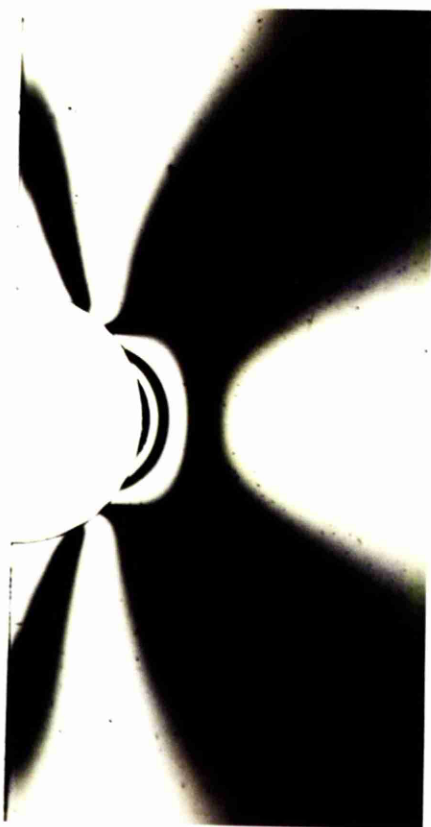


Fig.116 n.

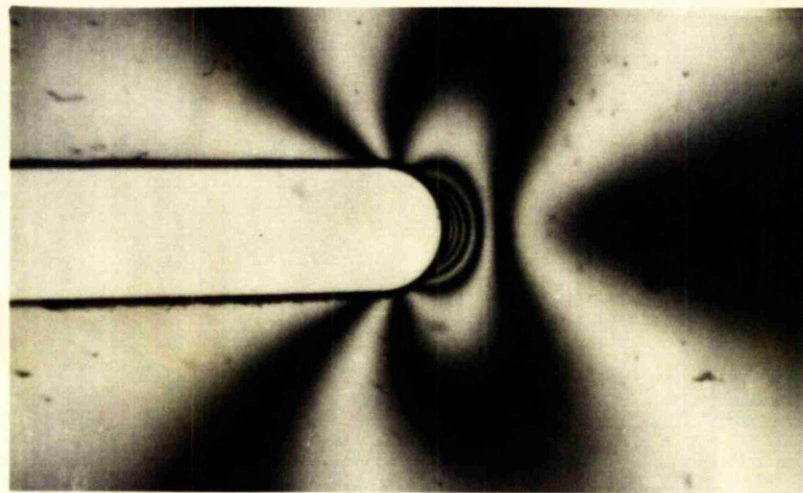
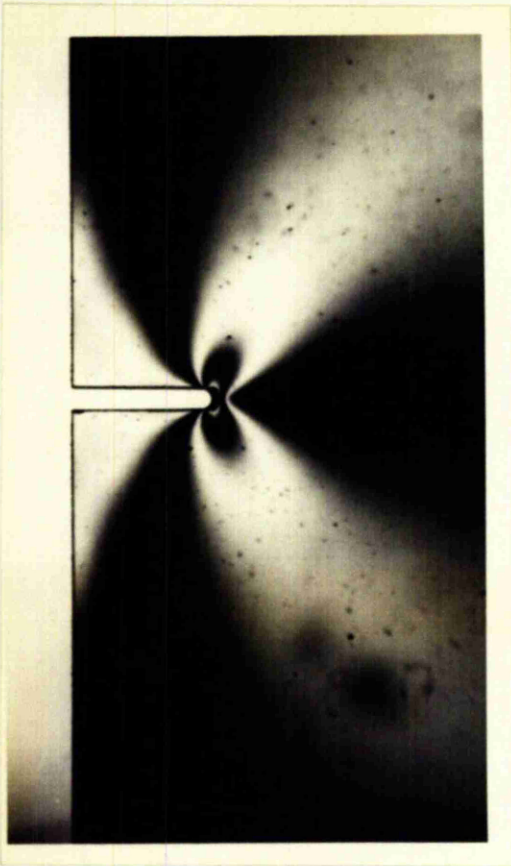


Fig.116 o.

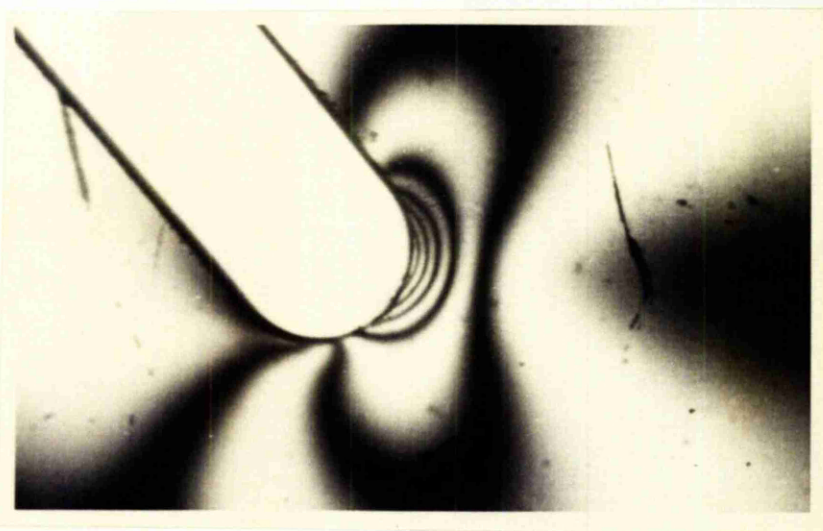
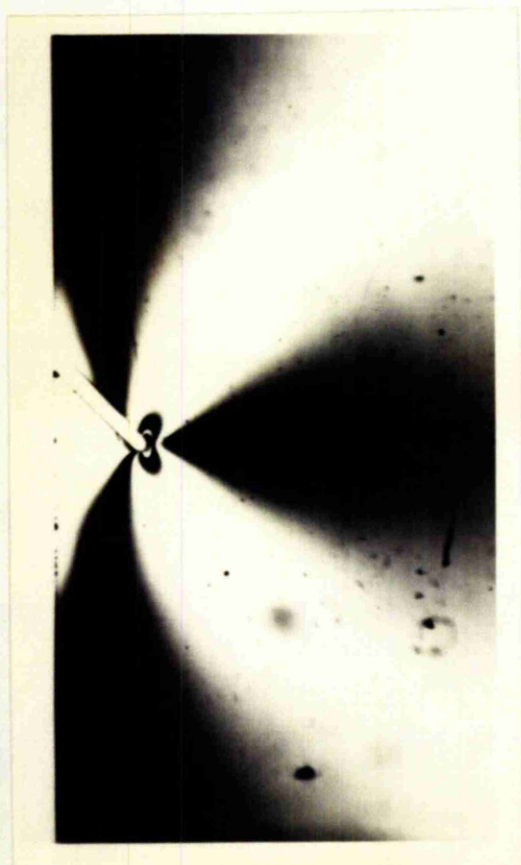


Fig.116 p.



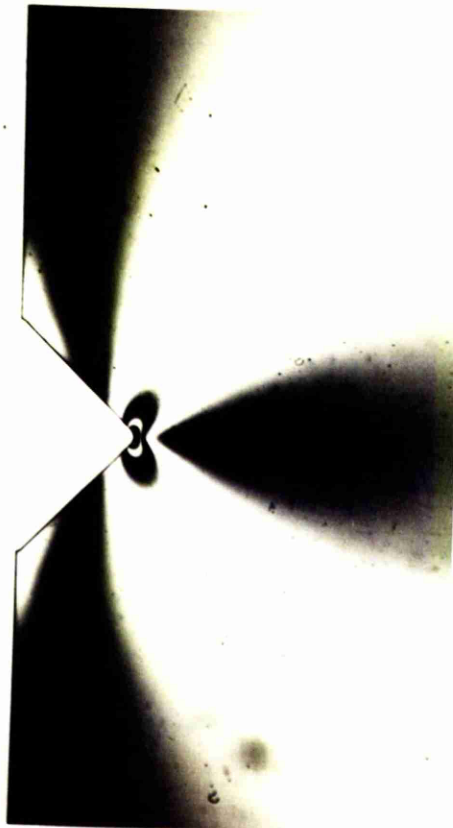


Fig.116 q.



Fig.116 r.

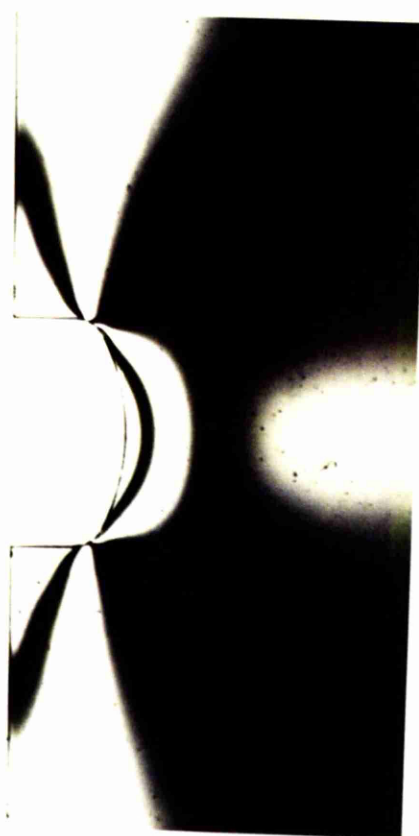
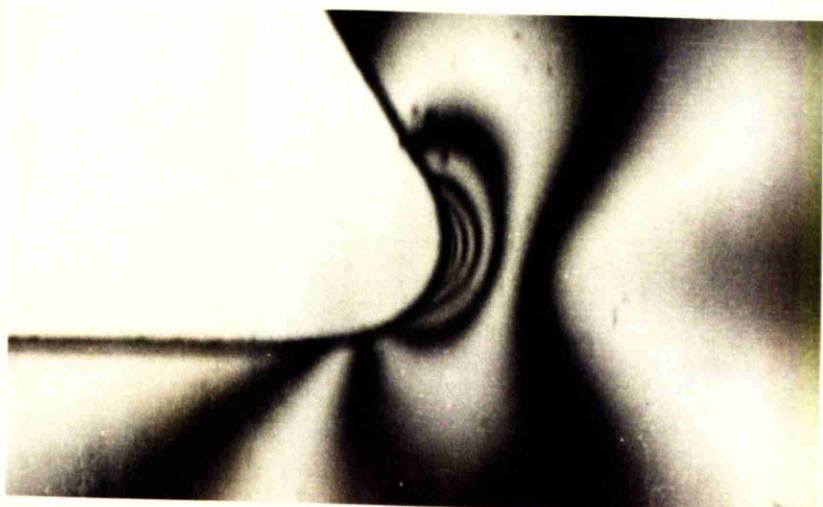
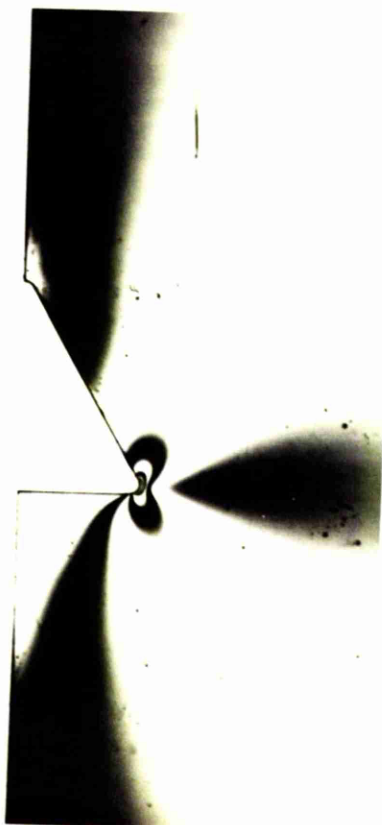


Fig.116 s.



Figs.117 - 125.

(STRESS DISTRIBUTIONS.)

Fig.117a.

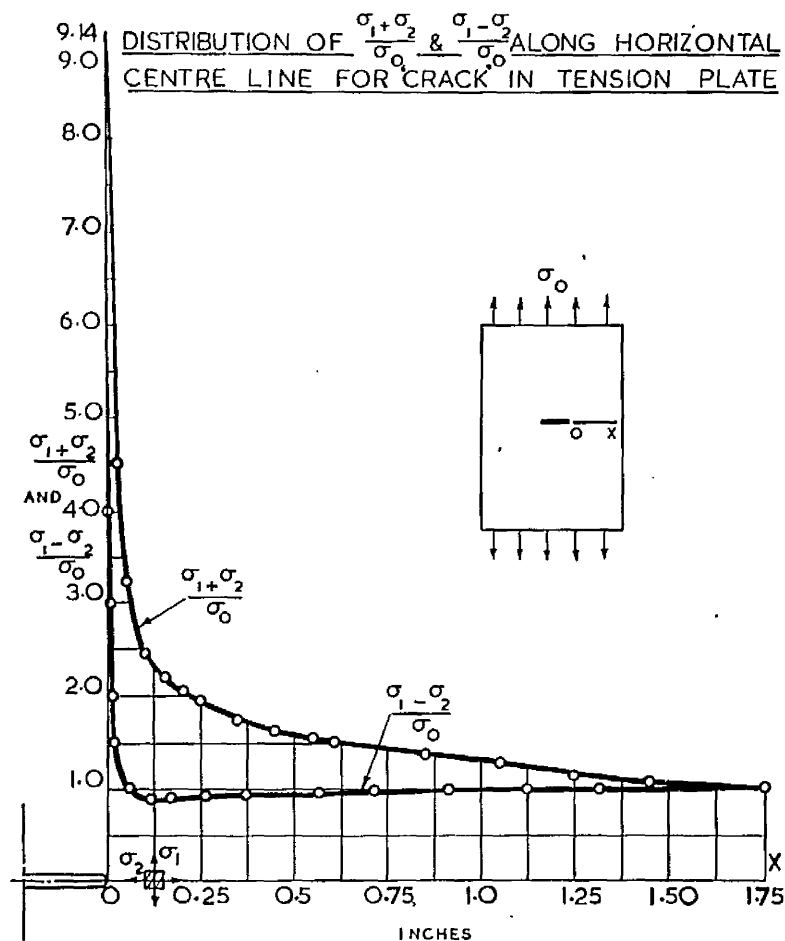
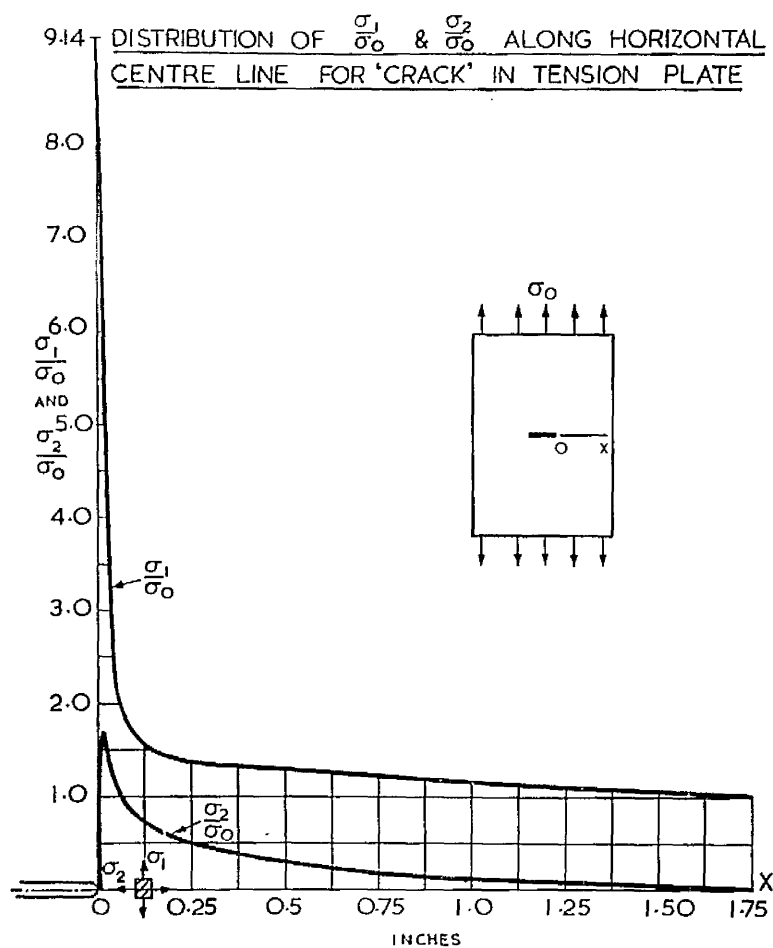


Fig.117b.



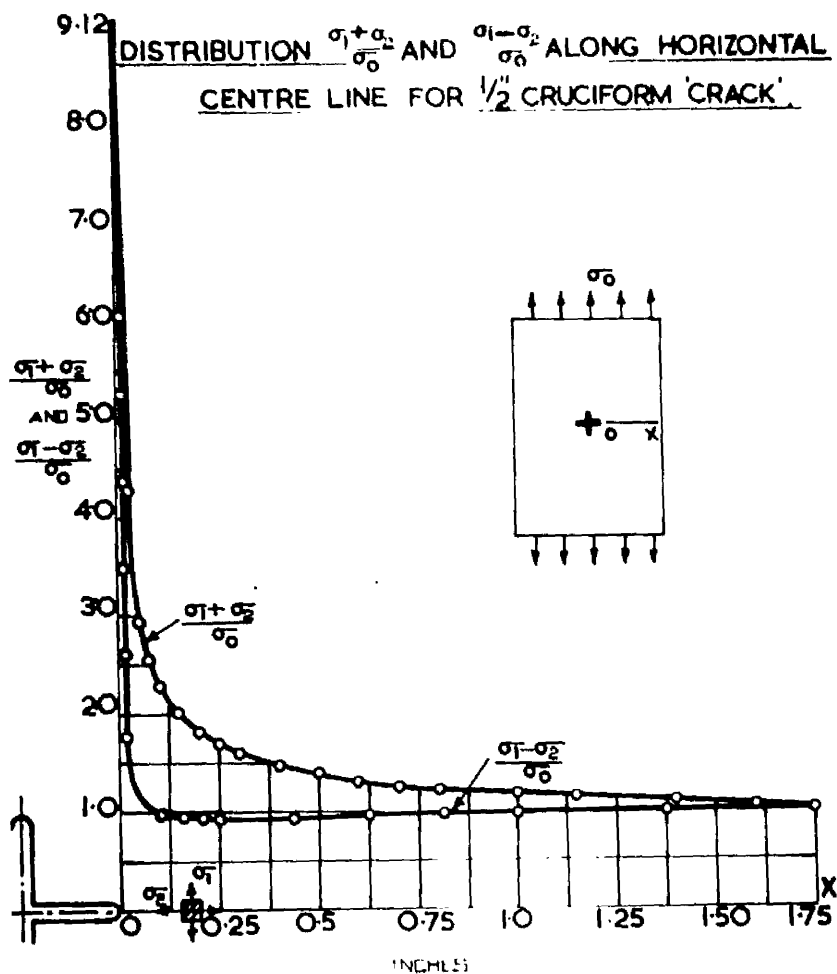


Fig.118a.

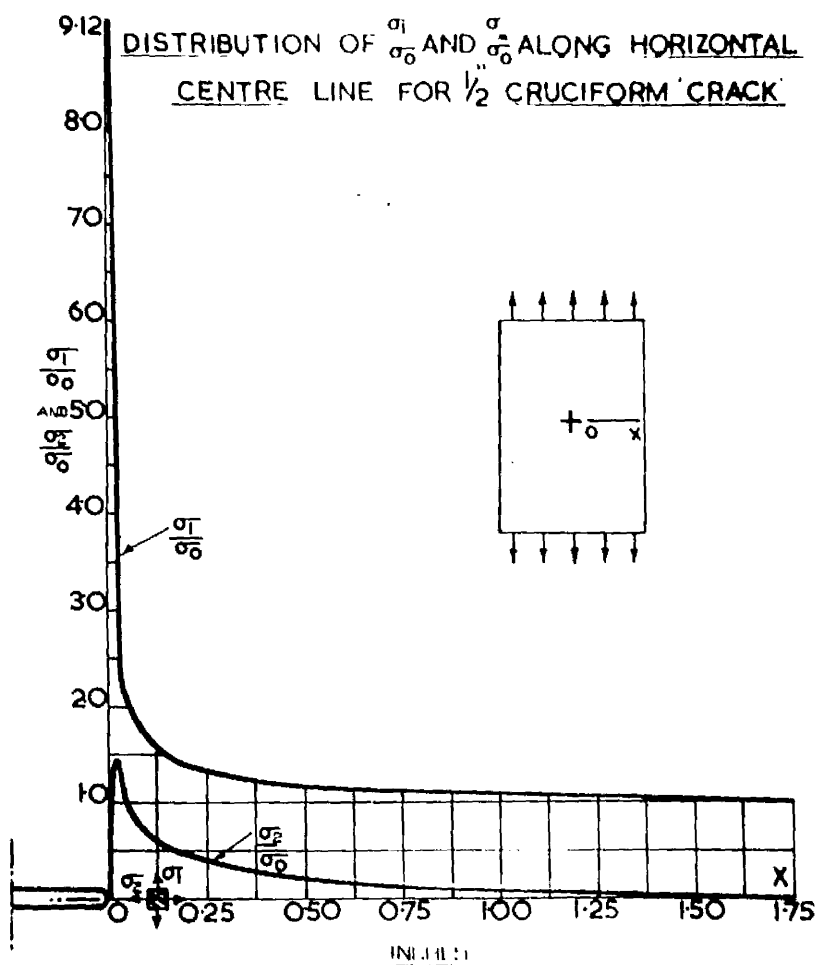


Fig.118b.

Fig.119a.

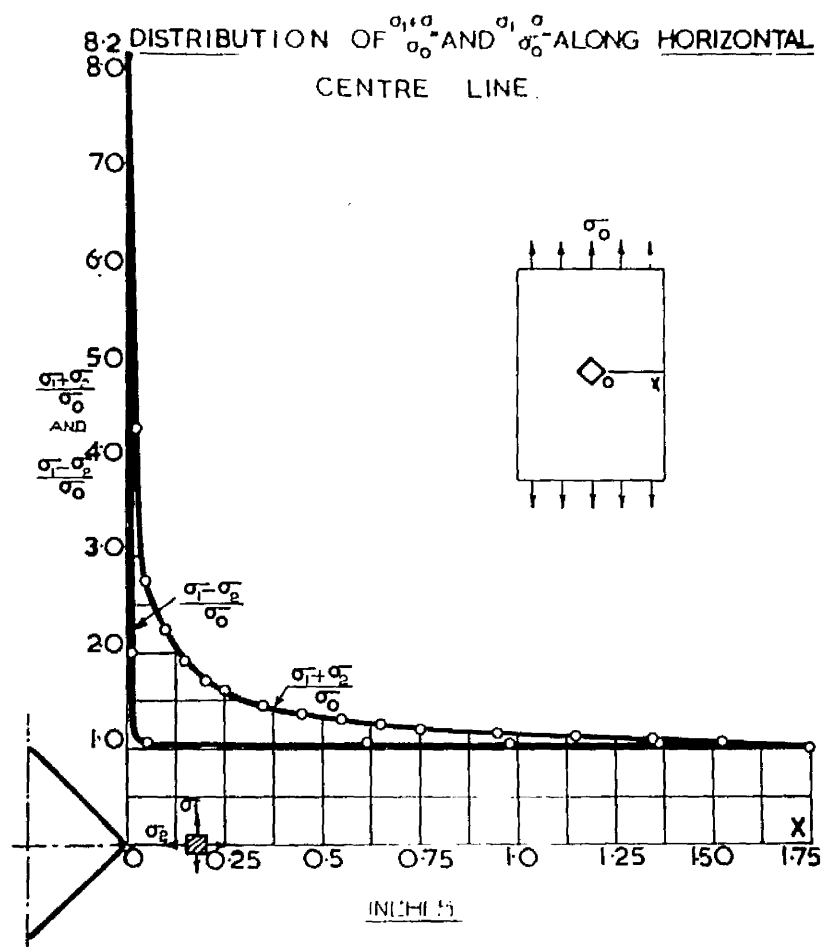
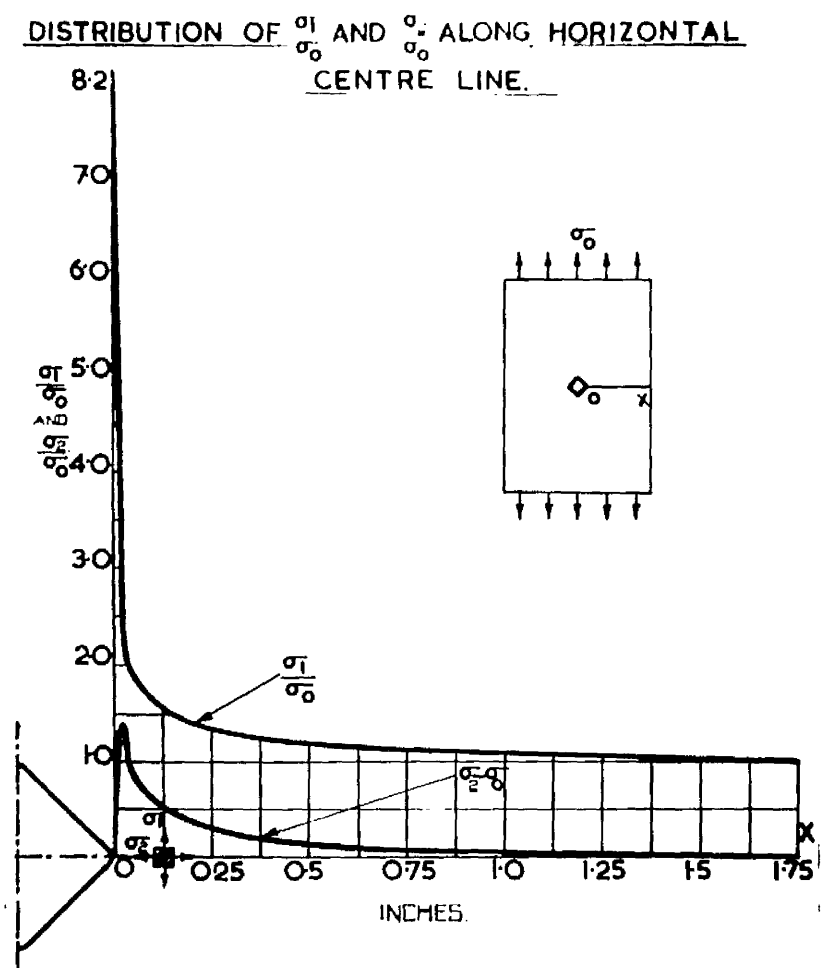


Fig.119b.





DISTRIBUTION OF DIFFERENCE OF PRINCIPAL STRESSES  
ALONG HORIZONTAL  $\zeta$

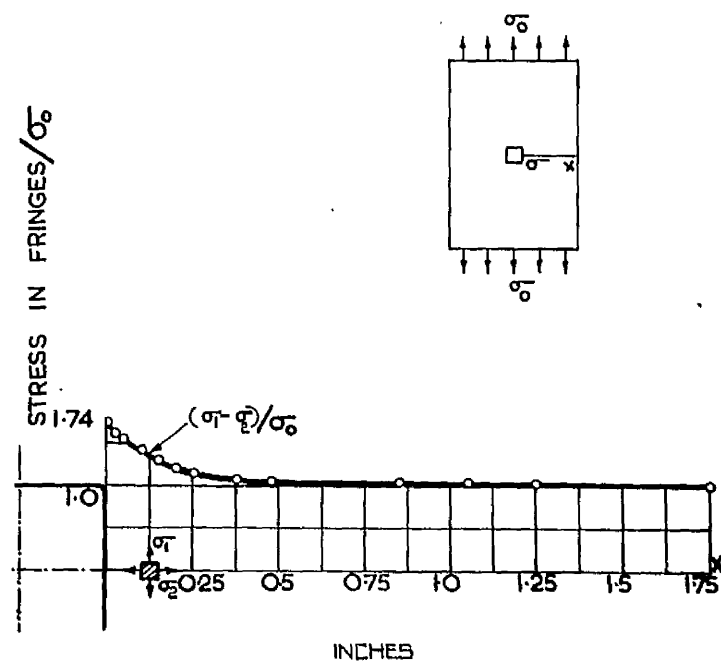


Fig. 120a.

DISTRIBUTION OF DIFFERENCE OF PRINCIPAL STRESSES  
ALONG VERTICAL  $\zeta$

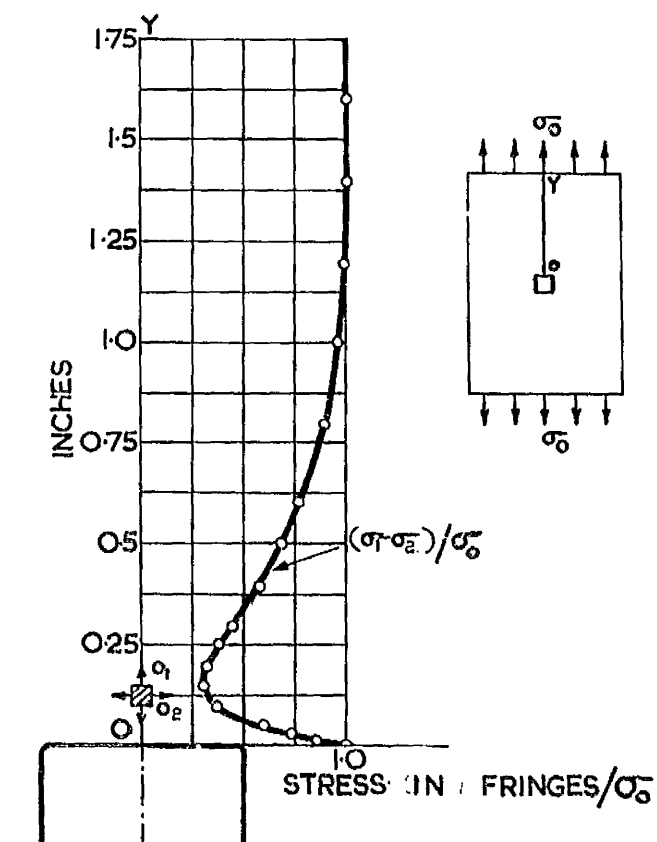


Fig. 120b.

DISTRIBUTION OF DIFFERENCE OF PRINCIPAL STRESSES  
ALONG HORIZONTAL SECTION THRO' MAX. FRINGE ORDER.

Fig.120c.

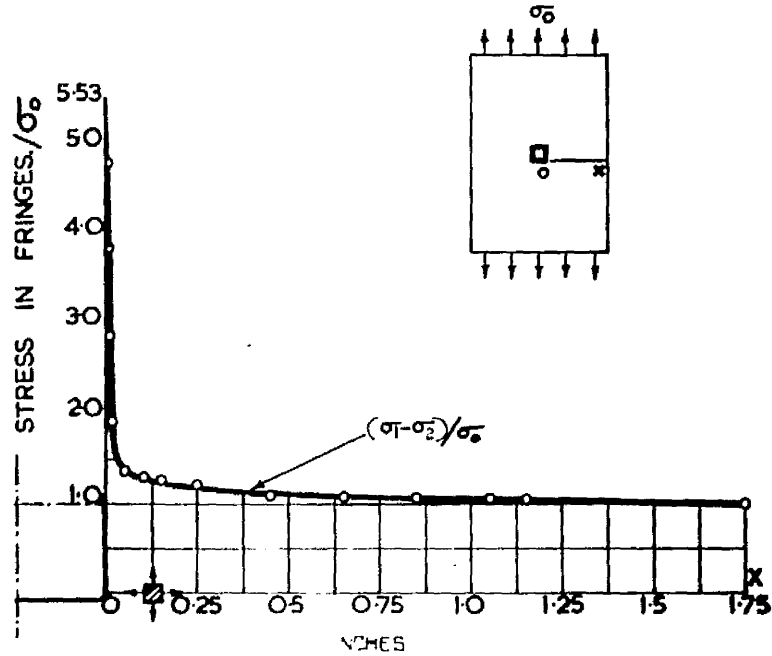
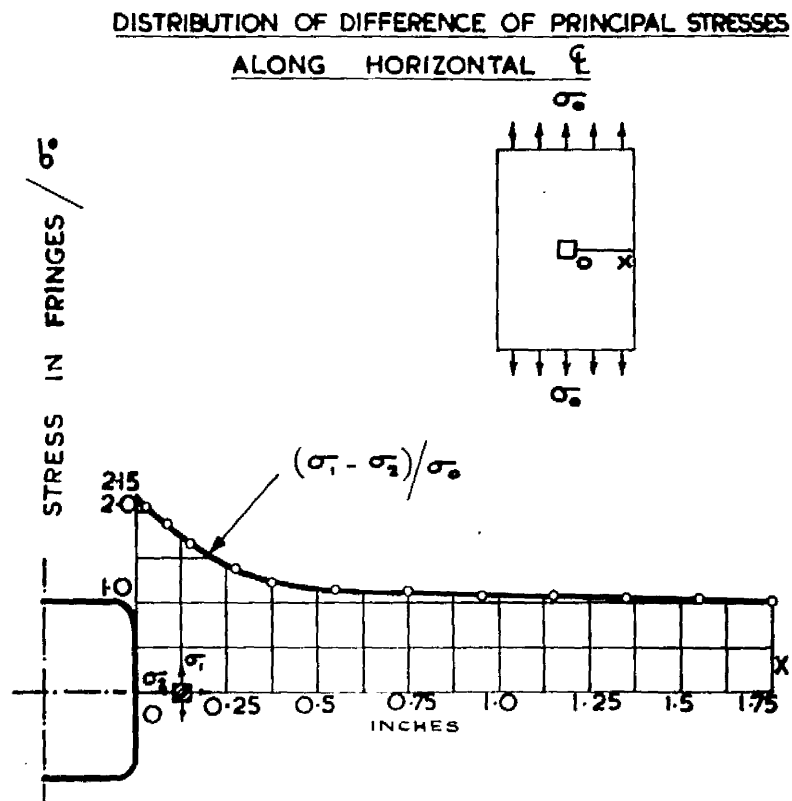


Fig.121a.



DISTRIBUTION OF DIFFERENCE OF PRINCIPAL STRESSES  
ALONG VERTICAL  $\ell$

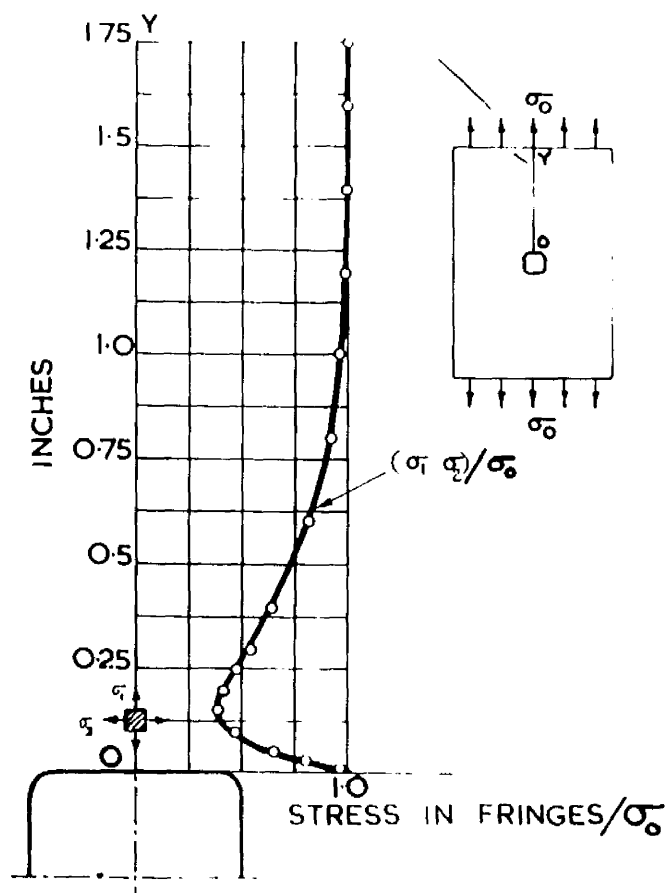


Fig.121b.

DISTRIBUTION OF DIFFERENCE OF PRINCIPAL STRESSES  
ALONG HORIZONTAL SECTION THRO' MAX. FRINGE ORDER

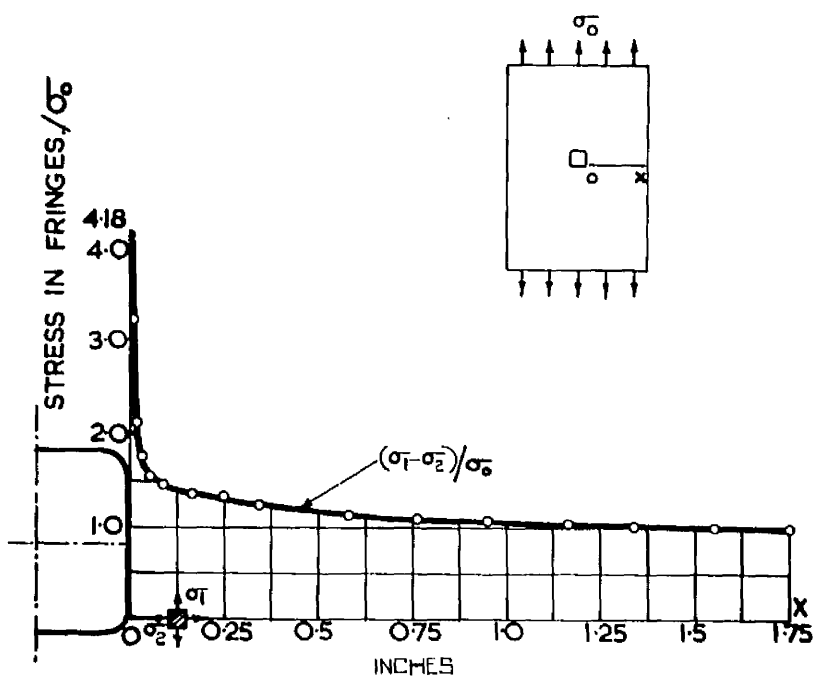
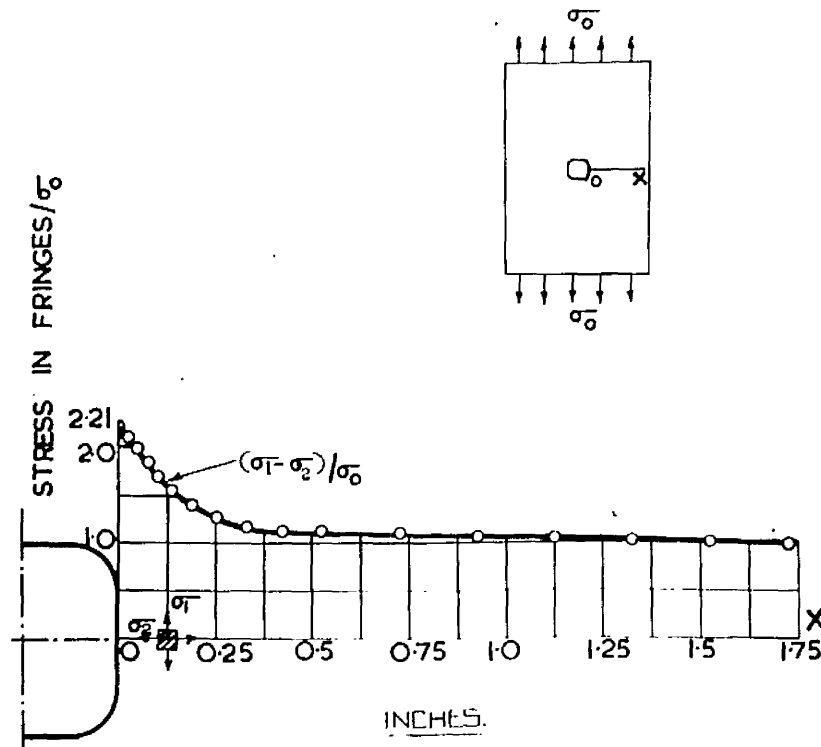


Fig.121c.

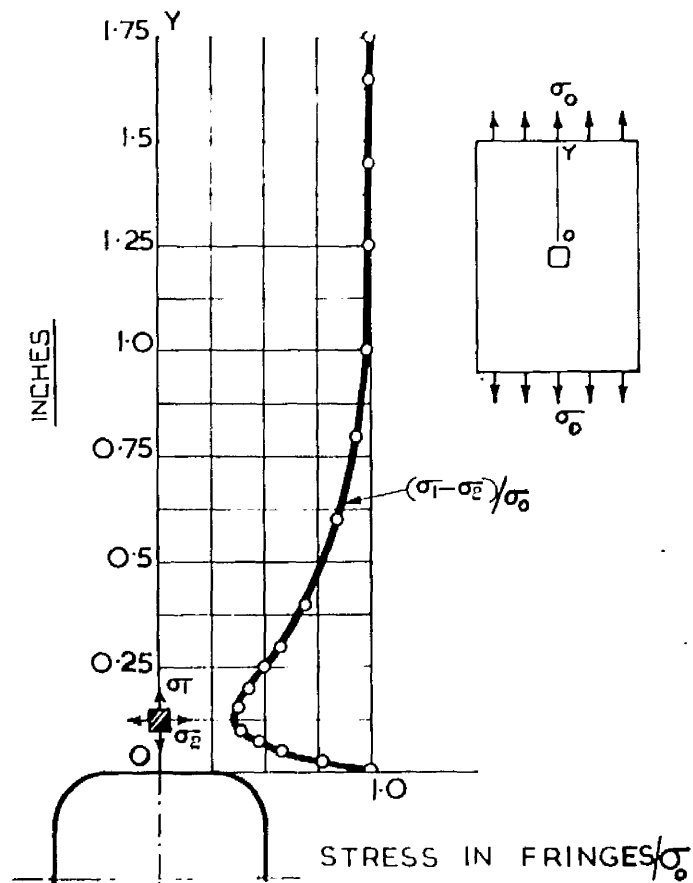
DISTRIBUTION OF DIFFERENCE OF PRINCIPAL STRESSES  
ALONG HORIZONTAL  $\zeta$

Fig.122a.



DISTRIBUTION OF DIFFERENCE OF PRINCIPAL  
STRESSES ALONG VERTICAL  $\zeta$

Fig.122b.



DISTRIBUTION OF DIFFERENCE OF PRINCIPAL STRESSES  
ALONG SECTION THROUGH MAX. FRINGE ORDER.

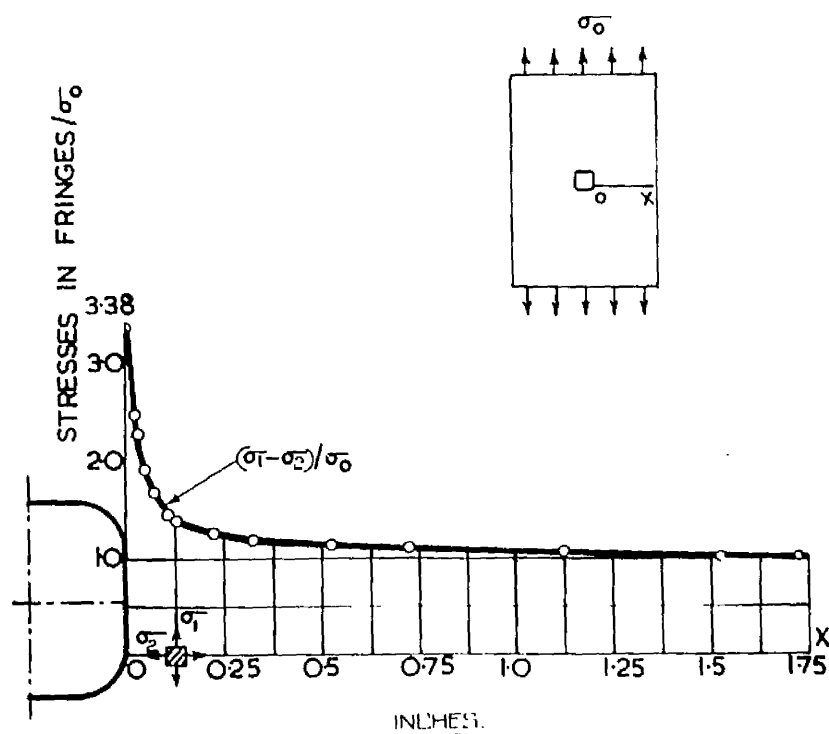


Fig.122c.

DISTRIBUTION OF DIFFERENCE OF PRINCIPAL STRESSES  
ALONG HORIZONTAL  $\phi$

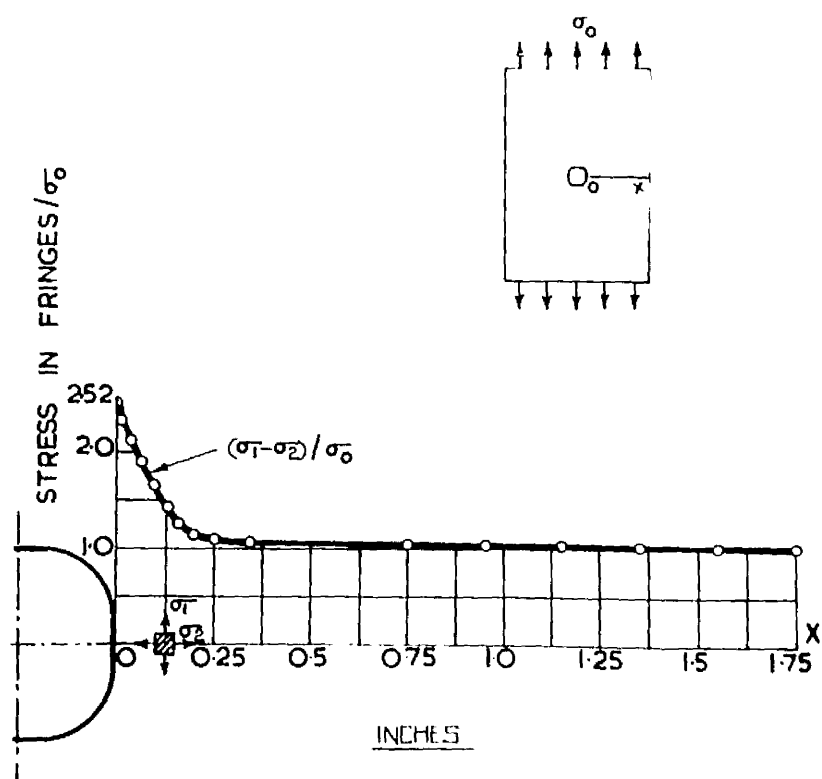


Fig.123a.

DISTRIBUTION OF DIFFERENCE OF PRINCIPAL STRESSES  
ALONG VERTICAL  $\phi$

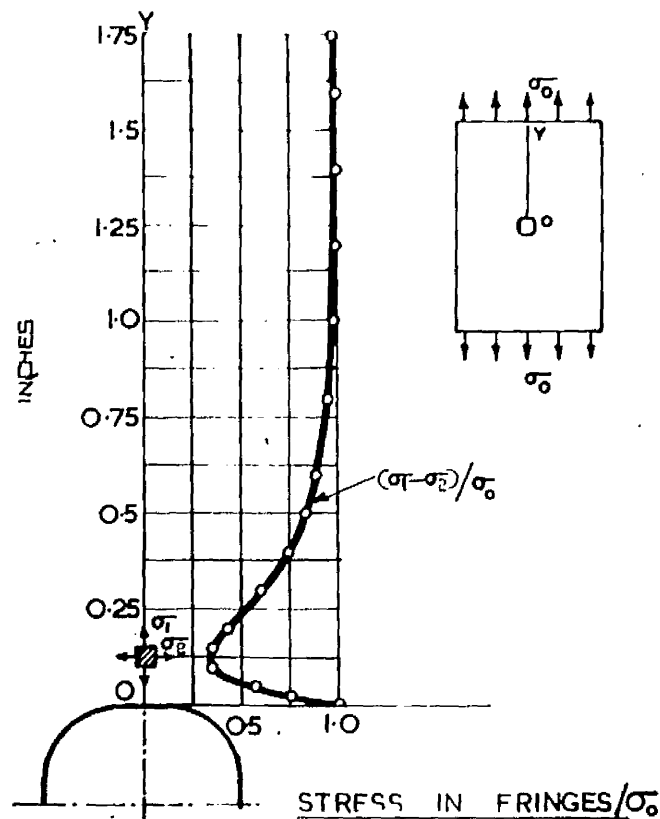


Fig.123b.

DISTRIBUTION OF DIFFERENCE OF PRINCIPAL STRESSES  
ALONG SECTION THROUGH MAX. FRINGE ORDER

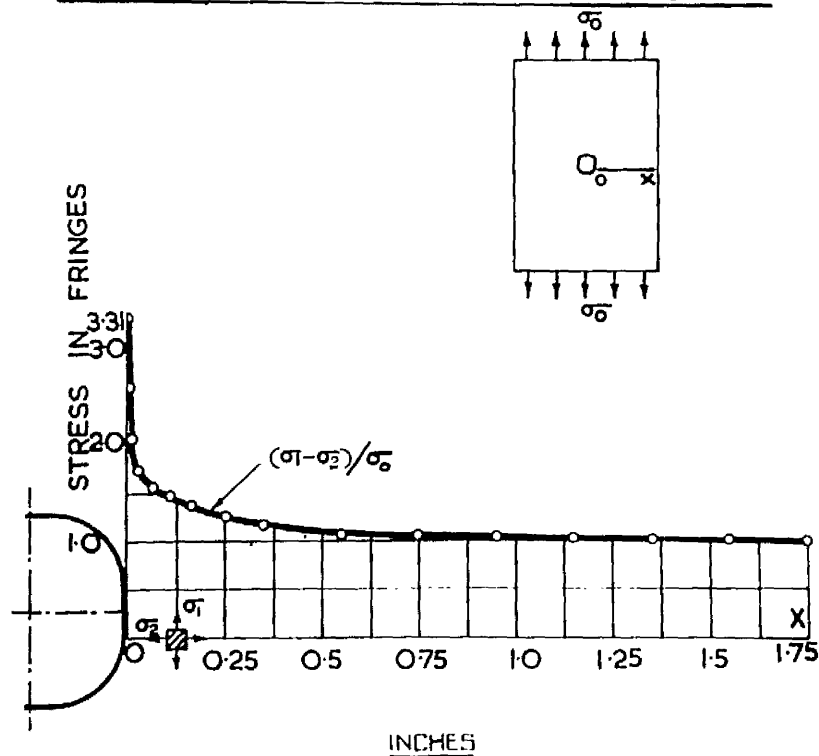


Fig.123c.

DISTRIBUTION OF DIFFERENCE OF PRINCIPAL STRESSES  
ALONG HORIZONTAL  $\zeta$

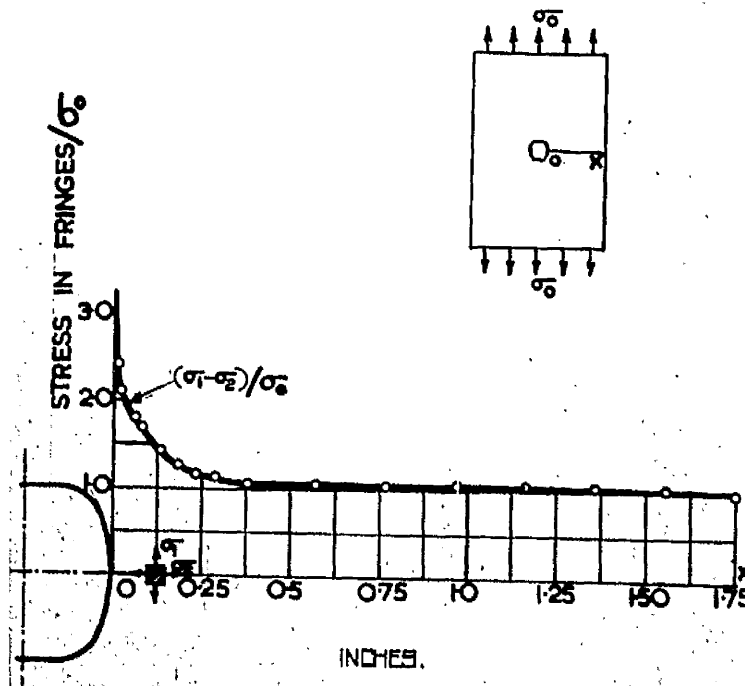


Fig.124a.

DISTRIBUTION OF DIFFERENCE OF PRINCIPAL  
STRESSES ALONG VERTICAL  $\zeta$

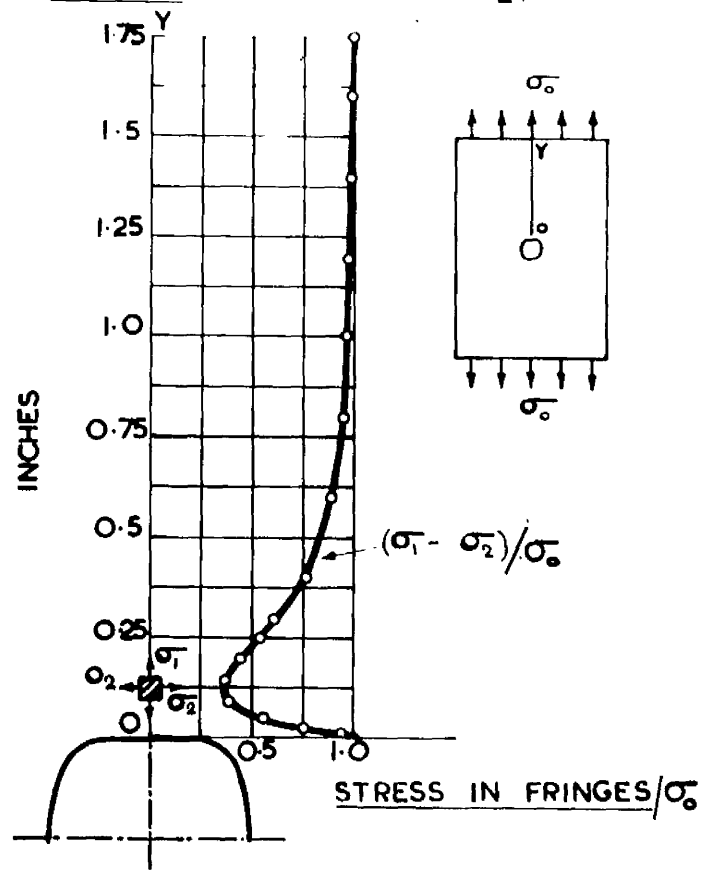


Fig.124b.

DISTRIBUTION OF DIFFERENCE OF PRINCIPAL  
STRESSES ALONG SECTION THROUGH MAX.  
FRINGE ORDER.

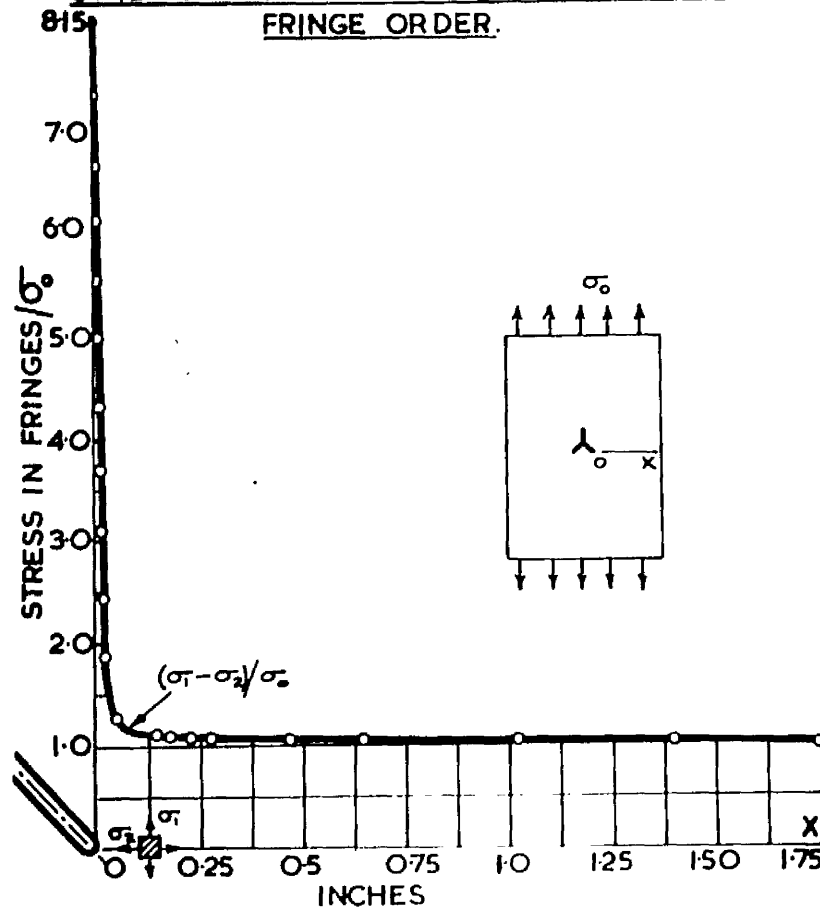


Fig.125a.

DISTRIBUTION OF DIFFERENCE OF PRINCIPAL  
STRESSES ALONG SECTION THROUGH MAX.  
FRINGE ORDER.

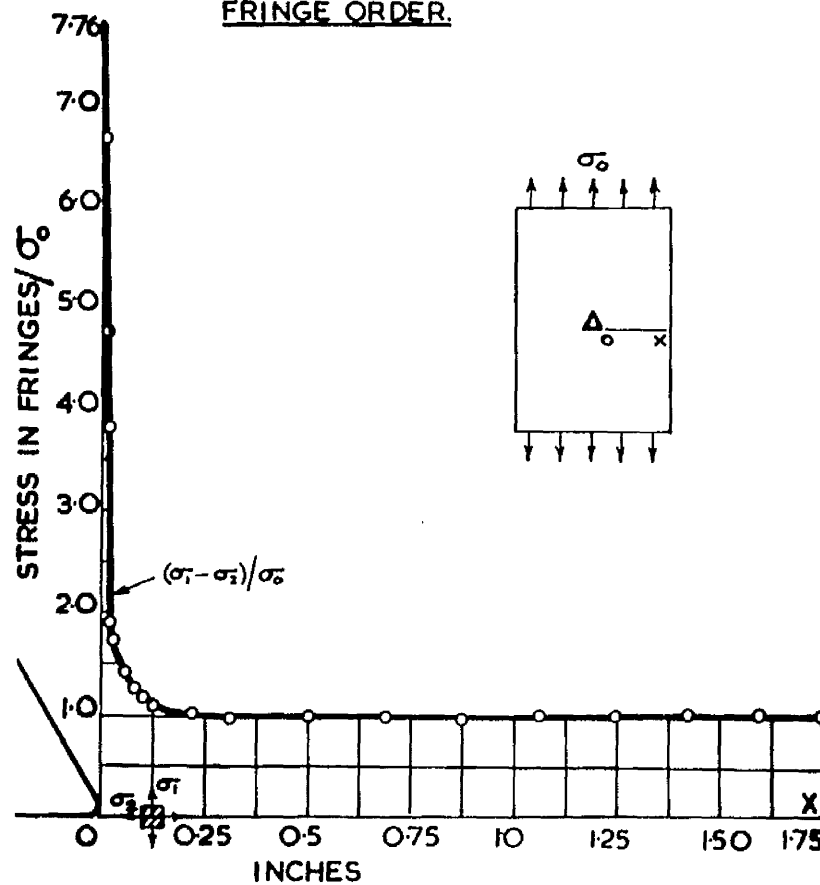
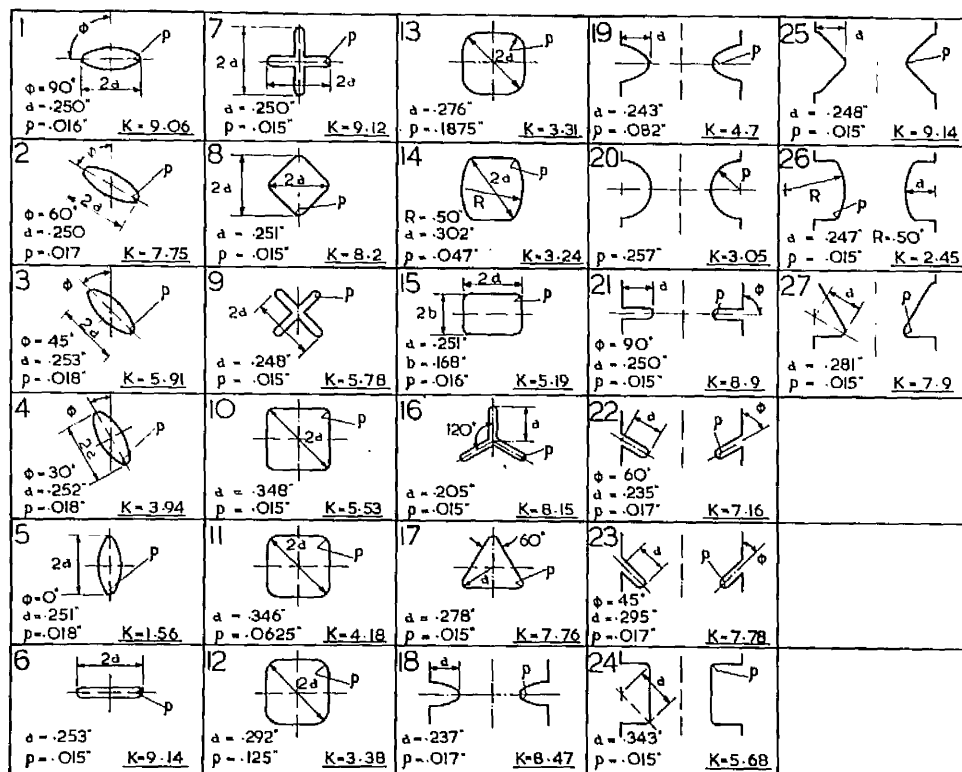


Fig.125b.





EXPERIMENTAL STRESS CONCENTRATION FACTORS

Fig.126.

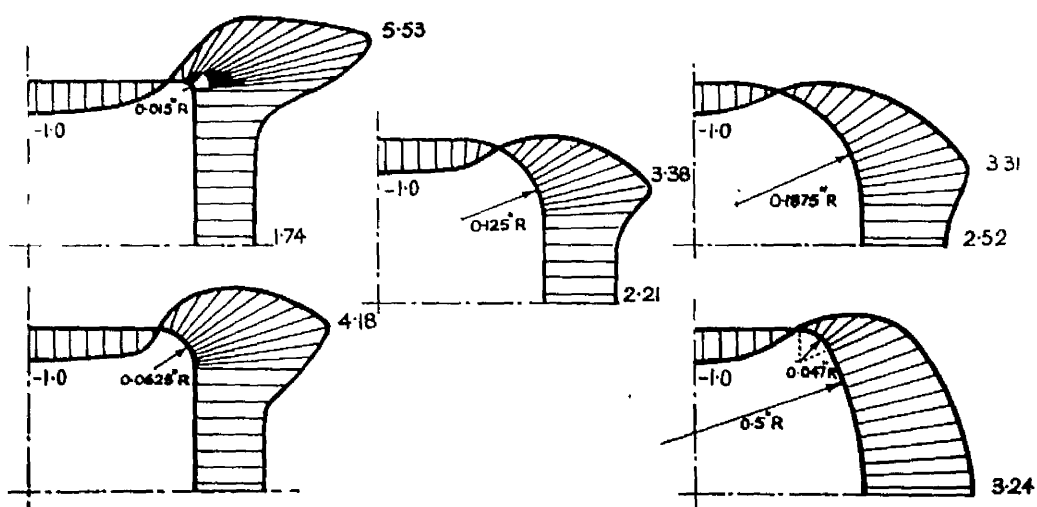


Fig.127.

CHAPTER IV      ANALYSIS AND DISCUSSION OF RESULTS

Fig.128.

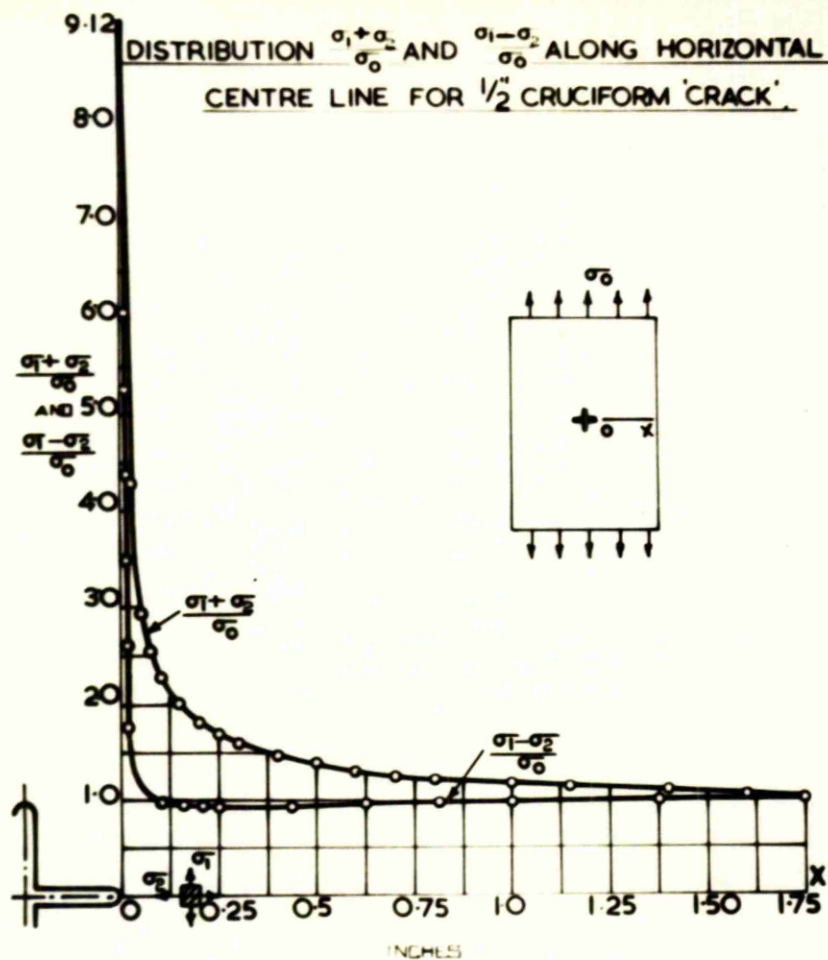
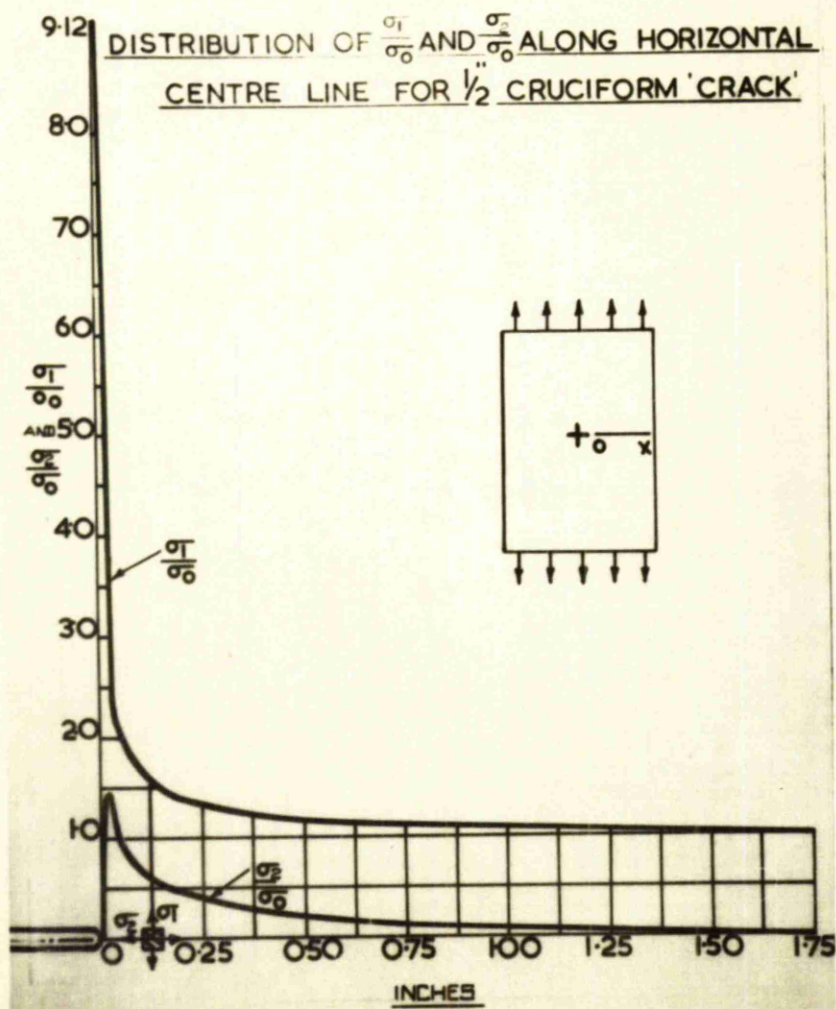


Fig.129.



(IV.1) The Cruciform Crack

In Figs. 128 and 129 the experimental results for the distributions of the sum and difference of the principal stresses along an axis at  $90^\circ$  to the direction of the applied tension are shown together with the separate values of these stresses along the same axis. Figs. 130 and 131 compare these results with the theoretical distribution obtained by the method given in Chapter II. It is seen that there is good agreement between the theoretical and experimental results. The slight divergence observable is regarded as a measure of the degree of approximation involved in using two terms only in the transformation series. It is considered that in view of the negligible order of deviation, the use of two terms only is both rational and acceptable.

It is also clear from the comparison of these results that for the discontinuity width to plate width ratio used, infinite plate conditions have been realised in the experimental specimens used. It is observable that in the graph of  $(\sigma_1 - \sigma_2)$  for the axis at  $90^\circ$  to the applied tension, that there is a decrease in  $(\sigma_1 - \sigma_2)/\sigma_0$  immediately prior to the final high increase at the point of maximum stress concentration. This is a feature which was shown to exist by JESSOP and SNELL in their experimental work on tension bars containing a circular hole. It should also be recalled that the theoretical solution for the circular hole given by KIRSCH shows a similar decrease in the  $(\sigma_1 - \sigma_2)$  distribution.

Another feature of interest is that the stress concentration factor for a cruciform crack is effectively the same as that for a slit of similar orientation, that is when the slit (in this case the arm of

Fig.130.

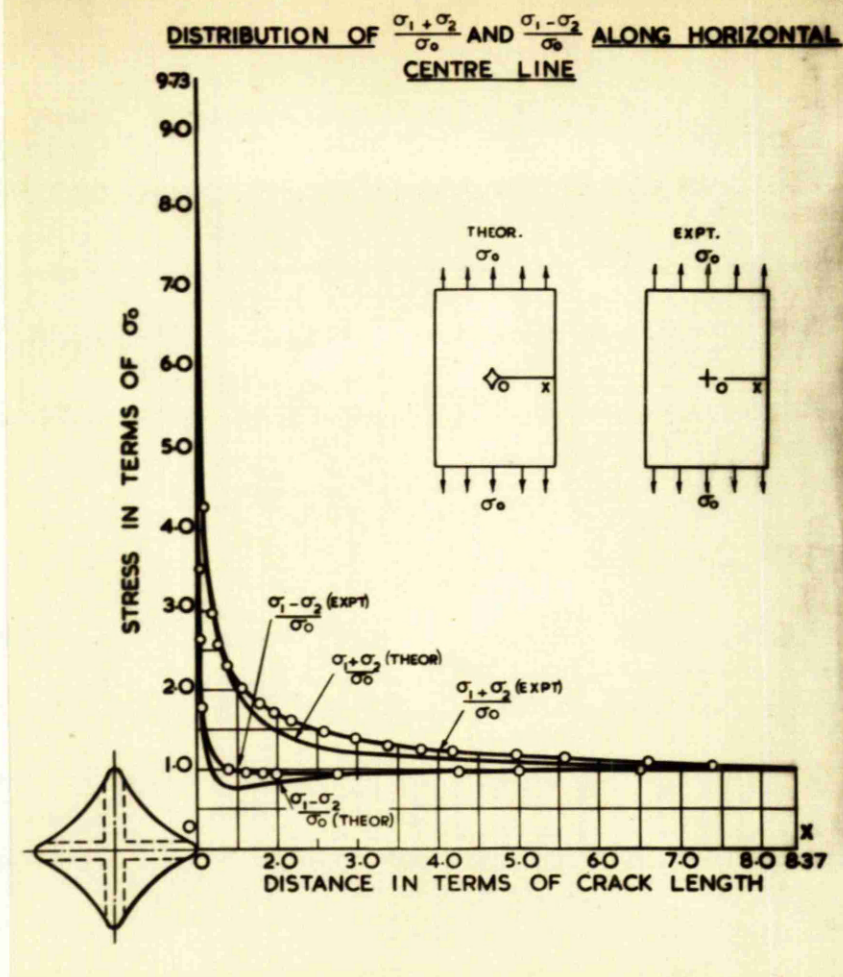
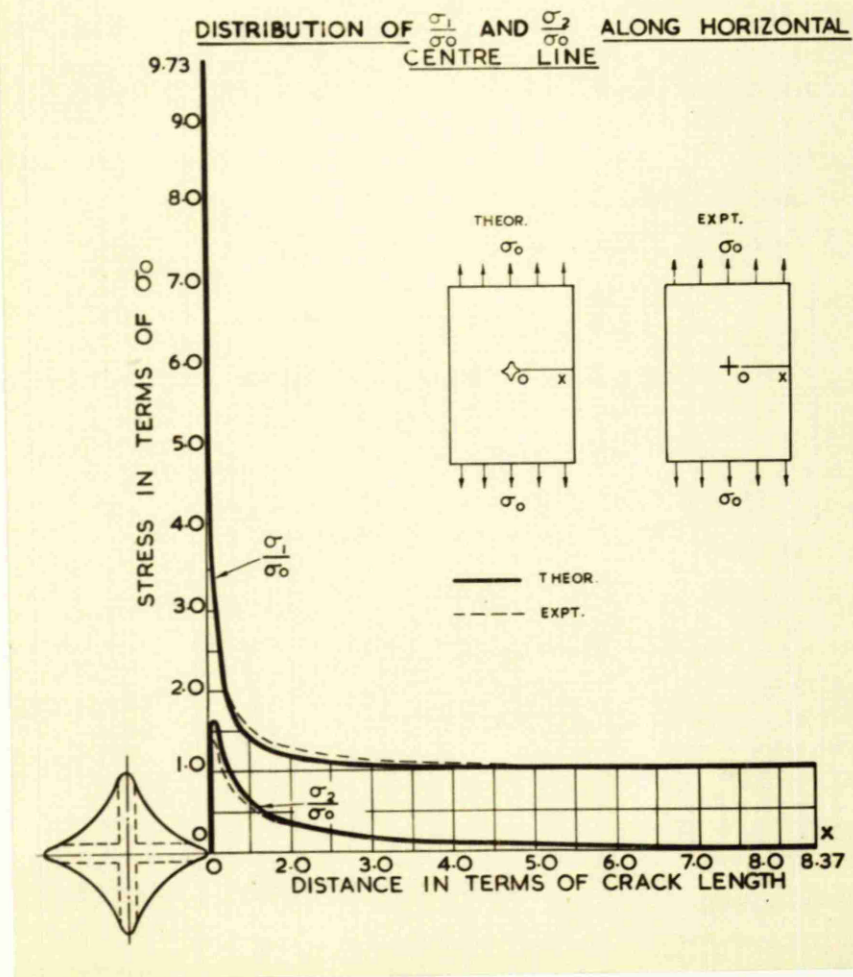


Fig.131.



of the cruciform crack) is at  $90^\circ$  to the direction of the applied tension. From this it may be inferred that a slit whose axis lies in the direction of the applied tension has no effect on the maximum stress concentration. The stress concentration factor would obviously be reduced as the number of 'arms' of the crack was increased, until the circular hole case was reached.

FORMS OF DISCONTINUITIES  
INVESTIGATED THEORETICALLY



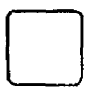



		<u>THEOR. S.C.F.</u>	<u>EXPTL. S.C.F.</u>	<u>% DIFFCE</u>
1.		9.73	9.12	-6.3
2.		8.8	8.2	-6.8
3.		5.67	5.53	-2.47
4.		6.0	5.78	-3.67
5.		7.58	7.75	+2.24
6.		7.93	8.15	+2.52

Fig.132.

Comparison of Theoretical and Experimental Stress Concentration Factors for a variety of Discontinuities.

The stress concentration factors for the forms of discontinuities investigated theoretically by the method given in Chapter II have been compared with the corresponding factors obtained by the photoelastic analysis, and the values are shown in Fig. 132. It can be seen that this comparison is a favourable one, the highest deviation between theory and experiment being 6.8%. It is of interest to note that the two highest deviations occur for the forms of discontinuities derived from the 'square hole' transformation form, when the diagonals of the holes lie along and at  $90^\circ$  to the axis of tension. As is shown later, the experimental value for the cruciform crack is in agreement with the value obtained by INGLIS'S elliptic formula  $K = 1 + 2\sqrt{a/\rho}$ . The writer is therefore of the opinion that the value obtained by the method given in Chapter II is slightly high, and that this may be due to the shortened transformation series which was used.

In the case of the second 'square hole', the value for the theoretical stress concentration factor may be slightly high for the same reason. In addition, the corresponding INGLIS value is higher than that given in Chapter II. For this particular type of discontinuity however, it is suggested later by the writer that the INGLIS method tends to over-estimate the stress concentration factor, and therefore it is claimed that the experimental figure is nearer to the true value.

Selected values of stress concentration factors calculated by INGLIS' formula (1.6) from the dimensions of the experimental discontinuities shown in Fig. 133 are given in Fig. 134.



# FORMS OF DISCONTINUITIES TESTED

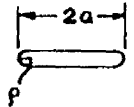

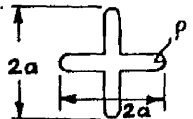
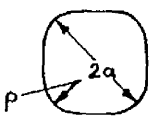
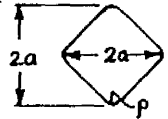
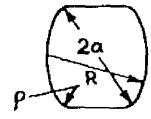
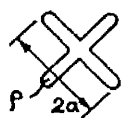
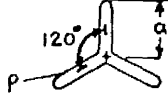
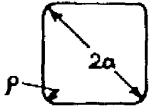
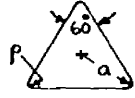
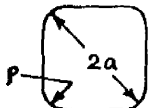
1. 	$2a = 0.506"$ $\rho = 0.015"$	7. 	$2a = 0.584"$ $\rho = 0.125"$
2. 	$2a = 0.500"$ $\rho = 0.015"$	8. 	$2a = 0.552"$ $\rho = 0.1875"$
3. 	$2a = 0.503"$ $\rho = 0.015"$	9. 	$2a = 0.604"$ $\rho = 0.047"$ $R = 0.500"$
4. 	$2a = 0.495"$ $\rho = 0.015"$	10. 	$2a = 0.510"$ $\rho = 0.015"$
5. 	$2a = 0.695"$ $\rho = 0.015"$	11. 	$2a = 0.556"$ $\rho = 0.015"$
6. 	$2a = 0.692"$ $\rho = 0.0625"$		

Fig.133.

## THEORETICAL & EXPERIMENTAL STRESS CONC. FACTORS.


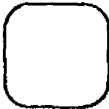
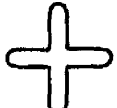
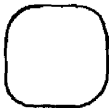
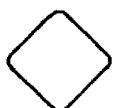


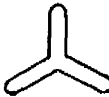
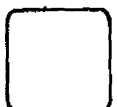

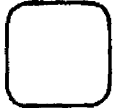
1. 	$K_T = 9.16$ $K_E = 9.14$	7. 	$K_T = 3.23$ $K_E = 3.38$
2. 	$K_T = 9.16$ $K_E = 9.12$	8. 	$K_T = 3.01$ $K_E = 3.31$
3. 	$K_T = 9.16$ $K_E = 8.2$	9. 	$K_T = 4.93$ $K_E = 3.24$
4. 	$K_T = 5.86$ $K_E = 5.78$	10. 	$K_T = 7.37$ $K_E = 8.15$
5. 	$K_T = 6.74$ $K_E = 5.53$	11. 	$K_T = 7.77$ $K_E = 7.76$
6. 	$K_T = 3.94$ $K_E = 4.18$		

Fig.134.

Examination of these results suggests that in general the INGLIS theory over-estimates the stress concentration factor for cases where the equivalent elliptic form is enclosed by the actual discontinuity (for example, the square hole with its diagonal parallel to the direction of tension), whereas if the discontinuity is enclosed by the equivalent elliptic form the theoretical stress concentration factor is in agreement with the experimental value, (such as for the horizontal slit and the cruciform).

Fig.135.

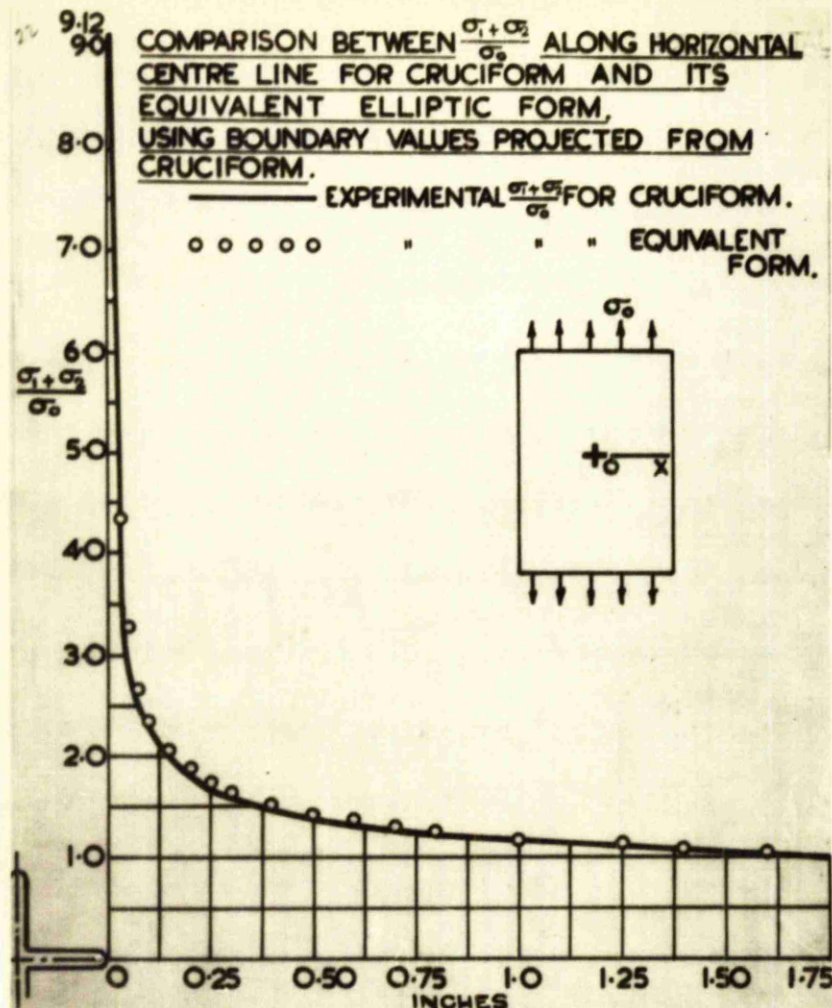
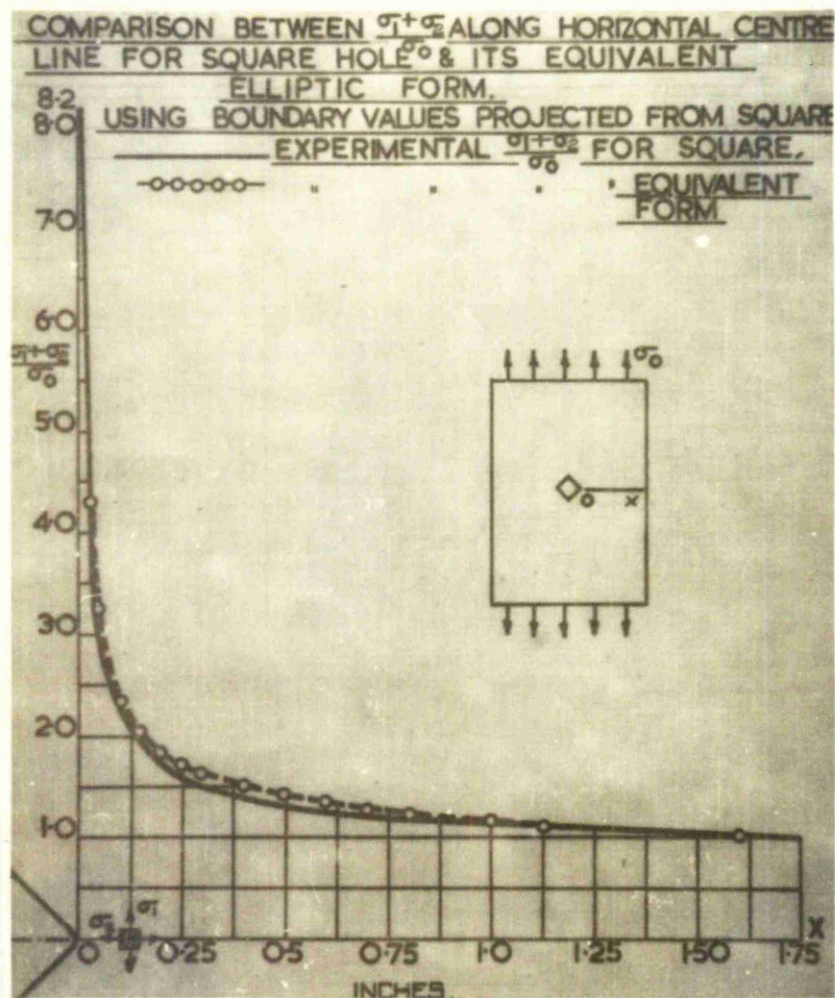


Fig.136.



(IV.5) Correlation of Stress Concentration Factors for Design Purposes

As a further check on the reliability of using an equivalent elliptic form in place of a non-elliptic form, the graphs of Figs. 135 and 136 were plotted. The conducting paper method was employed to determine the  $(\sigma_1 + \sigma_2)/\sigma_0$  distribution along the axis through the discontinuity at  $90^\circ$  to the direction of tension, for both the non-elliptic and its equivalent elliptic form. The boundary fringe values used in the conducting paper analogy for the non-elliptic opening were determined by the photoelastic method. These same boundary values were used for the equivalent elliptic opening. Their approximate positions on the boundary of the equivalent elliptic discontinuity were determined by projection from the non-elliptic boundary point to that on the equivalent ellipse, in a direction parallel to the applied tension. The  $(\sigma_1 + \sigma_2)/\sigma_0$  distributions were then compared.

From the graphs of Figs. 135 and 136 it can be seen that the concept of using an equivalent elliptic discontinuity in place of a non-elliptic one, is valid as far as the distribution of the sum of the principal stresses is concerned.

From all the work done, and as illustrated particularly by the cruciform approximation, it appears that the major factor of influence in stress concentration is the characteristic shape ratio  $\rho/a$ , where  $\rho$  is the smallest root radius of curvature and  $a$  is half the width of the discontinuity, related to this radius.

It was considered that a semi-empirical equation, if it could be established, purely for design purposes, would be of value. Therefore, an attempt has been made, based on INGLIS' theory, to relate the experimentally determined stress concentration factors for non-elliptic



Fig.137.

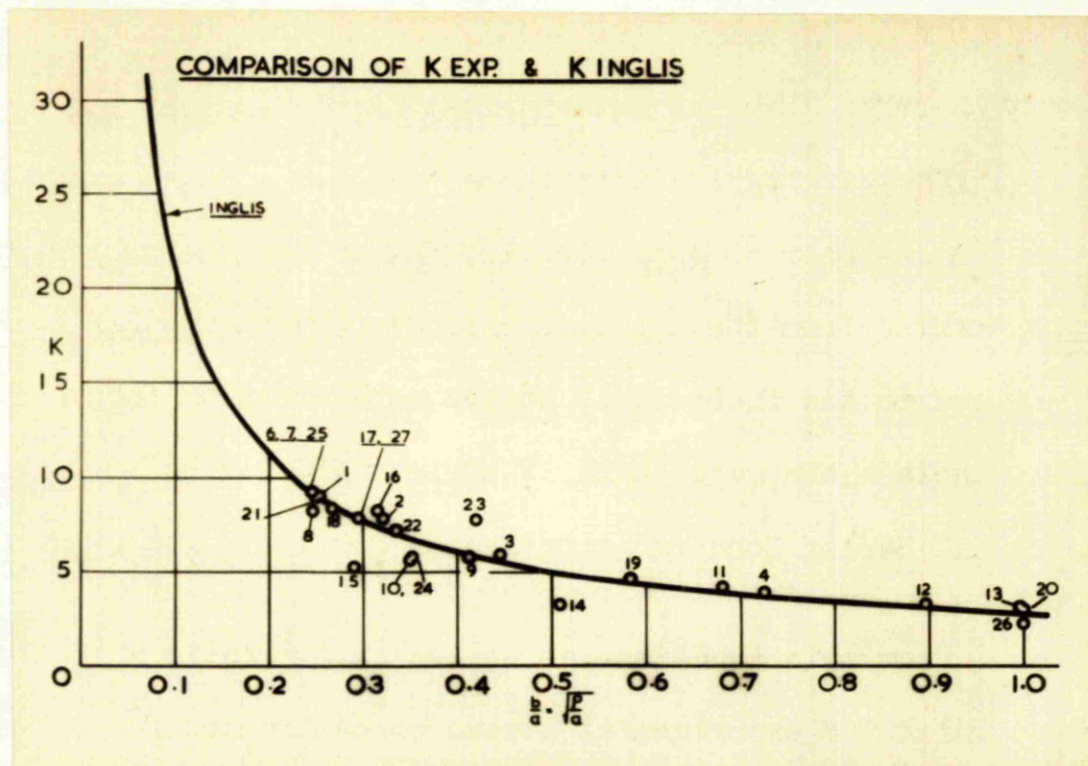
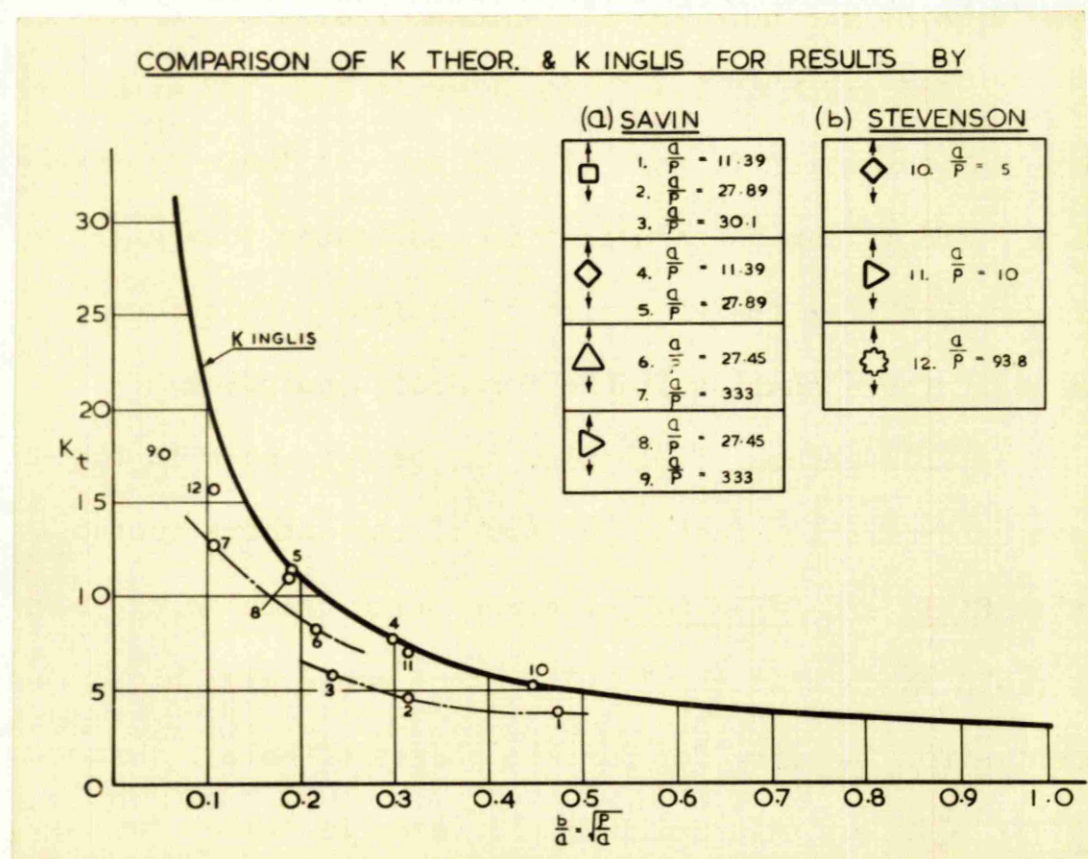


Fig.138.



elliptic and inclined elliptic holes to the theoretical stress concentration factors for equivalent elliptic holes whose major axes are perpendicular to the direction of tension applied to the plate. The theoretical stress concentration factor for the non-elliptic hole was calculated from the specimen dimension, using INGLIS equation (1.11) and equated to the theoretical stress concentration factor for an elliptic hole whose major axis is horizontal, giving

$$\text{Theoretical Stress Concentration Factor for Non-elliptic hole} = 1 + 2 \frac{a}{b} \dots\dots\dots(4.1)$$

From this equation, an 'equivalent'  $\frac{b}{a}$  ratio was determined, against which the experimental stress concentration factor was plotted. Since  $b = \sqrt{ap}$  for an ellipse, the 'equivalent'  $\frac{b}{a}$  ratio takes account of the size of the hole and its minimum radius of curvature.

The graph of  $1 + \frac{2a}{b}$  is shown in Fig. 137 with the experimental stress concentration factors plotted against their 'equivalent  $\frac{b}{a}$  ratios,' and it can be seen that in most cases this gives a reasonable approximation from the viewpoint of design. This form of correlation is a basis for a chart suitable for design purposes.

This method of plotting has been tried with the theoretical stress concentration factors of two of the authors quoted in the review, that is SAVIN and STEVENSON, the resulting graph being shown in Fig. 138. This graph shows that the INGLIS method would give higher stress concentration factors, for certain shapes of holes, than either SAVIN or STEVENSON, but this would in all cases be 'safe' for design purposes.

A suitable semi-empirical equation which approximates to the foregoing graphical forms has been found to be:-

$$K = 2 + \left(\frac{a}{p}\right)^{0.69} \dots\dots\dots(4.2)$$

**DESIGN CHART      STRESS CONCENTRATION FACTORS FOR EDGE AND INTERNAL DISCONTINUITIES IN TENSION PLATES**

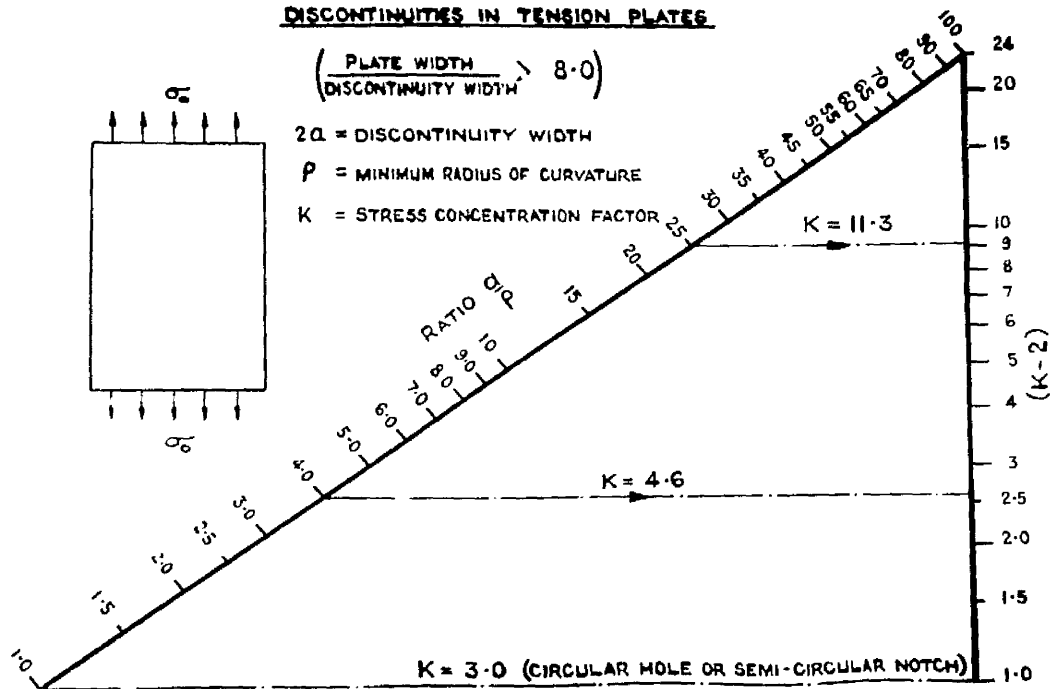


Fig.139.

where  $K$  is the stress concentration factor,

$\rho$  is the minimum radius of curvature of the 'equivalent' ellipse,

$a$  is the semi-major axis of the 'equivalent' ellipse.

From this equation, the design chart shown in Fig. 139 has been devised, the method of use being as indicated by the arrowed lines. Thus for any non-elliptic opening in a tension plate, an equivalent ellipse is 'fitted' to the opening and its  $\frac{a}{\rho}$  value determined, then from the design chart the approximate stress concentration factor may be found.



CHAPTER V      SUMMARY AND CONCLUSIONS

## V.1 The Cruciform Crack

### (i) Theoretical Analysis

The method of complex potentials applied to the stress analysis problem of a tension plate containing a cruciform crack has been shown to be completely satisfactory in all respects, even although the conformal transformation series form used to transform the cruciform boundary on to the unit circle was an abbreviated series.

It must be stated however, that this method of stress analysis, although mathematically more 'elegant', is a time consuming process, and that in order to obtain numerical results in a reasonable time it must be supplemented by the use of an electronic computer.

### (ii) Experimental Work.

The reliability of the results depends on the accurate determination of the photoelastic fringe patterns in regions of high stress. The use of a travelling microscope, together with a microscope camera, has been shown to give results of a high order of accuracy, even in regions of high stress and high stress gradient such as are encountered at the ends of two of the arms of the cruciform crack case investigated.

### (iii) Stress Concentration Factor

The theoretical analysis has been verified by the experimental work. It has been shown that the stress concentration factor for a cruciform 'crack' simulated in the experiments, whose axes are parallel and perpendicular to the direction of tension is sensibly the same as that for a slit of similar dimensions to one arm of the crack, lying at  $90^\circ$  to the axis of the tension. The arm of the 'crack' whose axis lies along the direction of the tension appears to have no effect upon the stress/

stress concentration at the end of the other arm. This has been shown also by comparison with INGLIS' theory, which for this form of discontinuity and orientation used gives an accurate stress concentration factor.

### Stress Distribution

The theoretical stress distribution along the axis of the cruciform at  $90^\circ$  to the direction of tension, has been verified by the experimental work. In particular, it has been definitely established that in the distribution of the difference of the principal stresses ( $\sigma_1 - \sigma_2$ ) along this axis, a decrease occurs below the uniform tension value, before the final increase to the maximum value at the end of the 'arm' of the crack.

## V.2 The Analogue Technique

### (1) The Function Generator and Analogue Computer

It has been shown that by the use of an analogue computer it is possible to determine in an extremely rapid manner, conformal transformations in series form, containing numerical coefficients, for an infinite number of geometric boundaries.

For any particular form of transformation, the effect of variations in the number of transformation terms, or in their coefficients, is readily determinable. The method may be employed to obtain a suitable transformation form which will 'fit' a chosen boundary, as was done for the case of the cruciform 'crack' boundary investigated.

It is concluded that this technique could be extended to cater for many transformation forms other than the type used in the work reported.

(ii) The Conducting Paper Analogue

This analogue has been proved to be a very accurate and rapid method for the determination of the distribution of the sum of the principal stresses in tension fields, and for cases of torsion, for the distribution of shear stress. The experimental techniques used by the writer for applying boundary voltages to conducting paper specimens and for measuring voltage distributions, have been most satisfactory.

V.3 Stress Concentration Factors

A representative range of geometric forms of discontinuities in tension plates has been investigated. In general, it has been shown that the experimental stress concentration factors are in agreement with those obtained theoretically. It has been shown that the stress concentration factor for any discontinuity, whether edge or internal, is dependent largely upon the size of the discontinuity and the minimum radius of curvature, that is upon a 'shape factor'  $a/\rho$ . It also depends in the case of uniform tension on the orientation of the discontinuity relative to the direction of applied tension, as illustrated by the five elliptic openings investigated photoelastically.

The INGLIS theory gives reasonable stress concentration factors for discontinuities where the equivalent elliptic form encloses the discontinuity being examined, but overestimates the stress concentration factors for discontinuities which enclose the equivalent elliptic form.

The 'barrel' shaped discontinuity suggested by HEYWOOD gives a relatively lower stress concentration factor than those for square boundaries of approximately similar dimensions.

The stress concentration factors for square and certain triangular discontinuities given by SAVIN are generally lower than those obtained for similar types of discontinuities by the experimental work of the writer, while the theoretical results of STEVENSON for square, triangular and polygonal boundaries are generally in agreement with the experimental results obtained by the writer.

The method of plotting the experimental stress concentration factor against an 'equivalent  $\frac{b}{a}$  ratio' for an elliptic discontinuity with major axis at  $90^\circ$  to the direction of the tension, provides a suitable means of comparing stress concentration factors for discontinuities of different basic shapes. This has also led to the drawing up of a design chart for discontinuities in plates in uniform tension.

#### V.4 Design Chart for Stress Concentration Factors

A design chart of the form presented is considered to be of value for the rapid assessment of stress concentration effect for any geometric shape of discontinuity for which a shape factor  $a/\rho$  can be estimated. The stress concentration factors determined from this chart will be sufficiently accurate for design purposes. It must be stated clearly that this chart applies only to discontinuities of geometric form in thin plates under uniform tension. The ratio of discontinuity, width to plate width is not greater than 1 : 8, to allow the plates to be considered as infinite relative to the size of the discontinuity.

For the values of  $\frac{a}{\rho}$  greater than 25 (that is, for  $\frac{b}{a}$  values less than 0.2), the chart may over-estimate the stress concentration effect. Since discontinuities within this range have extremely small radii of curvature, it is considered that for design purposes a 'self-contained' over-estimate in the chart is of practical value. As an example of this, for an  $\frac{a}{\rho}$  ratio of 100 (that is a  $\frac{b}{a}$  ratio of 0.1), the over-estimate in comparison with the INGLIS value is 24%. For  $\frac{a}{\rho}$  values between 25 and 100, the percentage over-estimate diminishes.

CHAPTER VI      BIBLIOGRAPHY AND AUTHOR INDEX

BIBLIOGRAPHY

1. 'Complex Potentials in Two-Dimensional Elasticity',  
A.C. STEVENSON; Proc.Roy.Soc.(London), Vol.184(1945), p.129.
2. 'Some Basic Problems of the Mathematical Theory of Elasticity',  
N.I. MUSKHELISHVILI; (1953).
3. 'Four Studies in the Theory of Stress Concentration',  
H.L. COX; A.R.C. Report and Memoranda (1953) R.C.M. No.2704.
4. 'Stress Concentration around Holes',  
G.N. SAVIN; A.R.C. Report No. 18460.
5. 'Stress Concentration Design Factors',  
R.E. PETERSON; Chapman and Hall, (1953).
6. 'Designing by Photoelasticity',  
R.B. HEYWOOD; Chapman and Hall, Ltd., (London).
7. 'A Theoretical Investigation of the Stresses in a Plate  
Containing a Crack',  
M. ROTHMAN; Engineering, Vol. 184, n.4770, Aug.9(1957),p.174-5.
8. B. KIRSCH; Z.V.D.I. Vol. 42(1898), p.797..
9. 'Three-dimensional Solutions for the Stress Concentration around  
a Circular Hole in a Plate of Arbitrary Thickness',  
E. STERNBERG and M.A. SADOWSKY; Trans. A.S.M.E. Vol.71(1949),  
p.A.27.

10. 'On the Stresses in the Neighbourhood of a Circular Hole in a Strip Under Tension',  
R.C.J. HOWLAND; Phil.Trans.Roy.Soc.(London),A.229(1929-30),p.49.
11. 'On the Stresses at the Edge of an Eccentrically Located Circular Hole in a Strip Under Tension',  
S. SJOSTROM; Aero.Res.Inst. of Sweden Report No.36 (1950).
12. 'Stress Distribution Round a Hole Near the Edge of a Plate',  
R.D. MINDLIN; Proc. S.E.S.A. Vol.5, No.2(1948), p.56.
13. Dissertation.  
G. KOLOSOFF; St. Petersburg (1910).
14. 'Stresses in a Plate due to the Presence of Cracks and Sharp Corners',  
C.H. INGLIS; Trans.Inst.Naval Arch. Vol.IV. Part I(1913),p.219.
15. 'A Treatise on Photoelasticity',  
E.G. COKER and L.W.G. FILON; Cambridge, England (1931).
16. 'Uber Eine partikulare losung des biharmonischer Problems fur den Aussenraum der Ellipse',  
T.L. POSCHL; Mathematische Zeitschrift (Berlin)(1921), p.89.
17. 'Stress Distribution around an Elliptical Discontinuity in any Two-dimensional, Uniform and Axial, System of Combined Stress',  
A.J. DURELLI and W.M. MURRAY; Proc. S.E.S.A. Vol. 1(1943),  
p.19.



18. 'Stress Concentrations due to Elliptical Discontinuities  
in a Plate Under Edge Forces',  
L.H. DONNELL; Theodore von Karman, Aniv. Vol. (1941).
19. 'Some Basic Problems of the Mathematical Theory of Elasticity',  
N.I. MUSKHELISHVILI; (1953), p.333.
20. 'The Phenomena of Rupture and Flow in Solids',  
A.A. GRIFFITH; Phil.Trans.Roy.Soc.(London), A.Vol.221(1920)  
p.163.
21. 'The distribution of Stress in the Neighbourhood of a Crack in  
an Elastic Solid',  
I.N. SNEDDON; Proc.Roy.Soc.(London) A.Vol.187(1946), p.229.
22. E. OROWAN; Zs. Kristallogr. Vol.89 (1934), p.327.
23. 'Stresses at a Crack, Size of the Crack and the Bending of  
Reinforced Concrete',  
H.M. WESTERGAARD; Proc.American Concrete Inst. Vol.30(1934),  
p.93.
24. 'Bearing Pressures and Cracks',  
H.M. WESTERGAARD; Trans. A.S.M.E., Vol.61(1939), p.A.49.
25. R. SACK; Proc.Roy.Soc.(London), A, Vol.187(1946), p.260.
26. 'The Moving Griffith Crack',  
E.H. YOFFE; Phil.Mag. Vol.42(1951), p.739.

27. 'Photoelastic Analysis for an Edge Crack in a Tensile Field',  
D. POST; Proc. S.E.S.A., Vol.XII, No.1 (1954), p.99.
28. 'Analysis of an Infinite Plate Containing Radial Cracks  
Originating at the Boundary of an Internal Circular Hole',  
O.L. BOWIE.
29. 'Stresses in Plates with Cracks and Notches',  
M. ROTHMAN and D.S. ROSS; Engineering, Feb.11(1955), p.175.
30. 'Some Boundary Value Problems of Two-dimensional Elasticity',  
A.C. STEVENSON; Phil.Mag. J.Sc., Vol.XXXIV (1945), p.766.
31. See Correction in Phil.Mag. J.Sc., Vol.XXXVI (1945), p.183.
32. 'Direct Determination of Stresses from the Stress Equations  
in Some Two-dimensional Problems of Elasticity',  
B. SEN; Phil.Mag. J.Sc., Vol.XXXIX (1948), p.992.
33. 'The Stresses Around a Rectangular Opening with Round Corners  
in a Uniformly Loaded Plate',  
S.R. HELLER, Jnr; J.S. BROCK; R. BART; Proc. 3rd U.S.  
National Congress of Applied Mechanics, (1958), p.357.
34. 'Effect of a Small Hole on the Stresses in a Uniformly Loaded  
Plate',  
M. GREENSPAN; Quart.App.Maths., Vol.2(1944), p.60-71.
35. 'Analytical Determination of the Stresses Around Square Holes  
with Rounded Corners',  
J.S. BROCK; David Taylor Model Basin Report 1149, 1957.

36. 'On the Stress Distribution at the Base of a Stationary Crack',  
M.L. WILLIAMS; J.App.Mechs., Vol.24, No.1 (March 1957), p.109.
37. 'Stresses in a Notched Plate Under Tension',  
F.G. MAUNSELL; Phil.Mag. J.Sc., Vol. XXI (1936), p.765.
38. 'Stresses in a Notched Strip Under Tension',  
C.B. LING; Trans. A.S.M.E., Vol.69 (1947), p.A.275.
39. 'On the Stresses in a Notched Strip',  
C.B. LING; Trans. A.S.M.E., Vol.74 (1952), p.A.141.
40. 'Kerbspannungslere',  
H. NEUBER; Editor J. SPRINGER, Berlin (1957).
41. 'Stress Concentrations in a Strip Under Tension and Containing  
Two pairs of Semi-Circular Notches Placed on the Edges  
Symmetrically',  
A. ATSUMI; J.App.Mechs., Vol.24 No.4 (Dec. 1957), p.565.
42. 'Ueber die Spannungserhdehung in Kerbstaebe',  
E. WEINEL; Fifth Inter.Cong.App.Mech., Cambridge, Mass. (1938),  
p.51.
43. 'Tension of Semi-infinite Plate with Notched Boundary',  
A.C. STEVENSON; Phil.Mag. J.Sc., Vol.XXXVI (1945), p.178.
44. 'The Effects of Holes and Semi-circular Notches on the  
Distribution of Stress in Tension Members',  
E.G. COKER; Proc.Phys.Soc., (1912), p.95.

45. 'Photoelastic Investigations of Stresses in Perforated Tensile Bars and About Rivet Holes',  
A. HENNIG; Forschung Gebiete Ing., Vol. 4, p.55.
46. 'Stress Concentrations Produced by Holes and Notches',  
A.M. WAHL and R. BEEUWKES; Trans. A.S.M.E., Vol.56(1934), p.617.
47. Discussion on Ref.46.  
M.M. FROCHT.
48. 'Photoelastic Studies in Stress Concentration',  
M.M. FROCHT, Mech.Eng., Vol.58(1936), p.485.
49. 'Photoelasticity - A Precision Instrument of Stress Analysis',  
M.M. FROCHT, R. GUERNSEY, Jr., D.LANDSBERG; Proc. S.E.S.A.,  
Vol. XI No.1(1953), p.105.
50. 'Results of Photoelastic Investigations of Stresses in a Tension Bar with Unfilled Hole',  
H.T. JESSOP and C. SNELL; J.Roy.Aero.Soc., Vol.59(1955), p.64.
51. 'The Effect of Holes, Cracks and Other Discontinuities in Ships Plating',  
E.G. COKER and A.L. KIMBALL, Trans.Inst.Naval Arch., Vol.62(1920) p.117.
52. Reports of Bristol Aircraft Ltd., on 'Slits in Tension Plates',  
J.R. DIXON; Reports E.D.L. 2/313 and E.D.L. 2/313 Addendum 1.

53. 'Factors of Stress Concentration for Slotted Bars in Tension and Bending',  
M.M. FROCHT and M.M. LEVENS; Trans. A.S.M.E., Vol.75(1957)  
p.A.107.
54. 'Stress Distribution in Tension Plates Containing Various Types of Discontinuities',  
D.S. ROSS; Conf.Exp. Stress Anal.Group Inst. of Physics, Glasgow (1958) - Unpublished.
55. 'Stress Concentrations due to Notches and like Discontinuities',  
E.G. COKER and P. HEYMANS; Brit.Ass.Adv.Sc.,  
Report of 90th Meeting (1921) p.291.
56. 'Factors of Stress Concentration in Bars with Deep Sharp Grooves and Fillets in Tension',  
M.M. FROCHT and D. LANDSBERG; Proc. S.E.S.A., Vol.VIII No.2(1951)  
p.149.
57. Discussion of Ref.56  
A.J. DURELLI and R.H. JACOBSON; Proc. S.E.S.A., Vol.VIII,  
No.2(1951), p.165.
58. Discussion of Ref.49  
A.J. DURELLI; Proc. S.E.S.A., Vol.XI No.1(1955), p.115.
59. 'Stress Concentration Produced by Holes and Fillets',  
S. TIMOSHENKO and W. DIETZ; Trans. A.S.M.E., Vol.47(1925),p.199.

60. 'Tension Tests of Materials',  
E.G. COKER; Eng. (Jan. 7, 1921), p.1.
61. 'Studies in Photoelastic Stress Determination',  
E.E. WEIBEL; Trans. A.S.M.E., Vol.56(1934), p.637.
62. 'Fillets Without Stress Concentration',  
R. LANSARD; Proc. S.E.S.A., Vol. XIII No.1(1955), p.97.
63. 'Photoelastic Investigation of Stress Relieving Fillet Curves',  
E. CHAPMAN; Product Eng., (May 1948), p.138.
64. 'Mathematical Theory of Elasticity',  
I.S. SOKOLNIKOFF; McGraw-Hill (1956).

VI.2 AUTHOR INDEX

<u>Name</u>		<u>Reference Nos.</u>	<u>Page Nos.</u>
ATSUMI,	A.	41	37
BART,	R.	33	31
BEEUWKES,	R.	46	43, 54
BOWIE,	D. L.	28	24
BROCK,	J. S.	33, 35	31
CHAPMAN,	E.	63	61
COKER,	E. G.	15, 44, 51, 55, 60.	15, 42, 47, 50, 54, 57.
COX,	H. L.	3	5, 7, 24, 31.
DIETZ,	W.	59	57
DIXON,	J. R.	52	48
DONNELL,	L. H.	18	18
DURELLI,	A. J.	17, 57, 58.	15, 47, 54, 55.
FILON,	L. N. G.	15	15, 50.
FROCHT,	M. M.	47, 48, 49, 53, 56.	43, 50, 54, 55, 57.
GREENSPAN,	M.	34	31
GRIFFITH,	A. A.	20	21
GUERNSEY,	R.	49	44, 55.
HELLER,	S. R.	33	31
HENNIG,	A.	45	42
HEYMANS,	P.	55	54
HEYWOOD,	R. B.	6	7
HOWLAND,	R. C. J.	10	12, 42.
INGLIS,	C. E.	14	15, 17, 21, 26.

<u>Name</u>		<u>Reference Nos.</u>	<u>Page Nos.</u>
JACOBSON,	A.J.	57	54
JESSOP,	H.T.	50	45
KIMBALL,	A.L.	51	47
KIRSCH,	B.	8	11
KOLOSOFF,	G.	13	15, 29.
LANDSBERG,	D.	49, 56.	44, 54, 55.
LANSARD,	R.	62	60
LEVENS,	M.M.	53	50
LING,	C.B.	38, 39.	37, 55.
MAUNSELL,	F.G.	37	37
MINDLIN,	R.D.	12	13, 45.
MURRAY,	W.M.	17	15, 47.
MUSKHELISHVILI,	N.I.	2, 19.	5, 7, 20, 29.
NEUBER,	H.	40	37, 55.
OROWAN,	E.	22	22
PETERSON,	R.E.	5	7
POSCHL,	T.L.	16	15
POST,	D.	27	23, 35, 48, 52, 55.
ROSS,	D.S.	29, 54.	24, 40, 48, 50, 53.
ROTHMAN,	M.	7, 29.	7, 24, 40, 48, 53.
SACK,	R.	25	22
SADOWSKY,	M.A.	9	12, 52.
SAVIN,	G.N.	4	5, 7, 20, 29.
SEN,	B.	32	28



<u>Name</u>		<u>Reference Nos.</u>	<u>Page Nos.</u>
SJOSTROM,	S.	11	15
SNEDDON,	I. N.	21	22
SNELL,	C.	50	45
SOKOLNIKOFF,	I. S.	64	127
STERNBERG,	E.	9	12, 52.
STEVENSON,	A. C.	1, 50, 43.	5, 20, 50, 40.
TIMOSHENKO,	S.	59	57
WAHL,	A. M.	46	45, 54.
WEIBEL,	E. F.	61	57
WEINEL,	E.	42	57
WESTERGAARD,	H. M.	25, 24	22
WILLIAMS,	M. L.	56	55
YOFFE,	E. H.	26	25

CHAPTER VII    APPENDICES

APPENDIX VII.1.      THEORY OF COMPLEX POTENTIALS

Theory of Complex Potentials in Two-Dimensional Elasticity

A thin plate in the XOY plane is considered, loaded in such a way as to produce conditions of plane strain or generalised plane stress.

If body forces are absent, the conditions of equilibrium are satisfied when

$$\frac{\partial \sigma_x}{\partial x} + \frac{\partial \tau_{xy}}{\partial y} = 0, \quad \frac{\partial \tau_{xy}}{\partial x} + \frac{\partial \sigma_y}{\partial y} = 0 \quad \dots\dots\dots(7.1)$$

and the conditions of compatibility are satisfied when

$$\left(\frac{\partial^2}{\partial x^2} + \frac{\partial^2}{\partial y^2}\right)(\sigma_x + \sigma_y) = 0 \quad \dots\dots\dots(7.2)$$

Changing to complex co-ordinates given by  $Z = x + iy$ ,  $\bar{Z} = x - iy$ , noting that

$$\frac{\partial}{\partial Z} = \frac{1}{2}\left(\frac{\partial}{\partial x} - i\frac{\partial}{\partial y}\right)$$

$$\frac{\partial}{\partial \bar{Z}} = \frac{1}{2}\left(\frac{\partial}{\partial x} + i\frac{\partial}{\partial y}\right)$$

and introducing the stress combinations

$$\Theta = \sigma_x + \sigma_y \quad \dots\dots\dots(7.3)$$

$$\Phi = \sigma_y - \sigma_x + 2i\tau_{xy}$$

equations (7.1) and (7.2) become

$$\frac{\partial \Theta}{\partial \bar{Z}} - \frac{\partial \Phi}{\partial Z} = 0 \quad \dots\dots\dots(7.4)$$

$$\frac{\partial^2 \Theta}{\partial Z \partial \bar{Z}} = 0 \quad \dots\dots\dots(7.5)$$

It is seen that  $\Theta$  is real, and as is shown later,

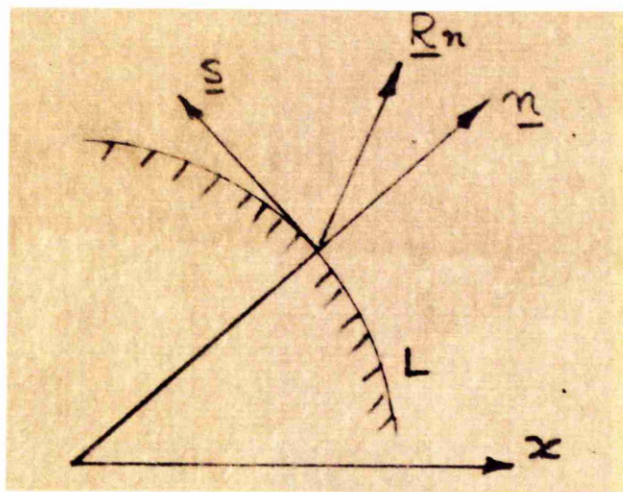
$$\Theta = 2 \left[ \phi'(Z) + \bar{\phi}'(\bar{Z}) \right] \quad \dots\dots\dots(7.6)$$

where the dashes denote differentiation with respect to the bracketed variable, and the bars denote the conjugate complex quantity.

Substituting for  $\Theta$  in (7.6) and integrating gives

$$\phi = 2 \left[ \bar{z} \phi''(z) + \psi'(z) \right] \dots\dots\dots (7.7)$$

Thus the stress components at any point in the  $Z$  region may be determined from two complex potentials  $\phi(z)$  and  $\psi(z)$  in terms of which all the other quantities may be obtained.



### Boundary Condition

Putting  $\underline{n}$  and  $\underline{s}$  as unit vectors normal and tangential to the boundary  $L$  of the opening in the  $Z$  plane, and  $\alpha$  as the angle of inclination of  $\underline{n}$  to the positive  $X$  axis as shown in Fig.140 the direction cosines of  $\underline{n}$  being  $(1, m, 0)$  and those of  $\underline{s}$  being  $(-m, 1, 0)$ , then the stress over an element of  $L$  can be represented by the vector  $\underline{R}_n$  which is related to the cartesian stress vectors  $\underline{R}_x$  and  $\underline{R}_y$  by

$$\underline{R}_n = \underline{R}_x + m \underline{R}_y$$

If  $X_n$  and  $Y_n$  are the components of  $\underline{R}_n$  then

$$X_n = 1\sigma_x + m\tau_{xy}$$

$$Y_n = 1\tau_{xy} + m\sigma_y$$

Taking  $X_n$  and  $Y_n$  to be known quantities, they may be related to the complex potentials, thus

$$X_n + iY_n = \frac{1}{2} e^{i\alpha} \Theta - \frac{1}{2} e^{-i\alpha} \bar{\Phi} \dots\dots\dots(7.8)$$

which on substitution for  $\Theta$  and  $\bar{\Phi}$ , gives

$$X_n + iY_n = \left[ \phi'(Z) + \bar{\phi}'(\bar{Z}) \right] e^{i\alpha} - \left[ Z\bar{\phi}''(\bar{Z}) + \bar{\psi}'(\bar{Z}) \right] e^{-i\alpha} \dots\dots\dots(7.9)$$

$$\text{Since } Z = x + iy, \frac{dZ}{dS} = \frac{dx}{dS} + i\frac{dy}{dS} = -m + il = ie^{i\alpha}$$

therefore

$$\begin{aligned} i(X_n + iY_n) &= \left[ \phi'(Z) + \bar{\phi}'(\bar{Z}) \right] \frac{dZ}{dS} + \left[ Z\bar{\phi}''(\bar{Z}) + \bar{\psi}'(\bar{Z}) \right] \frac{d\bar{Z}}{dS} \\ &= \frac{d}{dS} \left[ \phi(Z) + Z\bar{\phi}'(\bar{Z}) + \bar{\psi}(\bar{Z}) \right] \dots\dots\dots(7.10) \end{aligned}$$

Assuming the boundary to be a closed curve, and integrating round the boundary gives

$$i \int (X_n + iY_n) dS = \phi(Z) + Z\bar{\phi}'(\bar{Z}) + \bar{\psi}(\bar{Z}) + \text{constant.}$$

This integral is now written as  $f_1 + if_2$  so that the boundary condition becomes

$$\phi(Z) + Z\bar{\phi}'(\bar{Z}) + \bar{\psi}(\bar{Z}) = f_1 + if_2 + \text{constant} \dots\dots\dots(7.11)$$

### Resultant Force on the Boundary

The change in  $f(Z)$  when  $Z$  makes one circuit of the boundary  $L$  is denoted by  $C_y f(Z)$ , e.g.  $C_y \log Z = 0$  if  $L$  does not contain the origin and  $C_y \log Z = 2\pi i$  if  $L$  does contain the origin.

Also, if  $(X, Y)$  are the components of the resultant force on the boundary, then it may be shown that

$$(X + iY) = -\frac{1}{4} i C_y \left[ \phi(Z) + Z\bar{\phi}'(\bar{Z}) + \bar{\psi}(\bar{Z}) \right] \dots\dots\dots(7.12)$$

Displacement/

Displacement

Writing the complex displacement in the  $(x, y)$  plane as  $D = u + iv$ , then the stress combinations  $\phi$  and  $\Theta$  expressed in terms of the complex displacement are

$$\phi = -4\mu \frac{\partial \bar{D}}{\partial Z} \dots\dots\dots (7.13)$$

$$\Theta = \frac{2\mu}{1-2\nu} \left( \frac{\partial D}{\partial Z} + \frac{\partial \bar{D}}{\partial \bar{Z}} \right) \dots\dots\dots (7.14)$$

(Note: these expressions may be proved by substituting for  $D$  and expanding the right hand sides).

Substituting equations (7.15) and (7.14) in equation (7.4) leads to

$$K \frac{\partial^2 D}{\partial Z \partial \bar{Z}} + \frac{\partial^2 \bar{D}}{\partial \bar{Z}^2} = 0 \dots\dots\dots (7.15)$$

where  $K = 3 - 4\nu =$  bulk modulus for plane strain

$$= \frac{5 - \nu}{1 + \nu} \quad \quad \quad \text{" " " generalised plane stress}$$

Integration with respect to  $\bar{Z}$  gives

$$K \frac{\partial D}{\partial Z} + \frac{\partial \bar{D}}{\partial \bar{Z}} = C\phi'(Z) \quad \text{and its conjugate}$$

$$K \frac{\partial \bar{D}}{\partial \bar{Z}} + \frac{\partial D}{\partial Z} = C\bar{\phi}'(\bar{Z})$$

which when combined, reduce to

$$(K^2 - 1) \frac{\partial D}{\partial Z} = C \left[ K\phi'(Z) - \bar{\phi}'(\bar{Z}) \right]$$

Putting  $C = \frac{K^2 - 1}{2\mu}$  gives

$$2\mu \frac{\partial D}{\partial Z} = K\phi'(Z) - \bar{\phi}'(\bar{Z}) \dots\dots\dots (7.16)$$

which on integration with respect to  $Z$  may be shown to lead to

$$2\mu D = K\phi(Z) - Z\bar{\phi}'(\bar{Z}) - \bar{\psi}(\bar{Z}) \dots\dots\dots (7.17)$$

Writing (7.16) as

$$\frac{\partial D}{\partial Z} = \frac{1}{2\mu} \left[ K\phi'(Z) - \bar{\phi}'(\bar{Z}) \right] \quad \text{and its conjugate}$$

$$\frac{\partial \bar{D}}{\partial \bar{Z}} = \frac{1}{2\mu} \left[ K\bar{\phi}'(\bar{Z}) - \phi'(Z) \right] \quad \text{adding and substituting in equation}$$

(7.14) gives an expression for  $\Theta$  as

$$\Theta = \frac{2\mu}{1-2\nu} \cdot \frac{(K-1)}{2\mu} \left[ \phi'(Z) + \bar{\phi}'(\bar{Z}) \right]$$

$$\text{or } \Theta = \frac{K-1}{(1-2\nu)} \left[ \phi'(Z) + \bar{\phi}'(\bar{Z}) \right] \dots\dots\dots(7.18)$$

Since  $K = 3 - 4\nu$  for plane strain

$K - 1 = 2(1 - 2\nu)$ , and hence (7.18) reduces to formula (7.6), which is applicable also to generalised plane stress when  $K = 3 - \nu/1 + \nu$ .



Form of the Complex Potentials

The resultant boundary force condition stated in equation (7.12) is satisfied by complex potentials of the form

$$\phi(Z) = -\frac{(X + iY)}{2\pi(1+k)} \log Z + \sum_{-\infty}^{+\infty} a'_n Z^n \dots\dots\dots(7.19)$$

$$\psi(Z) = \frac{k(X - iY)}{2\pi(1+k)} \log Z + \sum_{-\infty}^{+\infty} b'_n Z^n$$

The series  $\sum_{-\infty}^{+\infty} a'_n Z^n$  and  $\sum_{-\infty}^{+\infty} b'_n Z^n$  must not contain terms in  $n > 2$ , if the stresses are to remain finite as  $|Z| \rightarrow \infty$  the plate being assumed to be large. These series may be written

$$\sum_{-\infty}^{+\infty} a'_n Z^n = a'_1 Z + \sum_{-\infty}^0 a'_n Z^n = a'_1 Z + a'_0 + \frac{a'_1}{Z} + \frac{a'_2}{Z^2} + \dots\dots\dots(7.20)$$

$$\sum_{-\infty}^{+\infty} b'_n Z^n = b'_1 Z + \sum_{-\infty}^0 b'_n Z^n = b'_1 Z + b'_0 + \frac{b'_1}{Z} + \frac{b'_2}{Z^2} + \dots\dots$$

Now put  $\phi_1(Z) = \sum_{-\infty}^0 a'_n Z^n$  and

$$\psi_1(Z) = \sum_{-\infty}^0 b'_n Z^n$$

with  $a'_1 = B + iC$

and  $b'_1 = B_1 + iC_1$  where  $B$ ,  $B_1$  and  $C_1$  are constants to be determined from the stresses at infinity, whilst  $C$  corresponds to a rigid body displacement, taken as zero.

Then the complex potentials become

$$\phi(Z) = -\frac{(X + iY)}{2\pi(1+k)} \log Z + (B + iC)Z + \phi_1(Z) \dots\dots\dots(7.21)$$

$$\psi(Z) = \frac{k(X - iY)}{2\pi(1+k)} \log Z + (B_1 + iC_1)Z + \psi_1(Z) \dots\dots\dots(7.22)$$

If the principal stresses at infinity are  $\sigma_o$  and  $\sigma_p$  with the direction of  $\sigma_o$  making an angle  $\alpha$  with the x-axis, then

$$\phi'(Z) = B + iC \quad \dots\dots\dots(7.23)$$

$$\bar{\phi}'(\bar{Z}) = B - iC$$

and from

$$\Theta = \sigma_x + \sigma_y = 2 [\phi'(Z) + \bar{\phi}'(\bar{Z})]$$

then  $\sigma_x + \sigma_y = 4B$ . At infinity,

$$\sigma_x + \sigma_y = \sigma_o + \sigma_p = 4B$$

$$\therefore B = \frac{1}{4} (\sigma_o + \sigma_p) \quad \dots\dots\dots(7.24)$$

Also, from equation (7.21), at infinity  $\phi''(Z) = 0$  and equation (7.7) gives

$$\begin{aligned} \sigma_y - \sigma_x + 2i\tau_{xy} &= 2\psi'(Z) \\ &= 2(B_1 + iC_1) \end{aligned}$$

$$\text{Since } (\sigma_y - \sigma_x) = (\sigma_p - \sigma_o)\cos 2\alpha$$

$$\text{and } 2\tau_{xy} = -(\sigma_p - \sigma_o)\sin 2\alpha$$

$$\text{therefore } (\sigma_y - \sigma_x) = 2B_1 = (\sigma_p - \sigma_o)\cos 2\alpha$$

$$2\tau_{xy} = 2C_1 = -(\sigma_p - \sigma_o)\sin 2\alpha$$

$$\begin{aligned} \text{giving } B_1 &= \frac{1}{2} (\sigma_p - \sigma_o)\cos 2\alpha \\ &\dots\dots\dots(7.25) \end{aligned}$$

$$C_1 = \frac{1}{2} (\sigma_o - \sigma_p)\sin 2\alpha$$

#### Application of Conformal Transformation

The region external to the boundary curve L of the actual hole is now mapped into the  $\zeta$ -region inside a unit circle Y by the

transformation  $Z = \omega(\zeta)$ , and when the point  $\zeta$  lies on the boundary of the unit circle it is denoted by  $\sigma$ . The complex potentials are now expressible in terms of  $\sigma$  in the form

$$\phi(Z) = \phi[\omega(\sigma)] = \phi(\sigma),$$

so that the equation for the boundary condition (7.11) now becomes

$$\phi(\sigma) + \omega(\sigma) \frac{\bar{\phi}'(\bar{\sigma})}{\bar{\omega}'(\bar{\sigma})} + \bar{\psi}(\bar{\sigma}) = f_1 + if_2 + \text{constant on } \gamma \dots\dots\dots (7.26)$$

If  $\zeta = \rho e^{i\theta}$ , combinations of the curvilinear stress components can be written in the form

$$\begin{aligned} \Theta' &= \sigma_\theta + \sigma_\rho = \Theta \\ \Phi' &= \sigma_\theta - \sigma_\rho + 2i\tau_{\rho\theta} = e^{2i\alpha} \Phi \end{aligned} \dots\dots\dots (7.27)$$

where  $\alpha$  is the angle which the normal to the curve  $\rho = \text{constant}$  makes with the X-axis.

Then in terms of the complex potentials, using equations (7.3),

$$\Theta' = 2 [\chi(\zeta) + \bar{\chi}(\bar{\zeta})] \dots\dots\dots (7.28)$$

$$\Phi' = \frac{2\zeta^2}{\rho^2 \bar{\omega}'(\bar{\zeta})} \left[ \bar{\omega}(\bar{\zeta}) \cdot \chi'(\zeta) + \psi'(\zeta) \right] \dots\dots\dots (7.29)$$

$$\text{where } \chi(\zeta) = \frac{\phi'(\zeta)}{\omega'(\zeta)} \dots\dots\dots (7.30)$$

Using the transformation form

$$Z = \omega(\zeta) = C \left[ \frac{1}{\zeta} + m_1 \zeta + m_2 \zeta^2 + \dots m_n \zeta^n \right] \dots\dots\dots (7.31)$$

Now, using equations (7.21) and (7.22) and substituting for  $Z$ , gives the complex potentials as

$$\phi(\zeta) = \frac{X + iY}{2(\mathbf{I} \cdot \mathbf{K})} \log \zeta + \frac{C}{\zeta} B + \phi_0(\zeta) \dots\dots\dots (7.32)$$

$$\psi(\zeta) = -\frac{K(X-iY)}{2\pi(1+K)} \log \zeta + \frac{c}{\zeta}(B_1 + iC_1) + \psi_0(\zeta) \dots\dots\dots(7.53)$$

where  $\phi_0(\zeta) = \sum_1^{\infty} a_n \zeta^n$  and  $\psi_0(\zeta) = \sum_0^{\infty} b_n \zeta^n$  are two functions of  $\zeta$  which are analytic inside the unit circle  $|\zeta| = 1$ .

The Theorem of HARNACK (see SOKOLNIKOFF'S 'Theory of Elasticity', page 160)<sup>(64)</sup> is now applied. This in effect states that if two expression in  $\zeta$  are to be equal at all points on the boundary of the unit circle, it is possible to multiply both sides by  $\frac{1}{2\pi i} \frac{d\sigma}{\sigma-\zeta}$  and integrate round the boundary, this resulting in equality of the two functions. Therefore, substituting the complex potentials (7.52) and (7.53) into the boundary condition (7.26),

$$\begin{aligned} & \frac{X+iY}{2\pi(1+K)} \log \sigma + \frac{cB}{\sigma} + \phi_0(\sigma) + \frac{\omega(\sigma)}{\bar{\omega}'(\bar{\sigma})} \left[ \frac{X-iY}{2\pi(1+K)} \sigma - \bar{c}B\sigma^2 + \bar{\phi}_0'(\bar{\sigma}) \right] \\ & + \frac{K(X+iY)}{2\pi(1+K)} \log \sigma + \bar{c}\sigma(B_1 - iC_1) + \bar{\psi}_0(\bar{\sigma}) = f_1 + if_2 \dots\dots\dots(7.54) \end{aligned}$$

By reformatting, this equation becomes

$$\begin{aligned} f_1 + if_2 &= \left[ \phi_0(\sigma) + \frac{\omega(\sigma)}{\bar{\omega}'(\bar{\sigma})} \cdot \bar{\phi}_0'(\bar{\sigma}) + \frac{X+iY}{2\pi} \log \sigma \right. \\ & \left. + \frac{cB}{\sigma} + \frac{\omega(\sigma)}{\bar{\omega}'(\bar{\sigma})} \left[ \frac{X-iY}{2\pi(1+K)} \sigma - \bar{c}B\sigma^2 \right] + \bar{c}\sigma(B_1 - iC_1) \right] \dots\dots\dots(7.55) \end{aligned}$$

The boundary condition for  $\phi_0(\zeta)$  and  $\psi_0(\zeta)$  is now written as

$$\phi_0(\sigma) + \frac{\omega(\sigma)}{\bar{\omega}'(\bar{\sigma})} \cdot \bar{\phi}_0'(\bar{\sigma}) + \bar{\psi}_0(\bar{\sigma}) = f_1^0 + if_2^0 \dots\dots\dots(7.56)$$

Applying HARNACK'S theorem, each term is multiplied by  $\frac{1}{2\pi i} \frac{d\sigma}{\sigma-\zeta}$  and integrated round the boundary  $\gamma$  of the unit circle, giving

$$\frac{1}{2\pi i} \int_{\gamma} \frac{\phi_0(\sigma) d\sigma}{\sigma-\zeta} + \frac{1}{2\pi i} \int_{\gamma} \frac{\omega(\sigma)}{\bar{\omega}'(\bar{\sigma})} \bar{\phi}_0'(\bar{\sigma}) \frac{d\sigma}{\sigma-\zeta} + \frac{1}{2\pi i} \int_{\gamma} \bar{\psi}_0(\bar{\sigma}) \frac{d\sigma}{\sigma-\zeta} = \frac{1}{2\pi i} \int_{\gamma} \frac{f_1^0 + if_2^0 d\sigma}{\sigma-\zeta}$$

Using CAUCHY'S integral formula, the first integral is

$$\frac{1}{2\pi i} \int_{\gamma} \phi_0(\sigma) \frac{d\sigma}{\sigma - \xi} = \phi_0(\xi)$$

and the third integral is

$$\begin{aligned} \frac{1}{2\pi i} \int_{\gamma} \frac{\bar{\psi}_0(\bar{\sigma}) d\sigma}{\sigma - \xi} &= \frac{1}{2\pi i} \int_{\gamma} \left( \sum_n \bar{b}_n \bar{\sigma}^n \right) \frac{d\sigma}{\sigma - \xi} = \frac{1}{2\pi i} \int_{\gamma} (\bar{b}_0 + \bar{b}_1 \bar{\sigma} + \dots) \frac{d\sigma}{\sigma - \xi} \\ &= \frac{1}{2\pi i} \int_{\gamma} \left( \bar{b}_0 + \frac{\bar{b}_1}{\sigma} + \dots \right) \frac{d\sigma}{\sigma - \xi} \\ &= \bar{b}_0 \end{aligned}$$

thus giving

$$\phi_0(\xi) + \frac{1}{2\pi i} \int_{\gamma} \frac{\omega(\sigma)}{\bar{\omega}'(\bar{\sigma})} \bar{\phi}_0'(\bar{\sigma}) \frac{d\sigma}{\sigma - \xi} + \bar{b}_0 = \frac{1}{2\pi i} \int_{\gamma} (f_1^{\circ} + if_2^{\circ}) \frac{d\sigma}{\sigma - \xi} \dots\dots\dots (7.57)$$

Taking the conjugate of equation (7.56)

$$\bar{\phi}_0(\bar{\sigma}) + \frac{\bar{\omega}(\bar{\sigma})}{\bar{\omega}'(\bar{\sigma})} \phi_0'(\sigma) + \psi_0(\sigma) = f_1^{\circ} - if_2^{\circ} \dots\dots\dots (7.58)$$

and performing the same integral process leads to

$$\psi_0(\xi) + \frac{1}{2\pi i} \int_{\gamma} \frac{\bar{\omega}(\bar{\sigma})}{\bar{\omega}'(\bar{\sigma})} \phi_0'(\sigma) \frac{d\sigma}{\sigma - \xi} = \frac{1}{2\pi i} \int_{\gamma} (f_1^{\circ} - if_2^{\circ}) \frac{d\sigma}{\sigma - \xi} \dots\dots\dots (7.59)$$

If the function  $\omega(\xi)$  is rational, equations (7.57) and (7.59) lead to the values of  $\phi_0(\xi)$  and  $\psi_0(\xi)$ , and therefore (7.52) and (7.55) give the complex potentials, from which the stresses and the displacement may be found.

Application to a Hole in a Tension Plate

Take the stress components  $\sigma_x^0$ ,  $\sigma_y^0$ ,  $\tau_{xy}^0$  to correspond to a plate without a hole under a given state of stress, and consider these components to be related to complex potentials  $\phi^0(Z)$  and  $\psi^0(Z)$ . Also take the stress components  $\sigma_x^*$ ,  $\sigma_y^*$ ,  $\tau_{xy}^*$  to be the additional amounts introduced by the presence of the hole, related to complex potentials  $\phi^*(Z)$  and  $\psi^*(Z)$ . The final state of stress  $\sigma_x$ ,  $\sigma_y$  and  $\tau_{xy}$  is then given by  $\sigma_x = \sigma_x^0 + \sigma_x^*$ , etc.

Since the effect of the hole will tend to be zero as  $Z$  tends to infinity, the functions  $\phi^*(Z)$  and  $\psi^*(Z)$  will be of the type

$$\sum_{-\infty}^{\infty} a_n Z^n \quad \text{and} \quad \sum_{-\infty}^{\infty} b_n Z^n \quad \text{and also} \quad \phi_1(Z) = \phi^0(Z) + \phi^*(Z) \text{ etc.}$$

The notation used on transformation to the  $\zeta$ -plane is:-

$$\phi_1[\omega(\zeta)] = \phi(\zeta) \qquad \psi_1[\omega(\zeta)] = \psi(\zeta)$$

$$\phi^0[\omega(\zeta)] = \phi^1(\zeta) \qquad \psi^0[\omega(\zeta)] = \psi^1(\zeta)$$

$$\phi^*[\omega(\zeta)] = \phi_0(\zeta) \qquad \psi^*[\omega(\zeta)] = \psi_0(\zeta)$$

$$\text{Then} \quad \phi(\zeta) = \phi^1(\zeta) + \phi_0(\zeta) \qquad \psi(\zeta) = \psi^1(\zeta) + \psi_0(\zeta)$$

$$\text{where} \quad \phi_0(\zeta) = \sum_1^{\infty} \alpha_n \zeta^n, \quad \psi_0(\zeta) = \sum_0^{\infty} \beta_n \zeta^n \dots\dots\dots(7.40)$$

These are the complex potentials which must be found and which must satisfy the necessary boundary conditions.

From (7.37) and (7.39) these conditions give

$$\phi_0(\zeta) + \frac{1}{2\pi i} \int_{\gamma} \frac{\omega(\sigma)}{\bar{\omega}'(\sigma)} \bar{\phi}_0'(\sigma) \frac{d\sigma}{\sigma - \zeta} + \bar{\beta}_0 = \frac{1}{2\pi i} \int_{\gamma} \frac{f_1^0 + if_2^0}{\sigma - \zeta} d\sigma \dots\dots\dots(7.41)$$

$$\psi_0(\zeta) + \frac{1}{2\pi i} \int_{\gamma} \frac{\bar{\omega}(\sigma)}{\omega'(\sigma)} \phi_0'(\sigma) \frac{d\sigma}{\sigma - \zeta} = \frac{1}{2\pi i} \int_{\gamma} \frac{f_1^0 - if_2^0}{\sigma - \zeta} d\sigma \dots\dots\dots(7.42)$$

Where  $f_1^0 + if_2^0$  is the derived boundary condition for  $\phi_0(\zeta)$  and

and  $\psi_0(\zeta)$  and is of the type

$$f_1^0 + if_2^0 = f_1 + if_2 - \left[ \phi(\sigma) + \frac{\omega(\sigma)}{\bar{\omega}(\bar{\sigma})} \bar{\phi}(\bar{\sigma}) + \bar{\psi}(\bar{\sigma}) \right] \dots\dots\dots (7.43)$$

### Plate Under Uniform Stress

For uniform stress  $\sigma_0$  at an angle  $\alpha$  to the x-axis, and the boundary of the hole in the plate unloaded, then  $X + iY = 0$  and  $f_1 + if_2 = 0$ . Hence from equations (7.24) and (7.25)

$$\begin{aligned} B &= \frac{1}{4} \sigma_0 \\ B_1 &= -\frac{1}{2} \sigma_0 \cos 2\alpha \\ C_1 &= \frac{1}{2} \sigma_0 \sin 2\alpha \end{aligned}$$

This stress state can be obtained from complex potentials  $\phi^0(Z) = \frac{1}{4} \sigma_0 Z$ ,  $\psi^0(Z) = -\frac{1}{2} \sigma_0 e^{-2i\alpha} Z$  which, using equations (7.5) give the above stress components.

$$\begin{aligned} \text{Then } \phi(\zeta) &= \frac{1}{4} \sigma_0 \omega(\zeta) + \phi_0(\zeta) \\ \psi(\zeta) &= -\frac{1}{2} \sigma_0 e^{-2i\alpha} \omega(\zeta) + \psi_0(\zeta) \end{aligned} \dots\dots\dots (7.44)$$

The boundary condition (7.43) now leads to

$$\begin{aligned} f_1^0 + if_2^0 &= -\frac{\sigma_0}{2} \left[ \omega(\sigma) + e^{2i\alpha} \bar{\omega}(\bar{\sigma}) \right] \\ f_1^0 - if_2^0 &= -\frac{\sigma_0}{2} \left[ \bar{\omega}(\bar{\sigma}) - e^{-2i\alpha} \bar{\omega}(\sigma) \right] \end{aligned} \dots\dots\dots (7.45)$$

Using equations (7.41) and (7.42) the complex potentials  $\phi_0(\zeta)$  and  $\psi_0(\zeta)$  can now be determined if the form of the transformation is given.

The stress combinations at any point in the Z region may be calculated using equations (7.5), for cartesian co-ordinates, thus

thus

$$\Phi = \sigma_x + \sigma_y = 2 \left[ \frac{\phi'(z)}{\omega'(z)} + \frac{\bar{\phi}'(\bar{z})}{\bar{\omega}'(\bar{z})} \right] \dots\dots\dots(7.46)$$

$$\phi = \sigma_y - \sigma_x + 2i\tau_{xy}$$

$$= 2 \left[ \bar{z} \left\{ \frac{\omega'(z)\phi''(z) - \omega''(z)\phi'(z)}{[\omega'(z)]^2} \right\} + \frac{\psi'(z)}{\omega'(z)} \right] \dots\dots\dots(7.47)$$

or for curvilinear co-ordinates, equations (7.28) and (7.29) may be employed.



APPENDIX VII.2     DIGITAL COMPUTER PROGRAMME  
FOR THEORETICAL STRESS DISTRIBUTION FOR  
CRUCIFORM CRACK CASE.

VII.2 Digital Computer Programme for Theoretical Stress Distribution for Cruciform Crack Case.

For the computation of values of  $(\sigma_{\theta} + \sigma_{\rho})$  and  $(\sigma_{\theta} - \sigma_{\rho} + 2i\tau_{\rho\theta})$  it was eventually decided to compute values along the axis through the point of maximum stress at  $90^{\circ}$  to the applied tension. The programme however was written and prepared for calculations for the axis at right angles to this. Since many of the cards were common, it was found possible to utilise these cards for both programmes, and for this reason the card numbering code is not consecutive in the  $(\sigma_{\theta} + \sigma_{\rho})$  programme, since certain cards had to be omitted from the  $(\sigma_{\theta} - \sigma_{\rho} + 2i\tau_{\rho\theta})$  programme to give the programme for  $(\sigma_{\theta} + \sigma_{\rho})$ . (Note: It is possible to utilise the computer to calculate values over the whole field of stress, and a programme was commenced with this in view. It was later abandoned however in favour of the more direct and shorter programmes given.)

Programme for  $\phi' = \sigma_{\theta} - \sigma_{\rho} + 2i\tau_{\rho\theta}$

For convenience in programming, expressions (2.79) and (2.80) were used to calculate the values of  $\sigma_{\theta} - \sigma_{\rho} + 2i\tau_{\rho\theta}$ , the sum of these equations giving the stress combination quoted, and on the axis of symmetry,  $\tau_{\rho\theta} = 0$ . Therefore this programme gives the difference of the principal stresses along the axis at  $90^{\circ}$  to the applied tensions.

Programme for  $\phi' = \sigma_{\rho} + \sigma_{\rho}$

For this programme, equation (2.50) was used. Cards common to the previous programme were employed where possible, and additional cards as required were added.

Note: It would have been possible to have combined both programmes so that the computer gave the result of the separate stresses in addition to the stress combinations, but it was considered easier to use a hand calculating machine to perform this function.

The results obtained from the computer, as reproduced from the punched card results on the tabulator, are shown immediately after each programme.



CRUCIFORM 'CRACK'

Q	r	R	A	B	FUNCTION	C	D	P S	NOTES
8			X5	X1	+	T1			$5m^4$ in X5
9			X6	X1	$\times$	T4			$5m^2 p^4$ in X6
0			X6	X6	-	X1			$5m^2 p^4 - 5m^4$ in X6
1			X7	X3	$\times$	T2			$2p^2$ in X7
2			X6	X6	-	X7			$5m^2 p^4 - 5m^4 - 2p^2$ in X6
3			X6	X6	+	T4			" " +m in X6
4			X6	X6	-	T1			" " " -1 in X6
5			X5	X5	$\times$	X6			$28 \times 54$ in X5
6			X6	T1	-	T4			$(1-m)$ in X6
7			X7	X4	$\times$	X4			$(5m^4 - 1)^2$ in X7
			X7	X6	$\times$	X7			$(1-m)(5m^4 - 1)^2$ in X7
			X5	X5	$\div$	X7			$55 \div 38$ in X5
			X5	X5	+	T1			$1 + 39$ in X5
			X2	X2	$\times$	X5			Equation(2.79) in X2
			1	1	RESULTS	X2	1		Print result of 41
			X5		-	X3		0	$-p^2$ in X5
			X8	X5	$\div$	X4			$45 \div 25$ in X8
			X9	T1	$\div$	X3			$1/p^2$ in X9
			X10	T4	$\times$	T4			$m^2$ in X10
			X10	T3	$\times$	X10			$5m^2$ in X10
			X10	X10	+	T1			$5m^2 + 1$ in X10
			X7	X10	$\div$	X7			$48 \div 38$ in X7
			X10	X5	$\times$	T3			$-5p^2$ in X10
			X10	X10	$\times$	X4			$50 \times 25$ in X10
			X11	X1	$\times$	T3			$9m^4$ in X11
			X11	X11	+	T1			$9m^4 + 1$ in X11
			X11	X6	$\times$	X11			$36 \times 55$ in X11
			X12	T2	$\times$	T2			4.0 in X12

CRUCIFORM 'CRACK'

[illegible]

COMPUTER RESULTS FOR  $\sigma_{\theta} - \sigma_{\rho} + 2\tau_{\rho\theta}$  with  $\theta = 90^{\circ}$ .

	1	1 0 0 0 0 0 0 0 0 +	= $\rho$	+
	1	9 9 9 9 9 9 9 9 9 +	= $\omega(\xi)$ .	1 -
1	0 0 1	1 0 2 7 0 6 1 4 2 -	= Equation(2.79).	2 +
1	0 0 1	1 1 2 4 4 1 9 2 2 +	= Equation(2.80).	2 +
2	0 0 1	9 7 3 5 7 8 0 2 4 +	= $\sigma_{\theta} - \sigma_{\rho} + 2i\tau_{\rho\theta}$	+
	1	8 9 9 9 9 9 9 9 9 +		1 -
	1	1 0 4 8 9 7 9 2 2 +		+
1	0 0 1	2 0 5 9 4 2 1 3 6 -		1 +
1	0 0 1	2 2 8 2 5 2 2 7 4 +		1 +
2	0 0 1	2 2 3 1 0 1 3 8 0 +		+
	1	8 5 0 0 0 0 0 0 0 +		1 -
	1	1 0 8 5 0 3 2 2 8 +		+
1	0 0 1	1 1 6 1 6 3 1 7 1 -		1 +
1	0 0 1	1 3 0 6 8 7 3 4 2 +		1 +
2	0 0 1	1 4 5 2 4 1 7 0 8 +		+
	1	8 0 0 0 0 0 0 0 0 +		1 -
	1	1 1 3 0 0 0 0 0 0 +		+
1	0 0 1	7 1 4 5 9 2 0 3 7 -		+
1	0 0 1	8 2 3 3 8 1 6 2 3 +		+
2	0 0 1	1 0 8 7 8 9 5 8 7 +		+
	1	7 5 0 0 0 0 0 0 0 +		1 -
	1	1 1 8 5 1 2 8 7 2 +		+
1	0 0 1	4 6 7 5 6 7 1 2 3 -		+
1	0 0 1	5 5 8 2 0 1 8 4 6 +		+
2	0 0 1	9 0 6 3 4 7 2 2 3 +		1 -
	1	7 0 0 0 0 0 0 0 0 +		1 -
	1	1 2 5 2 0 5 5 7 5 +		+
1	0 0 1	3 2 0 0 0 9 8 0 2 -		+
1	0 0 1	4 0 1 5 7 8 3 0 3 +		+
2	0 0 1	8 1 5 6 8 5 0 1 9 +		1 -



		1	6 4 9 9 9 9 9 9 9 +	1 -
		1	1 3 3 2 9 5 9 6 6 +	+
1	0 0 1		2 2 6 3 3 0 4 8 8 -	+
1	0 0 1		3 0 3 7 7 1 0 3 1 +	+
2	0 0 1		7 7 4 4 0 5 4 2 7 +	1 -
		1	6 0 0 0 0 0 0 0 0 +	1 -
		1	1 4 3 0 7 8 5 9 1 +	+
1	0 0 1		1 6 3 8 4 9 5 0 8 -	+
1	0 0 1		2 4 0 0 4 1 0 7 6 +	+
2	0 0 1		7 6 1 9 1 5 6 8 4 +	1 -
		1	5 0 0 0 0 0 0 0 0 +	1 -
		1	1 6 9 5 1 2 1 9 5 +	+
1	0 0 1		8 9 2 2 2 1 4 4 5 -	1 -
1	0 0 1		1 6 7 5 7 7 5 8 8 +	+
2	0 0 1		7 8 3 5 5 4 4 3 3 +	1 -
		1	4 0 0 0 0 0 0 0 0 +	1 -
		1	2 1 0 3 9 0 2 4 4 +	+
1	0 0 1		4 8 6 4 1 9 2 2 4 -	1 -
1	0 0 1		1 3 2 1 3 1 1 7 9 +	+
2	0 0 1		8 3 4 8 9 2 5 6 9 +	1 -
		1	3 0 0 0 0 0 0 0 0 +	1 -
		1	2 7 9 5 7 1 8 1 5 +	+
1	0 0 1		2 4 7 1 6 6 1 5 9 -	1 -
1	0 0 1		1 1 4 1 8 9 0 3 2 +	+
2	0 0 1		8 9 4 7 2 4 1 6 0 +	1 -



		1	2 5 0 0 0 0 0 0 0 +	1 -
		1	3 3 5 2 1 3 4 1 4 +	+
1	0 0 1		1 6 5 8 2 9 6 7 8 -	1 -
1	0 0 1		1 0 8 9 1 1 6 2 4 +	+
2	0 0 1		9 2 3 2 8 6 5 5 9 +	1 -
		1	2 0 0 0 0 0 0 0 0 +	1 -
		1	4 1 8 8 2 9 2 6 8 +	+
1	0 0 1		1 0 3 4 1 8 7 2 3 -	1 -
1	0 0 1		1 0 5 2 3 5 7 9 7 +	+
2	0 0 1		9 4 8 9 3 9 2 4 3 +	1 -
		1	1 7 5 0 0 0 0 0 0 +	1 -
		1	4 7 8 6 0 0 5 0 0 +	+
1	0 0 1		7 8 3 7 8 5 8 3 1 -	2 -
1	0 0 1		1 0 3 8 6 4 1 2 8 +	+
2	0 0 1		9 6 0 2 6 2 6 9 2 +	1 -
		1	1 2 5 0 0 0 0 0 0 +	1 -
		1	6 6 9 9 5 0 4 5 7 +	+
1	0 0 1		3 9 3 7 3 1 6 5 2 -	2 -
1	0 0 1		1 0 1 8 5 6 1 6 5 +	+
2	0 0 1		9 7 9 1 8 8 4 7 9 +	1 -
		1	1 0 0 0 0 0 0 0 0 +	1 -
		1	8 3 7 4 1 4 6 3 4 +	+
1	0 0 1		2 5 0 5 8 5 9 9 0 -	2 -
1	0 0 1		1 0 1 1 6 0 7 7 4 +	+
2	0 0 1		9 8 6 5 4 9 1 4 1 +	1 -

Calculation of  $\sigma_\theta + \sigma_\phi$  distribution along axes of symmetry for  $m = 1/5.5$

e.	For calculation of the stress combination $\sigma_{\theta} + \sigma_{\rho}$ along the $\theta = 0^{\circ}$ axis, card 69 must be removed.				
----	---	--	--	--	--

COMPUTER RESULTS FOR  $\sigma_\theta + \sigma_\rho$  with  $\theta = 90^\circ$ .

	1	1 0 0 0 0 0 0 0 0 +	= $\rho$	+
	1	9 9 9 9 9 9 9 9 9 +	= $\omega(\xi)$ .	1 -
1	0 0 1	9 7 3 5 7 8 0 2 8 +	= $\sigma_\theta + \sigma_\rho$	+
	1	8 9 9 9 9 9 9 9 9 +		1 -
	1	1 0 4 8 9 7 9 2 2 +		+
1	0 0 1	5 4 9 1 2 9 7 5 3 +		+
	1	8 5 0 0 0 0 0 0 0 +		1 -
	1	1 0 8 5 0 3 2 2 8 +		+
1	0 0 1	4 4 5 0 6 2 6 3 7 +		+
	1	8 0 0 0 0 0 0 0 0 +		1 -
	1	1 1 3 0 0 0 0 0 0 +		+
1	0 0 1	3 7 1 2 9 5 3 6 1 +		+
	1	7 5 0 0 0 0 0 0 0 +		1 -
	1	1 1 8 5 1 2 8 7 2 +		+
1	0 0 1	3 1 6 3 4 7 1 8 1 +		+
	1	7 0 0 0 0 0 0 0 0 +		1 -
	1	1 2 5 2 0 5 5 7 5 +		+
1	0 0 1	2 7 3 9 1 1 2 0 2 +		+
	1	6 4 9 9 9 9 9 9 9 +		1 -
	1	1 3 3 2 9 5 9 6 6 +		+
1	0 0 1	2 4 0 2 4 1 1 5 8 +		+
	1	6 0 0 0 0 0 0 0 0 +		1 -
	1	1 4 3 0 7 8 5 9 1 +		+
1	0 0 1	2 1 2 9 7 7 6 9 3 +		+

	1	5 0 0 0 0 0 0 0 0 +	1 -
	1	1 6 9 5 1 2 1 9 5 +	+
1	0 0 1	1 7 1 9 4 9 2 5 8 +	+
	1	4 0 0 0 0 0 0 0 0 +	1 -
	1	2 1 0 3 9 0 2 4 4 +	+
1	0 0 1	1 4 3 3 3 9 6 7 5 +	+
	1	3 0 0 0 0 0 0 0 0 +	1 -
	1	2 7 9 5 7 1 8 1 5 +	+
1	0 0 1	1 2 3 3 9 1 4 0 9 +	+
	1	2 5 0 0 0 0 0 0 0 +	1 -
	1	3 3 5 2 1 3 4 1 4 +	+
1	0 0 1	1 1 6 0 0 3 5 6 1 +	+
	1	2 0 0 0 0 0 0 0 0 +	1 -
	1	4 1 8 8 2 9 2 6 8 +	+
1	0 0 1	1 1 0 1 2 3 5 5 4 +	+
	1	1 7 5 0 0 0 0 0 0 +	1 -
	1	4 7 8 6 0 0 5 0 0 +	+
1	0 0 1	1 0 7 7 1 4 3 8 7 +	+
	1	1 2 5 0 0 0 0 0 0 +	1 -
	1	6 6 9 9 5 0 4 5 7 +	+
1	0 0 1	1 0 3 9 0 7 0 1 1 +	+
	1	1 0 0 0 0 0 0 0 0 +	1 -
	1	8 3 7 4 1 4 6 3 4 +	+
1	0 0 1	1 0 2 4 9 3 7 2 3 +	+

VII.3 Calculations for Theoretical Stress Concentration Factors

In order to determine suitable coefficients for the two term transformations used in the theoretical analysis, for a theoretical form of opening with the same  $\rho/a$  ratio as was used in the experimental specimens, the analogue computer was utilised to generate a family of openings for each basic shape. Enlarged photographs of these were used to determine (by measurement) their respective  $\rho/a$  ratios, then these were plotted against their corresponding  $1/m$  values. By interpolation on the resulting graph, it was possible to select suitable values of  $1/m$  to give shapes which corresponded with the actual forms of openings used in the experimental work.

The stress concentration factors for the shapes other than the cruciform, were calculated using the method of Chapter II. These are indicated in the following section.

(i) Cruciform 'Crack' with one arm of crack along axis of tension

As given by the computer programme.

(ii) Square Holes with Diagonal along Axis of Tension

The general solution was re-written in a slightly different form, in order to more easily determine the maximum stress concentration factor.

$$\begin{aligned} \text{Hence} \\ \chi(\xi) &= - \frac{\sigma_o \left[ -\frac{1}{4}\xi^2 + \frac{1}{2(1-m)} - \frac{m\xi^2}{4} \right] \xi^2}{1 - 3m\xi^4} \\ &= - \frac{\sigma_o \left[ -3m(1-m)\xi^4 + 2\xi^2 - (1-m) \right]}{4(1-m)(1-3m\xi^4)} \dots\dots\dots(7.48) \end{aligned}$$

$$\therefore \bar{\chi}(\xi) = - \frac{\sigma_o \left[ -3m(1-m)\xi^4 + 2\xi^2 - (1-m) \right]}{4(1-m)(1-3m\xi^4)} \dots\dots\dots(7.49)$$

$$\text{then } \Theta' = \sigma_{\theta} + \sigma_{\rho} = 2 \left[ (7.47) + (7.48) \right]$$

Putting  $\xi = \rho e^{in\theta} = \rho(\cos n\theta + i \sin n\theta)$ , with  $\rho = 1$ , and

$$\bar{\xi} = (\cos n\theta - i \sin n\theta)$$

in the above expressions, and collecting terms gives the stress concentration factor as

$$\begin{aligned} \text{Stress Concentration Factor} &= 2 \left[ \frac{A + iB}{C + iD} + \frac{A - iB}{C - iD} \right] \\ &= 4 \left[ \frac{AC + BD}{C^2 + D^2} \right] \dots\dots\dots (7.50) \end{aligned}$$

$$\text{where } A = (1-m) - 2 \cos 2\theta + 3m(1-m) \cos 4\theta$$

$$B = 3m(1-m) \sin 4\theta - 2 \sin 2\theta$$

$$C = 4(1-m) - 12m(1-m) \cos 4\theta$$

$$D = -12m(1-m) \sin 4\theta$$

Note: When  $m$  is numerically positive, one diagonal of the square lies along the axis of tension.

When  $m$  is numerically negative, the sides of the square are parallel to the axis of tension.

For this case, the point of maximum stress lies at the end of the diagonal which is at  $90^\circ$  to the axis of tension.

Therefore  $\theta = 90^\circ$ ,  $\cos 2\theta = -1$ ,  $\cos 4\theta = +1$  and

$$\text{Stress Concentration Factor} = 4 \frac{A}{C}$$

For the selected value of  $m$  to correspond with the experimental specimen,  $m = +0.182$ , giving  $3m = .546$

$$1 - m = .818$$

$$12m = 2.134$$

$$\begin{aligned}\text{Theoretical Stress Concentration Factor} &= \frac{(1-m) + 2 + 3m(1-m)}{(1-m) - 3m(1-m)} \\ &= \frac{3.266}{.372} \\ &= 8.8\end{aligned}$$

$$\text{Experimental Stress Concentration Factor} = 8.2$$

$$\text{Therefore \% Difference} = - \frac{8.8 - 8.2}{8.8} \times 100 = -6.8\%$$

(iii) Square Hole with Sides Parallel to Axis of Tension

Equation (7.50) again applies, with the value of  $m$  numerically negative with  $m = -0.216$  to correspond with experimental specimen.

$$\text{Then } m = -.216$$

$$3m = -.648$$

$$1 - m = 1.216$$

$$12m = -2.592$$

and after interpolation the value of  $\theta$  for the maximum stress concentration factor was found to be about  $48^\circ$ , giving

$$A = +2.197$$

$$B = -1.825$$

$$C = +1.779$$

$$D = -0.656$$

leading to

$$\begin{aligned}\text{Theoretical Stress Concentration Factor} &= 4 \frac{(2.197 \times 1.779 + 1.825 \times .656)}{(1.779)^2 + (.656)^2} \\ &= 5.67\end{aligned}$$

Experimental Stress Concentration Factor = 5.53

$$\text{Therefore \% Difference} = \frac{5.67 - 5.53}{5.67} \times 100 = -2.47\%$$

(iv) Cruciform 'crack' with arms of crack at 45° to axis of tension

For this case, using equation (7.50) and  $m = -0.222$  to correspond with the experimental specimen, an angle  $\theta = 48^\circ$  was again found to give the maximum stress concentration factor, so

$$\text{that } m = -0.222$$

$$3m = -0.666$$

$$1-m = 1.222$$

$$12 = -2.664$$

and

$$A = +2.217$$

$$B = -1.820$$

$$C = +1.703$$

$$D = -0.677$$

giving

Theoretical Stress Concentration Factor = 6.0

Experimental Stress Concentration Factor = 5.78

$$\text{Therefore \% Difference} = \frac{6 - 5.78}{6} \times 100 = -3.67\%$$

(v) 'Triangular' hole with one Median along the Axis of tension

From the derivation given in Section VII.1, for triangular holes, the following formula apply:-

$$\chi(\xi) = \frac{\sigma_0(-2m\xi^3 + 2\xi^2 - 1)}{4(2m\xi^3 - 1)} \dots\dots\dots(7.51)$$

$$\chi(\bar{\xi}) = \frac{\sigma_0(-2m\bar{\xi}^3 + 2\bar{\xi}^2 - 1)}{4(2m\bar{\xi}^3 - 1)} \dots\dots\dots(7.52)$$



and as before, using  $\xi = (\cos n \theta + i \sin n \theta)$

$$\bar{\xi} = (\cos n \theta - i \sin n \theta)$$

on the hole boundary, and substituting in the equation for  $\sigma_{\theta} + \sigma_{\rho}$  with some reduction leads to

$$\text{Stress Concentration Factor} = \left[ \frac{AC + BD}{C^2 + D^2} \right] \dots\dots\dots (7.52)$$

$$\text{where } A = -2m \cos 3 \theta + 2 \cos 2 \theta - 1$$

$$B = \sin 2 \theta - 2m \sin 3 \theta$$

$$C = 2m \cos 3 \theta - 1$$

$$D = 2m \sin 3 \theta$$

For a value of  $m = +0.317$  to give correspondence with the experimental specimen

$$A = -2.754$$

$$B = -0.7576$$

$$C = -0.370$$

$$D = -0.0695$$

and Theoretical Stress Concentration Factor = 7.58

Since Experimental Stress Concentration Factor = 7.75

$$\begin{aligned} \text{Therefore \% Difference} &= + \frac{7.75 - 7.58}{7.58} \times 100 \\ &= +2.24\% \end{aligned}$$

(vi) Triangular Star 'Crack' with one arm along the axis of tension

The same formulae as for (v) apply for this case, using

$m = 0.525$  to correspond with the experimental specimen, and this gives

$$A = -2.764$$

$$B = -0.761$$

$$C = -0.354$$

$$D = -0.068$$

and the \*

Theoretical Stress Concentration Factor = 7.95

Since Experimental Stress Concentration Factor = 8.15

$$\text{Therefore \% Difference} = + \frac{8.15 - 7.95}{7.95} \times 100 = +2.52\%$$

CHAPTER VII.4    INVESTIGATION OF ROTHMAN'S  
SUGGESTED COMPLEX POTENTIALS FOR CRUCIFORM CRACK  
AND DIGITAL COMPUTER PROGRAMME FOR SAME

(Note: This investigation was carried out prior to adopting the MUSKHELISHVILI method. In reporting this work it has been considered essential to adhere to STEVENSON'S forms of equations for  $\Phi$  and  $\bar{\phi}$ , as the potentials suggested by ROTHMAN are formed to suit these equations. As far as possible, the same symbols have been used as were used in the Muskhelishvili analysis).

VII.4 Investigation of ROTHMAN'S Suggested Complex Potentials for the Cruciform Crack Case and Digital Computer Programme for same.

The potentials given by ROTHMAN<sup>(7)</sup> are of the form

$$\phi(\xi) = (\sigma_p + \sigma_o) / \sqrt{2} + \frac{A\xi + B}{\xi + i\xi^2} \dots\dots\dots(7.54)$$

$$\psi(\xi) = (\sigma_p - \sigma_o) \xi^2/2 + \sum C_r/\xi^r \dots\dots\dots(7.55)$$

where  $\sigma_o$  and  $\sigma_p$  are the uniform tension stress parallel to the x and y axes, and the conformal transformation

$$Z = \omega(\xi) = (\xi^2 + 1/\xi^2)^{1/2}/\sqrt{2} \dots\dots\dots(7.56)$$

maps the Z-region exterior to the cruciform crack on to the

$\xi$  -region exterior to the unit circle;

To Show that the Potentials Satisfy the Boundary Conditions

The external boundary conditions are reached as  $Z \rightarrow \infty$ .

Using STEVENSON'S form of equation,

$$\Theta = \sigma_x + \sigma_y = \frac{1}{2} \left[ \frac{\phi'(\xi)}{\omega'(\xi)} + \frac{\bar{\phi}'(\bar{\xi})}{\bar{\omega}'(\bar{\xi})} \right] \dots\dots\dots(7.57)$$

and as  $Z \rightarrow \infty$

$$\sigma_x + \sigma_y = \frac{1}{2} \left[ \frac{(\sigma_o + \sigma_p)/\sqrt{2}}{1/\sqrt{2}} + \frac{(\sigma_o + \sigma_p)/\sqrt{2}}{1/\sqrt{2}} \right]$$

Therefore  $(\sigma_x + \sigma_y) = (\sigma_o + \sigma_p)$ , and for uniaxial tension in the x direction,  $\sigma_x = \sigma_o$ .

The potentials are thus satisfactory for this condition.

Again, using STEVENSON'S form of equation

$$\phi = \sigma_x - \sigma_y + 2i\tau_{xy} = -\frac{1}{2} \left[ \frac{\omega(z) [\bar{\phi}''(\bar{z}), \bar{\omega}'(\bar{z}) - \bar{\phi}'(\bar{z}) \bar{\omega}''(\bar{z})]}{[\bar{\omega}'(\bar{z})]^3} + \frac{[\bar{\psi}''(\bar{z}), \bar{\omega}'(\bar{z}) - \bar{\psi}'(\bar{z}) \bar{\omega}''(\bar{z})]}{[\bar{\omega}'(\bar{z})]^3} \right] \dots\dots\dots (7.58)$$

and as  $Z \rightarrow \infty$ ,

$$\sigma_x - \sigma_y + 2i\tau_{xy} = -\frac{1}{2} \left[ 0 + \frac{(\sigma_o - \sigma_p)(1/\sqrt{2})}{(1/\sqrt{2})^3} \right]$$

$$\text{Therefore } \sigma_x - \sigma_y + 2i\tau_{xy} = (\sigma_o - \sigma_p)$$

Since at infinity, with uniform tension  $\sigma_o$  parallel to the direction of the x-axis,  $\tau_{xy}$  is zero

$$\text{then } \sigma_x - \sigma_y = \sigma_o - \sigma_p$$

or  $\sigma_x = \sigma_o$ , and this again shows the potentials to be satisfactory for the boundary condition at infinity.

Determination of the Constants in the Complex Potentials from the Internal Boundary Conditions.

The normal and shear stresses round the boundary of the cruciform crack are zero, hence the equation for the boundary condition must be satisfied.

Therefore

$$\bar{\phi}(\bar{z}) + \bar{\omega}(\bar{z}) \cdot \frac{\phi'(z)}{\omega'(z)} + \frac{\psi'(z)}{\omega'(z)} = \text{a constant } K \text{ (or zero) round } z\bar{z} = 1 \text{ .. (7.59)}$$

$$\text{Round } z\bar{z} = 1, \quad \bar{z} = \frac{1}{z}.$$

The component parts of equation (7.59) are now formed.

$$\bar{\omega}(\bar{z}) = \bar{\omega}\left(\frac{1}{z}\right) = \frac{1}{\sqrt{2}} \left( z^2 + \frac{1}{z^2} \right)^{\frac{1}{2}}$$

$$\omega'(z) = \frac{1}{\sqrt{2}} \frac{\left( z - \frac{1}{z^3} \right)}{\left( z^2 + \frac{1}{z^2} \right)^{\frac{1}{2}}}$$

$$\text{Then } \frac{\bar{\omega}(\bar{z})}{\omega'(z)} = \frac{\left( z^2 + \frac{1}{z^2} \right)}{\left( z - \frac{1}{z^3} \right)} = \left( z + \frac{1}{z^3} \right) \left( 1 + \frac{1}{z^4} + \frac{1}{z^8} + \frac{1}{z^{12}} + \dots \right)$$

$$\begin{aligned} \text{Also } \frac{1}{\omega'(z)} &= \frac{\sqrt{2} \left( z^2 + \frac{1}{z^2} \right)^{\frac{1}{2}}}{\left( z - \frac{1}{z^3} \right)} \\ &= \sqrt{2} \left( 1 + \frac{1}{2z^4} - \frac{1}{8z^8} + \frac{1}{16z^{12}} \dots \right) \left( 1 + \frac{1}{z^4} + \frac{1}{z^8} + \frac{1}{z^{12}} \dots \right) \\ &= \sqrt{2} \left( 1 + \frac{3}{2z^4} + \frac{11}{z^8} + \dots \right) \end{aligned}$$

$$\bar{\phi}(\bar{z}) = \bar{\phi}\left(\frac{1}{z}\right) = \frac{(\sigma_o + \sigma_p)}{\sqrt{2}z} + \frac{A + Bz}{(1 - 1/z)}$$

$$= \frac{(\sigma_o + \sigma_p)}{\sqrt{2}z} + (A + Bz) \left( 1 + \frac{1}{z} - \frac{1}{z^2} - \frac{1}{z^3} + \frac{1}{z^4} \dots \right)$$

$$\phi'(z) = \frac{(\sigma_o + \sigma_p)}{\sqrt{2}} + -B/z^2(1 + iz) - i(A + B/z)$$

$$\begin{aligned}\phi'(z) &= \frac{\sigma_o + \sigma_p}{\sqrt{2}} + \frac{-\frac{B}{z^2} - \frac{iB}{z} - iA - \frac{iB}{z}}{-z^2(1/iz + 1)^2} \\ &= \frac{\sigma_o + \sigma_p}{\sqrt{2}} + \left(\frac{iA}{z^2} + \frac{2iB}{z^3} + \frac{B}{z^4}\right)(1 + \frac{2i}{z} - \frac{3}{z^2} - \frac{4i}{z^3} + \frac{5}{z^4} \dots)\end{aligned}$$

$$\psi'(z) = (\sigma_p - \sigma_o)z + \left(-\frac{C_1}{z^2} - \frac{2C_2}{z^3} - \frac{3C_3}{z^4} - \frac{4C_4}{z^5} \dots\right)$$

Substitution of these component parts into equation (7.59) followed by the equating of like powers of  $z$  gives the following constants:-

$$\begin{aligned}A &= i\sqrt{2} \sigma_p & B &= \frac{1}{\sqrt{2}}(\sigma_o - 3\sigma_p) \\ K &= \frac{i}{\sqrt{2}}(\sigma_o - \sigma_p) & C_1 &= \frac{i}{2}(\sigma_o - 9\sigma_p) \\ C_2 &= \frac{1}{4}(19\sigma_p - 3\sigma_o) & C_3 &= \frac{1}{6}(17\sigma_p - 3\sigma_o) \\ C_4 &= \frac{1}{2}(\sigma_o - 7\sigma_p)\end{aligned}$$

To satisfy the boundary condition (7.59), the constant  $K$  is included in the first part of the complex potential  $\phi(z)$ , thus giving the boundary equation as

$$\phi(z) + \omega(z)\bar{\phi}(\bar{z}) + \bar{\psi}(z) = 0 \text{ round the internal boundary.}$$

Inserting the values for the constants  $A$ ,  $B$ ,  $C$ , etc. into the equations for the potentials (7.54) and (7.55), and putting  $\sigma_p = 0$ , corresponding to simple tension  $\sigma_o$  parallel to the  $x$ -axis, the complex potentials are found to be:-

$$\phi(z) = \frac{\sigma_o}{\sqrt{2}}(z - 1) + \frac{\sigma_o}{\sqrt{2}(z + iz^2)} \dots \dots \dots (7.60)$$





The component parts of this expand as follows:-

$$\omega(\zeta) = \frac{1}{\sqrt{2}} \left( \zeta^2 + \frac{1}{\zeta^2} \right)^{\frac{1}{2}} \dots\dots\dots (7.62)$$

$$\bar{\omega}'(\bar{\zeta}) = \frac{1}{\sqrt{2}} \frac{\left( \bar{\zeta} - \frac{1}{\bar{\zeta}} \right)}{\left( \bar{\zeta}^2 + \frac{1}{\bar{\zeta}^2} \right)^{\frac{1}{2}}} \dots\dots\dots (7.63)$$

$$\bar{\omega}''(\bar{\zeta}) = \frac{1}{\sqrt{2}} \left[ \frac{\left( 1 + \frac{3}{\bar{\zeta}^4} \right)}{\left( \bar{\zeta}^2 + \frac{1}{\bar{\zeta}^2} \right)^{\frac{1}{2}}} - \frac{\left( \bar{\zeta} - \frac{1}{\bar{\zeta}} \right)^2}{\left( \bar{\zeta}^2 + \frac{1}{\bar{\zeta}^2} \right)^{\frac{3}{2}}} \right] \dots\dots\dots (7.64)$$

$$\frac{\bar{\phi}'(\bar{\zeta})}{\sigma_0} = \frac{1}{\sqrt{2}} \left[ 1 - \frac{(1 - 2i\bar{\zeta})}{(\bar{\zeta} - i\bar{\zeta}^2)^2} \right] \dots\dots\dots (7.65)$$

$$\frac{\bar{\phi}''(\bar{\zeta})}{\sigma_0} = \frac{1}{\sqrt{2}} \left[ \frac{2i}{(\bar{\zeta} - i\bar{\zeta}^2)^2} + \frac{2(1 - 2i\bar{\zeta})^2}{(\bar{\zeta} - i\bar{\zeta}^2)^3} \right] \dots\dots\dots (7.66)$$

$$\frac{\bar{\psi}'(\bar{\zeta})}{\sigma_0} = -\bar{\zeta} + \left[ \frac{i}{2\bar{\zeta}^2} + \frac{3}{2\bar{\zeta}^3} - \frac{5i}{2\bar{\zeta}^4} - \frac{2}{\bar{\zeta}^5} \dots \right] \dots\dots\dots (7.67)$$

$$\frac{\bar{\psi}''(\bar{\zeta})}{\sigma_0} = -1 + \left[ -\frac{i}{\bar{\zeta}^3} - \frac{9}{2\bar{\zeta}^4} + \frac{6i}{\bar{\zeta}^5} + \frac{10}{\bar{\zeta}^6} \dots \right] \dots\dots\dots (7.68)$$

Since  $\zeta = \rho e^{i\theta}$ , it is seen that by insertion of suitable values of  $\rho$  and  $\theta$  into these expressions, it is possible to obtain the distribution of the difference of the principal stresses throughout the stress field.

The Digital Computer Programme

The programme was written for the calculation of values of  $(\sigma_1 - \sigma_2)/\sigma_0$  in the Z-plane, corresponding to points in the  $\xi$ -plane, using four terms in the series  $\sum \frac{C_r}{r}$  contained in the  $\omega(\xi)$  potential.

In the Deuce Computer, complex operations (that is, 'Q-operations') are carried out using pairs of 'X'-stores, the real part of the complex number being stored in the odd X-store, and the imaginary part being carried in the even X-store. For any complex operation, only the relevant odd X-stores need be specified. Thus, multiplying  $(x + iy)$  by  $(u + iv)$  and getting the result as  $(m + in)$  is written as

$$X_5 = X_1 \text{ Q-mult. } X_3$$

This is a shorthand method of writing.

$x$  in  $X_1$ ,  $y$  in  $X_2$  multiplied by  
 $u$  in  $X_3$ ,  $v$  in  $X_4$  gives the result  
 $m$  in  $X_5$ ,  $n$  in  $X_6$

Constants may be stored in the 'T'-stores, of which there are eight. If a complex number is to be multiplied by a constant in a T-store, then the real and imaginary parts must be multiplied separately.

The programme was arranged so that points in the  $\xi$ -plane were located by various radii and angular intervals. The computer selected a radius value then proceeded through the calculation for angles between  $0^\circ$  and  $90^\circ$ , using  $10^\circ$  increments. On completion of the calculations for one radius, a new radius value was selected and the calculations repeated.

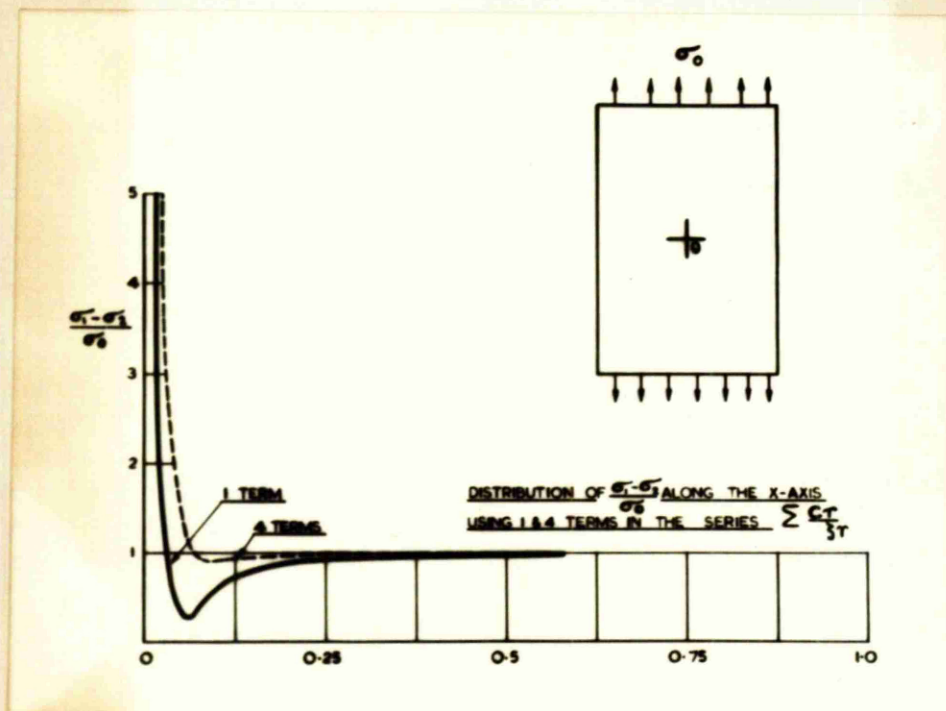


Fig.140a.

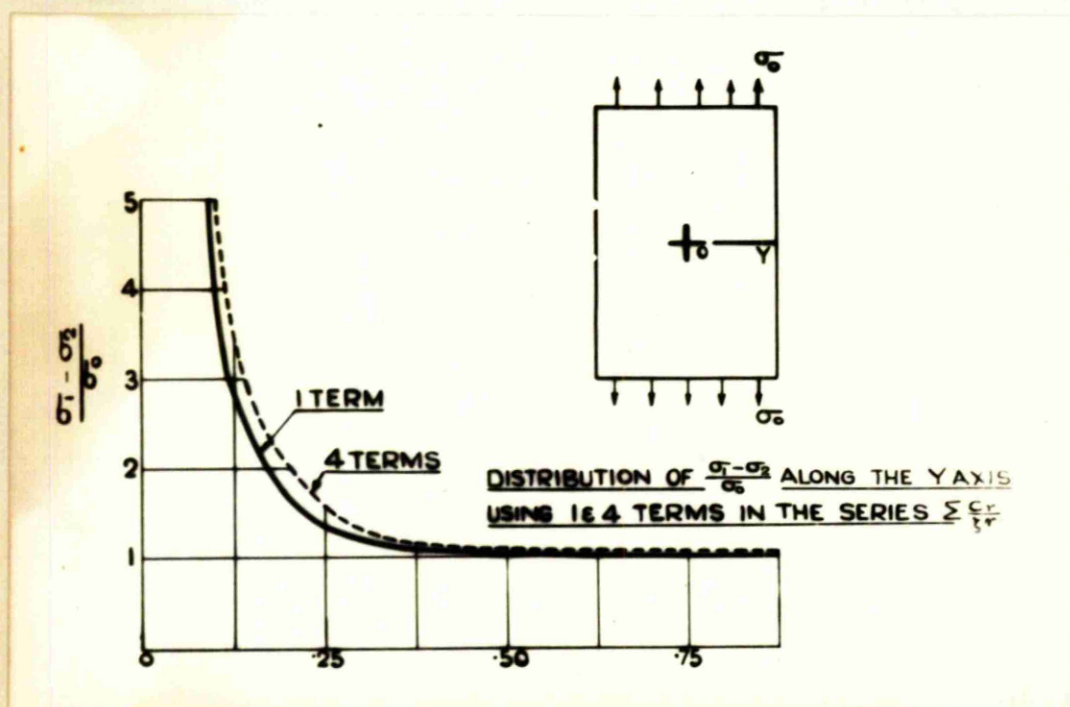


Fig.140b.

The distributions of  $(\sigma_1 - \sigma_2)/\sigma_0$  along the X and Y axes of the cruciform crack were drawn, using results obtained with one and with four terms in the series  $\sum C_r/r$  in the  $\psi$  potential.

(Figs 140a,b). The locus of  $(\sigma_1 - \sigma_2)/\sigma_0 = 2.0$  was drawn

(Figs 140c,d) using the same terms in the series.

Comparison of these results with the corresponding experimental results indicated disagreement to such an extent that further investigation of the potentials quoted by ROTHMAN was abandoned in favour of the MUSKHELISHVILI technique .

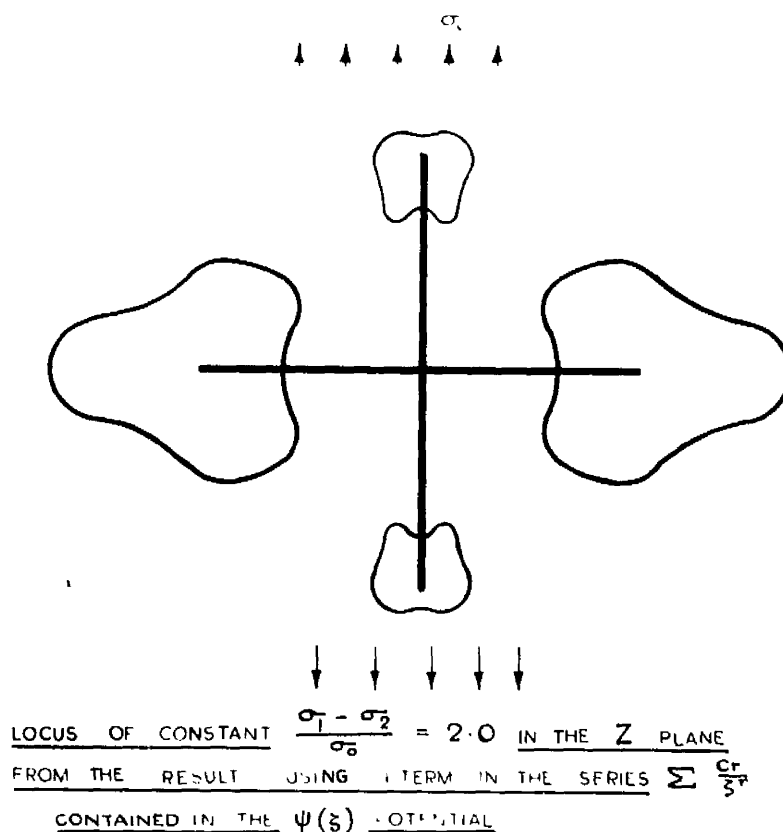
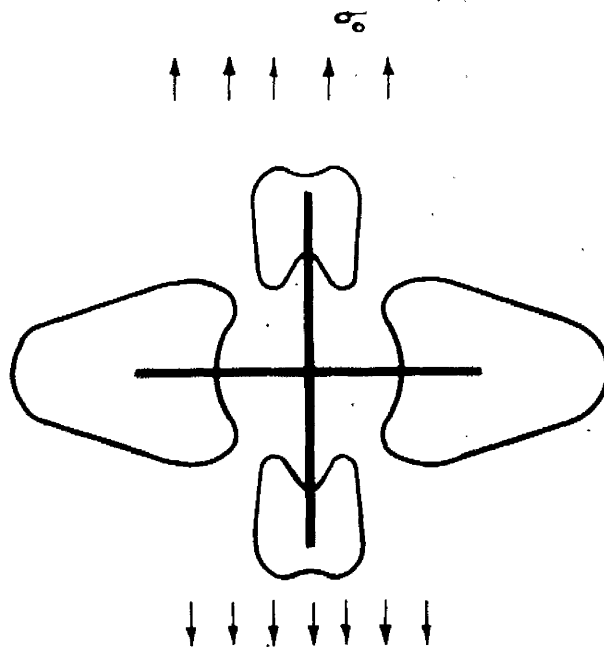


Fig.140c.



LOCUS OF  $\frac{\sigma_1 - \sigma_2}{\sigma_0} = 2.0$  IN THE  $z$  PLANE FROM  
 THE RESULTS USING 4 TERMS IN THE SERIES  $\sum \frac{c_r}{5^r}$   
 CONTAINED IN THE  $\psi(5)$  POTENTIAL

Fig. 140d.



## FOR CRUCIFORM TYPE 'CRACK' - USING ROTHMAN'S COMPLEX POTENTIALS

CALCULATION OF VALUES OF  $(\sigma_1 - \sigma_2)/\sigma_0$  AROUND THE DISCONTINUITY.

Nº	r	R	A	B	FUNCTION	C	D	P S	NOTES
00				1	DATA	X <sub>1</sub>			$1/\sqrt{2}$ in X <sub>1</sub>
01			T <sub>1</sub>		+	X <sub>1</sub>			$1/\sqrt{2}$ in T <sub>1</sub>
02				1	DATA	X <sub>1</sub>			2.0 in X <sub>1</sub>
03			T <sub>3</sub>		+	X <sub>1</sub>			2.0 in T <sub>3</sub>
04				1	DATA	X <sub>1</sub>			5.0 in X <sub>1</sub>
05			T <sub>4</sub>		+	X <sub>1</sub>			5.0 in T <sub>4</sub>
06				1	DATA	X <sub>1</sub>			5.0 in X <sub>1</sub>
07			T <sub>5</sub>		+	X <sub>1</sub>			5.0 in T <sub>5</sub>
08				10	DATA	X <sub>4</sub>			$\theta$ 's in X <sub>4</sub> to X <sub>15</sub>
09		R <sub>2</sub>		1	DATA	X <sub>1</sub>			r in X <sub>1</sub>
10			T <sub>2</sub>		+	X <sub>1</sub>			r in T <sub>2</sub>
11		R <sub>1</sub>		N <sub>1</sub>	MODIFY				
12			X <sub>2</sub>	X <sub>4</sub>	MOVED				$\theta$ in X <sub>2</sub>
13			X <sub>1</sub>		+	T <sub>2</sub>			
14			N <sub>2</sub>		MODIFY				
15			0	2	RESULTS	X <sub>1</sub>	1		r, $\theta$ values printed
16			X <sub>1</sub>	0	MOVED				
17			X <sub>1</sub>		Q EXP.	X <sub>1</sub>			$\cos \theta$ in X <sub>1</sub> $\sin \theta$ in X <sub>2</sub>
18			X <sub>1</sub>	X <sub>1</sub>	x	T <sub>2</sub>			$r \cos \theta$ in X <sub>1</sub> } $z = x + iy$
19			X <sub>2</sub>	X <sub>2</sub>	x	T <sub>2</sub>			$r \sin \theta$ in X <sub>2</sub> } $-X_1 - 2$
20			X <sub>15</sub>	X <sub>1</sub>	Qx	X <sub>1</sub>			$z^2$ in X <sub>15</sub>
21			X <sub>17</sub>	1	Q ÷	X <sub>15</sub>			$1/z^2$ in X <sub>17</sub>
22			X <sub>17</sub>	X <sub>17</sub>	Q+	X <sub>15</sub>			$(z^2 + 1/z^2)$ in X <sub>17</sub>
23			X <sub>17</sub>		Q	X <sub>17</sub>			$(z^2 + 1/z^2)^{1/2}$ in X <sub>17</sub>
24			X <sub>17</sub>	T <sub>1</sub>	x	X <sub>17</sub>			$z = w(z)$ in X <sub>17-18</sub>
25			X <sub>18</sub>	T <sub>1</sub>	x	X <sub>18</sub>			
26			X <sub>15</sub>	X <sub>17</sub>	MODULUS	X <sub>18</sub>			$\sqrt{x^2 + y^2} = R$ in X <sub>15</sub>
27			X <sub>16</sub>	X <sub>17</sub>	TAN <sup>-1</sup>	X <sub>18</sub>			$\delta$ in X <sub>16</sub>
28			N <sub>2</sub>		MODIFY				
29			100	4	RESULTS	X <sub>15</sub>	1		PRINT R, $\delta$ , x, $iy = z$



Nº	r	R	A	B	FUNCTION	C	D	P S	NOTES
50			X <sub>1</sub>		+	X <sub>1</sub>		}	$\bar{x} = x - iy$ in X1-2
51			X <sub>2</sub>		-	X <sub>2</sub>			
52			X <sub>19</sub>	X <sub>1</sub>	QX	X <sub>1</sub>			$\bar{x}^2$ in X <sub>19</sub>
53			X <sub>21</sub>	1	Q÷	X <sub>19</sub>			$1/\bar{x}^2$ in X <sub>21</sub>
54			X <sub>25</sub>	X <sub>21</sub>	QX	X <sub>21</sub>			$1/\bar{x}^4$ in X <sub>25</sub>
55			X <sub>25</sub>	X <sub>25</sub>	QX	X <sub>1</sub>			$1/\bar{x}^5$ in X <sub>25</sub>
56			X <sub>27</sub>	X <sub>1</sub>	Q-	X <sub>25</sub>			$(\bar{x} - 1/\bar{x}^5)$ in X <sub>27</sub>
57			X <sub>29</sub>	X <sub>19</sub>	Q+	X <sub>21</sub>			$(\bar{x}^2 + 1/\bar{x}^2)$ in X <sub>29</sub>
58			X <sub>29</sub>		Q√	X <sub>29</sub>			$(\quad)^{1/2}$ in X <sub>29</sub>
59			X <sub>51</sub>	X <sub>27</sub>	Q÷	X <sub>29</sub>			$(\bar{x} - 1/\bar{x}^5) / (\bar{x}^2 + 1/\bar{x}^2)^{1/2}$ in X <sub>51</sub>
40			X <sub>51</sub>	T <sub>1</sub>	x	X <sub>51</sub>			} $\bar{\omega}'(\bar{x})$
41			X <sub>52</sub>	T <sub>1</sub>	x	X <sub>52</sub>			
42			X <sub>25</sub>	T <sub>4</sub>	x	X <sub>25</sub>			} $5/\bar{x}^4$
43			X <sub>24</sub>	T <sub>4</sub>	x	X <sub>24</sub>			
44			X <sub>27</sub>	X <sub>27</sub>	QX	X <sub>27</sub>			$(\bar{x} - 1/\bar{x}^5)^2$ in X <sub>27</sub>
45			X <sub>27</sub>	X <sub>27</sub>	Q÷	X <sub>29</sub>		}	
46			X <sub>27</sub>	X <sub>27</sub>	Q÷	X <sub>29</sub>			$(\bar{x} - 1/\bar{x}^5)^2$
47			X <sub>27</sub>	X <sub>27</sub>	Q÷	X <sub>29</sub>			$(\bar{x} + 1/\bar{x}^2)^{5/2}$
48			X <sub>25</sub>	1	Q+	X <sub>25</sub>			$(1 + 5/\bar{x}^4)$
49			X <sub>25</sub>	X <sub>25</sub>	Q÷	X <sub>29</sub>			$(1 + 5/\bar{x}^4) / (\bar{x}^2 + 1/\bar{x}^2)^{1/2}$
50			X <sub>25</sub>	X <sub>25</sub>	Q-	X <sub>27</sub>			
51			X <sub>25</sub>	T <sub>1</sub>	x	X <sub>25</sub>			} $\bar{\omega}''(\bar{x})$
52			X <sub>24</sub>	T <sub>1</sub>	x	X <sub>24</sub>			
53			X <sub>21</sub>	i	QX	X <sub>1</sub>			$i\bar{x}$
54			X <sub>21</sub>	T <sub>5</sub>	x	X <sub>21</sub>			} $2i\bar{x}$
55			X <sub>22</sub>	T <sub>5</sub>	x	X <sub>22</sub>			
56			X <sub>21</sub>	1	Q	X <sub>21</sub>			$(1 - 2i\bar{x})$
57			X <sub>25</sub>	i	QX	X <sub>19</sub>			$i\bar{x}^2$
58			X <sub>25</sub>	X <sub>1</sub>	Q-	X <sub>25</sub>			$(\bar{x}^2 - i\bar{x}^2)$
59			X <sub>27</sub>	X <sub>21</sub>	Q÷	X <sub>25</sub>			$(1 - 2i\bar{x}) / (\bar{x} - i\bar{x}^2)$



Nº	r	R	A	B	FUNCTION	C	D	P S	NOTES
60			X <sub>27</sub>	X <sub>27</sub>	Q÷	X <sub>25</sub>			$(1-21\bar{f})/(\bar{f}-1\bar{f}^2)^2$
61			X <sub>27</sub>	1	Q-	X <sub>27</sub>			$[1-(1-21\bar{f})/(\bar{f}-1\bar{f}^2)^2]$
62			X <sub>27</sub>	T <sub>1</sub>	x	X <sub>27</sub>			$1/\sqrt{2} [ \quad ] \bar{\phi}'(\bar{f})$
63			X <sub>28</sub>	T <sub>1</sub>	x	X <sub>28</sub>			$1/\sqrt{2} [ \quad ]'$
64			X <sub>21</sub>	X <sub>21</sub>	Q÷	X <sub>25</sub>			$(1-21\bar{f})/(\bar{f}-1\bar{f}^2)$
65			X <sub>21</sub>	X <sub>21</sub>	Q÷	X <sub>25</sub>			$(1-21\bar{f})^2/(\bar{f}-1\bar{f}^2)^2$
66			X <sub>21</sub>	X <sub>21</sub>	Q÷	X <sub>25</sub>			$(1-21\bar{f})^2/(\bar{f}-1\bar{f}^2)^5$
67			X <sub>25</sub>	X <sub>25</sub>	QX	X <sub>25</sub>			$(\bar{f} - 1\bar{f}^2)^2$
68			X <sub>25</sub>	1	Q÷	X <sub>25</sub>			$1/(\bar{f} - 1\bar{f}^2)^2$
69			X <sub>25</sub>	X <sub>25</sub>	Q+	X <sub>21</sub>			$[\frac{1}{(\bar{f}-1\bar{f}^2)^2} + \frac{(1-21\bar{f})^2}{(\bar{f}-1\bar{f}^2)^2}]$
70			X <sub>25</sub>	X <sub>25</sub>	÷	T <sub>1</sub>			$\sqrt{[ \quad ]} \bar{\phi}''(\bar{f})$
71			X <sub>26</sub>	X <sub>26</sub>	÷	T <sub>1</sub>			$\sqrt{[ \quad ]}'$
72			X <sub>25</sub>	X <sub>25</sub>	QX	X <sub>51</sub>			$\bar{\omega}'(\bar{f}) \cdot \bar{\phi}''(\bar{f})$
73			X <sub>27</sub>	X <sub>27</sub>	QX	X <sub>25</sub>			$\bar{\phi}'(\bar{f}) \cdot \bar{\omega}''(\bar{f})$
74			X <sub>25</sub>	X <sub>25</sub>	Q-	X <sub>27</sub>			$[\bar{\omega}'(\bar{f})\bar{\phi}''(\bar{f}) - \bar{\omega}''(\bar{f})\bar{\phi}'(\bar{f})]$
75			X <sub>25</sub>	X <sub>25</sub>	Q÷	X <sub>51</sub>			
76			X <sub>25</sub>	X <sub>25</sub>	Q÷	X <sub>51</sub>			
77			X <sub>25</sub>	X <sub>25</sub>	Q÷	X <sub>51</sub>			$\bar{\phi}''(\bar{f})$
78			X <sub>25</sub>	X <sub>25</sub>	QX	X <sub>17</sub>			$\omega(\bar{f})\bar{\phi}''(\bar{f})$
79			X <sub>21</sub>	1	QX	X <sub>19</sub>			$1/\bar{f}^2$
80			X <sub>21</sub>	X <sub>21</sub>	÷	T <sub>5</sub>			$1/2\bar{f}^2$
81			X <sub>22</sub>	X <sub>22</sub>	÷	T <sub>5</sub>			
82			X <sub>27</sub>	T <sub>4</sub>	÷	T <sub>5</sub>			5/2
83			X <sub>27</sub>	X <sub>27</sub>	Q÷	X <sub>19</sub>			$5/2\bar{f}^2$
84			X <sub>27</sub>	X <sub>27</sub>	Q÷	X <sub>1</sub>			$5/2\bar{f}^5$
85			X <sub>29</sub>		+	T <sub>4</sub>			5
86			X <sub>29</sub>	X <sub>29</sub>	QX	X <sub>21</sub>			$51/2\bar{f}^2$
87			X <sub>29</sub>	X <sub>29</sub>	Q÷	X <sub>19</sub>			$51/2\bar{f}^4$
88			X <sub>17</sub>		+	T <sub>5</sub>			2
89			X <sub>17</sub>	X <sub>17</sub>	Q÷	X <sub>19</sub>			$2/\bar{f}^2$



Nº	r	R	A	B	FUNCTION	C	D	P S	NOTES
90			X <sub>17</sub>	X <sub>17</sub>	Q÷	X <sub>19</sub>			$2/\bar{f}^4$
91			X <sub>17</sub>	X <sub>17</sub>	Q÷	X <sub>1</sub>			$2/\bar{f}^5$
92			X <sub>21</sub>	X <sub>21</sub>	Q+	X <sub>27</sub>			$1/2\bar{f}^2 + 5/2\bar{f}^5$
93			X <sub>21</sub>	X <sub>21</sub>	Q-	X <sub>29</sub>			$1/2\bar{f}^2 + 5/2\bar{f}^5 - 51/2\bar{f}^4$
94			X <sub>21</sub>	X <sub>21</sub>	Q-	X <sub>17</sub>			" $-2/\bar{f}^5$
95			X <sub>21</sub>	X <sub>21</sub>	Q-	X <sub>1</sub>			" $-\bar{f} = \bar{\psi}'(\bar{f})$
96			X <sub>21</sub>	X <sub>21</sub>	QX	X <sub>25</sub>			$\bar{\psi}'(\bar{f}) \cdot \bar{\omega}''(\bar{f})$
97			X <sub>25</sub>	T <sub>5</sub>	x	T <sub>5</sub>			4
98			X <sub>25</sub>	X <sub>25</sub>	QX	X <sub>29</sub>			$61/\bar{f}^4$
99			X <sub>25</sub>	X <sub>25</sub>	Q÷	X <sub>1</sub>			$61/\bar{f}^5$
100			X <sub>29</sub>		+	T <sub>5</sub>			5
101			X <sub>29</sub>	X <sub>29</sub>	QX	X <sub>17</sub>			$10/\bar{f}^5$
102			X <sub>29</sub>	X <sub>29</sub>	Q÷	X <sub>1</sub>			$10/\bar{f}^6$
103			X <sub>17</sub>		+	T <sub>4</sub>			5
104			X <sub>17</sub>	X <sub>17</sub>	QX	X <sub>27</sub>			$9/2\bar{f}^5$
105			X <sub>17</sub>	X <sub>17</sub>	Q÷	X <sub>1</sub>			$9/2\bar{f}^4$
106			X <sub>27</sub>	i	Q÷	X <sub>19</sub>			$1/\bar{f}^2$
107			X <sub>27</sub>	X <sub>27</sub>	Q÷	X <sub>1</sub>			$1/\bar{f}^5$
108			X <sub>29</sub>	X <sub>29</sub>	Q+	X <sub>25</sub>			$10/\bar{f}^6 + 61/\bar{f}^5$
109			X <sub>29</sub>	X <sub>29</sub>	Q-	X <sub>17</sub>			" $-9/2\bar{f}^4$
110			X <sub>29</sub>	X <sub>29</sub>	Q-	X <sub>27</sub>			" $-1/\bar{f}^5$
111			X <sub>29</sub>	X <sub>29</sub>	Q-	1			$\bar{\psi}''(\bar{f})$
112			X <sub>29</sub>	X <sub>29</sub>	QX	X <sub>31</sub>			$\bar{\psi}''(\bar{f}) \cdot \bar{\omega}'(\bar{f})$
113			X <sub>29</sub>	X <sub>29</sub>	Q-	X <sub>21</sub>			$[\bar{\psi}''(\bar{f})\bar{\omega}'(\bar{f}) - \bar{\psi}'(\bar{f})\bar{\omega}''(\bar{f})]$
114			X <sub>29</sub>	X <sub>29</sub>	Q÷	X <sub>31</sub>			
115			X <sub>29</sub>	X <sub>29</sub>	Q÷	X <sub>31</sub>			
116			X <sub>29</sub>	X <sub>29</sub>	Q÷	X <sub>31</sub>			$\bar{\psi}''(\bar{f})$
117			X <sub>29</sub>	X <sub>29</sub>	Q+	X <sub>25</sub>			$\omega(\bar{f}) \cdot \bar{\phi}''(\bar{f}) + \bar{\psi}''(\bar{f})$
118			X <sub>29</sub>	X <sub>29</sub>	÷	T <sub>5</sub>			
119			X <sub>29</sub>		-	X <sub>29</sub>			$-\frac{1}{2} [\text{Real part}]$



[illegible]



VII.5      INVESTIGATION OF RELIABILITY AND  
SUITABILITY OF THE CONDUCTING PAPER ANALOGY  
FOR CASES OF TENSION AND TORSION

VII.5 Investigation of Reliability and Suitability of the Conducting Paper Analogy for Cases of Tension and Torsion.

The results of the investigation for the cases of tension plates with internal discontinuities have been given in Chapter III.2. The results of the investigation of the application to cases of torsion, while not directly related to the main work of the thesis, are included since the technique has been used for the determination of the stress concentration effect of a British Standard keyway in a shaft of circular cross-section, subjected to torsion.

As stated in Chapter III.2, the distribution of steady state potential  $V$  in a thin conducting sheet of constant thickness and uniform resistivity is governed by the LAPLACE equation

$$\frac{\partial^2 V}{\partial x^2} + \frac{\partial^2 V}{\partial y^2} = 0 \dots\dots\dots(7.69)$$

In the case of plane cross-sections under pure torsion, the distribution of the modified stress function  $\psi$  is governed by a similar equation,

$$\frac{\partial^2 \psi}{\partial x^2} + \frac{\partial^2 \psi}{\partial y^2} = 0 \dots\dots\dots(7.70)$$

$$\text{where } \psi = \phi + \frac{G\theta}{2} (x^2 + y^2) \dots\dots\dots(7.71)$$

and  $\phi$  = shear stress function

$\theta$  = angle of twist at section

$G$  = Modulus of rigidity

$x, y$  = Co-ordinates of points in the plane  
of the section.

From (7.71),

$\phi = \psi - \frac{G\theta}{2} (x^2 + y^2)$  and  $\phi$  may be a constant (or zero) on the boundary.

Putting  $\phi = 0$  gives  $\psi = \frac{G\theta}{2} (x^2 + y^2)$

$$\text{or } \frac{\psi}{G\theta} = \frac{1}{2} (x^2 + y^2) \dots\dots\dots (7.72)$$

Writing  $x_b$  and  $y_b$  for  $x$  and  $y$ , to represent co-ordinates of points on the boundary of the conducting paper specimen, the boundary voltage values used in the analogy are proportional to the values of

$$\frac{\psi}{G\theta} = \frac{1}{2} (x_b^2 + y_b^2) \dots\dots\dots (7.73)$$

Contours of constant  $\frac{\psi}{G\theta}$  may be obtained by probing over the area within the boundary. The shear stress contours, that is contours of constant

$$\frac{\phi}{G\theta} = \frac{\psi}{G\theta} - \frac{1}{2} (x^2 + y^2) \dots\dots\dots (7.74)$$

can then be obtained by calculation of the individual values over the region and sketching in the contours of common value.

#### Reliability Check

The technique was applied to the determination of the maximum shear stress values arising on the boundaries of specimens of rectangular cross-section subjected to torsion, for comparison with their known theoretical values. Four specimens were used, with breadth to depth ratios ranging from 1 : 1 to 8 : 1, the boundary voltages being determined by calculation using equation (7.73) and a suitable voltage scale.

Using the method described, the distributions of  $\frac{\phi}{G\theta}$  along the axes of symmetry were determined from all four rectangular sections, and in the cases of the square section and the 'thin' rectangular section, the distributions of  $\phi/G\theta$  were determined over the whole area. Also, the distribution of the shear stress  $\tau$  along these axes and along one side of the square were then found. Selected results are shown in Figs. 141 to 148.

The maximum shear stress values were determined from the maximum slope at the boundary of the  $\frac{\phi}{G\theta}$  distribution along the shortest axis of symmetry. This slope was found as accurately as possible, using the method of least squares to obtain an equation for the  $\frac{\phi}{G\theta}$  curve, the equation then being differentiated for the maximum shear stress value.

These results are shown (Fig.149) plotted on the theoretical curve for the maximum shear stress occurring on the boundary of a rectangular cross-section under torsion.

It is seen that there is excellent agreement between the theoretical and the conducting paper results.

The distribution of the shear stress  $\tau$  along the boundary of the square shaft was found by determining the  $\phi/G\theta$  distributions along lines parallel to the axis of symmetry through the centre of the square, as shown in Fig.150. The shear stress distribution is shown in Fig.151.

# **SQUARE SHAFT IN TORSION**

DISTRIBUTION OF  $\phi$  AND SHEAR STRESS  $\tau$  ALONG  
NORMAL LINES OF SYMMETRY CX AND OY

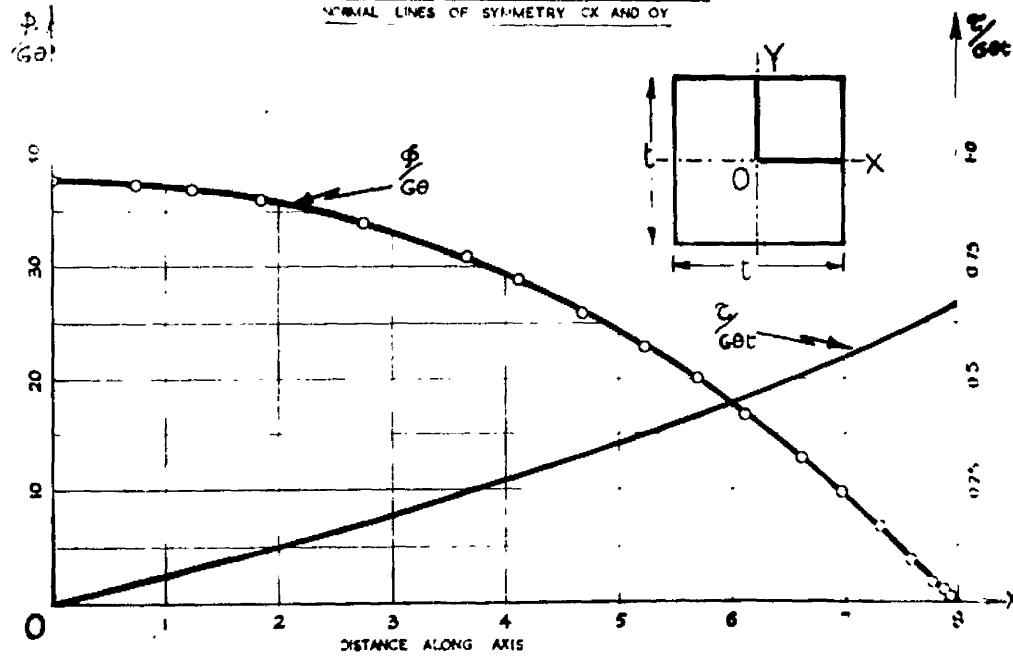


Fig.141.

# **SQUARE SHAFT IN TORSION**

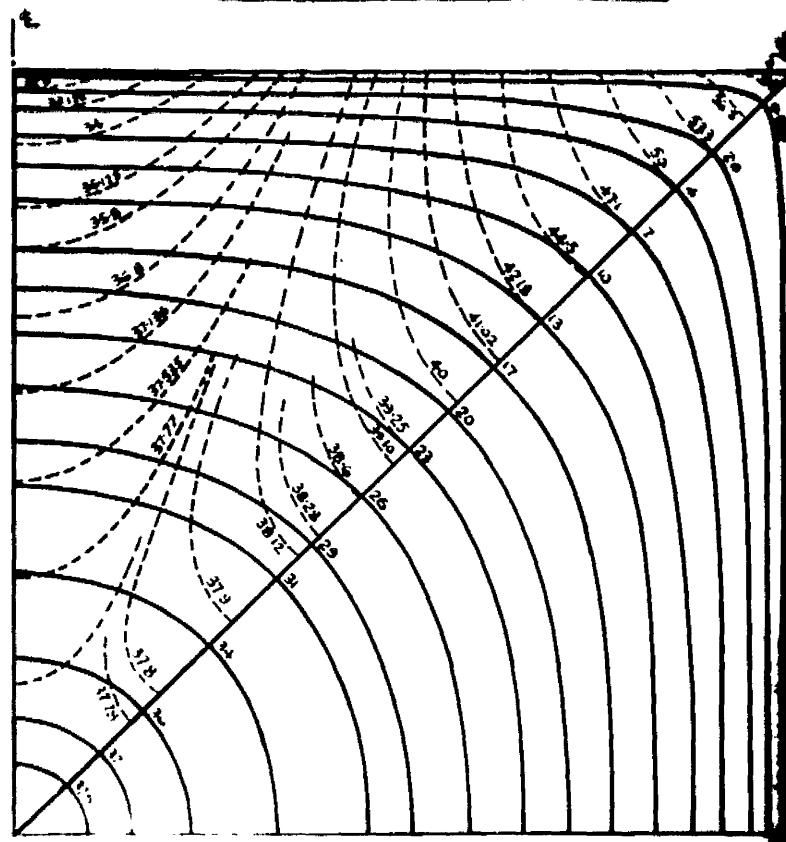


Fig.142.

# RECTANGULAR SHAFT IN TORSION

DISTRIBUTION OF  $\phi$  AND SHEAR STRESS  $\tau$  ALONG  
AXIS OY

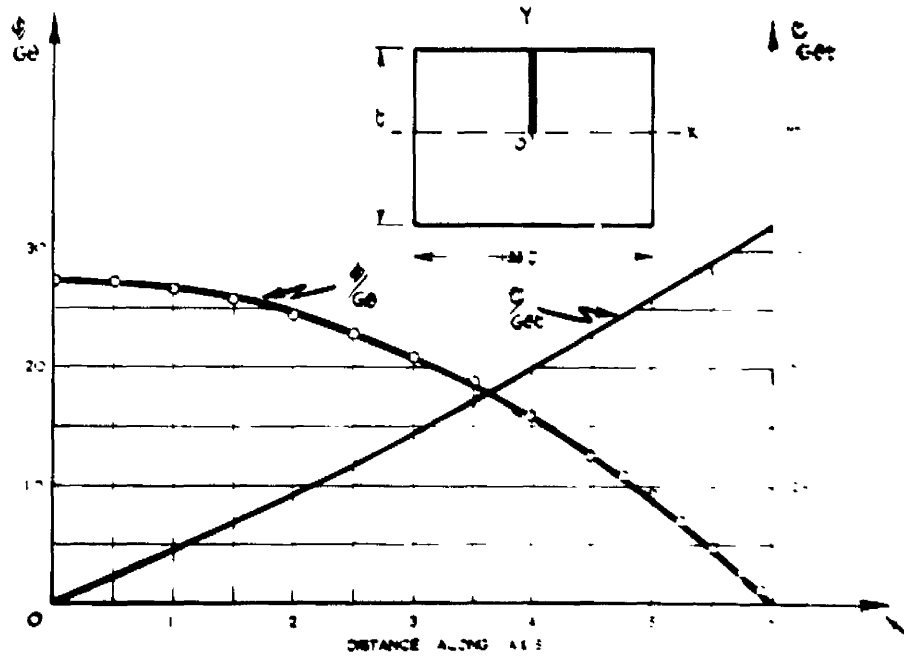


Fig.143.

# RECTANGULAR SHAFT IN TORSION

DISTRIBUTION OF  $\phi$  AND SHEAR STRESS  $\tau$  ALONG  
AXIS OZ

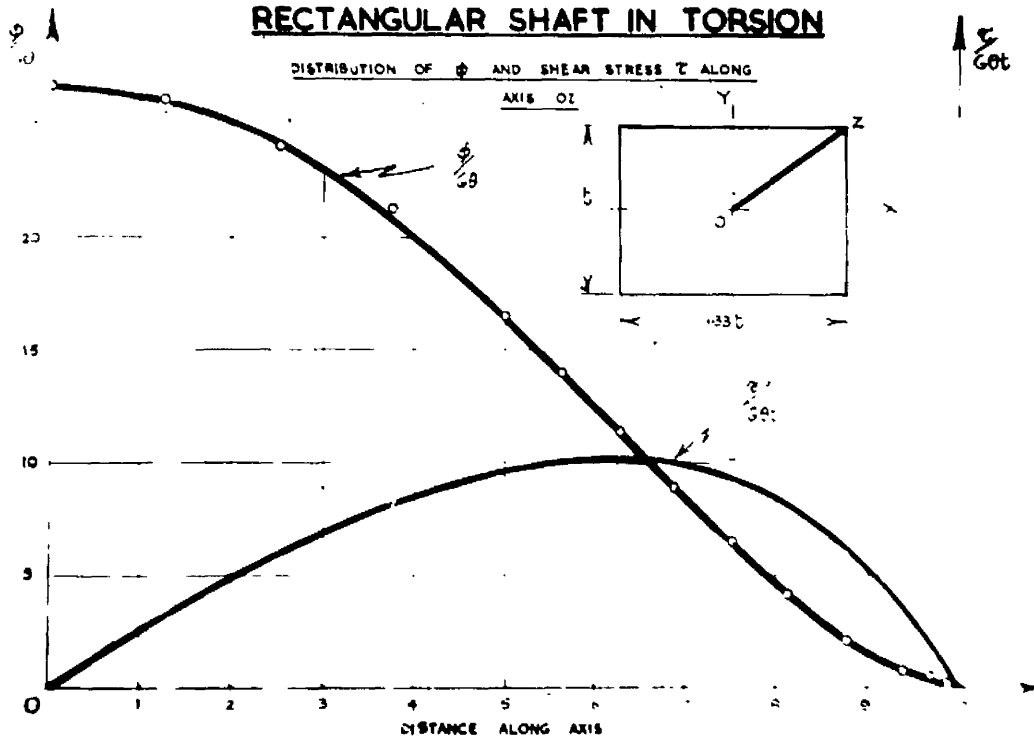


Fig.144.



# RECTANGULAR SHAFT IN TORSION

DISTRIBUTION OF  $\phi$  AND SHEAR STRESS  $\tau$  ALONG

AXIS  $OX$

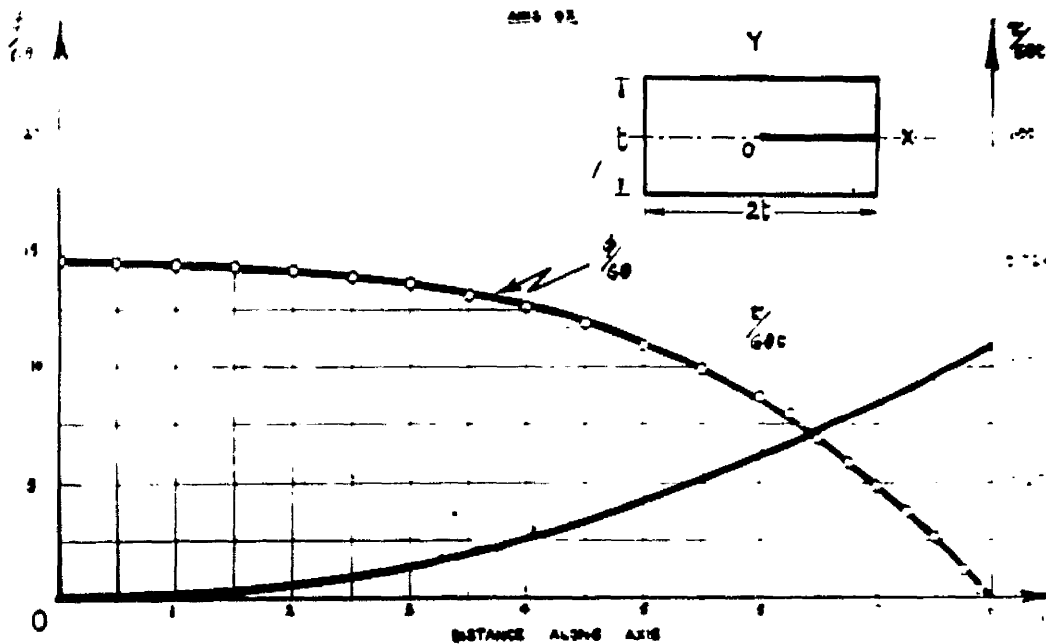


Fig.145.

# THIN RECTANGULAR SHAFT IN TORSION

DISTRIBUTION OF  $\phi$  AND SHEAR STRESS  $\tau$  ALONG AXIS  $OX$

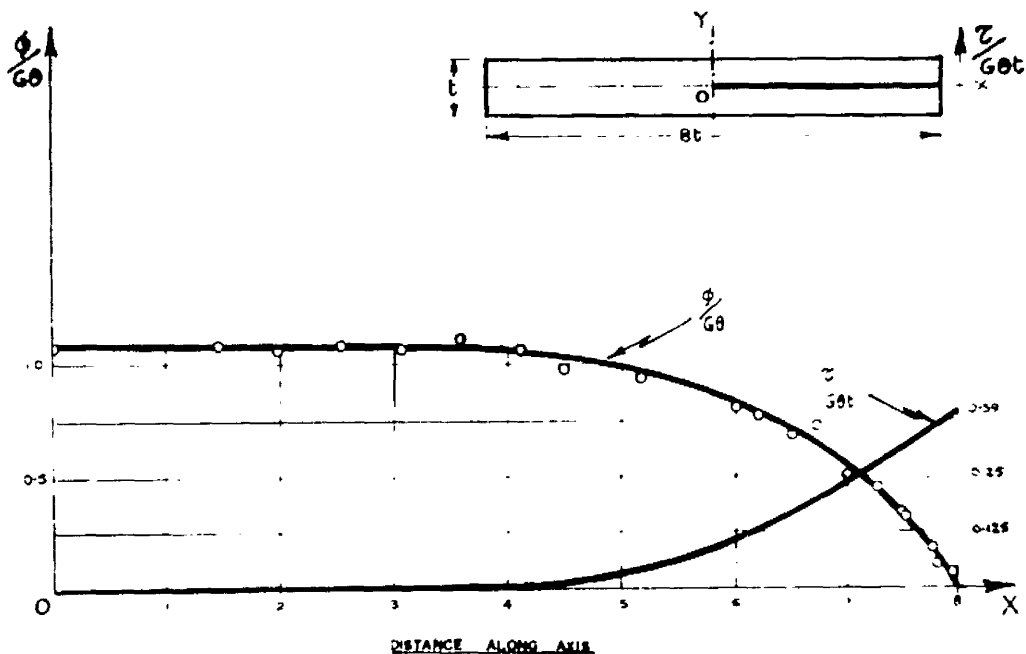


Fig.146.

# THIN RECTANGULAR SHAFT IN TORSION

DISTRIBUTION OF  $\phi$  AND SHEAR STRESS  $\tau$  ALONG AXIS OY

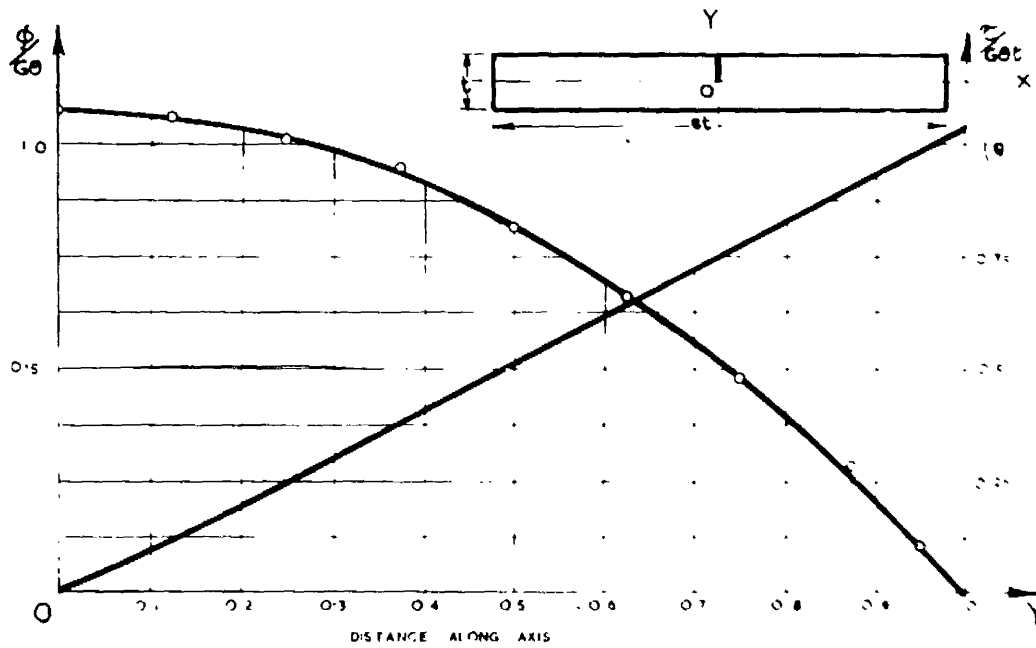


Fig.147.

# THIN RECTANGULAR SHAFT IN TORSION

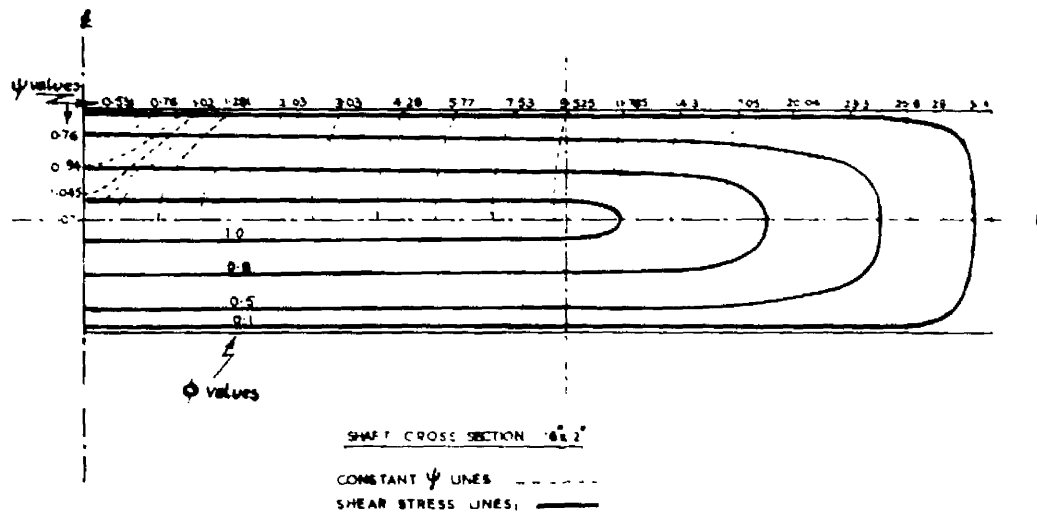


Fig.148.

# TORSION OF RECTANGULAR SHAFTS

THEORETICAL AND EXPERIMENTAL VALUES OF MAXIMUM  
SHEAR STRESS

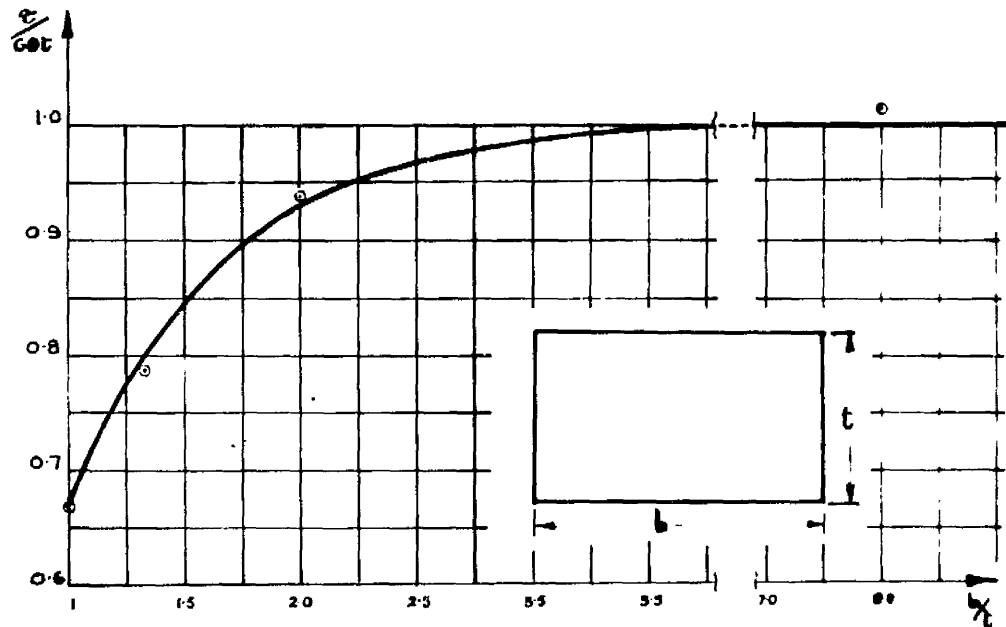


Fig.149.

## SQUARE SHAFT IN TORSION

MAXIMUM SHEAR STRESS LINES PARALLEL TO LINES  
OF SYMMETRY

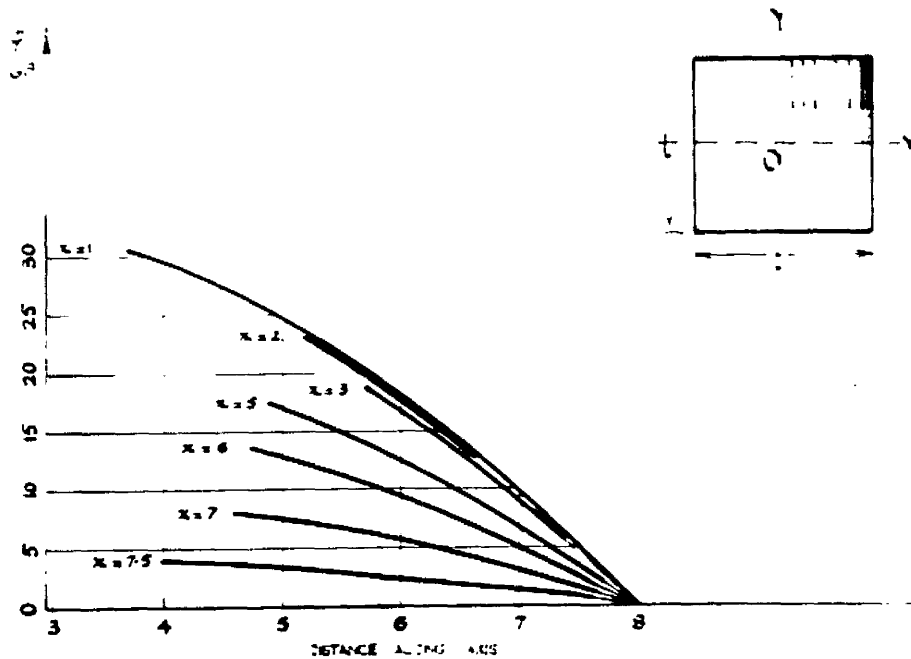


Fig.150.

# SQUARE SHAFT IN TORSION

DISTRIBUTION OF SHEAR STRESS  $\tau$  ALONG  
BOUNDARY AB

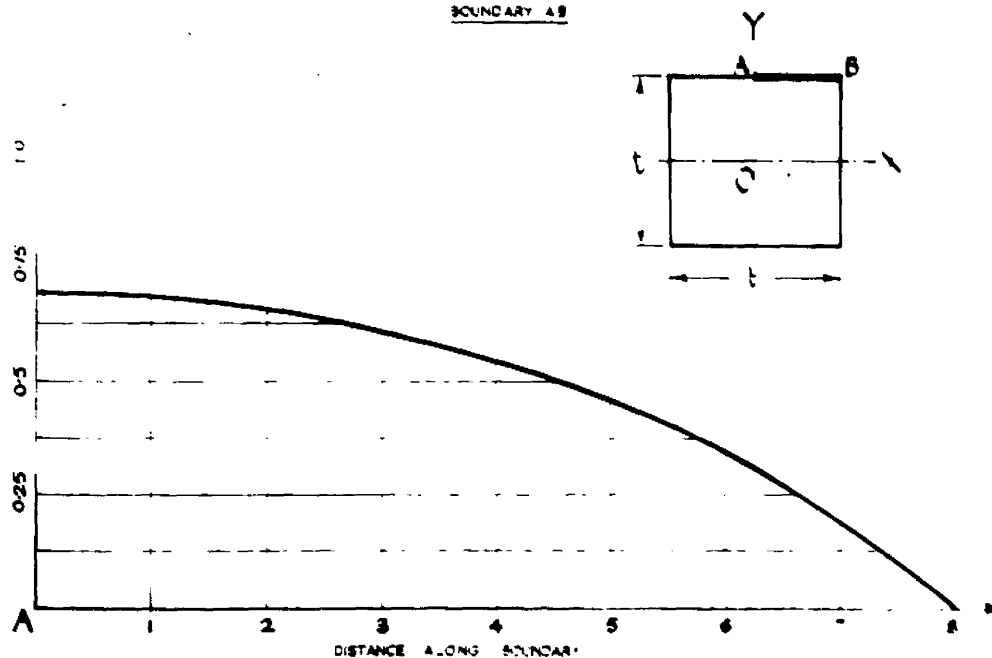


Fig.151.

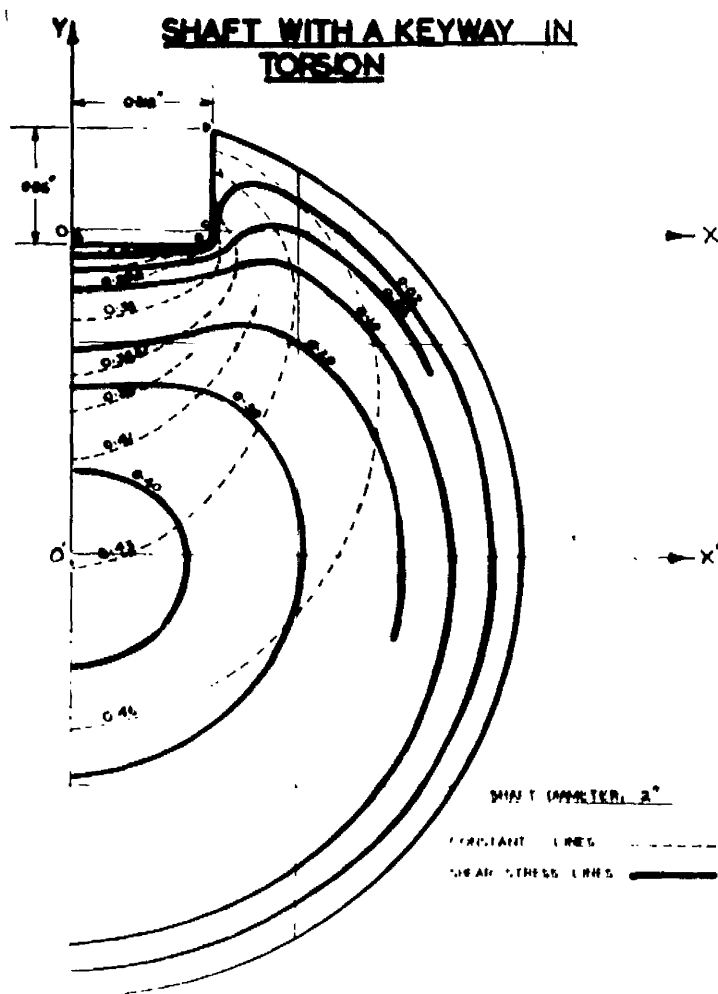


Fig.152.

# **CONSTANT $\psi$ LINES ON A TRANSFORMED SECTION**

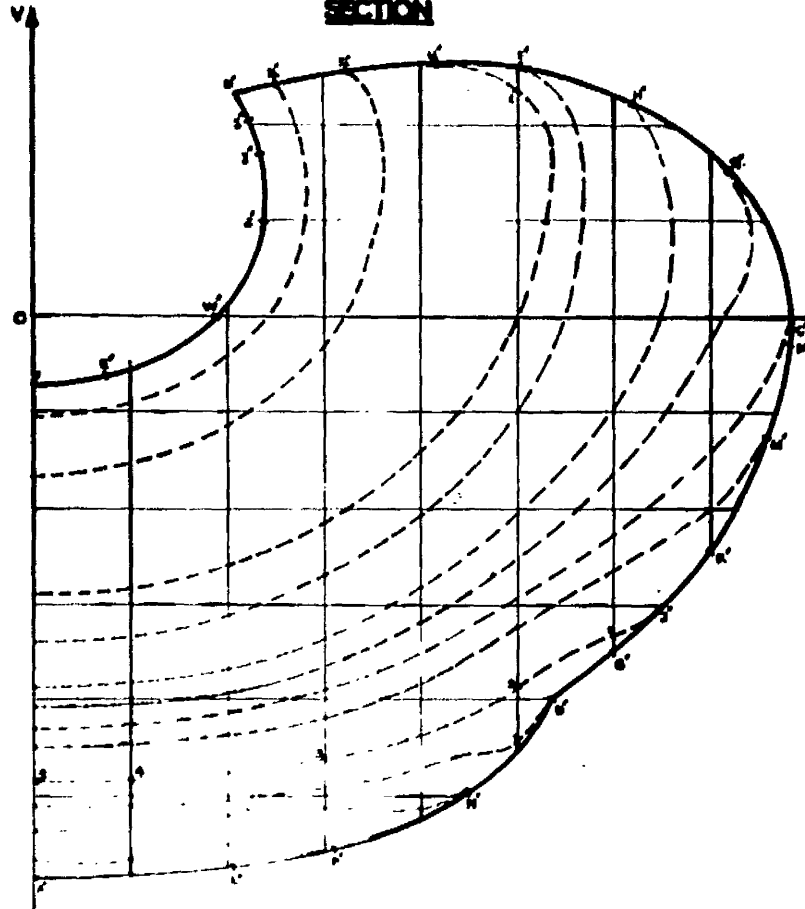


Fig.153.

## **FILLET REGION**

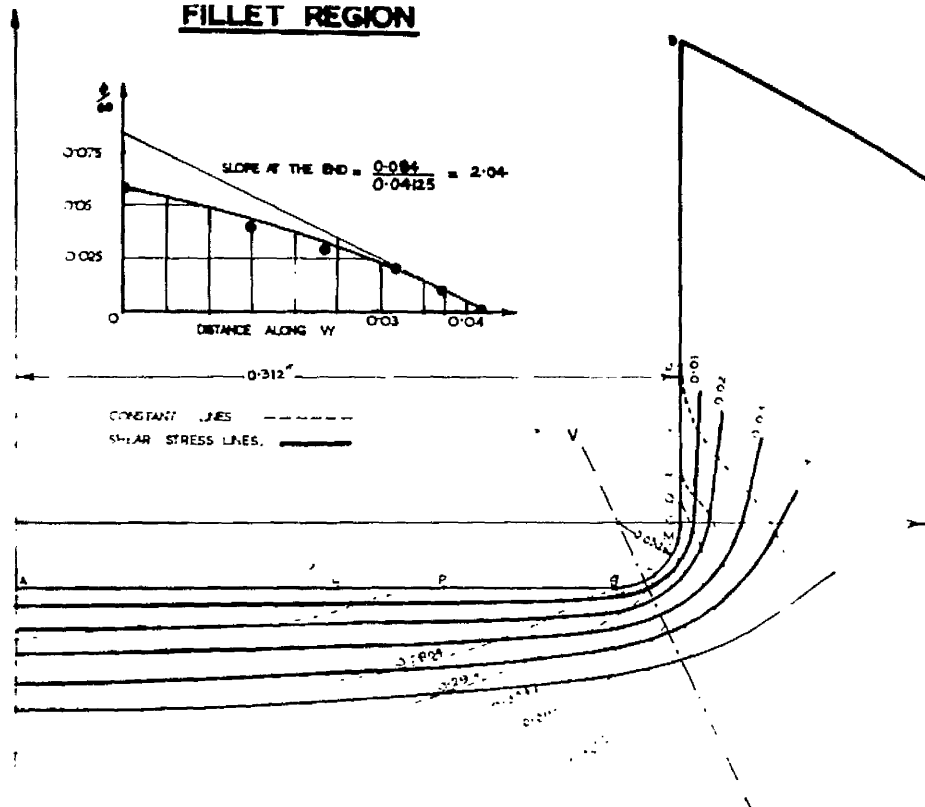


Fig.154.

Application to Stress Concentration Determination

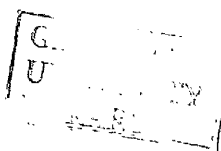
The analogue was applied to the case of a circular shaft containing a British Standard keyway (Fig.152). In this problem the difficulty of applying voltage connections along the short highly stressed region at the fillet, was overcome by transforming the shaft boundary to a more suitable form.

By the use of the transformation

$$x + iy = a \coth \frac{u - iv}{2} \dots\dots\dots (7.75)$$

the boundary shown in Fig.153 was obtained, so that the fillet region became enlarged. Lines of constant  $\psi/G\theta$  were obtained from a conducting paper specimen of the transformed shape. These contours were then re-transformed on to the original cross-section, on which the lines of constant  $\phi/G\theta$  were then constructed as shown in Fig.152.

The stress concentration factor for the keyway was determined by obtaining the slope, at the boundary, of the  $\phi/G\theta$  curve along a radial line drawn through the fillet radius centre, at the position on the boundary where the  $\phi/G\theta$  lines were most closely spaced. This is shown in Fig.154. This value, related to the maximum shear stress value in a shaft of the same diameter but with no keyway, and subjected to the same torque, gives a stress concentration factor for the keyway considered, of 2.95.



ACKNOWLEDGMENTS

The work presented in the thesis has been carried out in the Department of Mechanical, Civil and Chemical Engineering of The Royal College of Science and Technology, Glasgow. The writer wishes to record his grateful appreciation to Professor A.S.T. Thomson, D.Sc., Ph.D., A.R.C.S.T., M.I.C.E., M.I.Mech.E., and to R.M. Kenedi, C.H. (Lima), B.Sc., Ph.D., A.R.C.S.T., A.M.I.Mech.E., A.F.R.Ae.S., for their continued interest and encouragement.



GLASGOW  
UNIVERSITY  
LIBRARY